THE UNIVERSITY OF HULL

Pathways and Mechanisms of Aeration in *Phragmites australis*

being a Thesis submitted for the Degree of Doctor of Philisophy

in the University of Hull

by

Jean Armstrong, B.Sc., Dip.Ed.

April 1992

ACKNOWLEDGEMENTS

I thank my husband, Bill, very much for all his advice, encouragement and patience in supervising this project, and Dr. Peter M. Beckett for deriving the mathematical models of rhizome aeration. Also, I should like to thank Professor John Friend for the use of the Department's facilities.

I am very grateful to Miss Sarah Lythe for the preparation and sectioning of resin embedded material, Mr. Dick Holt and Mr. Keith Anderson for photography, Mrs. Janice Mundy and Mr. Anthony Sinclair for the preparation and photography of specimens for scanning electron microscopy, Mr. Michael Bailey for the production of glassware, especially for the Nuclepore experiments, and Miss Anne Braithwaite and Mr Victor Swetez of the University Botanic Gardens for the cultivation of *Phragmites* plants.

Finally, I am particularly grateful to the Water Research Centre (Swindon) and the Yorkshire Water Authority, for funding this research.

Frontispiece : Oxidation of methylene blue dye by the roots of *Phragmites*: (bottom left) solution culture, and (bottom right) waterlogged soil. In the latter iron oxidation is also clearly visible as an orange-brown precipitate in the rhizosphere. The upper figure shows the aerial parts of a dense stand of *Phragmites*.

Summary of Thesis submitted for the PhD degree

by Jean Armstrong

on

"Pathways and Mechanisms of Aeration in *Phragmites australis*"

This thesis describes an investigation into the aeration pathways, resistances to gas-movement, mechanisms of internal aeration and the locations and quantities of oxygen efflux from the underground parts of the common reed *Phragmites australis*. The "ventilating pressure concept" was also tested and reappraised.

Well-developed interconnecting gas-spaces within the culm, rhizome and roots offered relatively small resistance to either diffusive or convective gas transport, and the porosity of root-rhizome junctions was unusually high. Radial channels located at the nodes proved to be the only connecting points between cortex and pith in culms and rhizomes. Rhizome and old adventitious root surfaces were impermeable to oxygen but the young parts of adventitious roots and the numerous laterals readily released oxygen to anaerobic agar media and soil, markedly raising the redox potential of the rhizosphere.

It was discovered that callus readily forms in *Phragmites* in response to wounding and senescence, blocking the gas-spaces of root-rhizome junctions, leaf-sheath-culm junctions, and rhizome nodal diaphragms. However, the culm-rhizome junctions normally remain callus-free despite senescence of the culms, and gaseous connexion between the underground parts and the atmosphere is thus maintained thoughout the year.

A major discovery was that pressurised gas-flows are an important feature in *Phragmites*' aeration: Venturi- and/or Humidity-induced convections produced much higher rhizome oxygen

concentrations and radial oxygen loss from the roots than when rhizome aeration was chiefly diffusive. Both experiments and mathematical modelling demonstrated that comparatively slow rates of convection are sufficient to achieve this. The humidity-induced convection, the first reported in a grass, was shown to be initiated chiefly in living leaf sheaths, the convected gases being transmitted via gas-spaces in the culm to those of the underground rhizome, and vented via old broken culms. The flows are particularly rapid at low atmospheric humidities and increase with increasing PAR. The major mechanism promoting the convection appears to be a humidity-induced diffusion or transitional Knudsen diffusion of atmospheric gases into the plant, the concentration gradient being maintained by the difference in humidity between the interior of the plant and the outer air. The process was mimicked and further investigated using Nuclepore membranes providing important insights into the mechanism and its modelling, and it was shown that pore diameters within the Knudsen regime are not essential to produce the static pressure differentials and convective flows found in *Phragmites*.

The Venturi-induced convection, the first reported example in a plant, is created by the action of winds blowing across tall, dead, broken culms; air is drawn into the rhizome system via short broken culms in more sheltered positions.

Mathematical models and polarographic measurements of radial oxygen loss from roots were used to estimate the quantities of oxygen which might be released by *Phragmites* in the root-zone process of sewage treatment. It was concluded that 5 to 12 g O_2 m^{-2} day^{-1} would be a conservative estimate but that the amount could be greater or less depending upon root numbers and their physiological condition, as well as upon soil oxygen demand and diffusivities.

ABBREVIATIONS

ΔP = pressure differential (Pa)

ΔP_d = dynamic pressure differential (Pa)

ΔP_s = static pressure differential (Pa)

ΔT = temperature differential, °K (positive value indicates a higher temperature beneath Nuclepore membrane, and for plants, a higher temperature within the plant, compared to ambient, and *vice versa*).

ϵ = fractional porosity

η = viscosity of air (18.4×10^{-6} kg s^{-1} m^{-1})

HIC = humidity-induced convection

HID = humidity-induced diffusion

λ = molecular mean free path (μm)

MeB = methylene blue

MPD = pore diameter of membrane (μm)

mV = millivolts

Pa = Pascals

PAR = photosynthetically-active radiation (μmol m^{-2} s^{-1})

ϕ = capillary pressure flow resistance (Pa s m^{-3})

RH = relative humidity (%)

ρ = density of air or water (kg m^{-3}

RMM = relative molecular mass

ROL = radial oxygen loss (mass $area^{-1}$ $time^{-1}$)

R_{PV} = venting path resistance (Pa s m^{-3})

S = velocity of gas passing horizontally across Nuclepore membrane (m s^{-1})

SE = standard error of mean

SEM = scanning electron microscopy/micrograph

σ = surface tension of water (0.072 N m^{-1})

Si-rubber = silicone rubber

VIC = Venturi-induced convection

W = distance between water surface and Nuclepore membrane (mm or μm)

w/v = mass to volume ratio

CONTENTS

The following figures and tables have already been published and are the copyright of the journals concerned.

Figs. 2.03, 2.04, 2.05, 2.06, 2.07, 2.08, 2.09:

Armstrong *et al.* (1988).

Figs. 2.01, 2.02, 3.14, 3.15, 3.16, 3.20, 3.25; Table 4.01:

Armstrong & Armstrong. (1988)

Figs. 3.24, 5.01, 5.06, 5.07, 5.08 :

Armstrong & Armstrong (1990a)

Figs. 3.34, 3.02(b), 3.08 (a,b), 3.12, 3.14, 3.25, 5.10(b) 5.11, 5.12.

Armstrong & Armstrong (1990b).

Figs. 4.05, 5.01, 5.06, 5.07, 5.09(a) :

Armstrong *et al* (1990a).

Figs. 5.06, 5.08; Table 8.01 :

Armstrong *et al* (1990b).

Figs. 5.02(b), 5.04, 5.05, 5.12; Table 5.01 :

Armstrong & Armstrong (1991).

Figs. 5.09, 7.01, 7.02, 7.03, 8.01:

Armstrong *et al* (1992).

CHAPTER 1

GENERAL INTRODUCTION

This thesis is based upon work carried out during a three and a half year research programme funded by the Water Research Centre and the Yorkshire Water Authority to investigate "The Pathways and Mechanisms of Aeration in *Phragmites australis*". The ultimate goal of the project was to assess the suitability of the plant for use in the "root-zone treatment of waste-waters" by estimating its capacity to aerate the rooting zone, a process thought to be essential for effluent purification.

The notion of treating waste-waters by land-application is not new; to some extent it has been practised in the U.K. for more than a century. The purifying effects of natural fresh-water wetlands have been widely reported e.g. Seidel (1967), Toth (1972), De Jong (1976), De Jong *et al* (1977), Fetter *et al* (1978), and Sloey *et al* (1978).

The common reed, *Phragmites australis* (Cav.) Trin, ex Steud, is one of a number of species, (including *Typha, Scirpus, Eichornia and Pistia)*, which have been used extensively in recent years to stock wetlands and ponds especially constructed for the purposes of treating domestic, agricultural and industrial sewage. Reeds were chosen in the belief that they would be an aid to hydraulic conductivity, but more importantly (and in common with the other species: e.g. Reddy *et al*, 1987) would, by releasing oxygen from their roots, help in the removal of BOD, COD and 'nitrogen' (Seidel, 1976; Seidel & Happel, 1981; Finlayson & Chick, 1983; Kickuth, 1984; Kickuth *in* Boon, 1985; Lawson, 1985; Reddy & Smith, 1987; Athie & Cerri, 1987; Wathugala *et al*, 1987; Cooper & Findlater, 1990). It was estimated by Kickuth (1984) that in

the "root-zone method" up to 50 g O_2 m^{-2} d^{-1} could be transmitted by the plant into the substrate, but a report circulated to the Water Research Centre (Dorau, unpublished in Lawson, 1985) and based on calculations of oxygen diffusion through the reed, suggested that Kickuth's figures were too high by several orders of magnitude.

The theory underlying the "root-zone" purification process is as follows. The waste-water percolates through soil containing the plant's rhizomes and roots (Fig. 1.01a,b), and there comes into contact with a mosaic of reducing and oxidising zones, the latter being maintained by oxygen diffusing from the plant's roots and from the soil surface. The theory of nitrogen removal is as follows. In the oxidising regions, nitrification takes place through the activities of aerobic nitrifying bacteria; ammonium compounds may be converted to nitrites by for example, *Nitrosomonas* species. The nitrites are then oxidised to nitrates by species such as *Nitrobacter* (Fig. 1.01c). Subsequently, in the reducing regions of the soil, the denitrifying activities of facultative anaerobic bacteria such as *Pseudomonas* species convert the nitrates to oxides of nitrogen and, ideally, to nitrogen gas which escape into the atmosphere (Fig. 1.01c, and Stengel *et al*, 1987). In addition, both oxidation and reduction reactions are thought to be involved in the removal of phosphates (Stengel *et al*, 1987), while oxidations can also help to deposit iron (Armstrong, 1967; Green & Etherington, 1977; Taylor *et al*, 1984; Chen *et al*, 1980) and sulphur compounds (Engler & Patrick, 1975; Winter & Kickuth, 1989a,b). The removal of heavy metals e.g. Cu, Cd, Zn, Mn & Pb has been reported by, for example, Gambrell *et al* (1977), Gersberg *et al* (1985), and Dunbabin *et al* (1988). Metal removal is probably dominated by precipitations as metal oxides, complexing with the iron oxidised in the rhizosphere, and chelation with organic matter (Patrick & Gambrell, 1976).

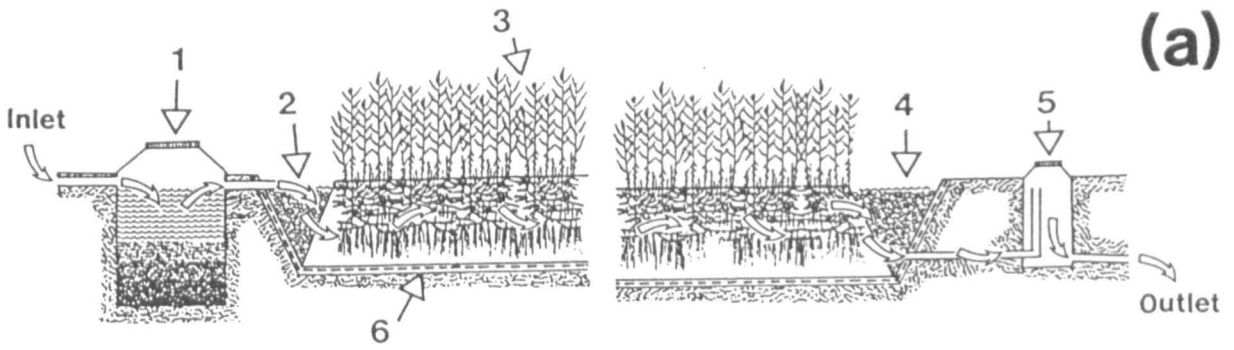

Schematic representation of a root-zone treatment plant. 1: Sedimentation tank;, 2: Inlet channel; 3: Wetland plants; 4: Outlet channel; 5: Outlet weel with vertical tube for control of water level in outlet channel; 6: Watertight membrane. (Hans Brix 1987)

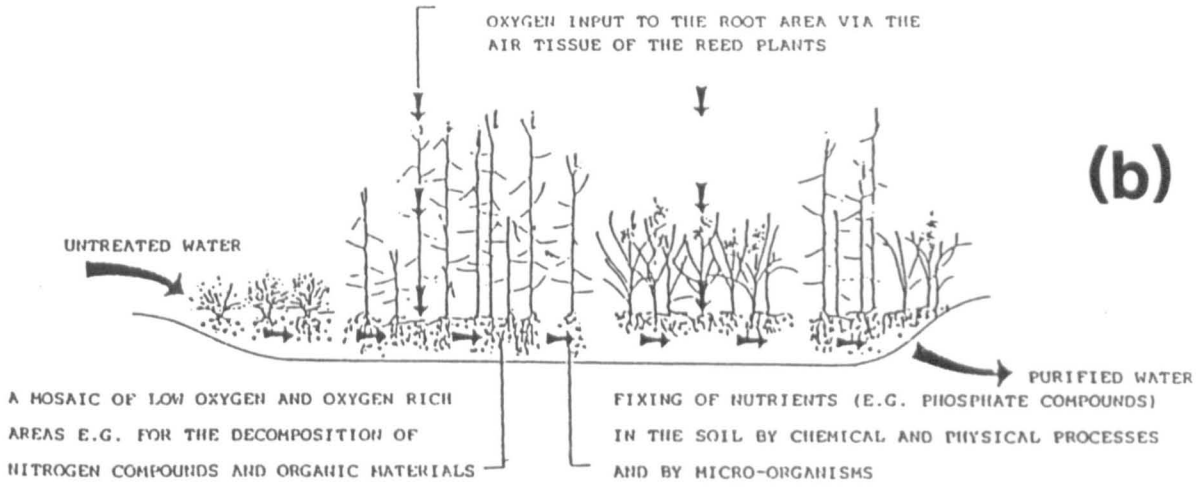

The purification of primary or secondary sewage in root zone beds (Thable 1984).

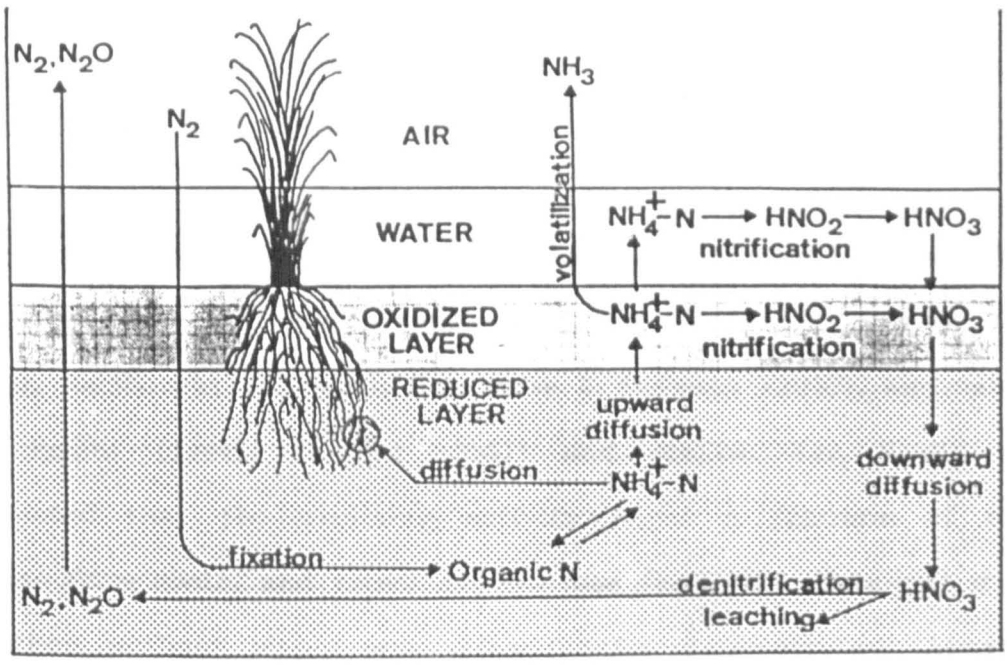

Nitrogen transformations in a flooded soil-plant system.

Figure 1.01

Potentially, macrophyte-based systems have several advantages compared to conventional treatment plants : they have low working costs and low energy and maintenance requirements, they can often be established at the very location where the waste water is produced, and, being "low technology" systems, they can be established and run by relatively untrained personnel (Brix, 1987). Thus, the use of "root-zone type" waste-water treatment plants could be suitable for small isolated communities, especially in developing countries.

Opinions as to the success of constructed wetlands and the role of the reed, are currently about as variable as bed design, soil type, loading rates, quality of effluent and vigour of the plants (Cooper & Findlater, 1990). The successful functioning of reed beds has been reported by Gersberg *et al* (1985, 1986), Geller, Kleyn & Lenz (1990), May *et al* (1990), and others, but at the present time many beds undoubtedly malfunction. In many cases this may be the result of faulty design or management (overloading), but critics have also questioned the ability of reeds to furnish sufficient quantities of oxygen for effluent purification (Brix & Schierup, 1990; Schierup, Brix & Lorenzen, 1990; Bucksteeg, 1990).

The ability of plants to oxidise the rhizosphere has been known for many years and was established by the pioneering work of Molisch (1888), Raciborski (1905a,b), Schreiner & Sullivan (1910), and later by van Raalte (1944), Bartlett (1961) and others. Van Raalte (1944) suggested that the oxidising activity might a function of oxygen release from roots, and radial oxygen loss from rice roots and a range of other wetland plants was subsequently demonstrated (Armstrong, 1964 & 1967). Later the dimensions of oxidised rhizospheres was found to accord with the limits of rhizosphere oxygenation by radial oxygen

loss (Armstrong, 1970), and the distribution of iron and other oxidations in rhizosphere and root Engler & Patrick (1975) and Green & Etherington (1977).

The continuity of gas-spaces between shoot and root systems of wetland plants was shown by Conway (1937) for *Cladium mariscus*, by Laing (1940) for *Nuphar*, and by van Raalte (1941, 1944) for rice. They also demonstrated the dependence of the submerged roots upon the shoot system for their oxygen supply, the assumption being that the oxygen was transported by diffusion through the gas-spaces.

The presence of large gas-spaces is a feature common to most wetland species and has two important effects. Firstly, it reduces the volume of respiratory tissue, thus decreasing the overall respiratory oxygen demands of the plant. Secondly, and more importantly (Armstrong, 1979) it forms a low resistance pathway for oxygen transport from the shoot into the root system. It has been shown elsewhere that the effectiveness of diffusive aeration in wetland plants depends upon the degree and distribution of (a) the gas-space (b) the respiratory demands of the plant and (c) leakage to the rhizosphere.

The diffusion of oxygen from submerged root surfaces is thought to be a useful, rather than a wasteful phenomenon : waterlogged soils invariably contain certain phytotoxins e.g. Mn^{2+}, Fe^{2+}, S^{2-} and volatile organic acids (e.g. Ponnamperuma, 1984; Gambrell & Patrick, 1978; Armstrong & Boatman, 1967; Jones & Etherington, 1970; Jones, 1972; DeLaune *et al*, 1983; Pezeshki *et al*, 1988). Thus, oxygen diffusing from the roots, which promotes the oxidation of these toxins and diminishes their potency, will create a more favourable medium for root growth. (e.g. Armstrong, in Etherington 1982; Laan *et al* 1989).

Prior to the start of this project very little previous work could be cited on rhizosphere oxidation by *Phragmites* apart from a paper by

Hansen & Andersen (1981). However, there was some literature regarding oxygen regimes within the plant viz. Yamasaki (1984), Krasovskii & Chashchukin (1974). Furthermore, little appeared to be known concerning the continuity of gas-spaces within the plant or about the mechanisms of gas-transport. Thus, it seemed desirable to examine the following aspects of aeration in *Phragmites*: (a) the nature of the gas-space system (Chapter 2), (b) the resistances to applied pressurized gas-flow (Chapter 3), (c) the potentials for radial oxygen loss from the roots and rhizosphere oxidation (Chapter 4), (d) the mechanisms for oxygen transport, particularly to see if diffusion was the only significant process (Chapters 5, 6 & 7). As the study progressed it was necessary to use mathematical modelling to try to reach conclusions concerning transport within the plant and the soil oxygenating capacity of the roots (Chapter 8).

Finally, it should be noted that during the course of this project several papers have appeared relating to the internal oxygen supply of *Phragmites*, to rhizosphere oxidations by the plant, BOD removal, nitrogen transformations etc. ; these publications are reviewed in Chapter 9.

CHAPTER 2

PRESSURIZED GAS-FLOW STUDIES TO DETERMINE GAS-SPACE CONNEXIONS, PRESSURE-FLOW AND DIFFUSIVE RESISTANCES, AND TO REAPPRAISE THE CONCEPT OF VENTILATING PRESSURE

PART I - GAS-SPACE CONTINUITY

2.1. INTRODUCTION

The intitial pressure flow experiments were designed to see if gas-space continuity exists between the culm, rhizome and roots of *Phragmites*, and if there were any such connections between the pith and aerenchyma channels of the rhizome. Attempts were made to blow air through the various parts, using similar methods to those described by Roberts, McComb & Kuo (1984) for investigating gas-space pathways within the sea grass *Halophila*. The pathways were also investigated and confirmed by anatomical studies, some of which were interspersed with the pressure flow investigations. For convenience, however, all the anatomy is collated in Chapter 3.

During these preliminary gas flow experiments, so-called "ventilating pressures" were also determined, i.e. minimum pressures required to force gas through a plant or plant organ to vent as bubbles beneath the water surface. However, the results found for *Phragmites* highlighted flaws in the ventilating pressure concept, and as a result of further experiments a critique of the concept is presented in Part II.

2.2. MATERIALS AND METHODS

2.2.1. *Plant material*

Horizontal and vertical rhizomes of *Phragmites*, collected from the banks of the Humber estuary during October and November, were either used immediately, or with the cut ends emergent, placed in stagnant 20% Hoagland's solution at 15°C, a PAR of 100 μmol m^{-2} s^{-1}, and an 18h daylength, to resume growth and root production.

2.2.2. *Gas space continuity using pressurized air-flow*

Gas-space continuity was studied by observing the release of gas-bubbles from rhizome, rhizome-root, and rhizome-root-shoot systems pressurized from one end and submerged at a depth of 10 mm. Accidental flooding was prevented by applying the gas-pressure before submergence. The method is similar to that reported by Roberts, McComb & Kuo (1984), but a compressed air cylinder was used as a gas source and pressures were recorded by means of either a water manometer or pressure transducer (Furness Controls Ltd).

2.2.2.1. H*orizontal rhizomes.*

First used were 100 mm lengths of rhizome (diam. *c.* 14 mm), each with two nodes and with apices excised. The points of gas loss, and the minimum pressures required to cause a flow were recorded when the pith cavity or aerenchyma channels were blocked with Si-rubber or Plasticene in various ways as indicated in Fig. 2.01. Minimum pressures required to cause a gas-flow from the intact apices of other rhizomes were also measured.

2.2.2.2. *Vertical rhizomes and culms.*

Pieces of rhizome, 80 mm long, each having adventitious roots and an aerial shoot were used. The minimum pressures recorded were those required to cause gas-flows through the various paths indicated in Fig. 2.02.

2.3. RESULTS AND DISCUSSION

The net minimum pressures required to force air through the submerged rhizome and culm through various routes are indicated in Figs. 2.01 & 2.02.

Since air could be forced through the rhizome pith cavity at comparatively low pressures (150–250 Pa), it would seem that the nodal septa offer little resistance to gas flow. Pressures were smaller for the pith cavity, larger for narrower aerenchyma channels, and largest for root gas-spaces, and the implications of these findings for the ventilating pressure concept described by Arikado & Aduchi (1955) and Arikado (1959) are discussed in Part II. The pressures associated with flow from stomata could not be determined owing to the permanent presence of leaf-surface gas-films.

Other conclusions to be drawn from these gas-flow experiments are that:

(a) Pith cavities of the the rhizome system connect with those of both dead and living culms.

(b) Within rhizomes there are gas-space connections between pith cavities and aerenchyma channels. The anatomical studies later showed (Chapter 3) that the rhizome aerenchyma did not constitute a longitudinal transport system that was independent from that of the pith. Rather, the aerenchyma channels at each

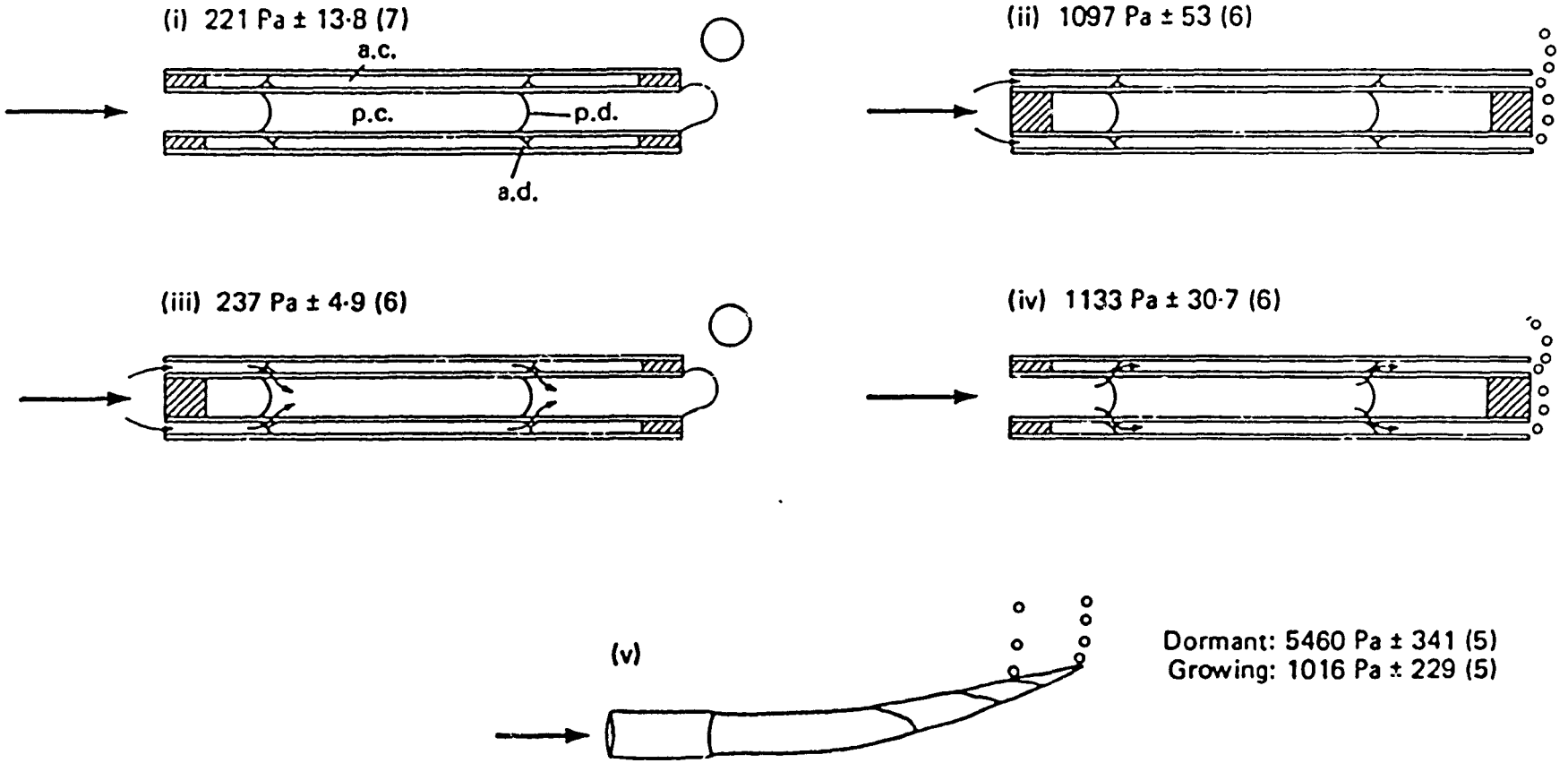

Fig. 2.01 The effect of pressured air flow and various patterns of blockage on gas movement through horizontal rhizomes with gas-pathways indicated by arrows. The minimum ventilating pressures are presented as; $\bar{X}$, SE and (n). a.d., aerenchyma diaphragm; p.d., pith diaphragm; a.c., aerenchyma channel; p.c., pith cavity. Hatching denotes artificial blockage.

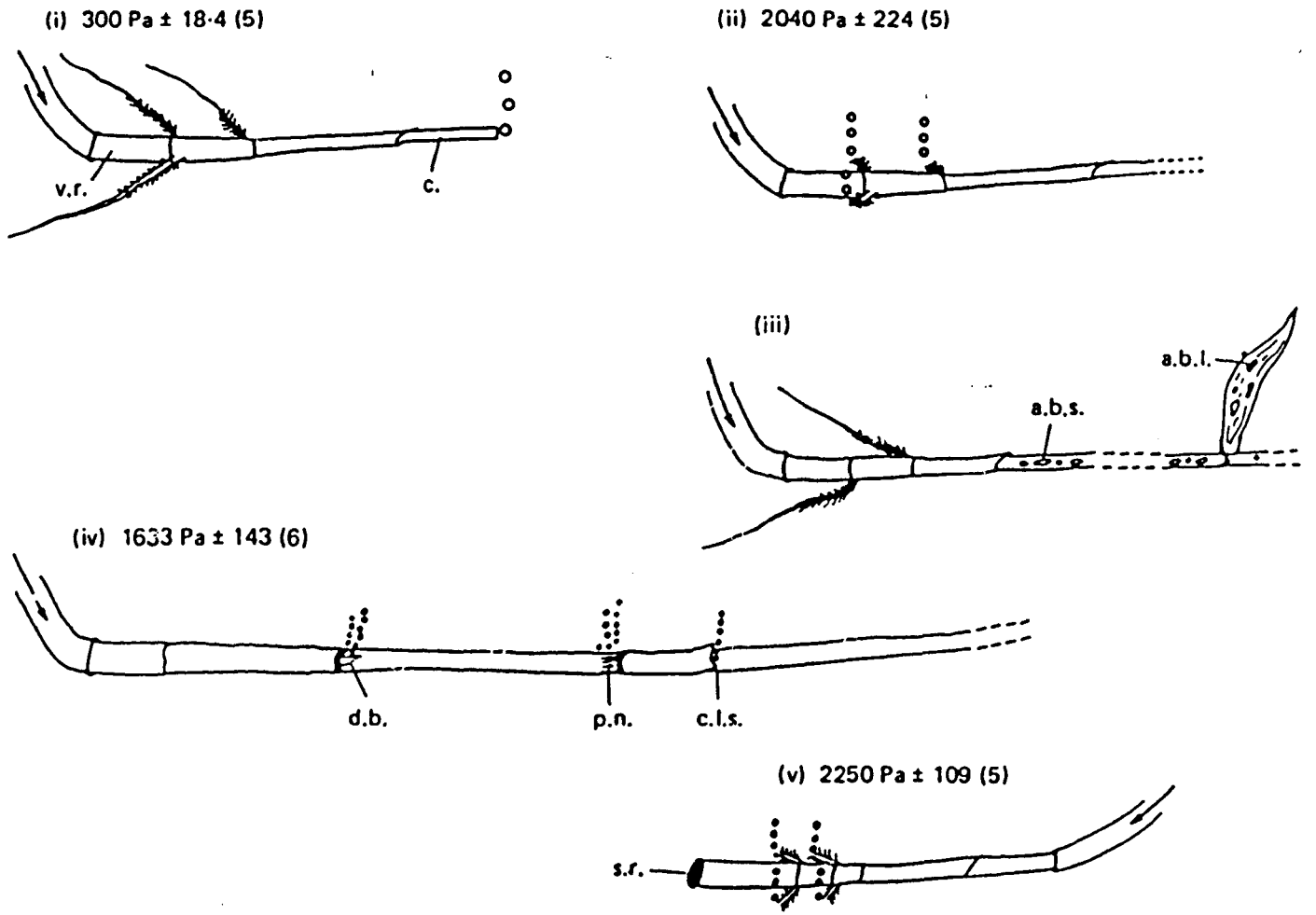

Fig. 2.02 The effects of pressured air flow through vertical rhizomes and culm. The minimum ventilating pressures are presented as: X, SE, (n) Arrows indicate direction of flow; broken lines denote an intact attached culm. In (iii) pressures could not be accurately measured; (i), (ii), (iii) and (v) represent young culms and (iv), an old one, (pressures were higher for senescing culms of the current year). c, culm; d.b., decayed bud; v.r., vertical rhizome; p.n., porous nodal region; c.l.s., cut leaf-sheath; a.b.l., air-bubbles forming on lamina; a.b.s., air-bubbles forming on leaf sheath; s.r., sealed rhizome.

end of an intact rhizome and at each node connect with the pith cavity via radial channels traversing the stele. Gas-transport from culm to rhizome is via the pith. When attempts were made to estimate simultaneously the relative rates of pressurised gas-flow through the aerenchyma and pith the experiments were abandoned when it was realised that flows in the two systems could be in opposite directions. From this, and the anatomy, it would seem that the aerenchyma may simply serve to aerate the cortex and (at the nodes) especially the developing buds and adventitious roots, and does not normally function significantly in *long*-distance gas-transport.

(c) There are gas-space connexions also between cortical aerenchyma channels of the rhizome and cortical gas-spaces in the roots.

(d) Ventilation of the underground parts can proceed via stomatal pores on the living leaves and culm, air spaces in the leaves and culm, and via both pith cavity and aerenchyma channels in the rhizome and aerenchyma in the roots.

These findings accord with anatomical studies on the interconnecting gas-transport pathways described in Sections 3.3 & 3.4.

The gas-flow studies also highlighted the surface porosities, due to stomata, of nodes in senescent culms, but gas did not escape from internodal regions. (In Chapter 4 it is shown that MeB dye oxidation occurred at the nodes but not around the culm internodes). From these results it was deduced that when the aerial shoots die in the winter, the lowermost of the exposed highly porous nodal surfaces could be major entry points for air to ventilate the subterranean parts (Armstrong & Armstrong 1988). A similar conclusion was reached by Brix (1989). However, it should be mentioned at this point that a *Venturi-induced* pressurised gas-flow, in which air enters and leaves

via the ends of dead culms, can considerably supplement the diffusive ventilation of the rhizomes during the winter (Chapter 7).

PART II - A CRITICAL APPRAISAL OF THE CONCEPT OF VENTILATING PRESSURE AND AN ANALYSIS OF RESISTANCE TO PRESSURIZED GAS-FLOW AND GASEOUS DIFFUSION IN HORIZONTAL RHIZOMES AND DEAD CULMS

2.4. INTRODUCTION

Ventilating pressure, i.e. the minimum pressure deficit required to force gas through a plant or plant organ, to vent as bubbles beneath a water surface, has been regarded as a reflection of internal resistance to gas flow. It has been claimed that interspecific differences in plant ventilating pressures reflect differences in flood tolerance (Arikado & Aduchi 1955; Arikado 1959). However, during the above preliminary pressure-flow experiments, it was noted that the ventilating pressure for rhizome segments was lowest when venting occurred through the pith cavity only, higher for venting through the aerenchyma channels only, and even higher for venting through the cut surfaces of adventitious roots. Hence, it was suggested that ventilating pressure might be more a function of surface-tension effects on the escaping bubbles than of gas flow resistance within the plant. It was also noted that the pith and aerenchyma channels of the *Phragmites* rhizome are regularly interrupted at the nodes by partitions (diaphragms) containing stellate parenchyma. Although such partitions must offer resistance to pressurized and diffusive gas flow,

it seemed unlikely that these resistances would even be detectable by the conventional ventilating-pressure measurements.

This section includes an analysis of the surface-tension contribution to ventilating-pressure measurements, and presents a more meaningful method for assessing internal resistances to pressurized flow. Also, it is shown that the data so obtained can be used to estimate the effective pore diameters and the diffusive resistances of the nodal diaphragms.

2.5. THEORY

2.5.1. *Ventilating pressures and surface-tension*

The pressure difference, ΔP_d, developed along a capillary of radius r, when venting occurs from a submerged end, is given by the equation:

$$\Delta P_d = h\rho g + 2\sigma/r + \phi F, \qquad (2.01)$$

where h is the depth of submersion (m) above the mouth of the capillary: ρ, the density of water (kg m^{-3}); g, the gravitational constant (m s^{-2}); σ the surface tension of water (0.072 N m^{-1}); ϕ, the pressure-flow resistance of the capillary (Pa s m^{-3}) and F, the volume flow rate (m^3 s^{-1}). The expression ϕF is therefore the contribution to the pressure-difference caused by gas flow along the capillary and $2\sigma/r$ is the surface-tension contribution. Since ventilating pressure has been treated in the literature as a measure of internal resistance to gas flow, the inevitable conclusion must be that it has been mistakenly assumed to be some measure of the term ϕF. If the term $2\sigma/r$ is very small compared with ϕF there is no real problem but, by definition, ventilating-pressure represents the minimum pressure difference required to force gas from a plant. Consequently, as flow rate diminishes towards zero, as it must do to obtain a measure of the

minimum pressure required for flow, then $\phi F \rightarrow 0$ and the true minimum pressure-difference becomes largely a surface-tension effect, namely:

$$\Delta P_{d_m} = h\rho g + 2\sigma/r \qquad (2.02).$$

Also, since $\Delta P_{d_m} - h\rho g \propto 1/r$, the surface-tension component will increase with a decreasing radius of the capillary. If the capillary is elliptical rather than circular (applicable to some rhizome pith and aerenchyma channels), the term 2/r can be replaced by $1/r_1 + 1/r_2$, where r_1 and r_2 are the maximum and minimum radii of the ellipse. It is assumed that at the moment of escape the bubble also has a radius equal to that of the capillary; the general formula for the pressure difference across the interface is $2\sigma/r_c$, where r_c is its radius of curvature. If, in practical terms, the so-called ventilating pressure for plants does indeed represent largely a surface-tension effect then the plot of 2/r (or $1/r_1+1/r_2$) *vs.* $P_{d_m} - h\rho g$ should depart little from the theoretical line for glass capillaries, and the slope of the line should give the value of σ.

2.5.2. P*ressure differences vs. flow rate in the absence of surface tension or other external resistances*

Simple capillaries. For laminar gas flow through a capillary of uniform bore, the pressure difference, ΔP, between the ends of the capillary is given by the Poiseuille equation:

$$\Delta P = F [\ 8\eta L / \pi r^4\ ], \qquad (2.03),$$

where η is the viscosity of the gas (air = 18.4 x 10^{-6} kg s^{-1} m^{-1} ≡ N s m^{-2}), F is the volume flow rate (m^3 s^{-1}), r is the radius of the capillary and L its length. The ΔP is expressed in Pa (i.e. kg m^{-1} s^{-2}) and the resistance to flow (Pa s m^{-3}) is given by the expression, $8\eta L/\pi r^4$.

It follows that for any given resistance, the flow rate is directly

proportional to the pressure difference, and the resistance is given by the slope $\Delta P/F$. Further, the relationship between flow rate and path length for a given pressure difference will show a smooth decline inversely proportional to the length. Thus, it is possible to determine the radius of the capillary from the pressure difference, flow rate and length. It is also implicit in equation (2.03) that for any value of $\Delta P > 0$, there will always be a flow, and this again contrasts with the original concept of ventilating pressure.

Multiple capillaries. The axial ventilation system of a *Phragmites* horizontal rhizome consists of not one but of several parallel capillaries in the internodal regions (namely aerenchyma channels and pith cavity), while at the nodes there are diaphragms of stellate parenchyma with very many capillaries. Where gas flow occurs through a number of parallel and similar capillaries, a slightly modified solution to the Poiseuille equation is required. If n is the number of parallel capillaries, and r_1 the radius of each individual capillary, the solution is:

$$\Delta P = F \left[8\eta L / (n\pi r_1^2) r_1^2 \right] \qquad (2.04).$$

If the multiple capillary system is used to replace a single capillary of the same total cross-sectional area, i.e. $n\pi r_1^2$ [equ. 2.04] = πr^2 [equ. 2.03], it will be appreciated that the resistance will be increased: for n = 100 the resistance will be x 100 greater than for the single capillary, for n = 1000 the resistance will be x 1000 greater, and so on. Apart from demonstrating the effect of pore radius on pressure flow resistance, equation (2.04) also helps to provide an alternative check on pore radius, and this is particularly relevant if there is a need to estimate the diffusive resistance of nodal diaphragms. The anatomical studies (Chapter 3) suggest a porosity of c. 50% for nodal diaphragms

both in the distal small stellate and the proximal large stellate parenchyma layers. Since the observed capillary diameters of the small stellate layer seem to be very much less than 10 μm, whilst those of the large stellate parenchyma are much greater (50-80 μm), it follows that the small stellate parenchyma should dominate the nodal pressure-flow resistance. For the small stellate parenchyma of a domed nodal diaphragm in the pith cavity of the *Phragmites* rhizome, equation (2.04) can therefore be modified to:

$$\Delta P = [8\eta L_1 \; / \; \{\epsilon_1 \; \pi(a^2 + d^2) \; r_1^2\}] \qquad (2.05),$$

where L_1 is the longitudinal thickness of the small stellate parenchyma layer, ϵ_1 its fractional porosity, r_1 its average pore radius, a *is* the radius of the pith cavity at the insertion of the diaphragm and d, the height of the small stellate parenchyma dome, i.e. $\epsilon\pi(a^2 + d^2) = n\pi r_1^2$.

Equation (2.05) can be further modified to include the resistance due to the large stellate parenchyma:

$$\Delta P = (R_1 + R_2) \; F, \qquad (2.06),$$

where R_1 is the resistance due to the small, and R_2 the resistance of the large stellate parenchyma layers. The latter can be derived by:

$$R_2 = 8\eta L_2 \; / \; \epsilon_2\pi(a^2 + d^2) \; r_2^2 \qquad (2.07),$$

where L_2 is the longitudinal thickness of the large stellate parenchyma layer, ϵ_2 its fractional porosity, and r_2 its average pore radius. Thus from appropriate ΔP and flow-rate data, and by substituting the values for ϵ, a, d, L and r_2 in equation (2.06), an estimation of the individual pore radii of the small stellate parenchyma (r_1) in the diaphragm becomes possible.

2.5.3. *Diffusive resistance*

For gaseous diffusion through a non-tortuous single or multi-capillary system, diffusive resistance can be determined from the expression

L/DA where L is the length and A the total cross-sectional area of the diffusion path, and D is the diffusion coefficient of the gas in air (20.1 x 10^{-6} m^2 s^{-1} at 20°C, Armstrong, 1979). For a porous partition with n capillaries each of radius r_1 then, provided that the capillary diameters are considerably greater (by an order of magnitude) than the mean free path length of the diffusing molecules (10^{-7} m for O_2 at 20°C), the expression becomes $L/Dn\pi r^2$. Consequently if the fractional porosity of the partition is ϵ and its radius *is* a, the diffusive resistance, R, will be:

$$R = L/D\epsilon\pi a^2. \qquad (2.08)$$

In contrast to pressure-flow resistance, the dimensions of the individual capillaries should not unduly influence the overall diffusive resistance. In the case of the nodal partitions in the *Phragmites* rhizome, however, it is again important to take account of the domed nature of the structure. If the partition is domed, the area term will be that used in equation (2.05). It should also be noted that if pore sizes much exceed the mean free diffusion path of the molecules, fractional porosity will be the major factor governing diffusive resistance. Consequently the diffusive resistance offered by the small stellate parenchyma may often be less than that of the large stellate parenchyma since the latter is always the thicker layer.

2.6. MATERIALS AND METHODS

2.6.1. *Rhizomes*

Horizontal rhizomes of *Phragmites* were collected from the banks of the Humber estuary in November, December and February, and were used immediately or kept for a few days in moist air at 5°C until required.

2.6.2. *Ventilating pressures in partially submerged rhizomes*

Standard lengths of internode (30 mm) were used and either the pith or the aerenchyma channels were blocked with silicone rubber. The rhizome was connected to a water manometer and an air supply and submerged under 10 mm of water ($h\rho g$ = 100 Pa). Accidental flooding was prevented by applying pressure before submergence. Minimum pressures required to force air through either the pith cavity or aerenchyma channels were measured. Transverse sections were cut from each piece of rhizome, and the radii of the pith cavity, or those aerenchyma channels from which bubbles emerged, were measured using a Vernier microscope. Values $2/r$ for cavities round in cross section, or $1/r_1 + 1/r_2$ for cavities oval in cross section, were plotted against $\Delta P d_m - h\rho g$ (see Theory).

2.6.3. *Pressurized flow in "non-submerged" rhizomes*

A length of horizontal rhizome was connected at one end, (in parallel with a water manometer), to a flow meter and compressed-air cylinder. The other end was connected to the atmosphere by rubber tubing. The rhizome itself was then submerged in water. In contrast to the previous "ventilation pressure" experiment, however, the rhizome's cut ends remained dry and in air, hence the "non-submerged" condition.

(Immersion served only to confirm that there were no surface gas-leaks, and that the joints were airtight.)

Various procedures were used:

(a) At a fixed pressure differential of 375 Pa, gas-flow rates were recorded during progressive shortening of a long rhizome. Measured lengths of internodal and nodal tissue were alternately removed from one end of the rhizome after it had been temporarily removed from the water, care being taken to keep the cut ends dry. Internodal tissue was cut each time to within 2.5 mm of the scale-leaf scar. Each piece of nodal tissue removed was 5 mm long. The percentage porosity for each piece of internode cut off was measured on a transverse section by projection and tracing using a microprojector and leaf area meter.

(b) Rhizomes were progressively shortened by removing a node, together with half of the internodal segment on each side of it, and pressures required to cause a variety of flow rates: 100, 250 and 300 x 10^{-6} m^3 min^{-1} were measured. The relationship between pressure difference and gas-flow rates for different lengths of the same rhizome containing differing numbers of nodes was determined.

(c) Pressure *vs* flow measurements were used to estimate effective pore dimensions of the diaphragms of horizontal rhizomes. Non-submerged single nodes (length = 20 mm) were used with the aerenchyma channels sealed with silicon rubber at both ends. The longitudinal thicknesses of both small and large stellate parenchyma layers, and the average pore diameter of the large stellate parenchyma were measured using a calibrated eye-piece; the diameter of the pith cavity at the insertion of the diaphragm, and the height of the small stellate parenchyma "arc" as seen in radial longitudinal section were measured in each case using a travelling Vernier microscope.

2.7. RESULTS AND DISCUSSION

2.7.1. *Ventilating pressures in partially submerged rhizomes*

By fitting the appropriate data into equation (2.02) it becomes apparent that the surface-tension effects at the end of the channels form a major resistance to gas flow in a shallowly submerged capillary system. In Fig. 2.03 it should be noted that the broken line, the theoretical relationship for gas flow from submerged glass capillaries, corresponds closely with the regression line for the *Phragmites* data points. Also, the slope of the line correctly corresponds with the surface tension for water: 0.07 N m^{-1}. This serves to confirm the original premise that ventilating pressures, as described above and by Arikado (1959), will not necessarily reflect the resistance to gas transport within the plant. Instead, they are very much a function of the gas space dimensions at the submerged cut end of the organ.

2.7.2. P*ressurized flow in "non-submerged" rhizome*

The removal of an internode of non-submerged rhizome increased the flow rates by only small amounts (0.5-2.5 x 10^{-6} m^3 min^{-1}; Fig. 2.04), whereas the removal of relatively small lengths of nodal tissue increased the rates considerably (10-110 x 10^{-6} m^3 min^{-1}). The effects were more obvious the shorter the length of the rhizome. The conclusion must be that nodal regions offer much more resistance to pressurized gas-flow than internodes, and since the pith cavity and aerenchyma channels are interrupted at the nodes by transverse partitions (the diaphragms), it is clearly these which are responsible

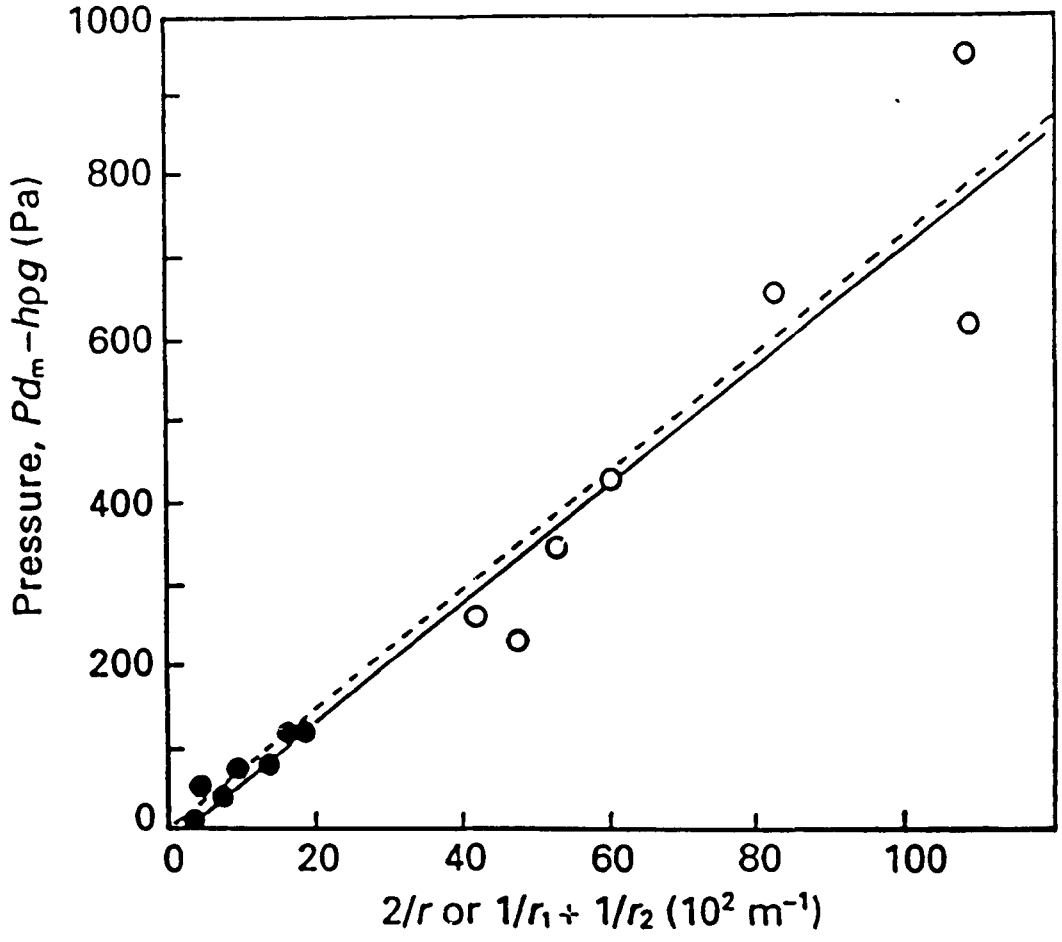

Fig. 2.03 Submerged internodes: the relationship between traditional 'ventilating-pressure' $pd_m - h\rho g$ (Pa) and the radius r (cm) of the submerged venting channels (see Theory). Pith cavities (●); aerenchyma channels (○); correlation coefficient for the linear regression (continous line), is 0·965; broken line shows the theoretical relationship for glass capillaries.

for the increased resistance. Anatomically (in both culm and rhizome) they comprise three zones, a basal layer of large stellate parenchyma, a middle zone of small stellate parenchyma and an apical layer of over-arching, anastomosing vascular tissue (Sections 3.3.2 & 3.3.3 & Armstrong & Armstrong, 1988). The relationship between gas flow rate and applied pressure for pieces of the same rhizome containing differing numbers of nodes is shown in Fig. 2.05. For each piece of rhizome there was a direct linear relationship between flow rate and pressure.

A comparison of Figs. 2.05, 2.06 & 2.07 shows that the relationship between gas-flow at fixed pressure and resistance (indicated by the number of nodes) is similar to the relationship between current and electrical resistance in a simple circuit; there is some departure from an ideal curve, however, because of the tapering nature of the rhizome. When a range of single rhizome nodes was used [pith cavity diameter 3.7-15 mm; method (c)], the values of nodal diaphragm resistance lay between 6 and 200 MPa s m^{-3} (Fig. 2.08). Factors other than pith diameter contributing to this variation must include the degree of doming of the diaphragm, usually greater in the narrower rhizomes (and which increases pore numbers), morphological and anatomical variation associated with bud initiation, the thickness of the small stellate parenchyma layer, and the pore size within that layer. All but the first will also have contributed to the variation in the resistance per unit area of these diaphragms the mean of which was 3 kPa s m^{-1} (SD±1, n = 22).

Estimates of the smallest pore space diameters in the various nodal diaphragms were made by substituting appropriate data into equation (2.06). The resultant mean: 5 ± 1 μm (n = 22), agrees well with the pore sizes found in the small stellate parenchyma layer by

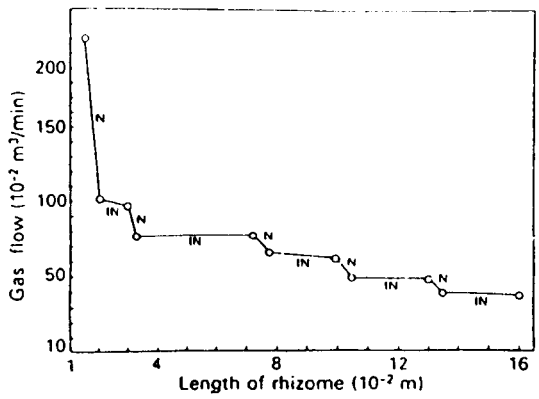

Fig. 2.04 'Non-submerged' horizontal rhizome: the effect on pressurized gas flow at 375 Pa of a progressive shortening of the rhizome by alternately removing lengths of internode (IN), and standard lengths of nodal tissue (N).

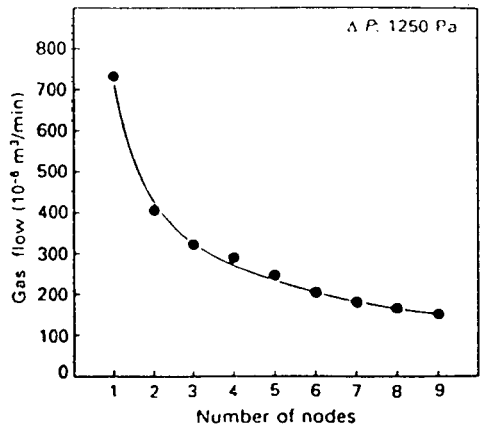

Fig. 2.06 Non-submerged' horizontal rhizomes: showing the effect of nodal numbers on gas-flow rates at 1250 Pa (data transposed from Fig. 3).

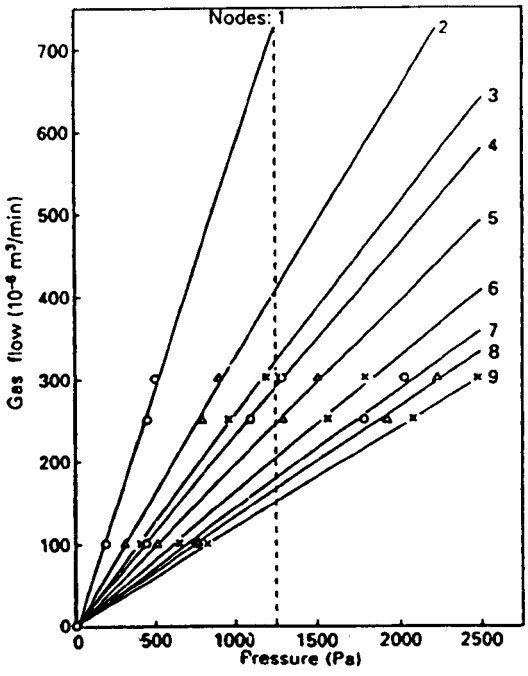

Fig. 2.05 'Non-submerged' horizontal rhizome: the relationships between gas flow and applied pressure with different numbers of nodes (1–9). Broken line highlights the flow rates at 1250 Pa (see also Fig. 4).

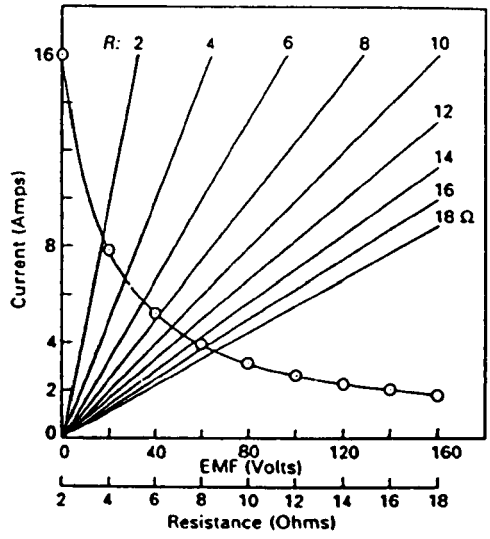

Fig 2.07 The relationship between current, voltage and resistance in a simple electrical circuit. Curved line shows the effect of increased resistance (lower x axis, equivalent to increased numbers of nodes) on current; data transposed from the currents at 32 V.

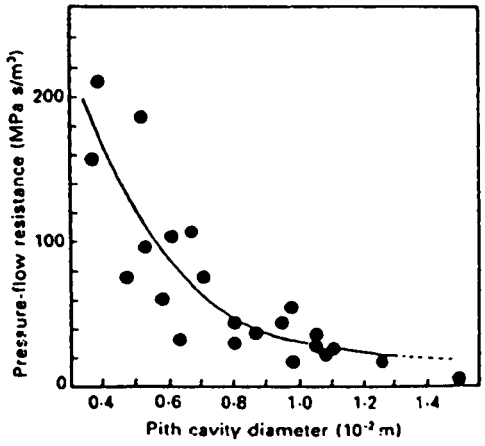

Fig. 2.08 Horizontal rhizome diaphragms: the relationship between pressure-flow resistance of individual pith-cavity diaphragms and pith-cavity diameter.

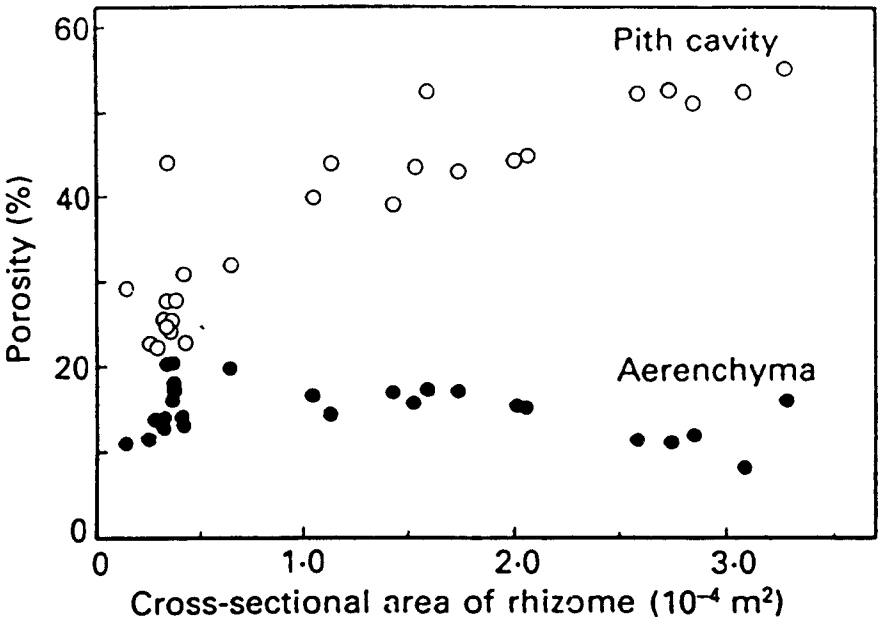

Fig. 2.09 Horizontal rhizomes: the per cent porosity due to the pith cavity (○) or cortical aerencyma channels (●) for rhizomes of various cross-sectional areas.

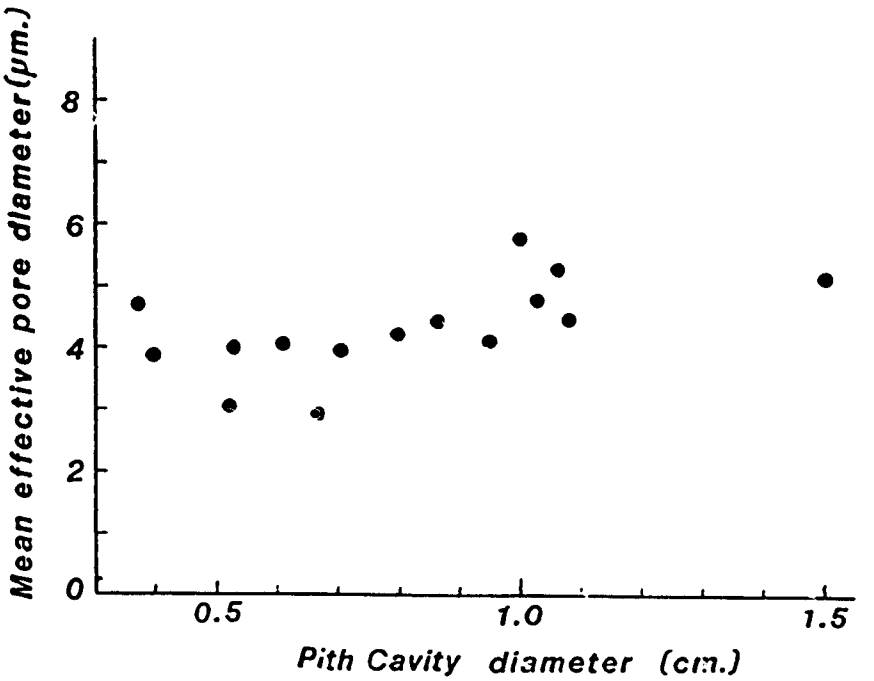

Fig. 2.10 *Phragmites: mean effective pore diameters in diaphragms estimated from pressure/flow data*

scanning electron microscopy (Section 3.3.3 & Armstrong & Armstrong, 1988). The pore size did not seem to vary with rhizome diameter (Fig. 2.10). Some of the variation in the estimates, however, could be related to the assumed porosity of the system, but variations in the thickness and the pore diameters in the large stellate parenchyma should have had little influence: applying equation (2.07) revealed that the pressure-flow resistance of the large stellate parenchyma, and of the anastomosing but porous vascular layer, will be insignificant in comparison with that of the small stellate parenchyma layer. Internodal pith cavity pressure-flow resistance was minute also, in comparison with the small stellate parenchyma layer namely 0.0015–0.39 MPa s m^{-3} for path lengths of 100 mm, and it must be must concluded, therefore, that it is the small stellate parenchyma layers of diaphragm material which offer the greater resistance to pressurized gas flow within the *Phragmites* rhizome system. This contrasts with the diffusive resistance of these layers where total cross sectional area of gas space is the main consideration, and where the large stellate parenchyma layer, because of its greater thickness, will offer the greater resistance (see below).

Pressure-flow studies on lengths of dead culms each of fairly uniform diameter produced similar graphs to Figs. 2.05, 2.06 & 2.08. For dead culms, pressure-flow resistances for individual nodes of diameters 2–5 mm ranged from 108–28 MPa s m^{-3}. These values are less than for living rhizomes (Fig. 2.08), and this is probably due to a combination of doming in the culm diaphragm and a higher porosity due to a drying-out of the tissues. It should be noted that there is a similarity in the porosity of the small stellate parenchymas in the nodal diaphragms of both fresh culm and rhizome (Sections 3.3.2 & 3.3.3). It seems likely, however, that culm nodal diaphragms, being more steeply

domed, will offer less resistance than those of rhizomes of similar diameter.

Pressure-flow resistance due to aerenchyma diaphragms ranged from 540-1600 MPa s m^{-3} per node, but it was not possible to deduce resistance per unit area because of the difficulty in determining diaphragm surface areas. From their anatomical appearance, however, the diaphragm tissues could be expected to exhibit approximately the same specific resistance as the pith diaphragms.

2.7.3. *Diffusive resistances*

The pressure: flow measurements support the conclusions arrived at earlier from scanning electron microscope examination of diaphragm material prepared by critical-point drying (Armstrong & Armstrong, 1988), namely that the smallest pores in the nodal diaphragms are located in the small stellate parenchyma layer and are of the order of 3-7μm diameter. As such, they are more than an order of magnitude greater than the mean free-path length of diffusing gas molecules such as oxygen, and consequently, diffusion will depend only upon concentration gradients and on the frequency and types of intermolecular collisions (Leuning, 1983). Axial diffusive resistance at the nodes will therefore be mainly a function of path length and porosity and will be readiiy calculable for each of the diaphragm layers by appropriate use of equation (2.08). Although pore sizes are relatively small, the porosities of each of the diaphragm layers is relatively high ($\geq$ 50%) and hence, the diffusive resistance of the diaphragms must be relatively low. For the pith cavity diaphragms the predicted values range from 1-13 Ms (Mega seconds) m^{-3} (in accordance with diaphragm thickness and surface area). No attempt has been made to deduce the diffusive resistance of the aerenchyma

partitions since their morphology is difficult to ascertain with accuracy, and within any node a proportion of the channels and their partitions are greatly modified by the presence of lateral buds and adventitious root initials. However, it seems likely that specific resistance of partitions in unmodified channels will be similar to that of nodal diaphragm material. Rhizome porosity as a whole varied with rhizome diameter largely as a result of pith cavity size (Fig. 2.09), and axial diffusive resistance of internodal pith cavity and aerenchyma channels are easily deduced using equation (2.08). For path lengths of 100 mm, the pith cavity axial diffusive resistance was much higher than diaphragm resistance ranging from 28 - 1100 Ms m^{-3} (pith cavity diameters 2.4 - 15 mm), and for aerenchyma channels the figures were 160 - 2850 Ms m^{-3}. It should be noted that the aerenchyma channels and pith cavity are resistances in parallel and that their combined resistance is less than the smaller of the two. This combined effective resistance can also be computed from equation (2.08) where ϵ is the fractional porosity of the rhizome internode and r, the rhizome radius; values ranged from c. 26 - 796 Ms m^{-3}. A direct numerical comparison of nodal and internodal diffusive resistances suggests that the diaphragm resistance may be almost small enough to be ignored at times in assessing or modelling the overall diffusive resistance and aeration of the rhizome system. In practice, however, this may not really be so since oxygen concentration gradients depend not only upon the physical aspects of diffusive resistance but on the amount and distribution of the oxygen demand (Armstrong, 1979). Since respiratory consumption per unit volume at the nodes is very much higher than at the internodes (Chapter 8), the concentration deficits across nodal tissues may be greater than anticipated. In the most general terms, however, it is clear that axial diffusive resistance in the

Phragmites rhizome is very low and in keeping with the need for effective long-distance gas transport in wetland conditions.

2.8. FINAL COMMENTS

During the experiments on pressure flow through single nodes of non-submerged rhizomes, a much greater than normal resistance was sometimes found due to a type of callus (tylosoid-like growths) within and emanating from the small stellate parenchyma. Only data from nodes free from these "tylosoids" have been included in the present results: the structure and possible function of the callus is described in Section 3.3.5. Although the pressure *vs* flow studies served to confirm the pore-sizes in the small stellate parenchyma of the nodal diaphragms and so helped towards the calculation of diffusive resistance within the *Phragmites* rhizome, any direct relevance of pressure-flow resistance values to *Phragmites* aeration may not be immediately apparent. Later research showed, however, that convective flows of gases do indeed take place naturally within *Phragmites* rhizomes and culms (see Chapters 5 & 7).

Since the aeration of *Phragmites* involves both convection and diffusion, a knowledge of both pressure flow and diffusive resistance is essential for a full understanding of *Phragmites* aeration. Whichever mechanism dominates, however, the relatively low values of resistance demonstrated here highlight the adapted nature of *Phragmites* rhizomes and culms for long-distance gas transport. For a wide rhizome 1 m long (pith cavity radius, 7.5 mm) and with diaphragms at 100 mm intervals, a total pressure drop of 100 Pa will be sufficient to drive a convective gas-flow of 1.67×10^{-6} m^3 s^{-1} (100 cm^3 min^{-1}) through the rhizome; for a much narrower rhizome (pith cavity radius, 1.85 mm),

the rate would be 4.33 x 10^{-8} m^3 s^{-1} (2.6 cm^3 min^{-1}). Also, because of the high porosity (30-70 %) and low respiratory demand (<10 mg m^{-3} s^{-1} at 20°C, see Chapter 8), it is theoretically possible for diffusion to support fully the aeration in rhizomes up to 1 m in length. It should be noted, that if culm resistance is taken into account, the figure could be significantly reduced.

SUMMARY

The concept of plant "ventilating pressures" is considered by comparing the pressures required to cause various rates of gas-flow through rhizomes of *Phragmites australis* venting either beneath water or into air. The resistances to pressurized flow in nodal and internodal regions are quantified, and the pressure: flow data analysed mathematically to deduce effective pore-space diameter in the nodal diaphragms, and the diffusive resistances of the diaphragms and internodes.

The value traditionally termed "ventilating-pressure", the minimum pressure required to cause a venting of gas into water, is shown to be a function of surface tension effects at the venting surfaces and not a measure of gas-flow resistance within the plant.

With venting to air rather than water, gas-flows occurred at all applied pressures greater than atmospheric, and pressure-flow resistance within the plant was determined from the gas-flow: pressure relationship. Pressure-flow resistance was much greater in the nodal pith diaphragms (6 - 210 MPa s m^{-3}) than in internodal pith cavities (0.0015 - 0.40 MPa s m^{-3}; path length, 100 mm) and was chiefly a function of pore-size, pore numbers and path length within the small stellate parenchyma layers of the diaphragms. The domed nature of

diaphragms reduces resistance by increasing the pore numbers. The effective pore diameters within the small stellate parenchyma of the diaphragms were estimated from the pressure : flow data using a modification of the Poiseuille equation. The values obtained ranged from ca. 3 - 7 μm, and corresponded closely with diameters found previously by scanning electron microscopy.

It is concluded that both large and small stellate parenchyma must contribute significantly to the diffusive resistance of the diaphragms in accordance with path lengths and porosity, and that, in contrast with pressure-flow resistance, the internodes, because of their length, should have the greater impedance. Estimated values for the pith diaphragm diffusive resistance were 1 - 13 Ms m^{-3} (path length, 1.7 - 3 mm), whilst pith cavity resistances, (path length 100 mm), were 28 - 1100 Ms m^{-3}. In the latter, the variation was attributable chiefly to the widely varying rhizome diameters: porosities of wide rhizomes were greater than those of narrower ones because of large pith cavities (Fig. 2.09). The fractional porosity due to cortical aerenchyma channels (10-20%) was not related to rhizome thickness.

It is concluded that gas-flow resistances in *Phragmites* are sufficiently small to allow for substantial long-distance transport by convection or diffusion.

CHAPTER 3

AN ANATOMICAL STUDY OF THE GAS-SPACE SYSTEM

3.1 INTRODUCTION

The presence of extensive gas-spaces within both the aerial and submerged parts is a feature common to emergent aquatic macrophytes (Arber, 1920; Sculthorpe, 1967). It is generally acknowledged that these spaces provide a low resistance pathway for atmospheric and photosynthetic oxygen to pass into the submerged organs (Armstrong, 1979). There is, however, comparatively little published information describing the anatomy of *Phragmites per se*, apart from the work of Rudescu, Niculscu & Chiru (1965). Their extensive monograph describes both morphological and anatomical aspects of the plant, including some detail of the pith, and cortical aerenchymatous gas-space systems of the culm, rhizome and adventitious roots. However, no clear details are presented of gas-spaces within the transition zones between leaf-sheath and culm, culm and rhizome, rhizome and adventitious root, adventitious root and lateral, and between aerenchymatous channels and pith cavities in rhizomes and culms. Such information is necessary in order to obtain a clear picture of gas-space continuity within the plant, and the possible barriers to gas-transport from one plant organ to another. It was felt that this latter information could be important in assessing the suitability of *Phragmites* and any other plant for use in the "root-zone method" of sewage treatment; an ideal plant would act as a "low resistance gas-space connector", enabling the rapid transportation of oxygen between the atmosphere and the rooting zone. Pressure-flow studies in Chapter 2 suggested that *Phragmites* might

well meet these criteria.

As the project progressed it became apparent that gas-transport in *Phragmites* was not solely dependent upon diffusion, but that two types of pressurized gaseous throughflow, namely *humidity-induced convection* (Chapter 5) and *Venturi-induced convection* (Chapter 7), were inportant in rhizome and root aeration. The anatomical studies helped to explain why these *throughflow convections* were possible. Additional anatomical studies on stomata were undertaken in order to investigate the nature of the porous membrane within the plant which could be effective in supporting *humidity-induced convection.*

3.3. MATERIALS AND METHODS

3.2.1. *Plant material*

Horizontal and vertical rhizomes of *Phragmites* collected from the banks of the Humber estuary during October and November were either used immediately, or with the cut ends emergent, placed in stagnant 20% Hoagland's solution at 15°C, a PAR of 100 µmol m^{-2} s^{-1}, and an 18h daylength, to resume growth and root production.

3.2.2. *Anatomy*

3.2.2.1. *Light microscopy.*

(a) Using fresh material, transverse and longitudinal sections of rhizomes and culms, and transverse sections of the roots, leaf laminae and sheaths were cut by hand and stained with Sudan III to indicate suberisation or cuticularisation, or with phloroglucinol and concentrated hydrochloric acid to show lignification. Any lignification was confirmed using aniline sulphate. The sections were examined and photographed

using a Zeiss photomicroscope.

(b) For resin embedding, samples of culm nodes, leaf sheaths and laminae, and rhizomes and roots were first evacuated in a detergent solution (3 drops Triton in 800 ml of water), fixed in 3% $KMnO_4$ for 6 days, dehydrated in alcohol (16 h) and embedded in a mixture of Spurr's resin (pure resin for 5 days and then resin plus accelerator for 19 days). The samples were then transferred to an oven at 70°C for 3-4 days. Transverse sections (1 µm) were either left unstained or stained with toluidine-blue (1% w/v in 1% w/v borax solution) and examined and photographed by light microscopy.

3.2.2.2. *Scanning electron microscopy.*

Samples of culm nodes, leaf sheaths, rhizomes and roots were fixed in a mixture of 3% glutaraldehyde, 15% acrolein and 15% paraformaldehyde in phosphate buffer (pH 6.8), dehydrated in acetone and dried by the carbon dioxide critical-point drying technique, and coated in gold. The cut surfaces were examined by scanning electron microscopy.

To display stomatal surfaces it was necessary to immerse the leaf sheath sections in warm acetone in order to dissolve the surface waxes.

In order to examine stomatal structure, slivers of tissue were removed using a razor blade from surfaces of leaf sheath and culm nodes which had already been dehydrated and gold coated. The exposed surface was then recoated in gold and examined by SEM. A similar procedure was also adopted for examining radial and tangential intercellular spaces in adventitious roots.

3.3. RESULTS AND DISCUSSIONS

3.3.1. *Stomata*

"Zooming" in on leaf sheaths (Fig. 3.01) shows that the stomata lie in rows in grooves on the leaf sheath abaxial surface. The culm nodal stomata similarly lie in grooves. Wax is abundant on the surfaces of the epidermal cells adjoining the pore (Fig. 3.02, 3.03, 3.04 & 3.05). A comparison of Fig. 3.03 and 3.04 indicates that when viewing an entire stoma from the surface, the epidermal cells slightly overarch the slit, and the stomatal slit itself lies between and below ledges on the outer surface of each guard cell. These ledges part when the stoma is open (Figs. 3.02 & 3.04), and come together in the closed state (Fig. 3.03a). When stomata are viewed superficially the auxilliary cells are not visible ; this can be deduced from Fig. 3.04.

The stomatal structure appears to be typical of the monocot type, the guard cells being dumb-bell shaped, about 15 µm in length, with large adjoining auxilliary cells (Fig. 3.04, 3.05 & 3.06). The length of the superficial stomatal slit between the guard cells is 11 - 12 µm, and the depth of the whole pore, including the epidermal cells is *ca.* 12 µm. The sectional topography of the pore itself is related to the cells bounding it at the various levels: the pore is at its widest between the epidermal cells, 2 - 2.4µm across the middle of the stoma, while the distances between the guard cells depends upon the degree of stomatal opening, the range of values observed being 1 - 2.5 µm across the middle of the pore in the open condition (i.e. between the guard cell ledges). However, because of the sculpturing, the width of the narrowest part was difficult to ascertain, and it appears from Fig. 3.04 that the auxilliary cells subtend the guard cells and the distance

between the former may be the narrowest region of the stomatal pore. In Fig. 3.04 this distance is 0.14 - 0.2 µm. This narrow region may be the most important for the development of the ***humidity-induced convective throughflows*** described in later in Chapters 5 & 6. Because of the superficial waxes, and the sculptured nature of the pore itself, it was difficult to ascertain from initial scanning electron microscopy of leaf sheath surfaces how the pore width varies in light and darkness. However, plunging leaf sheaths, from plants exposed to either light or darkness for at least six hours, into liquid N_2, prior to fixation and dehydration when waxes were removed, led to the impression from SEM that the distance between guard cells is greater in the light than darkness, as would be expected. Also, Si-rubber impressions taken in the field and preliminary pressure flow studies on living excised culms suggested that stomata were more open in the light than in darkness. Nevertheless, it is still unclear as to how the narrowest region of the pore may or may not change in light or darkness.

3.3.2. *Leaf laminae, leaf sheaths and culm*

The leaf laminae have no aerenchyma channels, (Fig. 3.08a), and do not appear to be important in the throughflow aeration of the plant (Sections 5.3.1.2 & 5.3.1.3), but rather primarily for photosynthesis. On the other hand, the leaf sheaths contain prominent, longitudinal aerenchyma channels (Fig. 3.08b).

The leaf sheath stomata are subtended by chlorenchyma (Figs. 3.08b & 3.09), in which are small intercellular spaces of diameters 1.1 - 2.9 µm, (Fig. 3.10). Beneath the chlorenchyma are the leaf sheath aerenchyma channels which lead to "pockets" of aerenchyma within the nodal regions of the culm. These latter connect, via radially-running intercellular spaces in the culm cortex, with the culm pith cavity. In

these nodal regions are also stomata on the culm surface which connect via intercellular spaces in the subtending chlorenchyma with the aforementioned 'pockets' of aerenchyma (Fig. 3.08c). The intercellular spaces immediately subtending the culm stomata are larger than those beneath the leaf sheath stomata. Culm stomata can generate slow humidity-induced convections in senescing shoots, when the leaf sheaths have died (Section 5.3.1.4.), but they probably contribute only slightly during the growing season. The lowermost culm stomata are important for aerating the underground parts by diffusion when convections are not occurring (Brix 1989).

It should be noted that stomata and aerenchyma channels are normally absent from the culm internodal regions, but where culms have emerged from sediment into water (e.g. beneath lake surfaces) aerenchyma channels continuous with those of the vertical rhizome are found. The channels terminate where the culm emerges into the air. The surface of the aerial stem is covered in a cuticle, and there is suberisation of the sub-epidermal layers ; it appears (Section 4.3.1.) that oxygen mainly enters a culm pith cavity directly via nodal stomata, or indirectly *via* the leaf sheath stomata and aerenchyma.

The culm pith cavity is interrupted at each node by a dome-shaped diaphragm (Fig. 3.11), which has three distinct regions: an upper part composed of vascular tissue, a narrow middle band of small, unlignified stellate parenchyma, below which is a thick layer of highly porous, lignified, large stellate parenchyma. Although light microscopy showed the small stellate parenchyma as a rather dense layer, the SEM indicated its highly porous nature (pore diameters of approx. 3 - 7 µm; porosity = >50%)(Figs.3.11 and 3.12). Across such a diaphragm there are clearly intercellular gas-spaces connecting the pith cavities above and below it. Nodal diaphragms offer little resistance to Poiseuille or

diffusive gaseous flow (Sections 2.3, 2.7.2, 2.7.3 & 2.8). Nodal diaphragms of similar structure are also present in vertical and horizontal rhizomes (Section 3.3.3). Neither side of a diaphragm is easily wetted and this feature may temporarily prevent the flooding of a damaged culm or rhizome (also Goebel 1905).

As a culm ages its tissues become increasingly lignified and it tends to persist for two to three years, after which they may be snapped at various levels by the wind (Haslam, 1969). Old culms maintain gaseous connection with the rhizome for several years. This is important in both *humidity-* and *Venturi-induced* convections (Chapters 5 and 7 respectively), as well as for the diffusive aeration of the rhizome. During senescence of the leaf sheaths the basal ends of the aerenchyma channels become sealed by a callus-like (tylosoidal) growth of parenchyma cells (Fig. 3.19c, and Section 3.3.5).

3.3.3. *Rhizome*

Rhizomes are of two kinds which are anatomically very similar: horizontally-growing rhizomes colonise the soil, while vertical rhizomes, produced either from upwardly-growing tips or lateral buds of horizontal rhizomes, give rise to the aerial shoots when they emerge into the air (Haslam 1969). The rhizomes bear scale-leaves at their apices which are generally not persistent in mature parts; these are not differentiated into laminae and sheaths but are aerenchymatous throughout. These aerenchyma channels eventually become sealed at the scale-leaf : rhizome junction by callus (tylosoids).

Rhizomes are covered in a thick waxy cuticle (Fig. 3.13, and Section 4.3.1) which together with suberisation and lignification of the sub-epidermal layers (Fig. 3.21a) appear to prevent the passage of oxygen (Section 4.3.1). There are no stomata on either the nodal or

internodal surfaces of the rhizome.

The pith cavity of the horizontal rhizome (Figs. 3.14 & 3.15) is a major component of the gas-space system and it connects directly with similar cavities in the vertical rhizome and culm. Nodal diaphragms (Fig. 3.15) are similar in structure to those of the culm, but flatter in shape ; the large stellate parenchyma (Fig. 3.16) is highly lignified (Fig. 3.17). The pressure-flow and diffusive resistances of the diaphragms are low (Sections 2.7.2 & 2.7.3), the greatest resistance being in the small stellate parenchyma which has similar pore size (3 - 7 μm diameter) and porosity (>50%) to the culm.

Unlike the culm, discrete aerenchyma channels run longitudinally through the inner cortex of the internodes in the horizontal rhizome (Fig. 3.14a), and in all but the shortest internodes of the vertical rhizome where sometimes they lose their separate identities. They normally cease where the vertical rhizome emerges to become the culm. At the rhizome nodes the aerenchyma channels are interrupted by porous stellate-parenchyma porous partitions. Also at the nodes are radial channels within the stele (similar to those in the culm) which form gas-space connections between the aerenchyma channels of the cortex and the pith cavity (Fig. 3.14b). They cross the stelar cylinder just above the insertion of the pith diaphragms (Fig. 3.14a), and connect via stellate parenchyma partitions with the cortical aerenchyma channels of the "lower" internode and the cortical aerenchyma of the "upper" internode which, at this point, always exists for a short distance as a continuous cylinder rather than discrete channels (Figs. 3.21 & 3.24). It should be noted that the aerenchyma channels *per se* form a blind-ending longitudinal pathway within an intact rhizome system. However, at the nodes, they connect with the pith cavity *via* the radial channels, and also connect with each other where they

merge to form a "nodal ring". The latter may serve to facilitate circumferential gas-transport in the region of developing adventitious root primordia and buds.

It should be noted that there can be no significant radial oxygen transport between the pith cavity and the aerenchyma channels in the internodal regions (Section 4.3.1). Thus, transport between pith and cortex only appears to be possible in the nodal regions via the radial channels.

An intercellular gas-space system is visible at the tips of horizontal and vertical rhizomes (Fig. 3.18) prior to aerenchyma and pith cavity differentiation. Presumably oxygen diffuses into these spaces from the rhizome pith and aerenchyma to supply the growing tip.

Callus (tylosoid) development occurs in diaphragms adjacent to wounded and\or rotting regions of a rhizome, (Figs. 3.19a,b and 3.20); the significance of this is discussed in Section 3.3.6.

3.3.4. *Roots*

Adventitious roots are produced from rhizome nodal primordia. It is interesting to note the relative lack of suberisation and lignification in the rhizome sub-epidermal layers immediately external to a root primordium, (Fig. 3.21a). Perhaps this facilitates the emergence of the young root from the rhizome. Even within the root primordium gas-space connections can be detected, via stellate parenchyma, between the developing lysigenous root aerenchyma and the rhizome aerenchyma, (Fig. 3.21a). This helps to account for dye oxidation observed around roots which have newly emerged from the rhizome, (Section 4.3.1).

SEM's of the rhizome-"mature root" junctions, (Fig. 3.24a), also

show a narrow zone of stellate parenchyma linking the rhizome aerenchyma with that of the adventitious root. The zone is ca. 200 µm in L.S. and the stellate parenchyma-type cells 14 - 20 µm diameter with intercellular spaces of 8 - 17 µm diameter (Fig. 3.24b). Although this tissue will offer the greatest resistance to diffusion, within the aerenchyma at the rhizome-root junction, nevertheless, its unusually porous nature: 30%, compared to other species examined, (Gaynard & Armstrong 1987; Justin & Armstrong, 1983), ensures that this resistance is relatively small. The applied pressure-flow experiments (Section 2.3) also indicated the gas-space continuity between the rhizome and adventitious roots.

Adventitious roots can be long, >1m. Their anatomical features are mostly typical of wetland grasses, and they develop lysigenous cortical aerenchyma 10 - 20 mm behind the apex (Fig.3.21b). In the apical non-aerenchymatous region, longitudinally-running, quadrangular intercellular gas-spaces are present, like those in Fig 3.21b. In tangential section, small, radially-running intercellular spaces are visible, which are oval in cross-section: 6-8 µm x 3-4 µm (Figs. 3.22 and 3.23), and it is likely too, that circumferential intercellular spaces, triangular in cross-section (side : 4 - 5 µm), like those found between the persisting cells of the maturing cortex, are also present (Fig. 3.28). In adventitious roots in regions very close to the apex, (apical 0.5 cm), no suberisation or lignification of the hypodermal and sub-epidermal layers are detected, and this helps to account for these regions showing ROL (Sections 4.3.1 & 4.3.2). However, as differentiation proceeds, these layers develop increasingly thickened, suberised and lignified cell walls, (Figs. 3.21b and 3.26a), and become impermeable to oxygen (section 4.3.1). This latter process is concomitant with aerenchyma development and prevents ROL from the highly porous,

mature regions of the root; hence the oxygen is available for longitudinal transport down the root. Suberisation and possibly lignification of these outer layers may also prevent the uptake of phytotoxins from a waterlogged soil. It is noteworthy that hypodermal regions opposite lateral root primordia lack cell wall suberisation and lignification, (Fig. 3.21b). It would be interesting to discover if these "windows" and those in the rhizome form due to a loss of cell wall materials, i.e secondarily to root development, or whether the thickening just fails to develop opposite the primordia.

As differentiation proceeds, the aerenchyma becomes prominent, (Figs. 3.25a, 3.26a & 3.27a), but triquetral non-aerenchymatous intercellular spaces, (sides = 4 - 5 µm), run circumferentially between the persistent cortical cells (Figs. 3.27 & 3.28). These cells form intact radial longitudinal" ribbons" between the aerenchyma spaces (Figs. 3.27b & 3.29a). In the root's most basal regions, most of the cortex may be composed of gas-space traversed by the fine laterals, but the cortical cells persist around those parts of the laterals embedded in the cortex, (Figs. 3.25a, 3.29a & 3.30 *below*).

It should be noted that the persisting cortical cells in the basal root aerenchyma have been shown to be metabolically active since they develop chlorophyll when the root is exposed to light (Fig. 3.32), as also do cells of the lateral root cortex (Figs.3.33).

In the stele, intercellular spaces are present only in the pith. The endodermis in the mature parts of adventitious roots is strongly lignified and suberised (Fig. 3.26) probably forming a very significant resistance to the radial diffusive inflow of oxygen. However there may be a small amount of longitudinal transport from the shoot within the pith, but no attempt was made to confirm this.

Fine lateral roots (length *ca.* 10 - 15 mm; diameter 230 µm), can

develop in large numbers in the basal 30 - 60 mm of the adventitious roots of length >150 mm. In those roots examined their numbers varied from 90 - 120 per centimetre of adventitious root. Dye oxidation and polarographic oxygen measurements (Sections 4.3.1, 5.3.1.5 & 5.3.1.7), and mathematical modelling (Section 8.2.2), have indicated that they are an important means of oxygenating the rhizosphere. Aerenchyma does not form in these laterals (Figs. 3.25b, 3.30 *above*, 3.31 & 3.33a), and no hypodermal suberisation or lignification was found; this correlates with their apparently high permeability to ROL. Within the narrow cortex, which is only two to three cells thick, there is a scattering of small intercellular spaces (Fig. 3.25b), and an estimated porosity for these roots is *ca.* 1.4%. The cells of the cortex will form chlorophyll if the roots are exposed to light (Fig. 3.33).

Close to the junction between a lateral root and the stele of the parental adventitious root (Figs. 3.30 *below*, & 3.31) the intercellular spaces of the lateral appear to connect with the aerenchyma of the adventitious root via intercellular space of the intact parenchyma cells which ensheath the lateral. Further from the stele a more normal non-porous epidermis develops (Fig. 3.29 *above*, & 3.30 *above*). It is interesting that calculations of the maximum lengths that lateral roots could attain in waterlogged soils when supported by internal gas-transport from the adventitious root (Section 8.2.2), are very close to observed lengths. However, such limited growth occurs whether in stagnant nutrient media or waterlogged soil, and this might be indicative of a genetical control mechanism to withstand fluctuating oxido-reduction regimes within the soil.

3.3.5. *Callus*

In the pressurised gas-flow experiments described in Chapter 2. it was

sometimes found that axial flow could not be effected. Anatomical investigation showed that this was due to outgrowths of cells blocking the gas-flow pathway at nodes where an adjacent internode showed signs of decay. The growths were of large tylosoid-like cells, probably callus, with thin lignified walls apparently produced by a renewal of growth of the small stellate parenchyma (Fig. 3.19b) and possibly the circumvascular parenchyma of the nodal diaphragms (Fig. 3.19a & 3.20). Cell-packing in these extraordinary structures is so close as to form an apparently impenetrable layer devoid of gas-space.

No record of similarly modified partitions in other plants could be found, but in *Phragmites* they had formed 1-2 days after wounding and submergence, and were inducible in *Equisetum* within a day (unpublished). In *Phragmites* they act as a barrier to gas-flow, to flooding and, probably, to the spread of rots in the rhizome. A similar process of "sealing" can occur at rhizome junctions with decaying roots, scale leaves and culms, and at the bases of leaf-sheath aerenchyma spaces when the leaf-sheaths die in the autumn (Section 3.3.2 & Fig. 3.19c). In the latter case, callus development may reduce the risk of desiccation which could otherwise occur via stomata of persistent leaf-sheaths. Callus can also form within aerenchyma partitions, but in all the cases examined this developed secondarily to pith callus formation. Rhizomes were often found with blocked pith diaphragms but open aerenchyma partitions.

It should be noted that the gas-space connections between a dead culm and the vertical rhizome remain callus-free for at least two to three years; this is important for rhizome aeration by humidity- and Venturi- induced convections (Chapters 5 and 7 respectively), and by diffusion.

3.4. FINAL COMMENTS

The system of interconnecting gas-spaces within the culm, rhizome and roots of *Phragmites* links the atmosphere with the extremities of the buried roots and rhizomes, and is summarized in Fig. 3.34. These pathways help to account for the results of dye oxidation experiments (Chapter 4), applied pressurised gas-flows through the plant (Chapter 2), and humidity- and Venturi-induced convections (Chapters 5 & 7 respectively).

In general, all tissues in which there is a paucity of gas-space will offer considerable resistance to gas transport (Armstrong, 1979). In the rhizomes and roots of *Phragmites,* however, where there had been a failure to oxidize the methylene-blue, there were invariably additional features such as waxy cuticles or suberised and/or heavily lignified cell walls. Suberin, in particular, is known to offer a high resistance to oxygen diffusion. The epidermis of horizontal and vertical rhizomes had thick lignified walls and the outer tangential wall had appreciable quantities of silicon and a waxy cuticle, 1 - 2 µm thick. Lignified and suberised fibres formed cylinders beneath the epidermis, beneath the inner tangential surface of the aerenchyma channels, and centrifugal to the lining of the pith cavity. Regions of the rhizome wall opposite adventitious root initials either lacked lignin or suberin or had developed much less than elsewhere: the presence of a waxy cuticle presumably accounts for the lack of oxygen efflux in these parts. The hypodermal layers in the older parts of the adventitious roots were lignified and suberised as were the endodermis and stelar parenchymas. Suberisation and lignification were not visible in younger regions or in the fine laterals. It was interesting to note that those

regions of the hypodermis opposite lateral root initials were not lignified or suberised (see also Justin & Armstrong, 1987). It is possible that oxygen may be lost from the root at these points.

Although many aspects of the *Phragmites* anatomy and morphology are typical of wetland plants (Justin & Armstrong, 1987), certain features may specially contribute to its success as a coloniser and competitor in waterlogged habitats. These include: (a) the lignification and persistence of the aerial shoot system for at least two to three years, which will provide a low resistance pathway for atmospheric oxygen to enter the rhizome system by diffusion and convection throughout the year; (b) the large proportion of gas-space within the rhizome system which probably enables the rhizome to colonise new ground rapidly and economically in terms of carbohydrate utilisation. Also, the gas-spaces help to ensure efficient rhizome and root aeration; (c) the unusually porous rhizome and root junctions comprised of stellate parenchyma which are a particularly advantageous ventilating feature; (d) the dense groups of fine basal non-suberised laterals which can be expected to produce coalescing oxidised rhizospheres (Section 4.3.1).

SUMMARY

The gas-space anatomy of *Phragmites* was investigated by scanning electron microscopy and light microscopy. It revealed an intricate system of interconnecting passages linking the atmosphere with aerenchyma and intercellular spaces in the culm, rhizome and roots. Notable features included: (a) the non-aerenchymatous nature of the leaf laminae as opposed to the highly aerenchymatous leaf sheath; (b) the localisation of nodal stomata on the culm, and details of stomatal

structure; (c) the presence of highly porous small stellate parenchyma within the culm and rhizome nodal diaphragms; (d) the existence of nodal radial channels crossing the steles of rhizome and culm and connecting the pith cavity with the cortical aerenchyma, and also the presence of stellate parenchyma within these channels; (e) the presence of unusually porous rhizome-root junctions with stellate parenchyma at the junction between the aerenchyma of the rhizome and that of the root; (f) suberisation/cuticularisation (accompanied by lignification) in those parts of the plant which appear to impermeable to ROL e.g. the outer layers of both the rhizome, and older parts of adventitious roots; (g) the existence of "windows" lacking suberisation and lignification in the outer layers of rhizomes and adventitious roots opposite developing root primordia; (h) the development of callus (tylosoids) in response to wounding and senescence which seal nodal diaphragms, leaf-sheath aerenchyma at the junction with the culm, and rhizome-root junction.

The anatomical study also helped to elucidate the pathways for *humidity-induced* convection (Chapter 5), *Venturi-induced* convection (Chapter 7) and diffusion which are the principal means of rhizome and root aeration.

Figure 3.01 (overleaf)

Fig. 3.01. Scanning electron photomicrograph series showing leaf sheath stomata at increasing magnification.

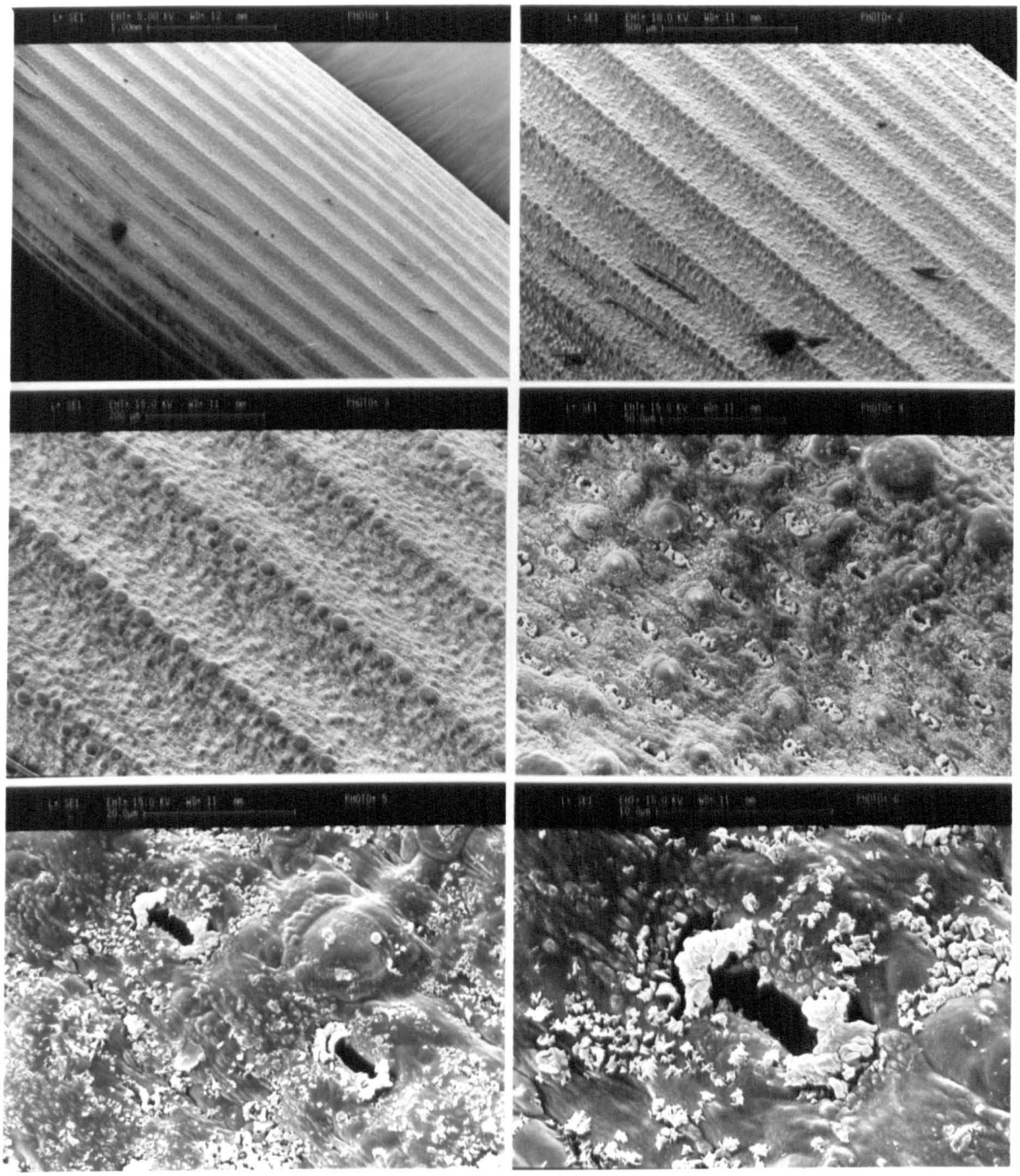

FIG. 3.01

Figure 3.02 (overleaf)

Fig. 3.02. Scanning electron photomicrographs of leaf-sheath stomata : e = epidermal cell; g = guard cell. Note: surface waxes of epidermal cells in (a) ; in (b) and (c) the waxes have been partially removed.

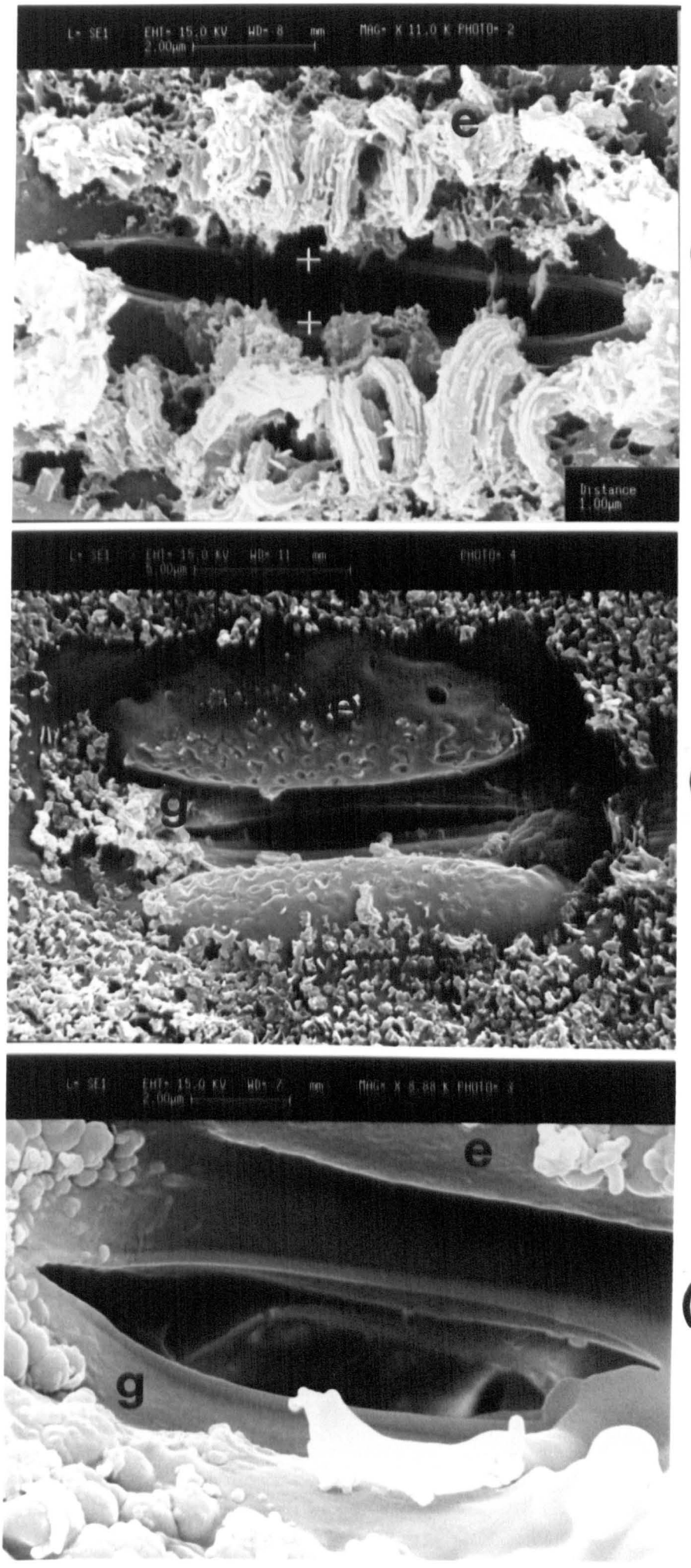
e
Distance
1.00μm
(a)
e
g
(b)
e
g
(c)

Figure 3.03 (overleaf)

Fig. 3.03. Scanning electron photomicrographs of leaf-sheath stomata : e = epidermal cell; g = guard cell. In (a) the stoma is in the "closed" condition, and in (b) it is partially open.

(a)

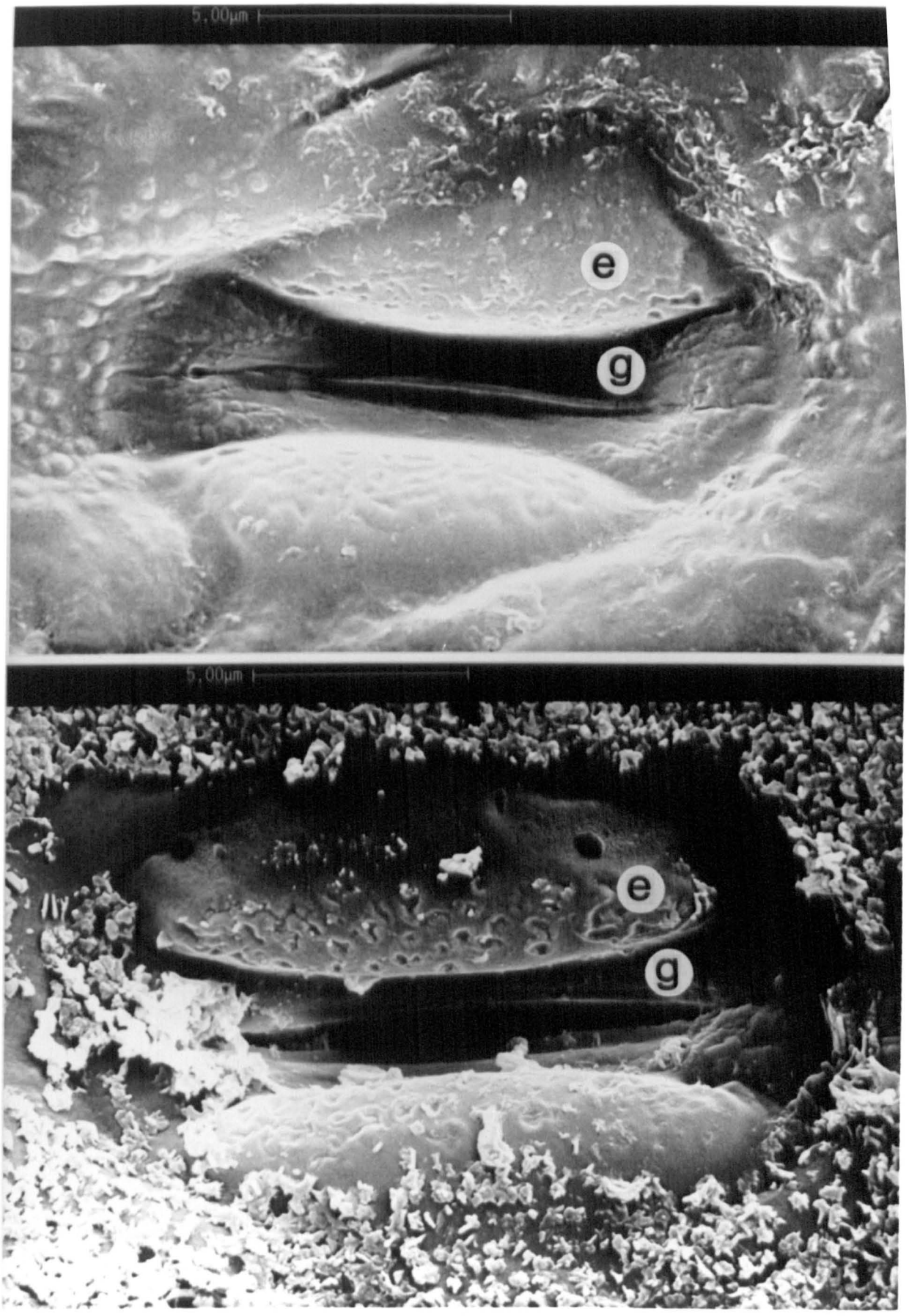

(b)

Fig. 3.04. Scanning electron photomicrographs of leaf-sheath stoma in transverse section in the mid-region of the guard cells: a = auxilliary cell; e = epidermal cell; g = guard cell. Note: epidermal cells with surface waxes, guard cells with protruding "ledges" (cf. Fig. 3.03b), and large auxilliary cells which appear to subtend the guard cells.

Fig. 3.05. Scanning electron photomicrographs of leaf-sheath stoma in transverse section at "dumbell" ends of guard cells: a = auxilliary cell; e = epidermal cell; g = guard cell.

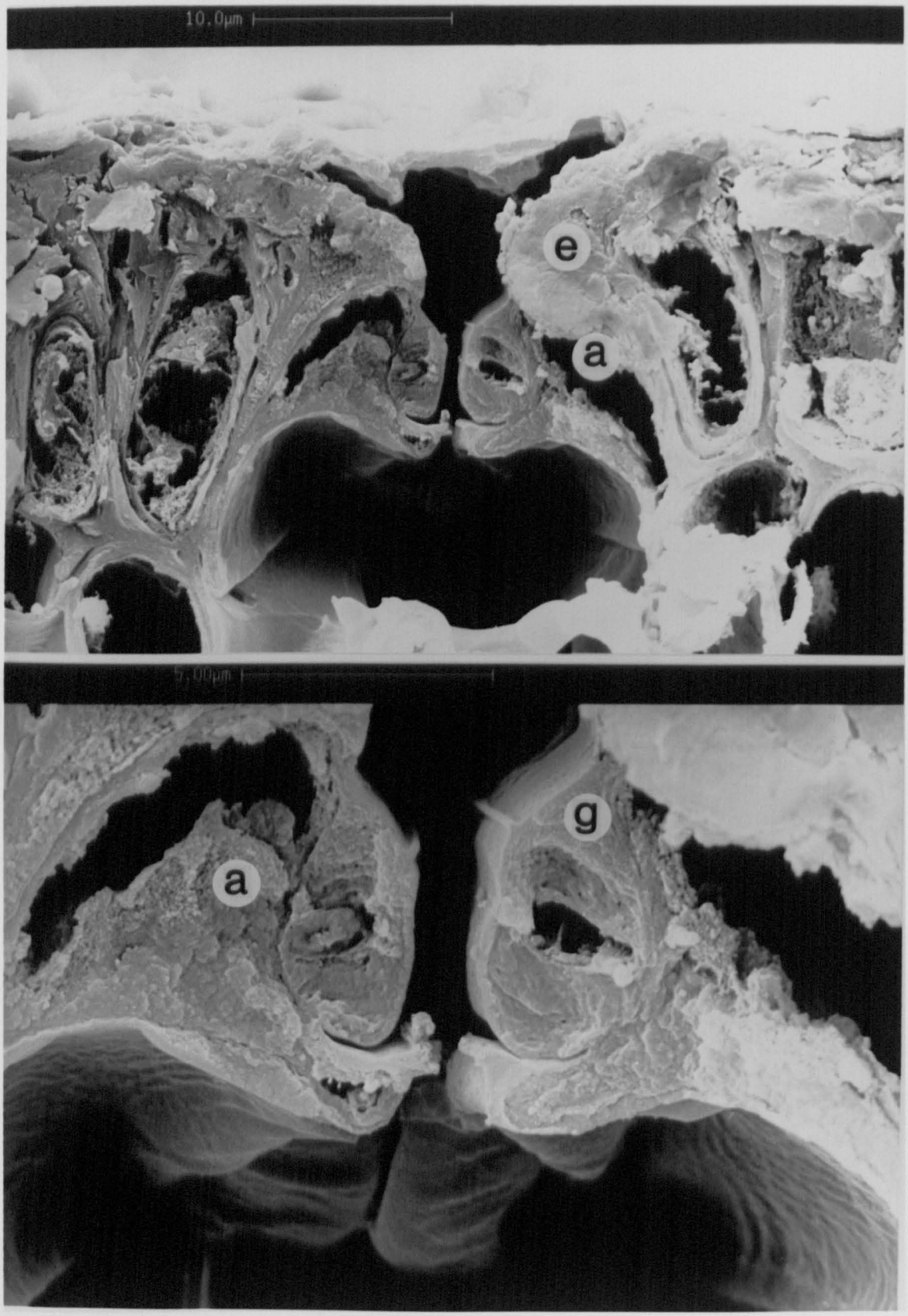

FIG. 3.04

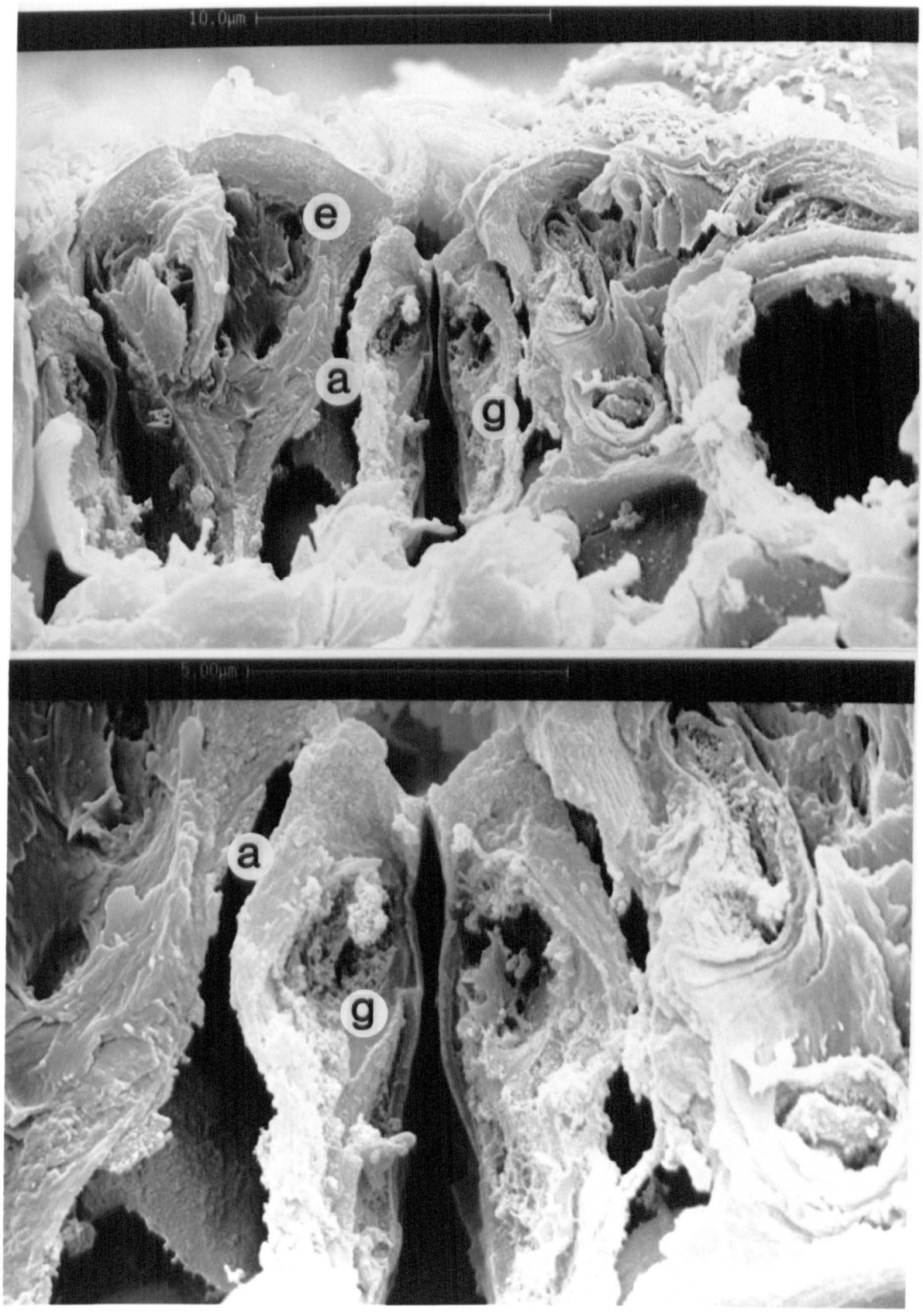

FIG. 3.05

Fig. 3.06. Scanning electron photomicrographs of leaf-sheath stoma in longitudinal section with *thin* superficial layer removed: a = auxilliary cell; g = guard cell. Note dumbell-shaped guard cells.

Fig. 3.07. Scanning electron photomicrographs of leaf-sheath stoma in longitudinal section with *thick* superficial layer removed: a = auxilliary cell; g = guard cell.

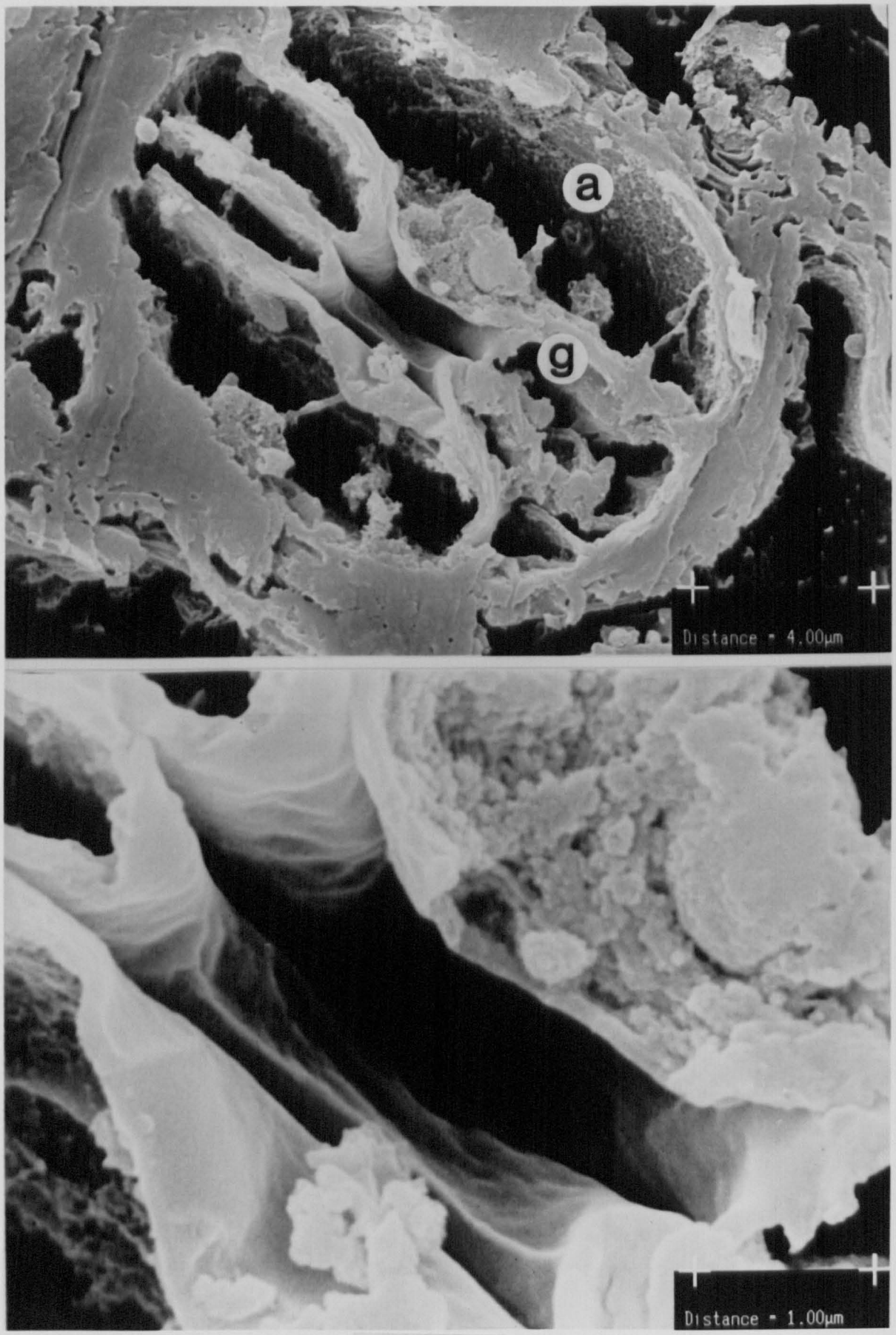

FIG. 3.06

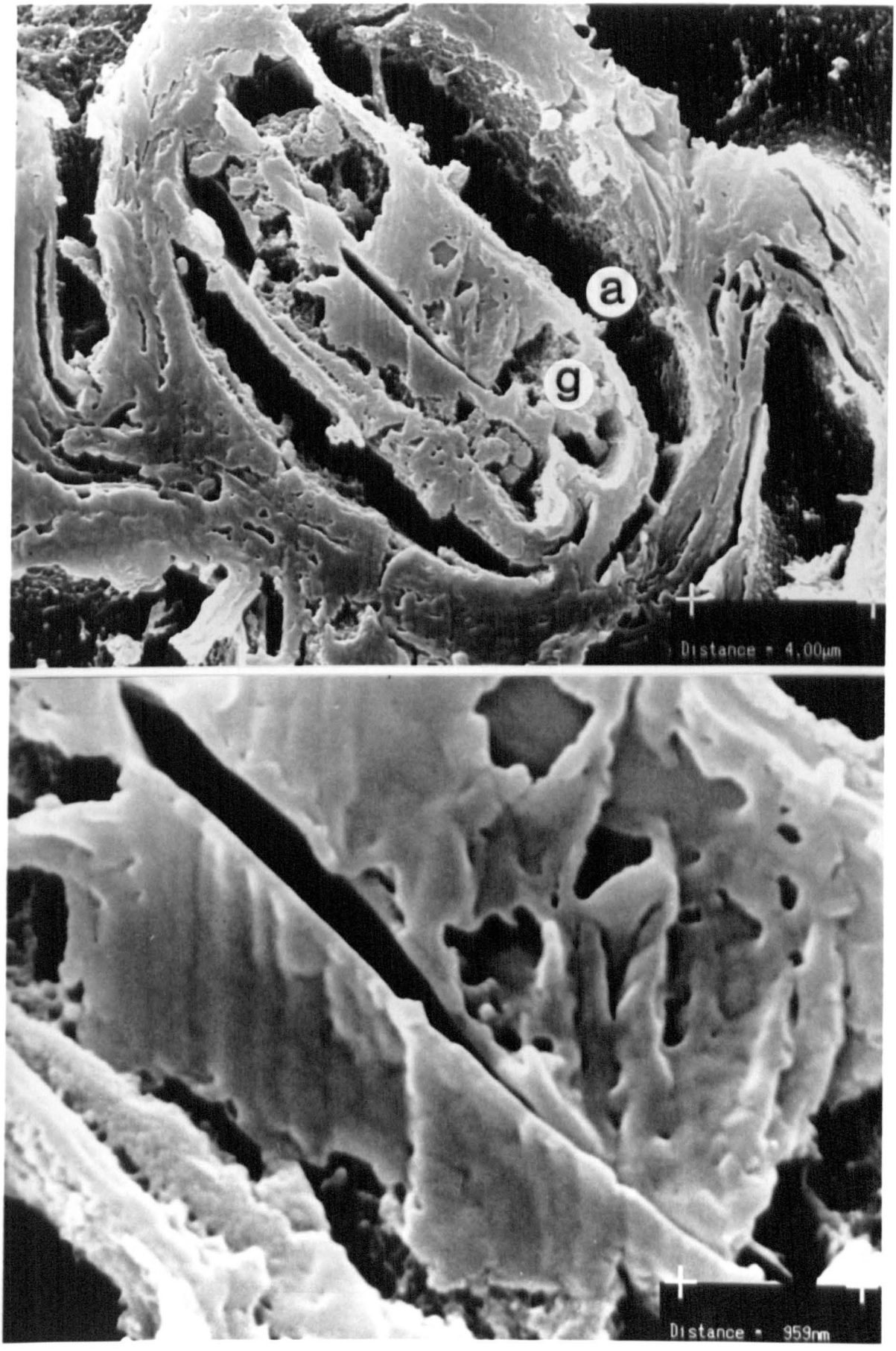

FIG. 3.07

Figure 3.08 (overleaf)

Fig. 3.08. (a) Transverse section of leaf lamina (x165) stained with safranine. Note the absence of aerenchyma channels.

(b) Transverse section of leaf sheath (x165). Note aerenchyma channels with abaxial chlorenchyma and stomata. Beneath is stem internode in T.S.

(c) Nodal region of aerial stem (x200) with radial channel, r, connecting cortical aerenchyma pockets, a, with pith cavity, p. Note sub-surface chlorenchyma and nodal stomata.

All material was resin embedded.

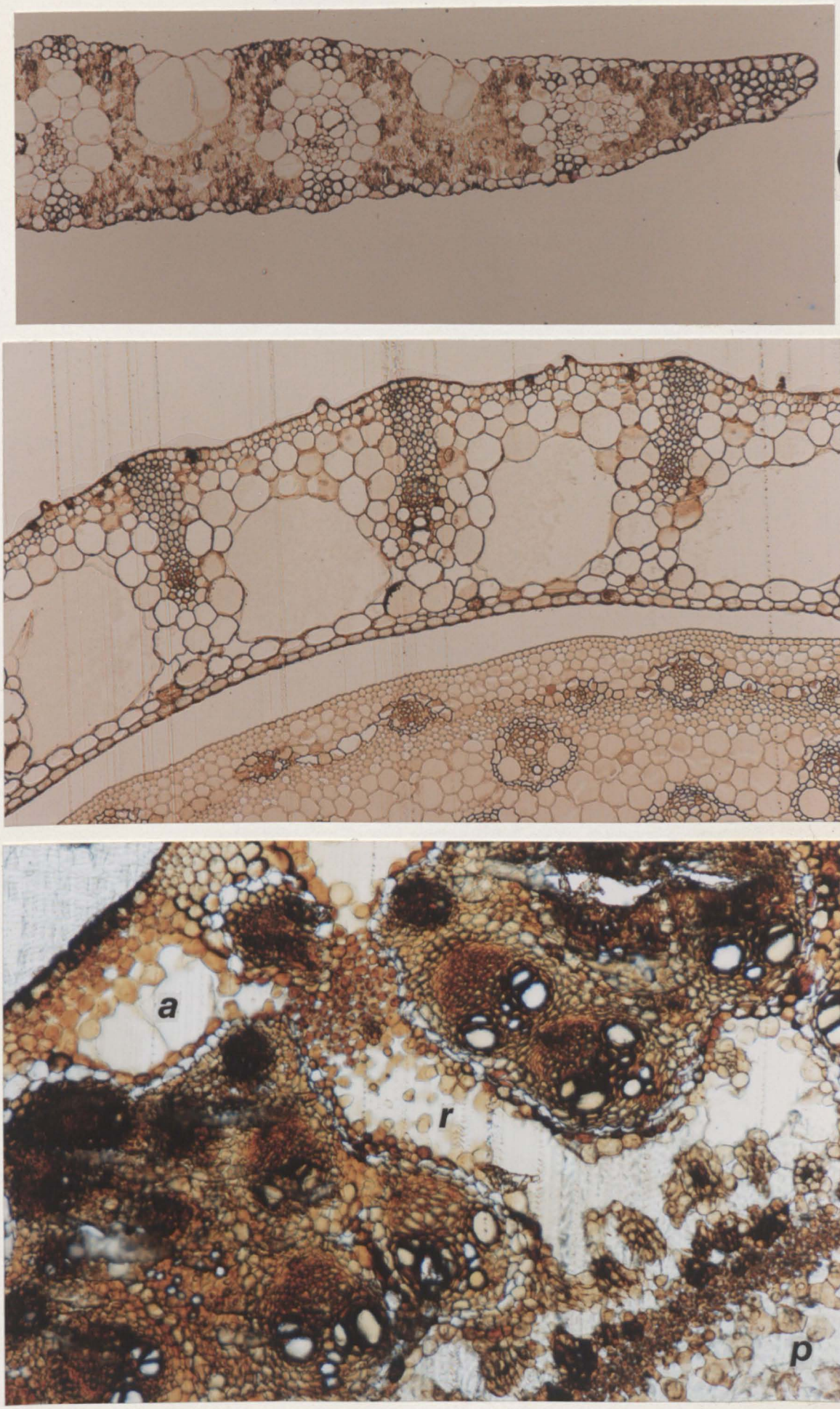

FIG. 3.08

Figure 3.09 (overleaf)

Fig. 3.09. Fresh, hand-cut, transverse section of leaf-sheath showing stomata. Note epidermal, subsidiary and guard cells and subtending chlorenchyma with intercellular spaces.

Above : stained with phloroglucinol & conc. HCl; (X720).

Below : stained with methylene blue; (X1500).

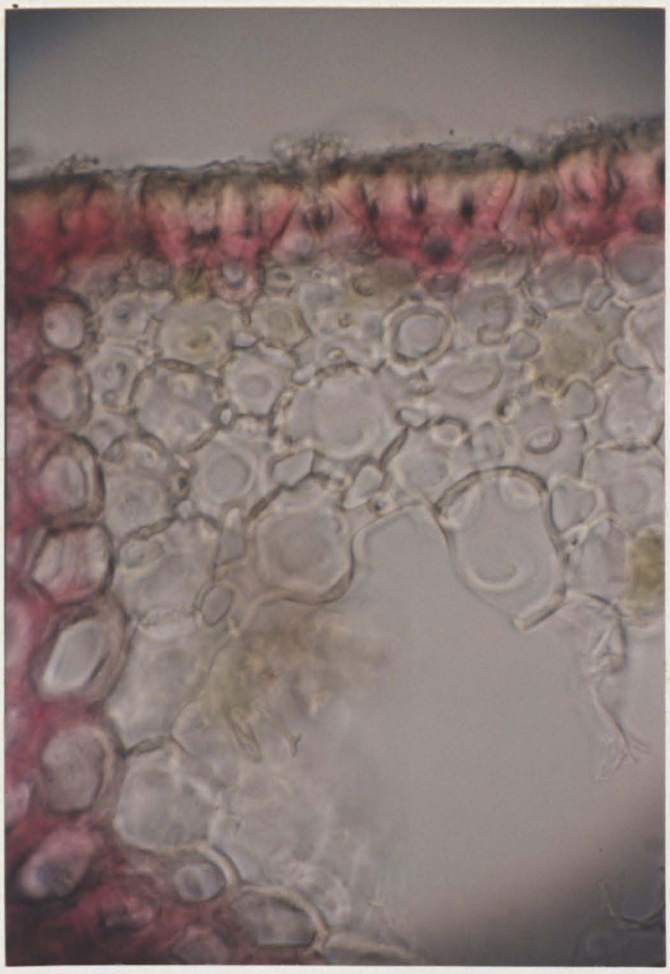

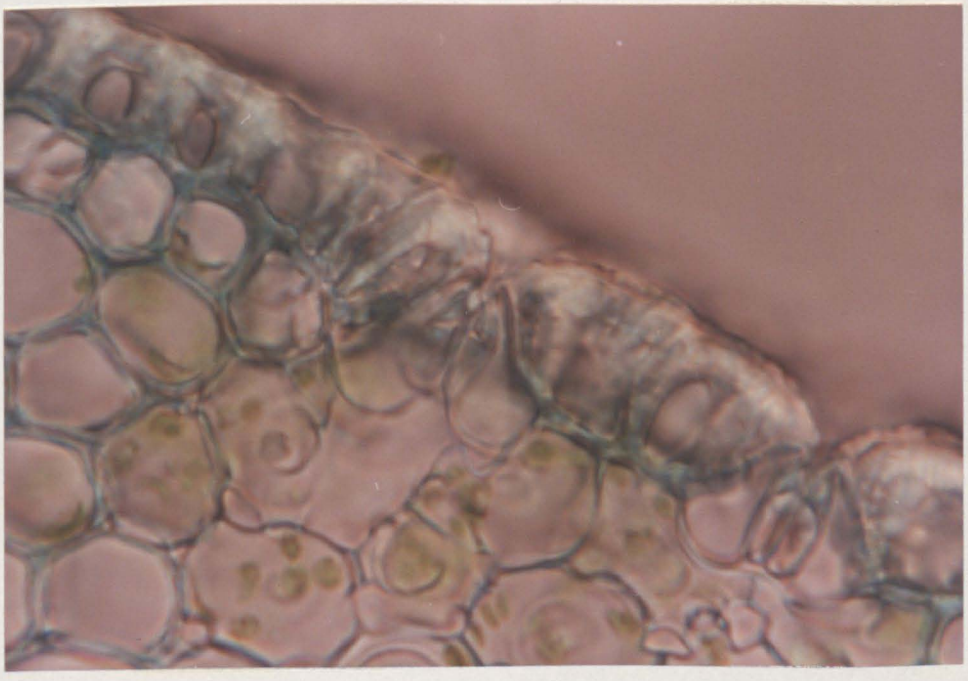

FIG. 3.09

Figure 3.10 (overleaf)

Fig. 3.10. Scanning electron photomicrographs of leaf-sheath with abaxial epidermal layer removed, showing intercellular spaces within chlorenchyma. (cf. Fig. 3.09).

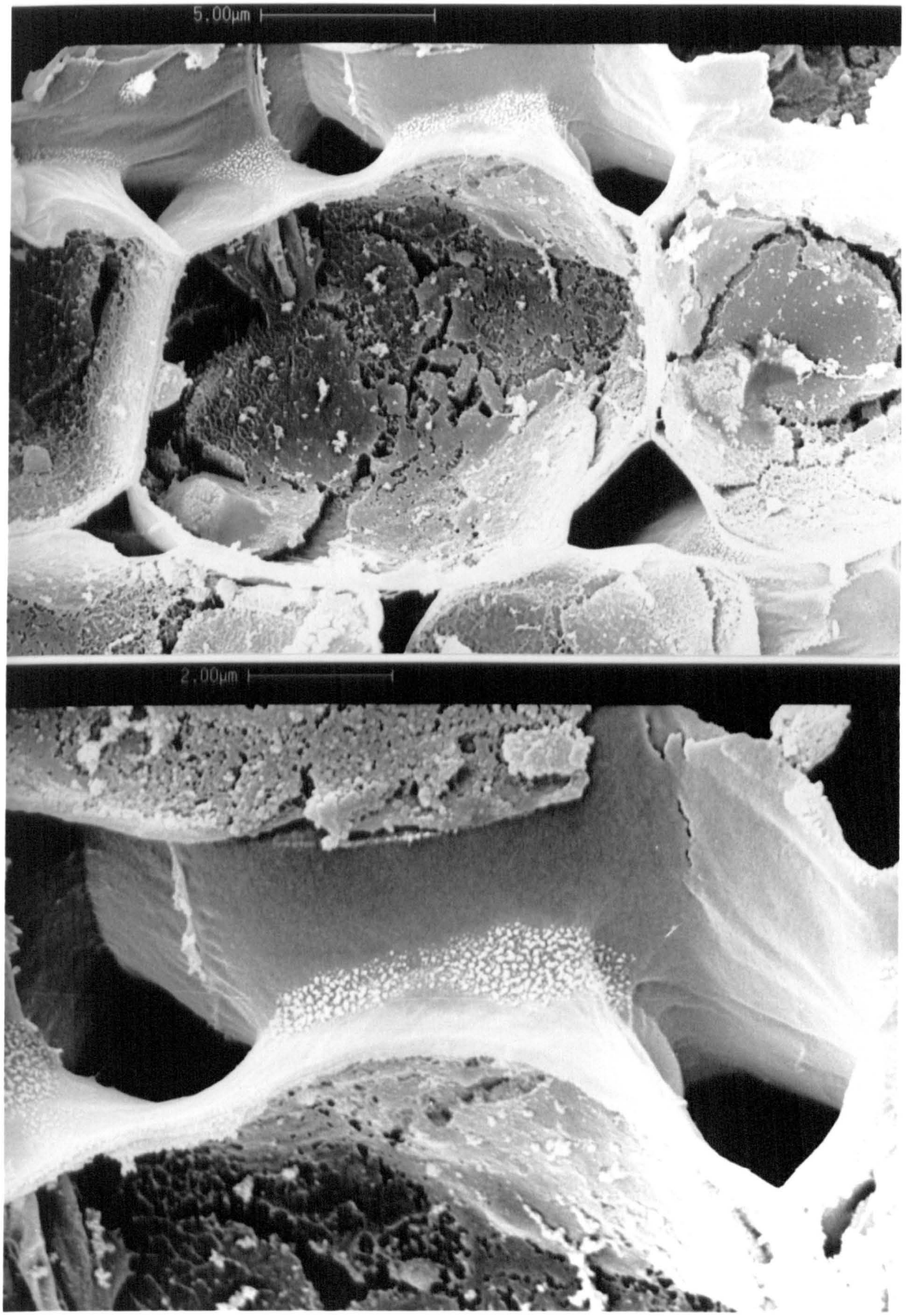
5.00µm
2.00µm

Figure 3.11 (overleaf)

Fig. 3.11. Scanning electron photomicrograph of a culm nodal diaphragm in longitudinal section:

ls = leaf sheath; p = pith cavity; S = large stellate parenchyma; s = small stellate parenchyma; v = vascular tissue.

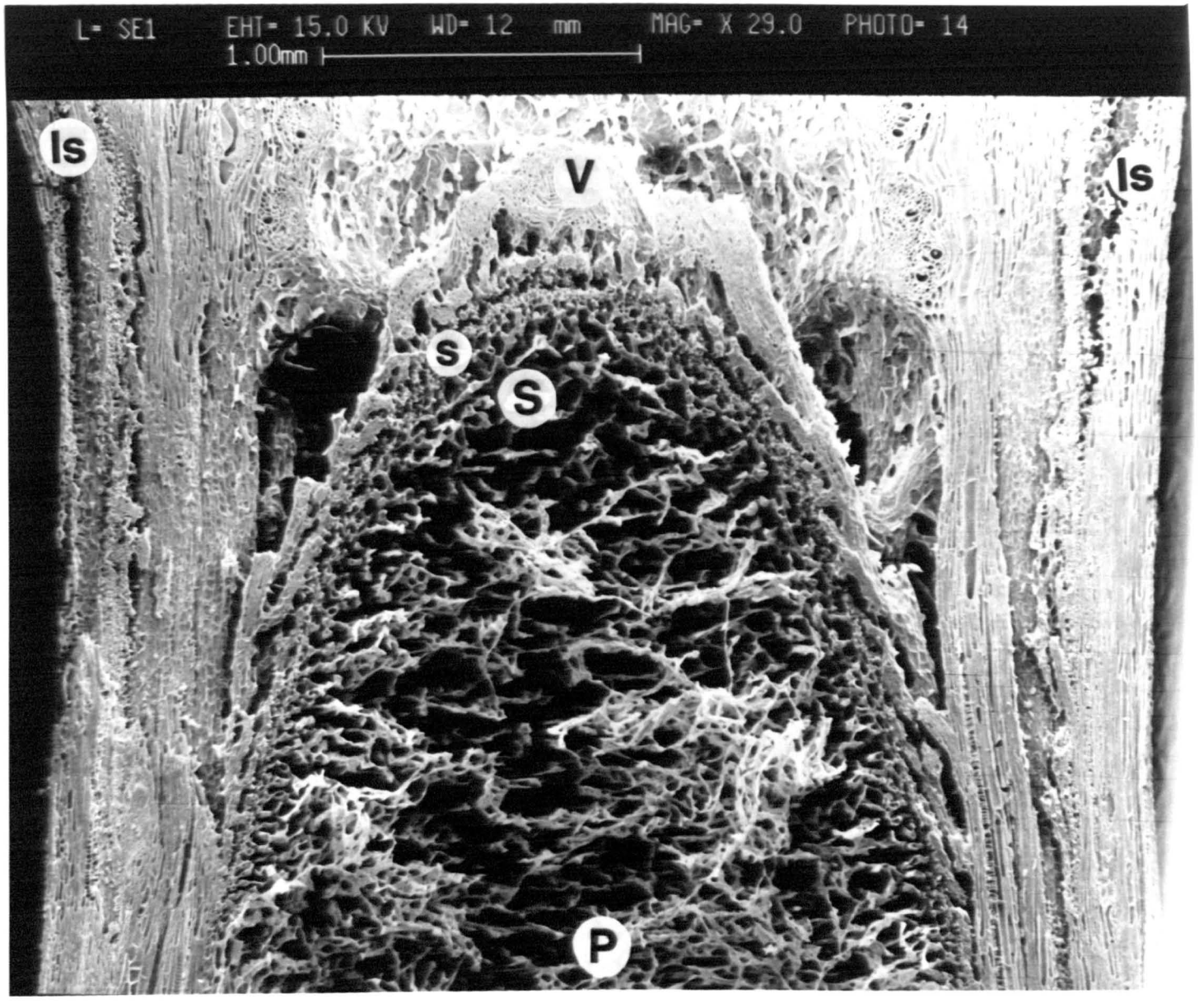
L= SE1 EHT= 15.0 KV WD= 12 mm MAG= X 29.0 PHOTO= 14
1.00mm
ls
V
ls
s
S
P

Figure 3.12 (overleaf)

Fig. 3.12. Scanning electron photomicrographs:

(Above) Culm nodal diaphragm in longitudinal section: S = large stellate parenchyma; s = small stellate parenchyma; v = vascular tissue.

(Below) Small stellate parenchyma from (a); note its highly porous nature.

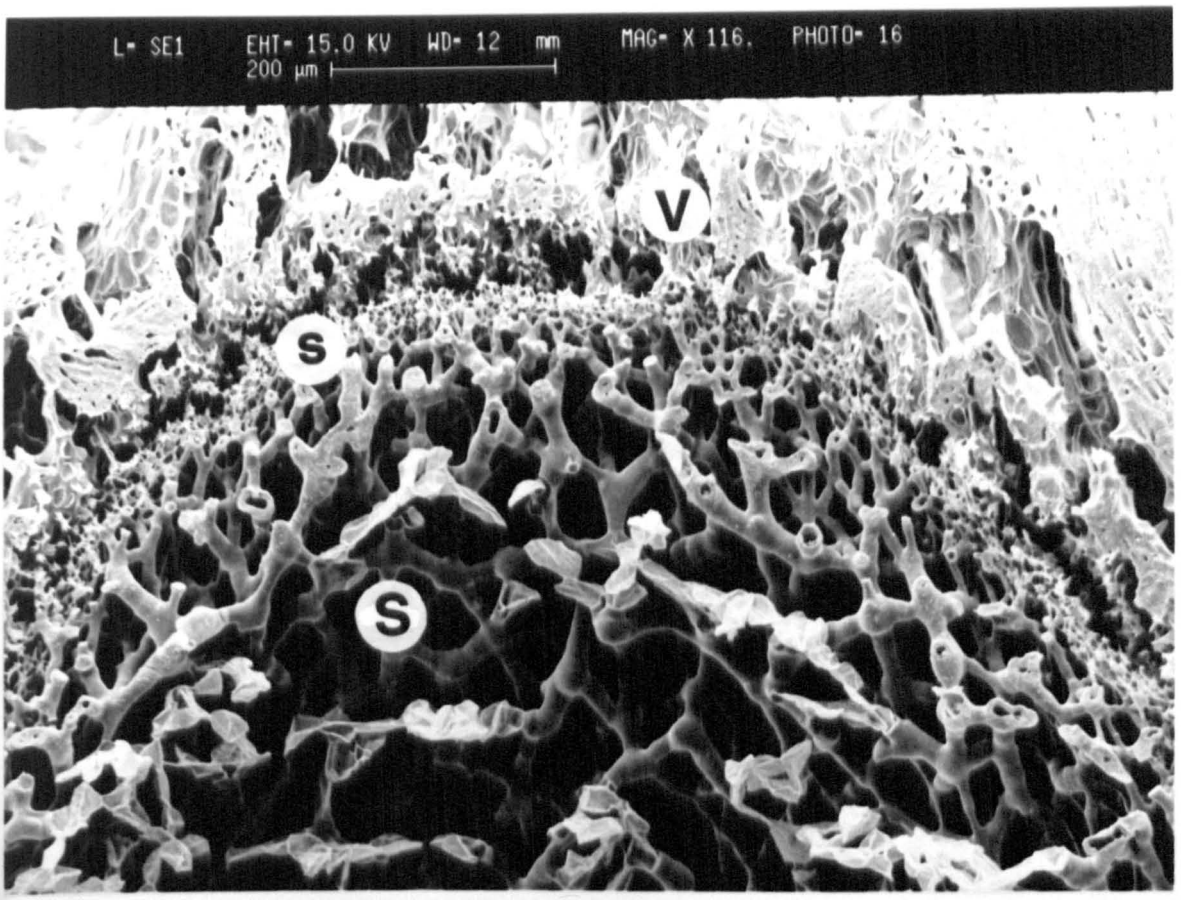
L= SE1 EHT= 15.0 KV WD= 12 mm MAG= X 116. PHOTO= 16
200 µm
V
S
S

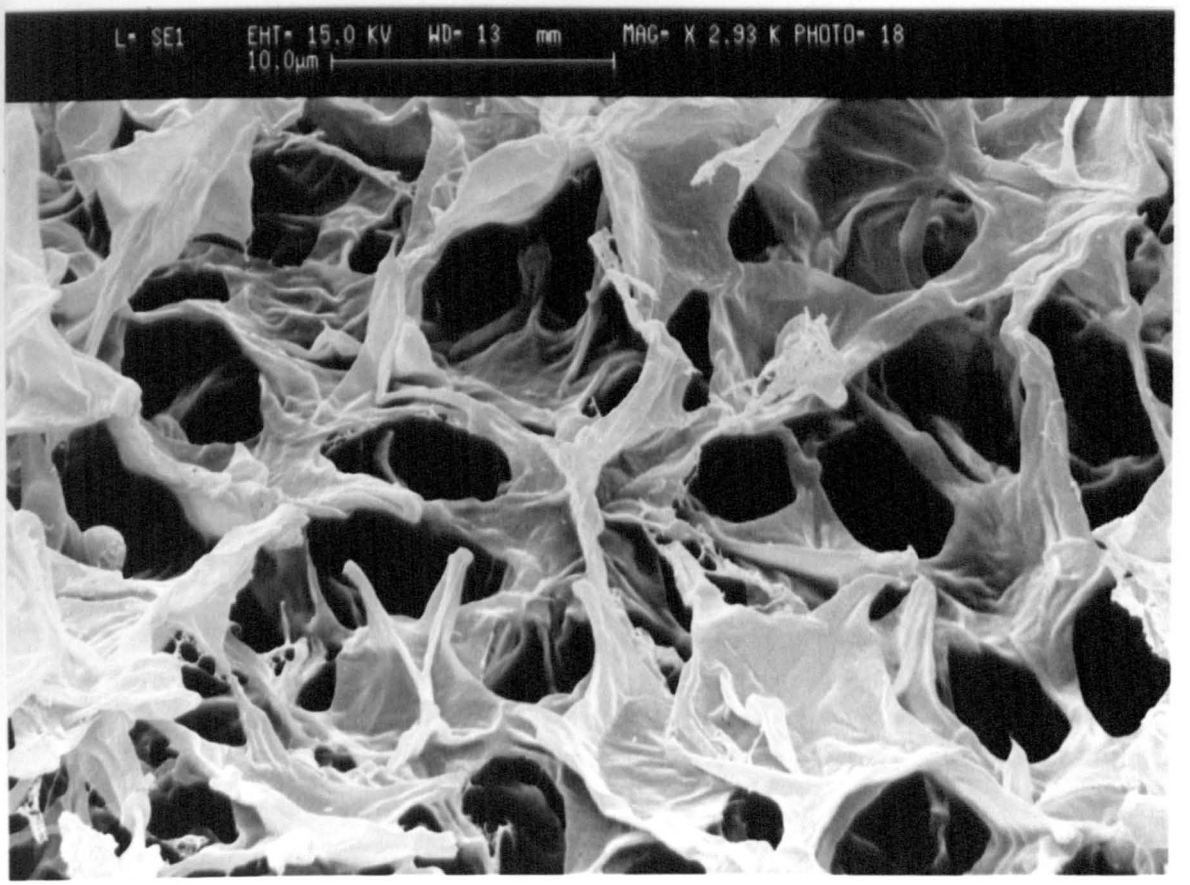
L= SE1 EHT= 15.0 KV WD= 13 mm MAG= X 2.93 K PHOTO= 18
10.0µm

Figure 3.13 (overleaf)

Fig. 3.13.

Above. Scanning electron photomicrograph of epidermis of horizontal rhizome showing waxy cuticle and thickened cell walls.

Below. Fresh, hand-cut, transverse section from horizontal rhizome showing waxy cuticle and suberised sub-epidermal layers (X1200). Stained with Sudan III.

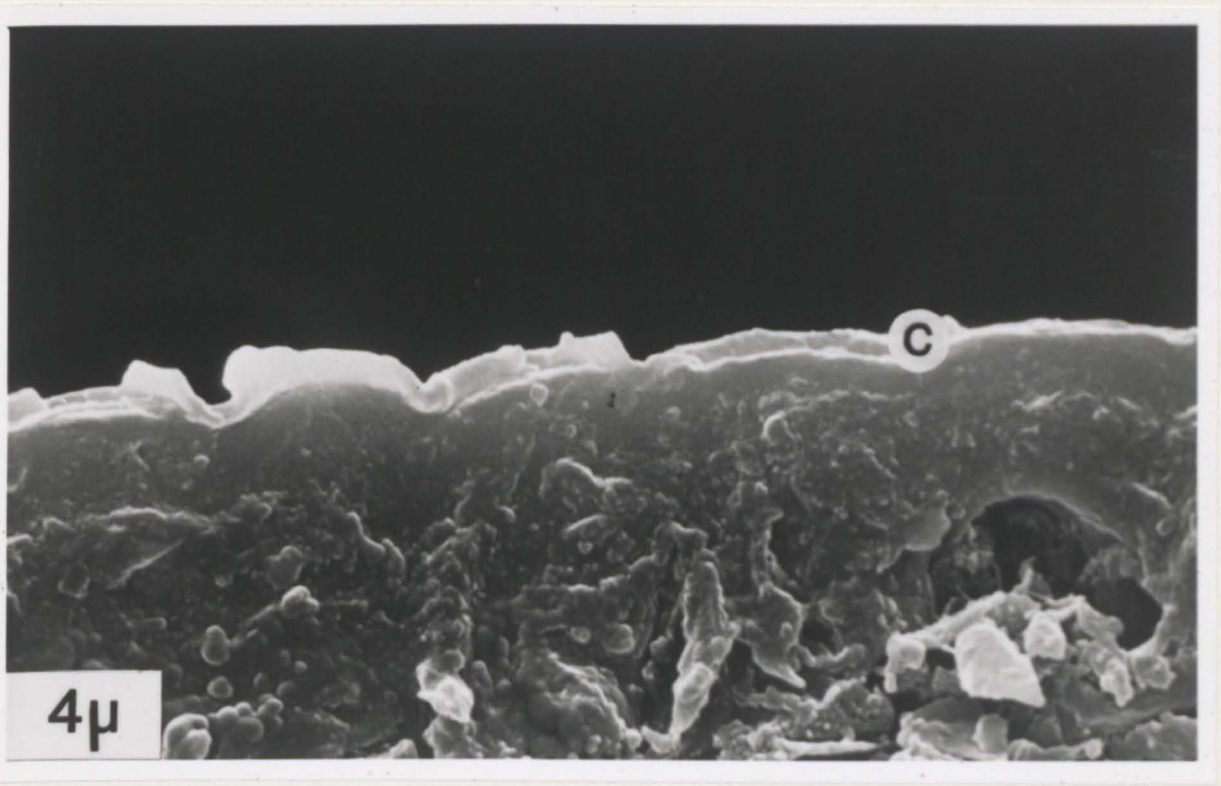
C
4μ

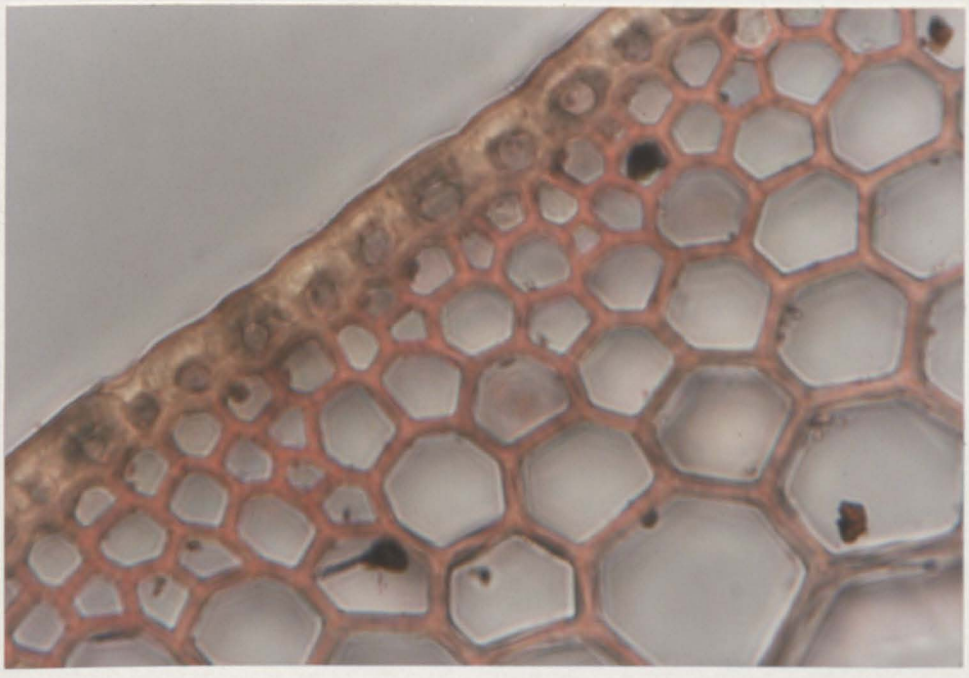

Figure 3.14 (overleaf)

Fig. 3.14. Scanning electron photomicrographs:

(a) Transverse section of internodal region of horizontal rhizome showing the lack of gas-space connexion between the pith cavity (P) and the cortical aerenchyma (A).

(b) Transverse section of nodal region of horizontal rhizome showing the radial gas-channels (R) which traverse the stelar cylinder. These connect (*via* stellate parenchyma, S), with the pith cavity above (P) and below (P') the pith diaphragm, with the cortical aerenchyma channels (A) below the leaf origin, and with the cortical aerenchyma band (A') above the leaf origin.

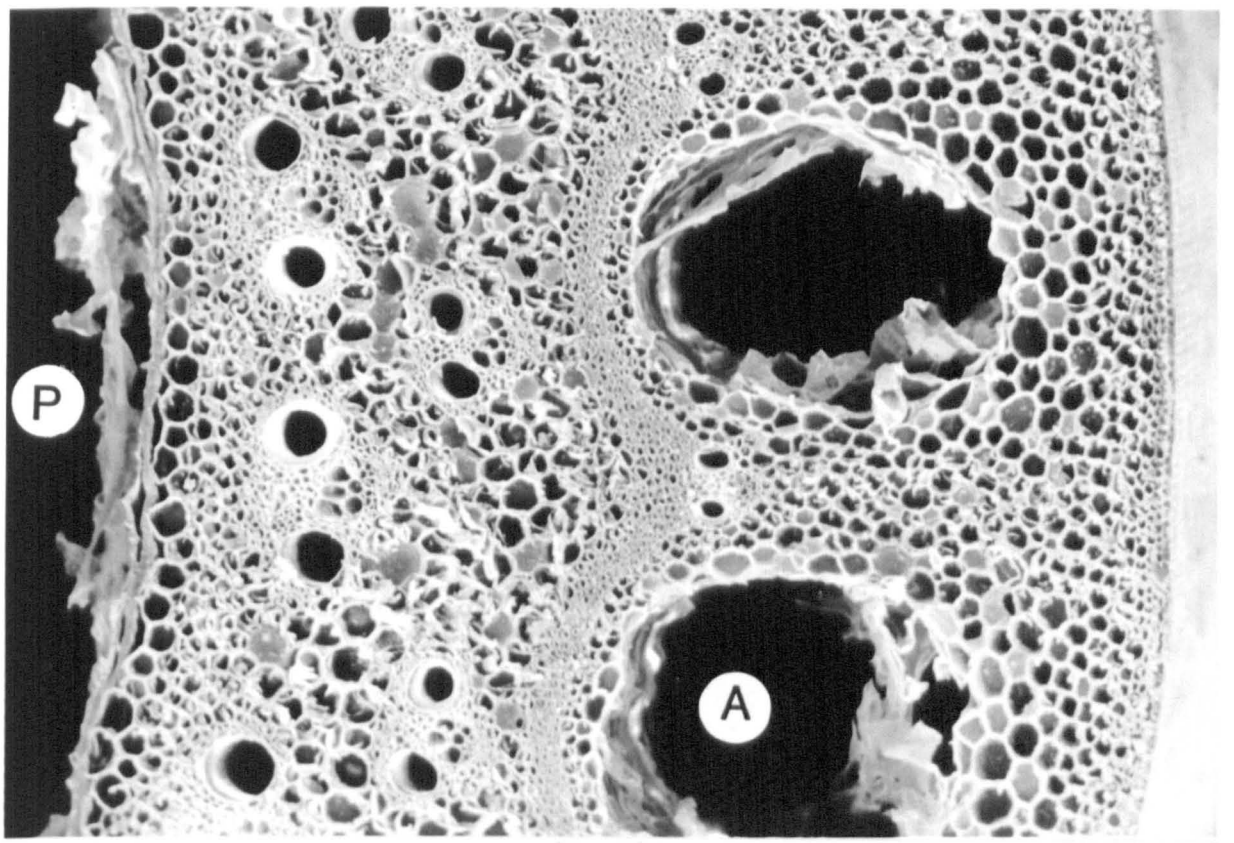

(a)

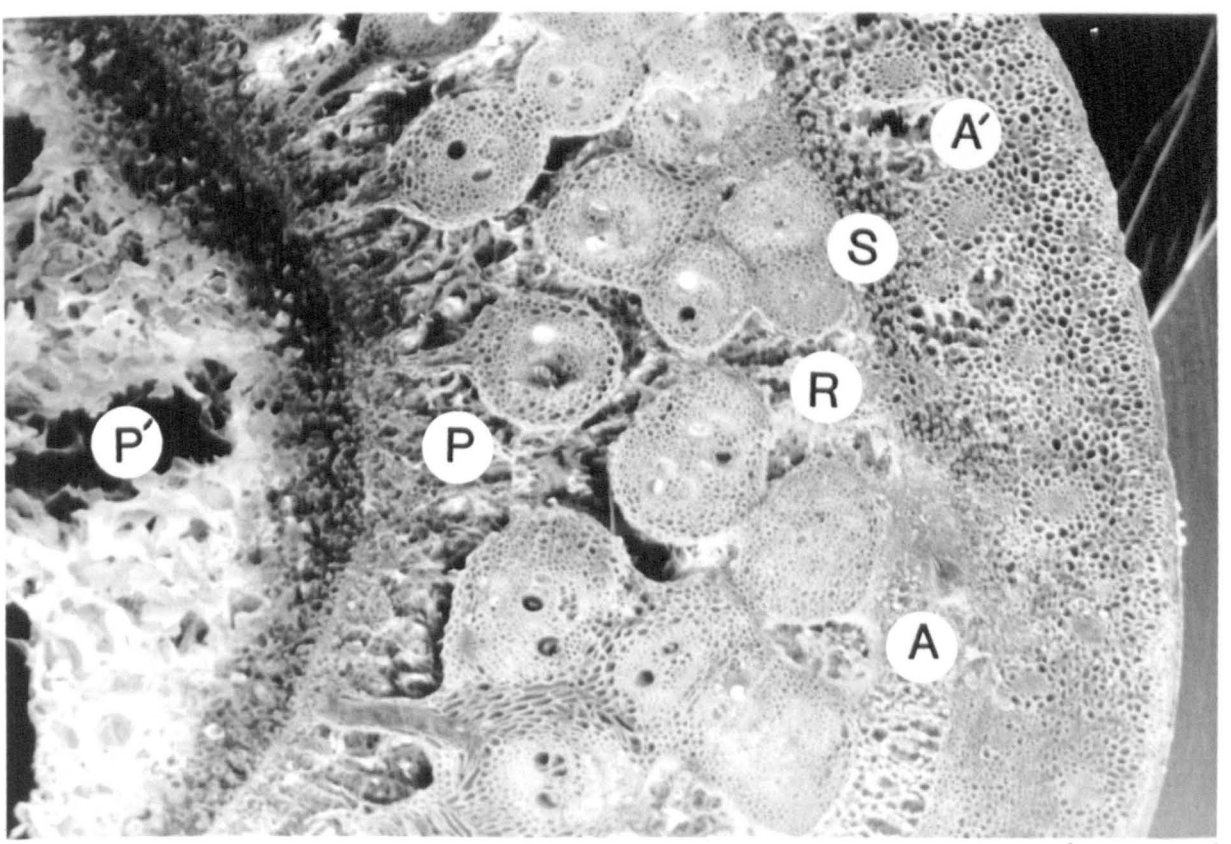

(b)

Figure 3.15 (overleaf)

Fig. 3.15. Scanning electron photomicrographs:

Above. Longitudinal section of horizontal rhizome through nodal diaphragm, consisting of upper anastomosing vascular strands (V), small stellate parenchyma (S), and large stellate parenchyma (S'). Also shown is the pith cavity (P) and one of the radial channels (R) which connect the pith cavity with the cortical aerenchyma above (A), and below (A') the scale-leaf junction (J).

Below. High power nodal diaphragm.

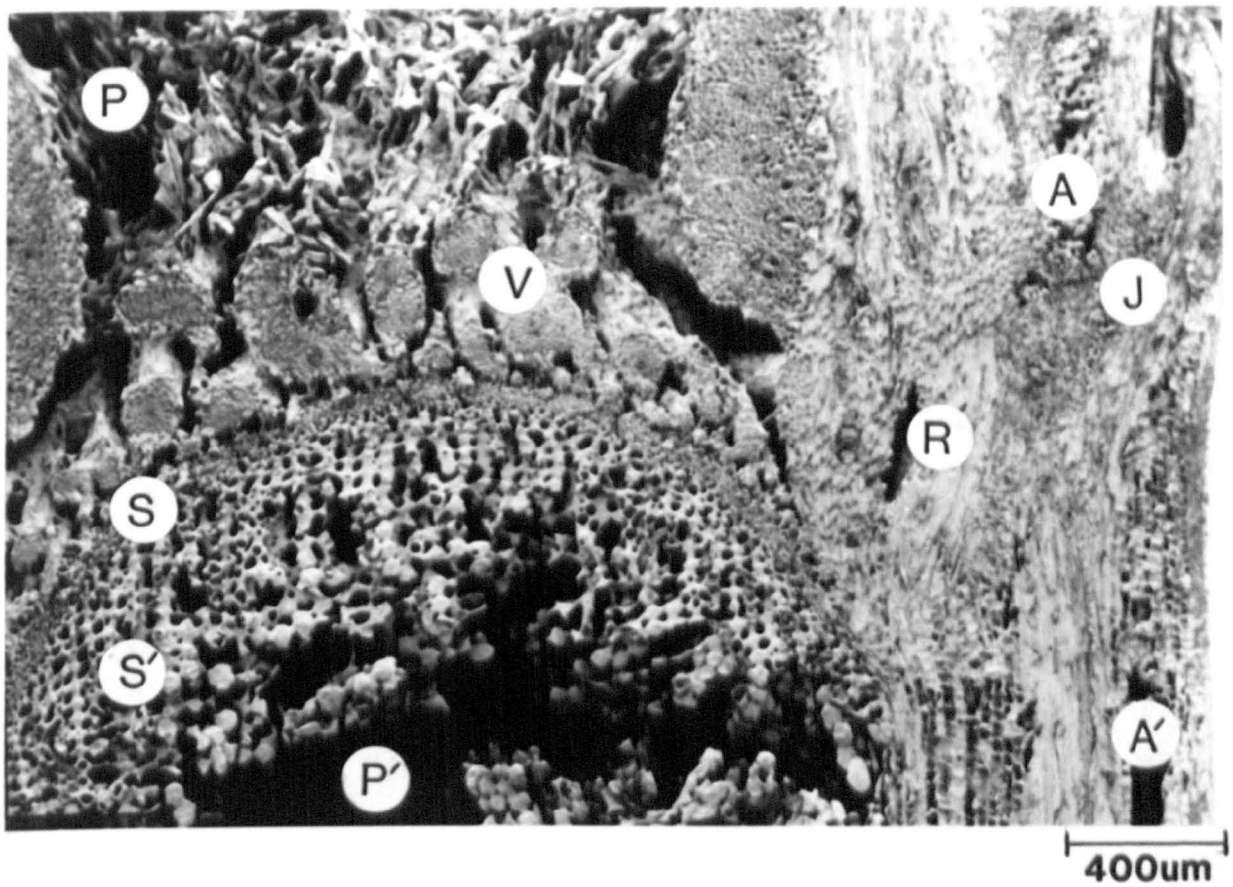
P
V
A
J
R
S
S′
P′
A′
400um

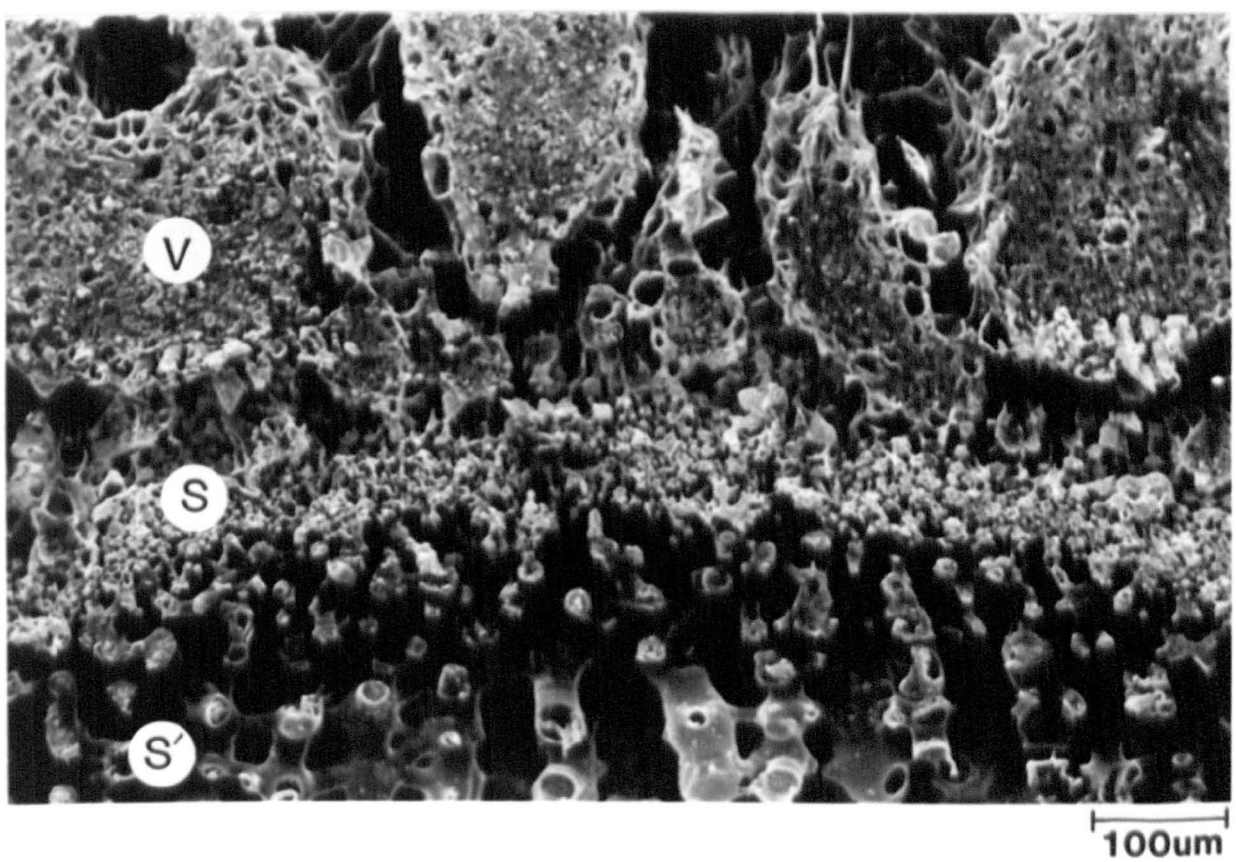
V
S
S′
100um

Figure 3.16 (overleaf)

Fig. 3.16. Scanning electron photomicrographs from longitudinal section of nodal diaphragm of horizontal rhizome:

Above. Small stellate parenchyma.

Below. Large stellate parenchyma.

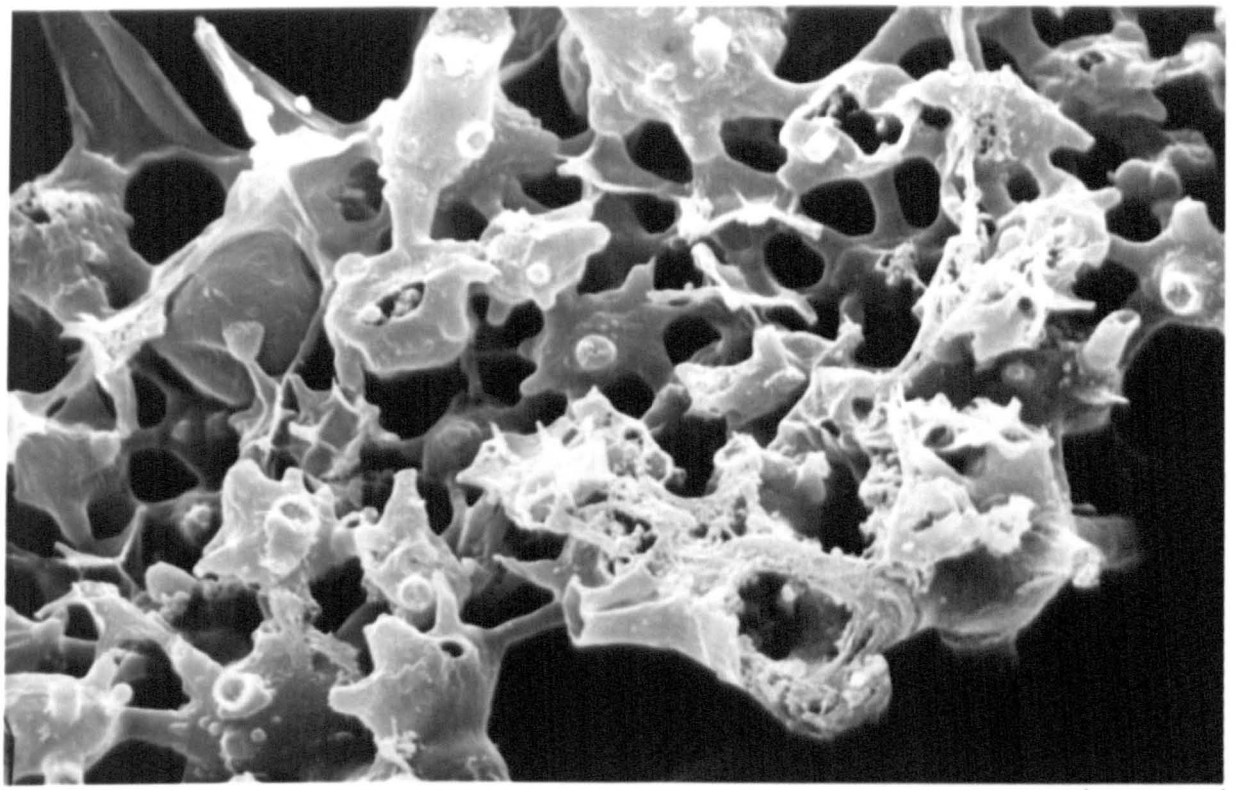
10um

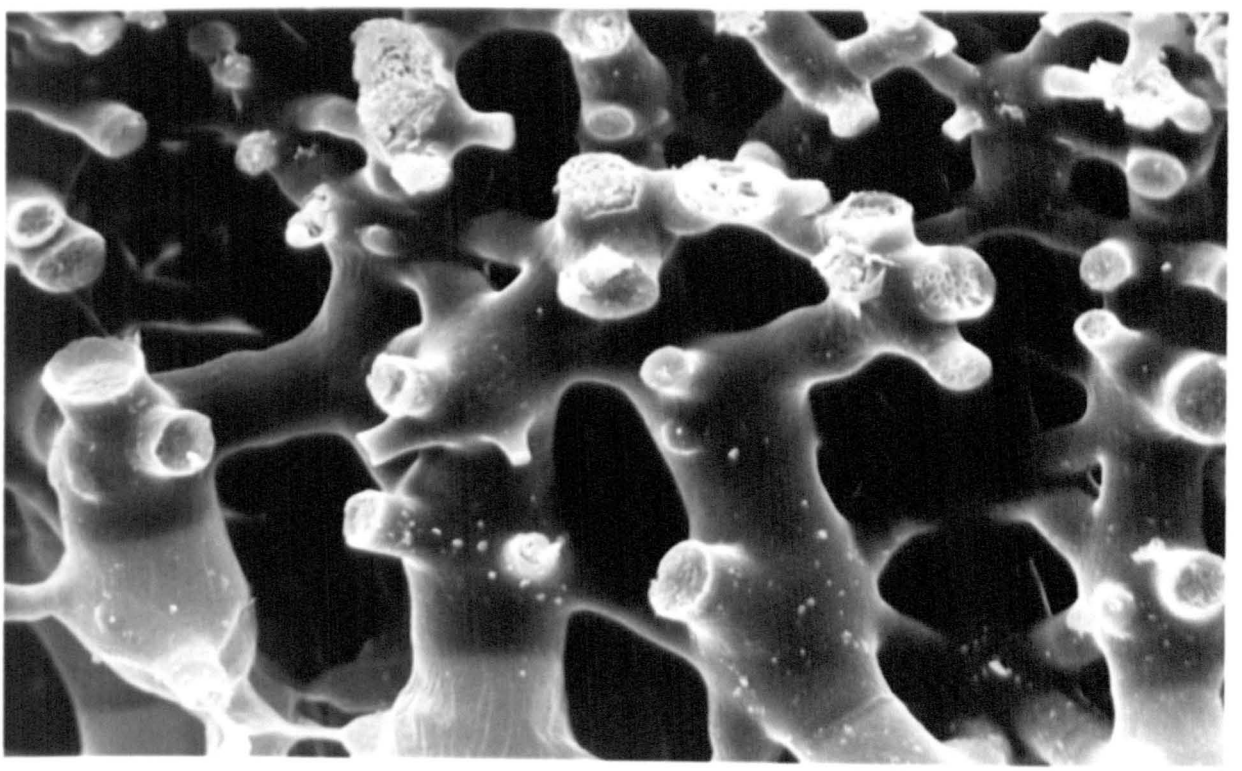
40um

Figure 3.17 (overleaf)

Fig. 3.17. Fresh, hand-cut, longitudinal section of part of rhizome nodal diaphragm stained with phloroglucinol and conc. HCl showing unlignified small stellate parenchyma and lignified large stellate parenchyma (X640).

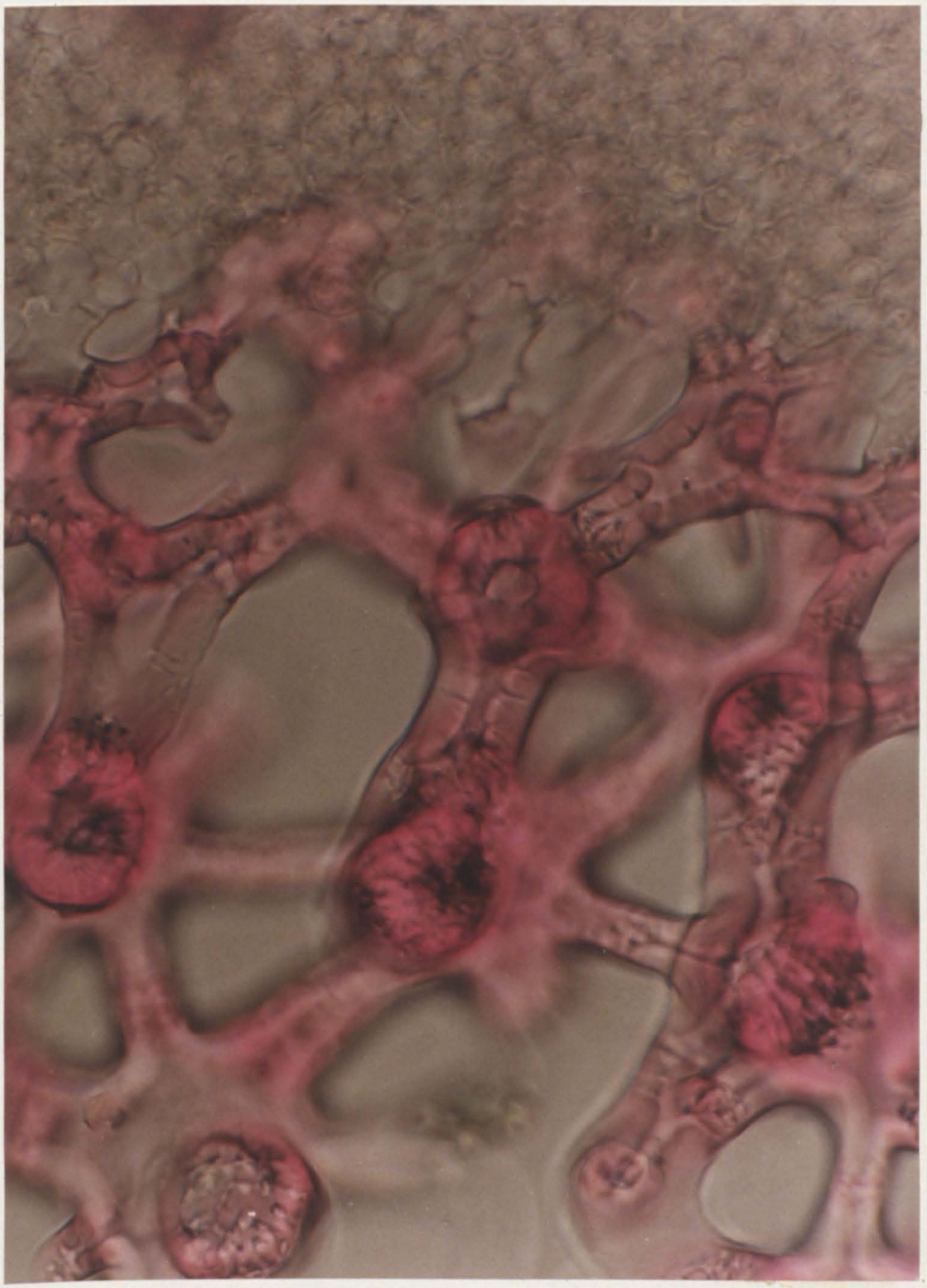

Figure 3.18 (overleaf)

Fig. 3.18. Fresh, hand-cut, longitudinal section of rhizome tip prior to aerenchyma and pith-cavity development, showing intercellular gas-space connexions (black) especially obvious in developing nodal diaphragm, and in apical meristem region. Note gas-space connexions between what will become leaf sheath aerenchyma and rhizome cortical aerenchyma, and nodal radial channels between rhizome cortex and developing pith.(x42)

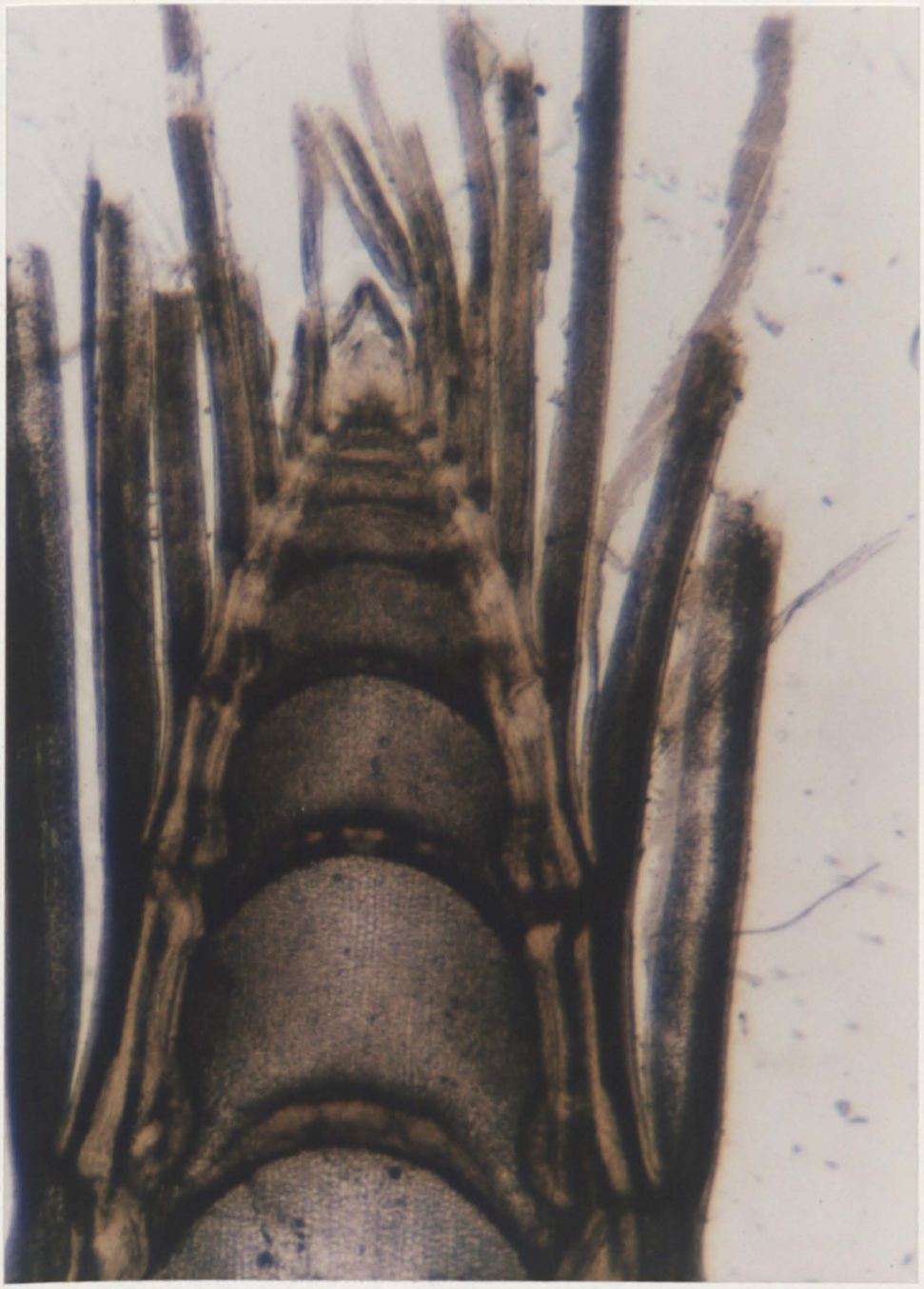

Figure 3.19 (overleaf)

Fig. 3.19. Fresh, hand-cut, longitudinal sections of:

(a) rhizome diaphragm (x60)

(b) diseased rhizome nodal diaphragm, showing palisade callus (tylosoids) with lignified walls, developed from small stellate parenchyma (bottom right) (x100)

(c) base of senesced leaf sheath showing callus (tylosoids) blocking an aerenchyma channel (x270)

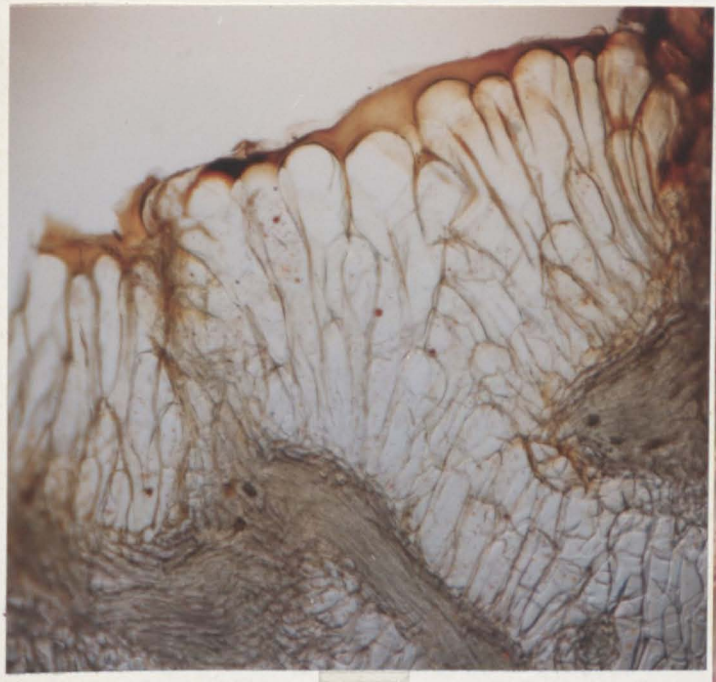

(a)

(b)

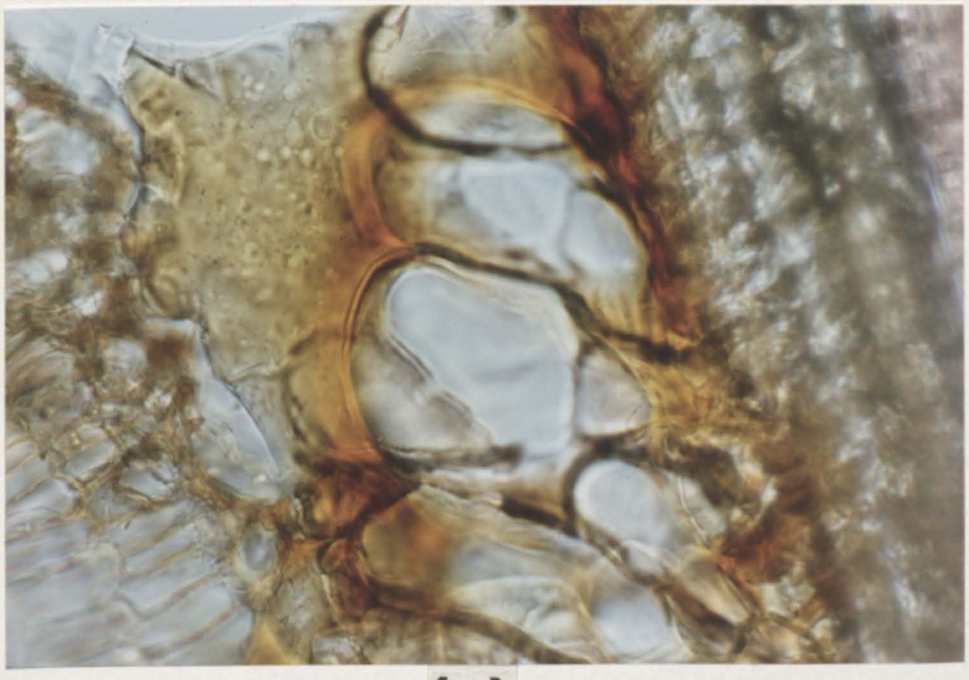

(c)

Figure 3.20 (overleaf)

Fig. 3.20. Scanning electron photomicrograph of vertical section through nodal diaphragm of diseased horizontal rhizome showing callus (tylosoid-like) growths (T) which occlude the former gas-spaces around the vascular strands (V), and which have their origin in circumvascular parenchyma and small stellate parenchyma. The impenetrable upper surface of the callus can be seen (top right).

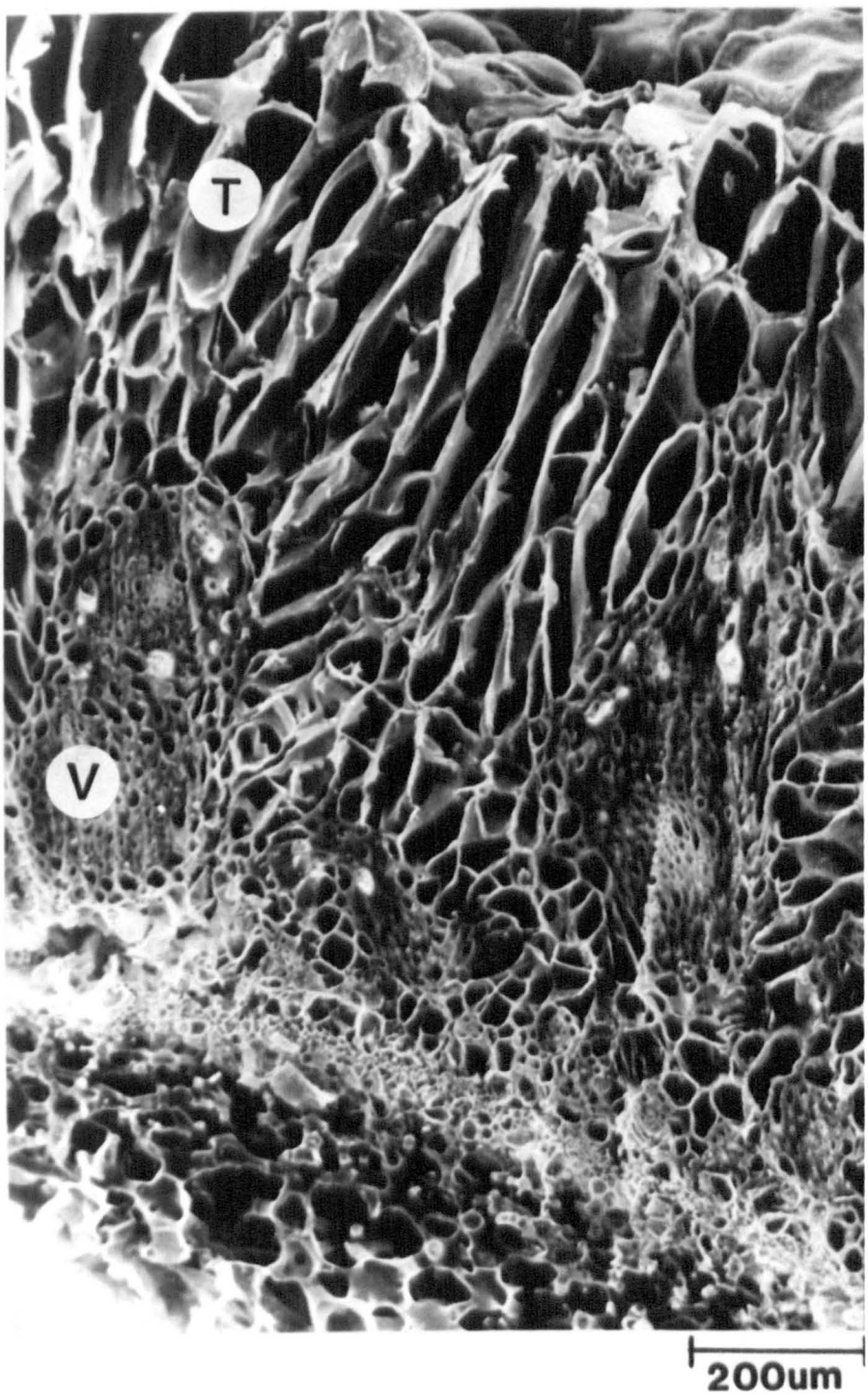
T
V
200um

Figure 3.21 (overleaf)

Fig. 3.21 Fresh, hand-cut, transverse sections of:

(a) rhizome node across adventitious root primordium stained with phloroglucinol and conc. HCl showing reduced lignification in rhizome cortex opposite the primordium. Note also intercellular gas-space connexions (arrow) via stellate parenchyma between rhizome aerenchyma and root cortex. (X125).

(b) adventitious root at 10 mm from apex stained with Sudan III to show relative absence of hypodermal suberisation and wall thickening opposite a developing lateral. Note concave quadrangular shape of longitudinally running non-aerenchymatous cortical gas-spaces and also early stages of aerenchyma development. (X 330).

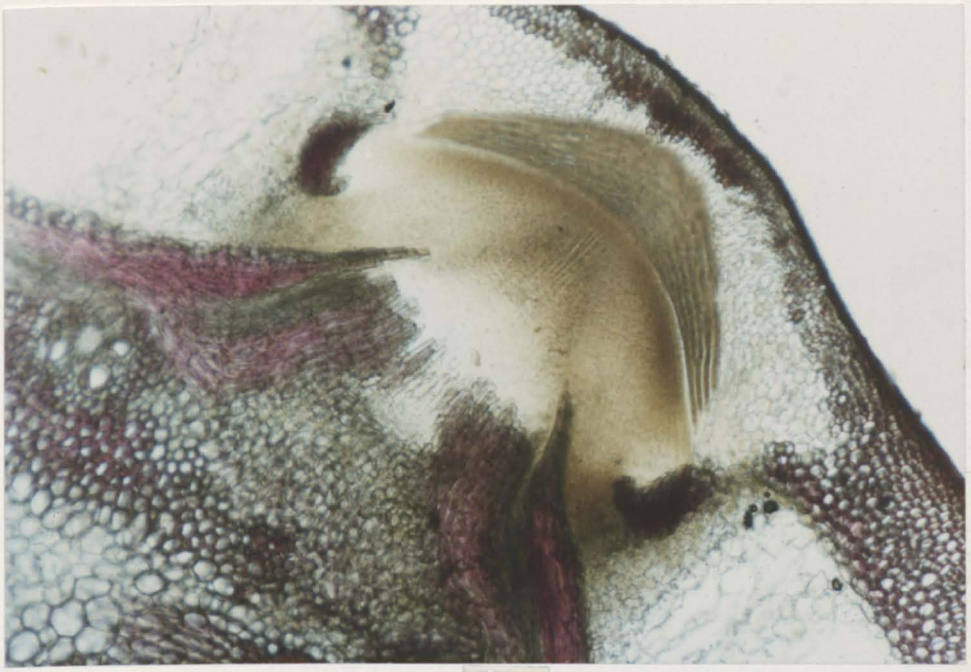

(a)

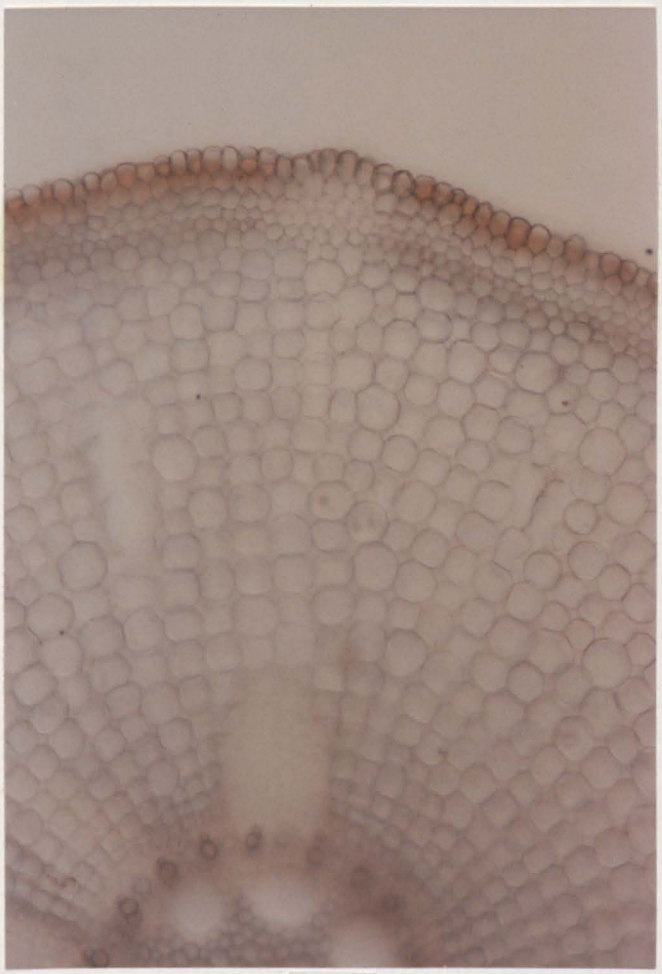

(b)

Fig. 3.22. Scanning electron photomicrographs of tangential longitudinal section of adventitious root < 5 mm from the apex showing radially-running intercellular spaces in the cortex: (Above) X 1580; (Below) X 3000.

Fig. 3.23. Scanning electron photomicrographs of tangential longitudinal section of adventitious root < 5 mm from the apex showing radially-running intercellular spaces in the cortex: (Above) X 6430; (Below) X 6000.

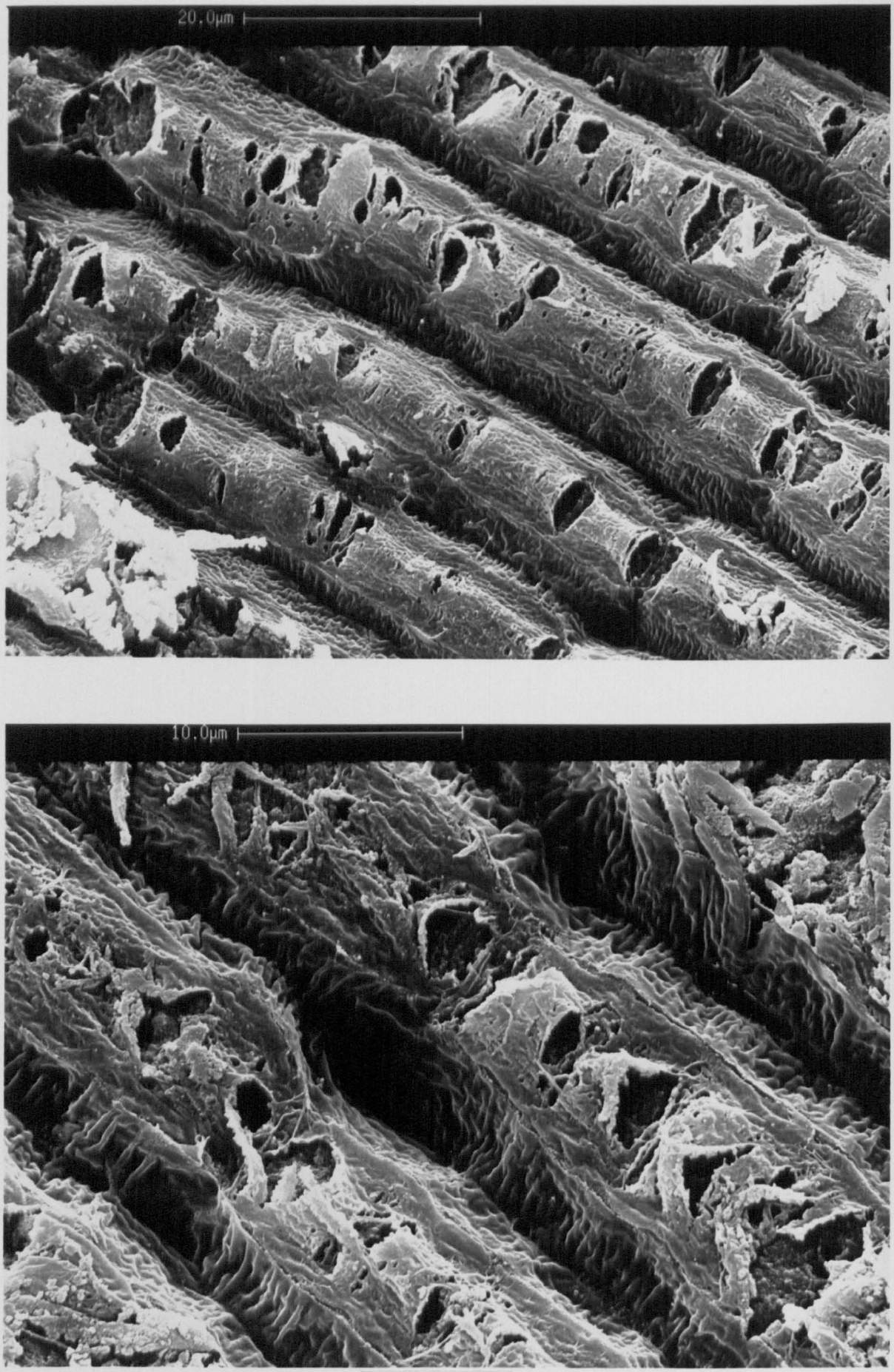

FIG. 3.22

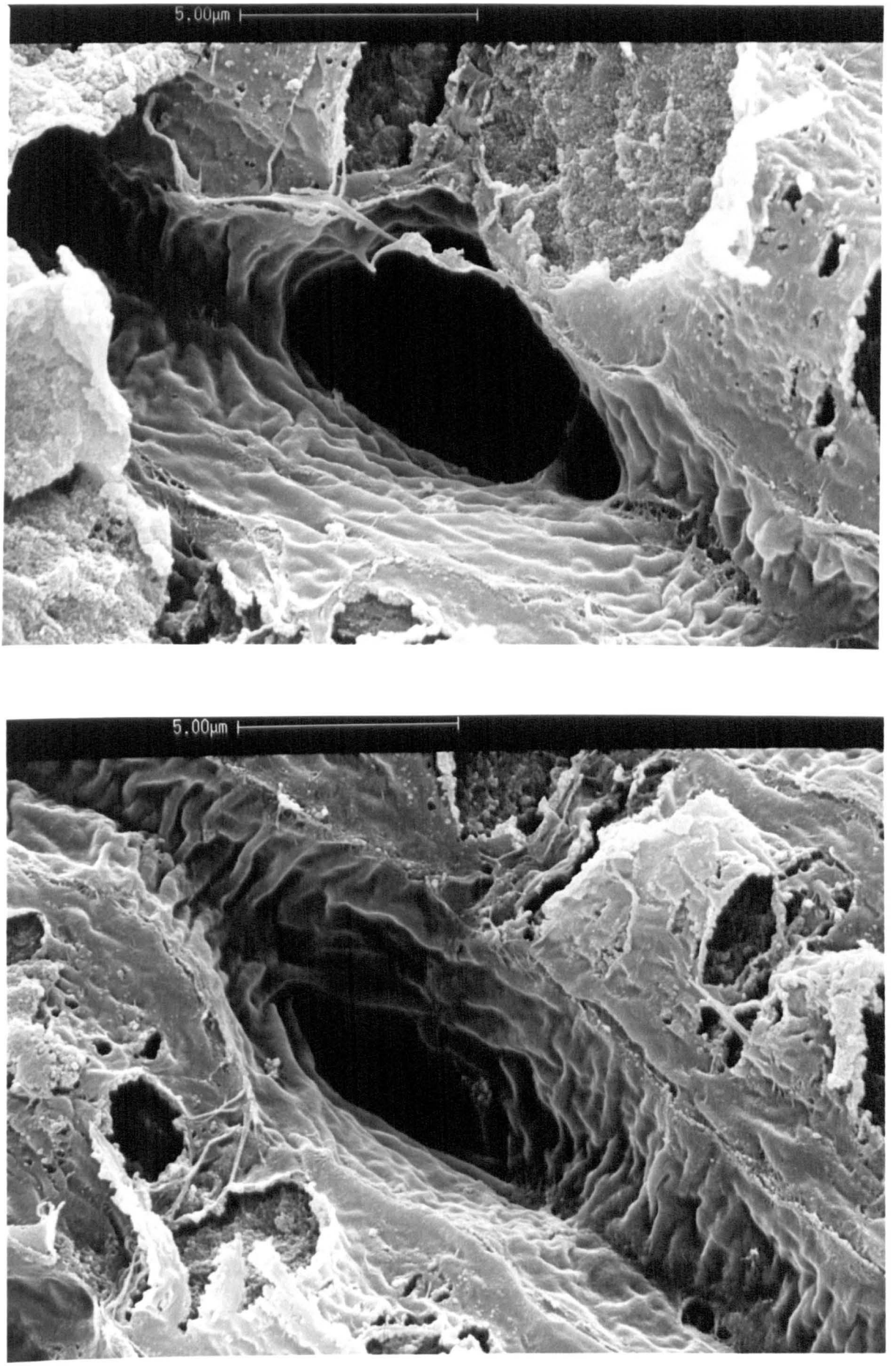

FIG. 3.23

Figure 3.24 (overleaf)

Fig. 3.24. Scanning electron photomicrographs:

(a) Transverse section of horizontal rhizome at rhizome-root junction showing cortical aerenchyma of the rhizome (A), and root (A'), and stellate parenchyma (S) at the junction.

(b) Stellate parenchyma of highly porous rhizome-root junction; these gas-spaces form a link between the cortical aerenchymas of rhizome and root.

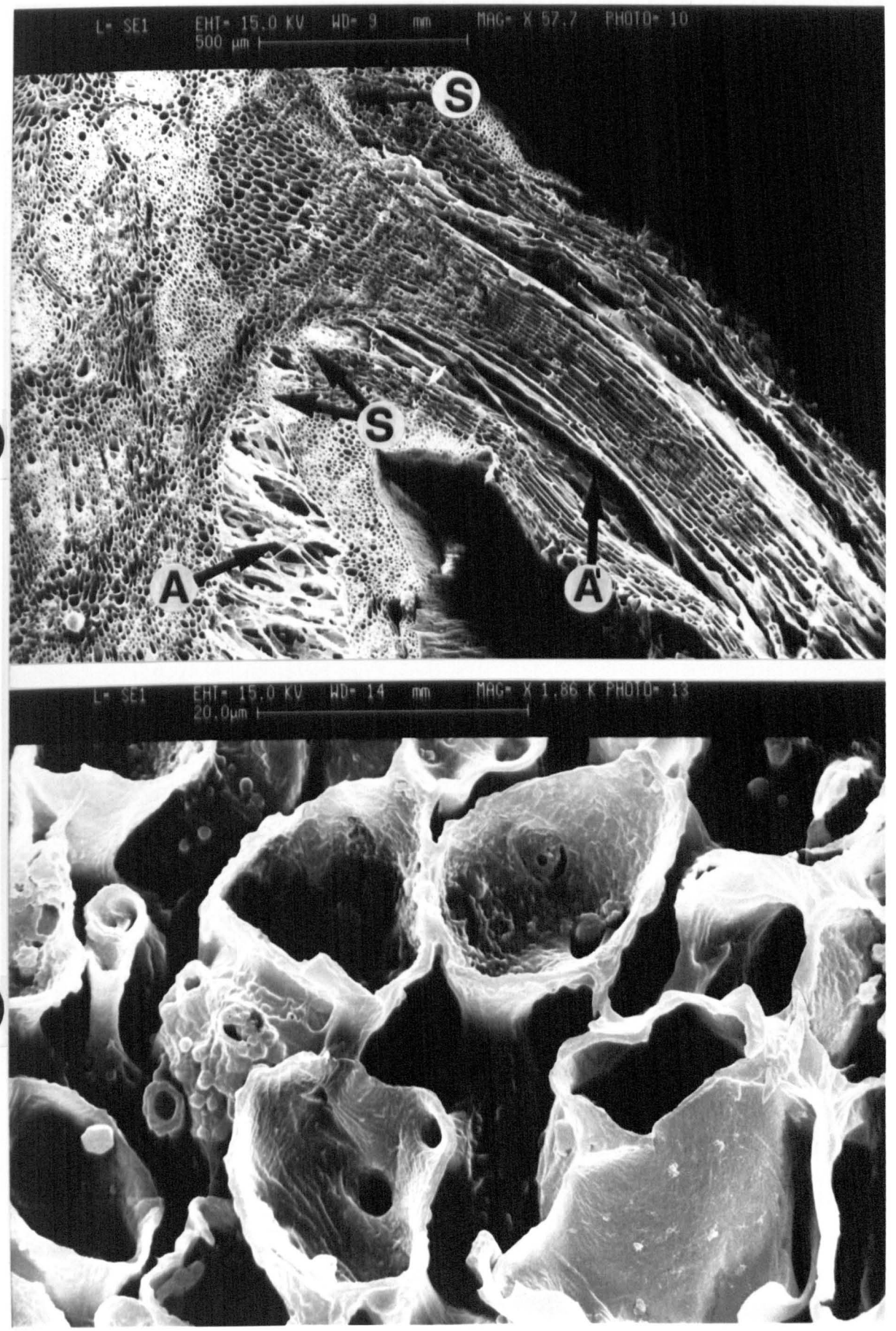
L= SE1 EHT= 15.0 KV WD= 9 mm MAG= X 57.7 PHOTO= 10
500 µm
S
S
A
A'
(a)
L= SE1 EHT= 15.0 KV WD= 14 mm MAG= X 1.86 K PHOTO= 13
20.0µm
(b)

Figure 3.25 (overleaf)

Fig. 3.25. Scanning electron photomicrographs:

(a) Transverse section of adventitious root through a region of basal laterals and showing aerenchyma channels. Lateral roots, ensheathed in persistent cortical parenchyma may be seen crossing the adventitious root cortex.

(b) Transverse section of a basal lateral showing the occasional concave quadrangular intercellular gas-spaces, and the lack of cortical aerenchyma.

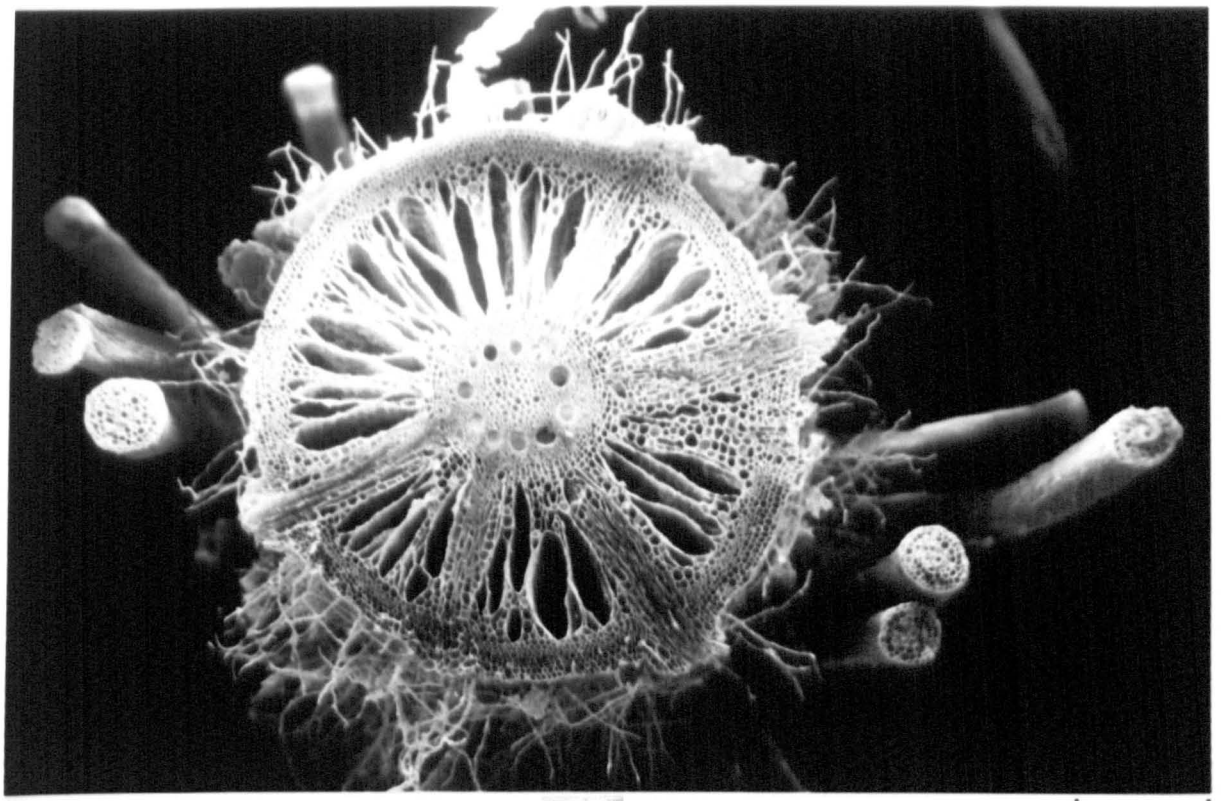

(a)

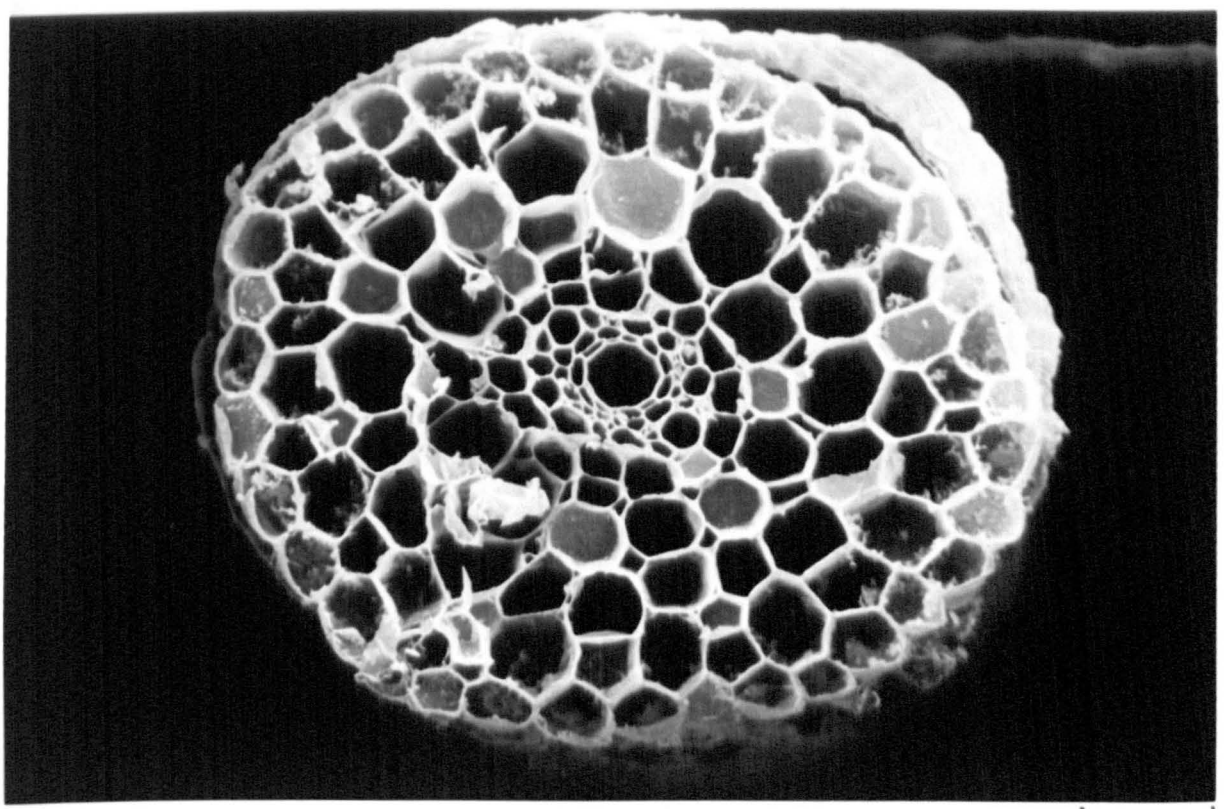

(b)

Figure 3.26 (overleaf)

Fig. 3.26. Fresh, hand-cut, transverse sections in basal 10 mm region of adventitious root (length *ca.* 200 mm) stained with phloroglucinol and conc. HCl.:

(a) Note lysigenous cortical aerenchyma with persisting radial strands of cells, lignified and suberised hypodermal layers and endodermis (X 160).

(b) high power (X 1600) of endodermal region from (a). Note thick lignified inner tangential and radial walls.

(a)

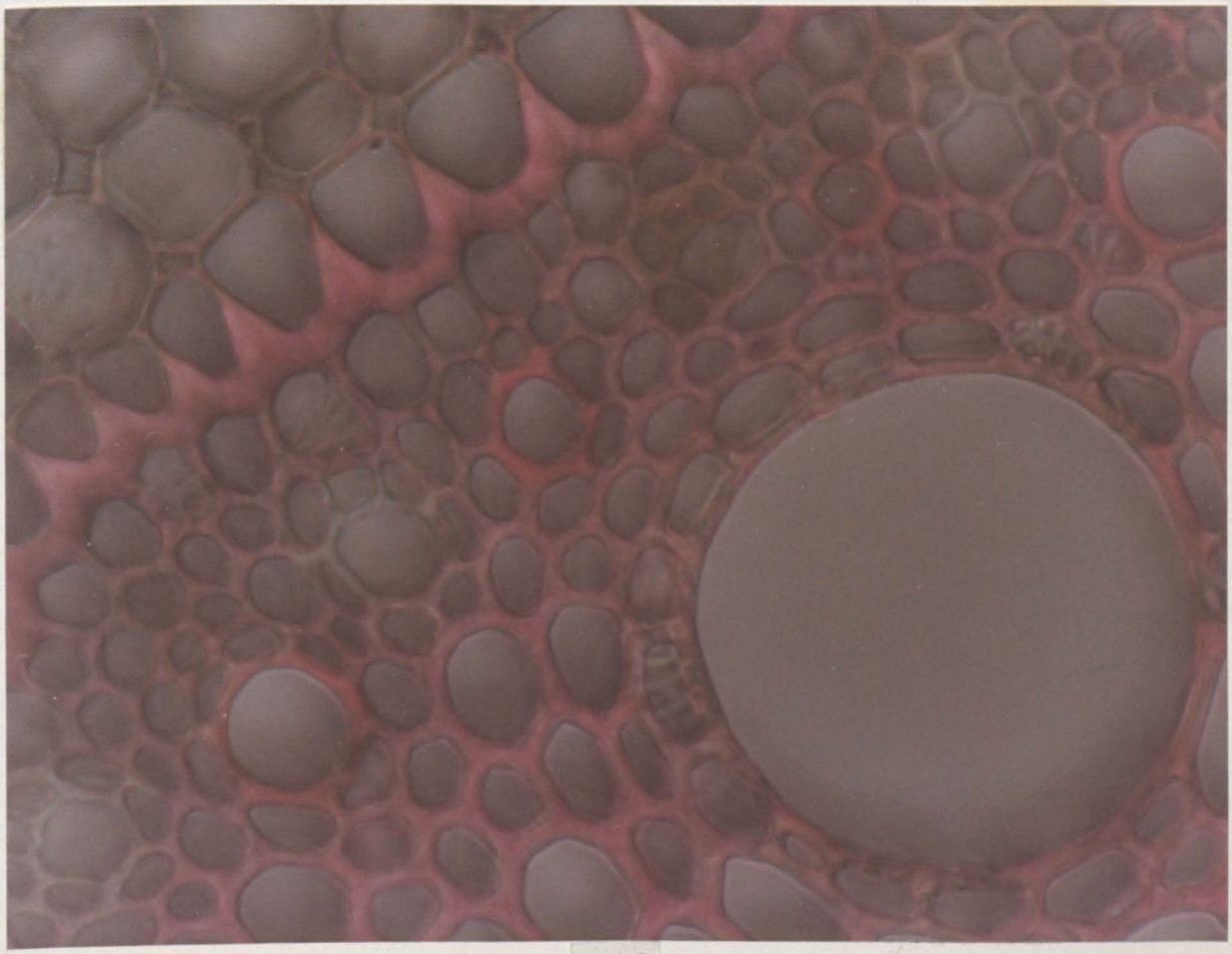

(b)

Fig. 3.27. Scanning electron photomicrographs from transverse section of basal region of adventitious root (length *ca.* 150 mm):
(Above) Note circumferentially-running triangular intercellular spaces in the bounding walls of the cortical aerenchyma channels (arrows);
(Below) Enlarged wall of aerenchyma channels from SEM above.

Fig. 3.28. Further enlargements from Fig. 3.27 of the circumferentially-running triangular intercellular spaces in the bounding walls of the cortical aerenchyma.

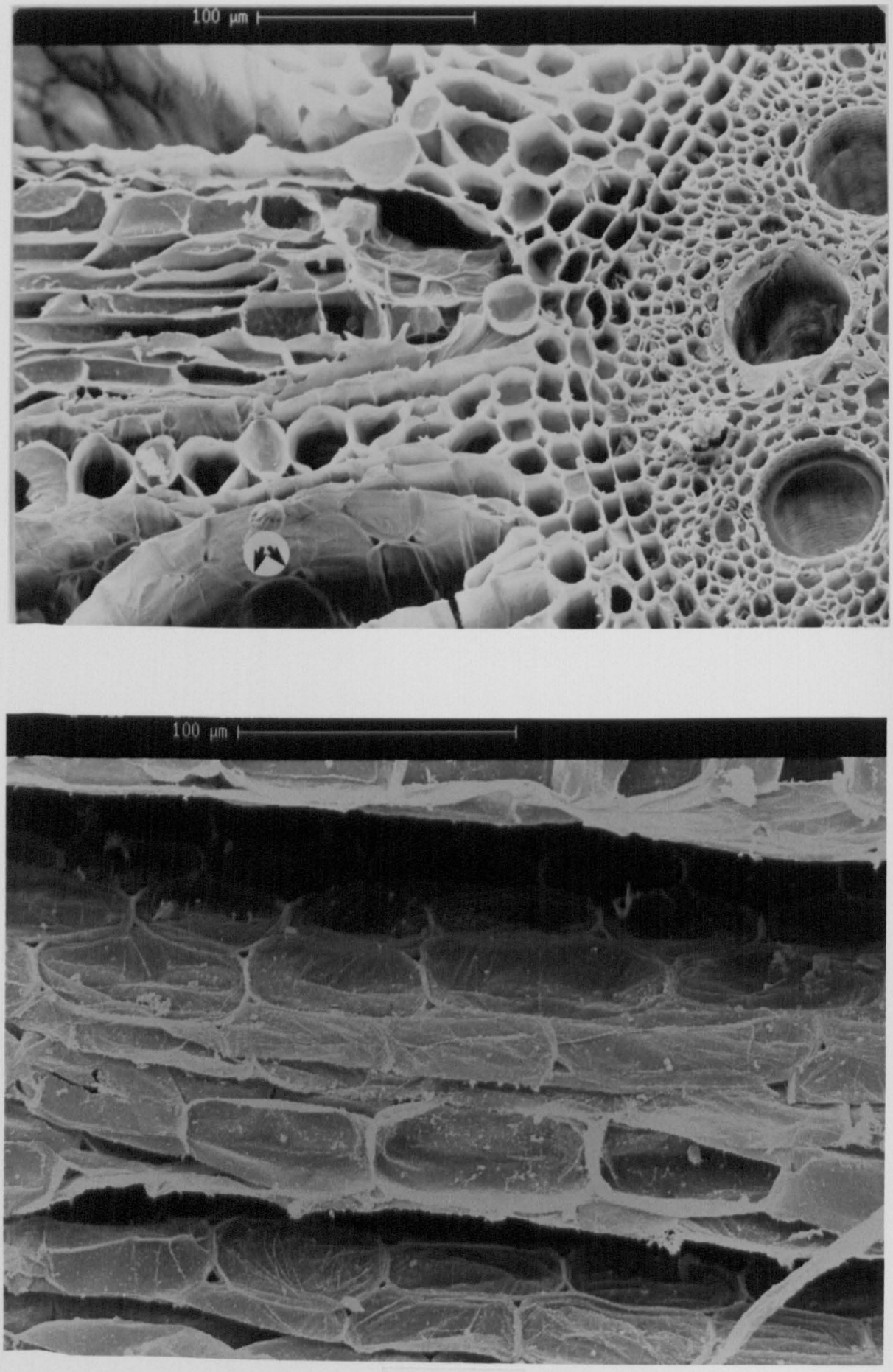

FIG. 3.27

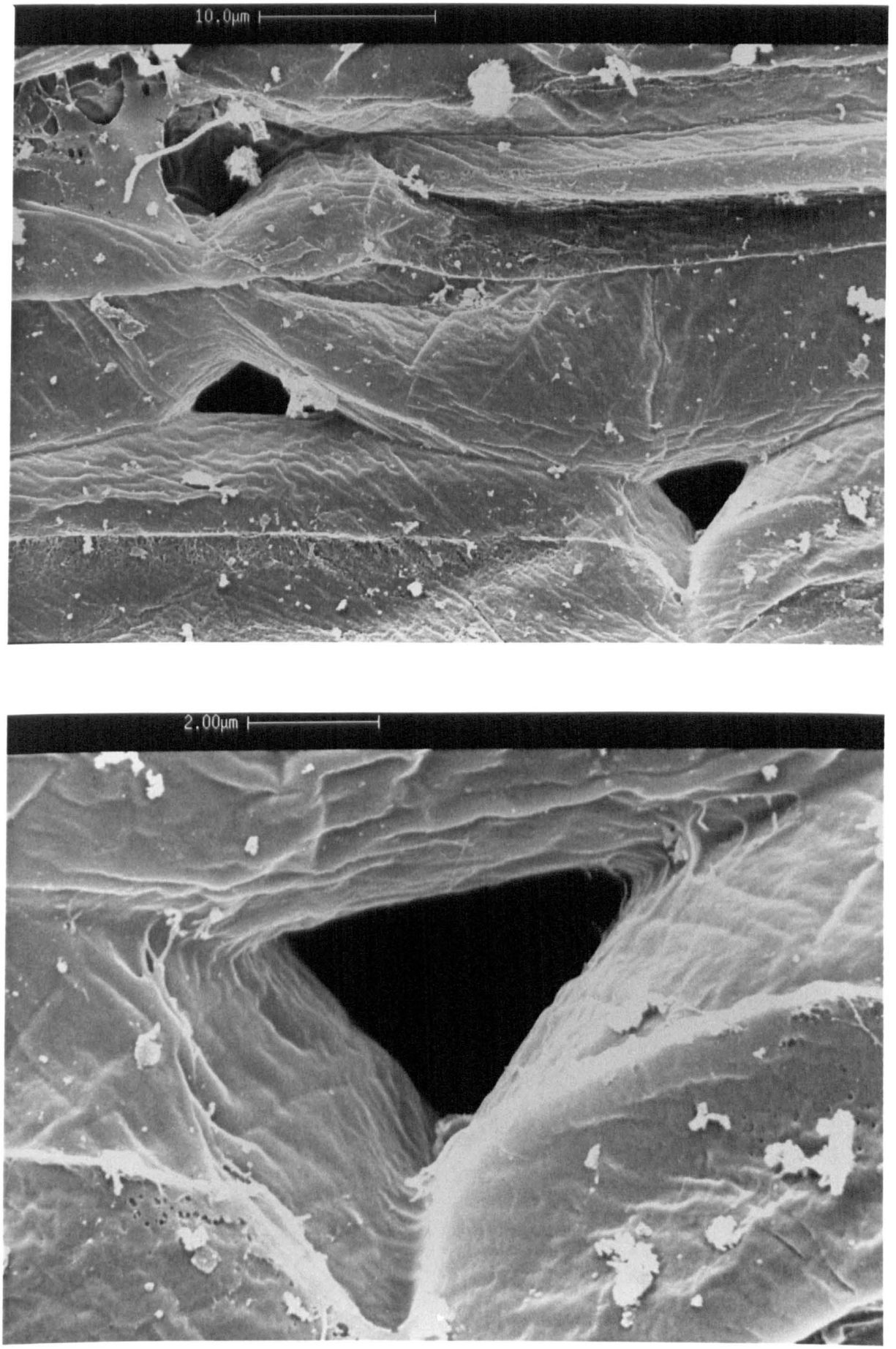

FIG. 3.28

Figure 3.29 (overleaf)

Fig. 3.29. Scanning electron photomicrographs from tangential section of basal region of adventitious root (length *ca.* 150 mm):

(Above) Showing files of intact cells running longitudinally and forming the bounding walls of the cortical aerenchyma spaces. Note the persisting cortical cells around the lateral roots (*cf.* Figs. 3.25a & 3.32a).

(Below) Persisting cortical cells enlarged from SEM above, and showing developing lysigenous aerenchyma.

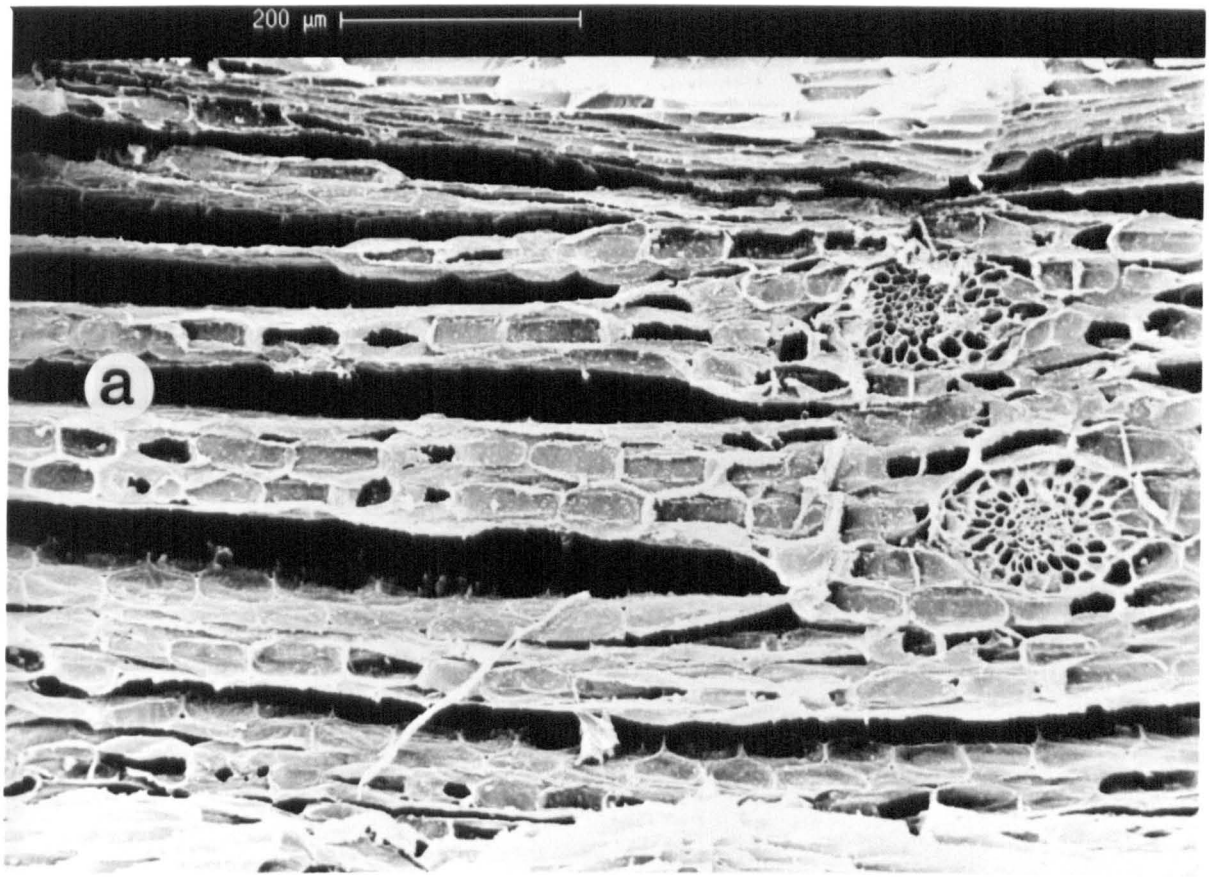
200 µm
a

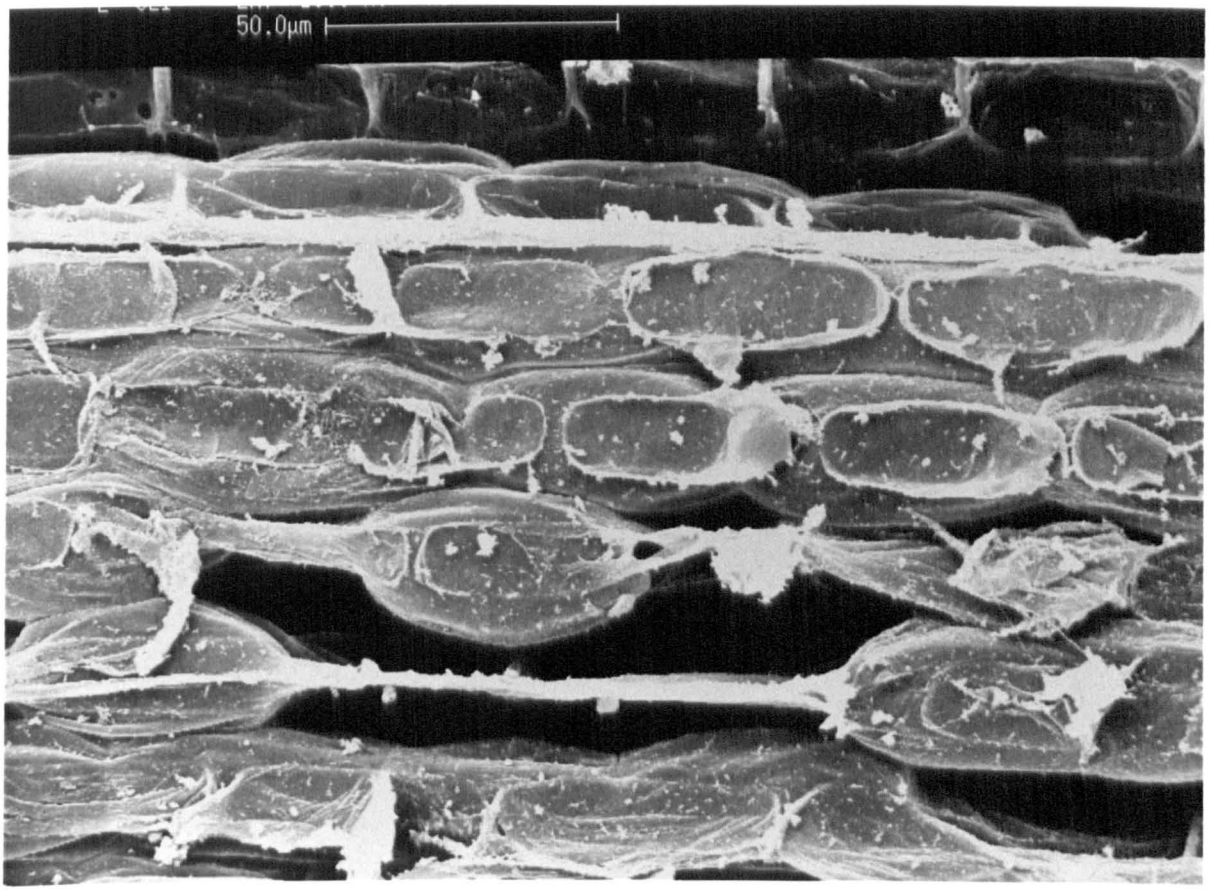
50.0µm

Fig. 3.30. Scanning electron photomicrographs :

(Above) Tangential section of basal region of adventitious root in mid-cortex showing lateral root in transverse section with epidermis complete and no obvious gas-space connexions with adventitious root cortex.

(Below) Transverse section of basal region of adventitious root showing the connexion between a lateral root and the stele. Note proximity of lateral root base to cortical aerenchyma spaces of the adventitious root.

Fig. 3.31. Scanning electron photomicrographs from tangential sections across emergent laterals close to the stele of adventitious root (length *ca.* 150 mm). Note intercellular gas-space connexion between lateral and adventitious root cortex (*cf.* Fig. 3.30).

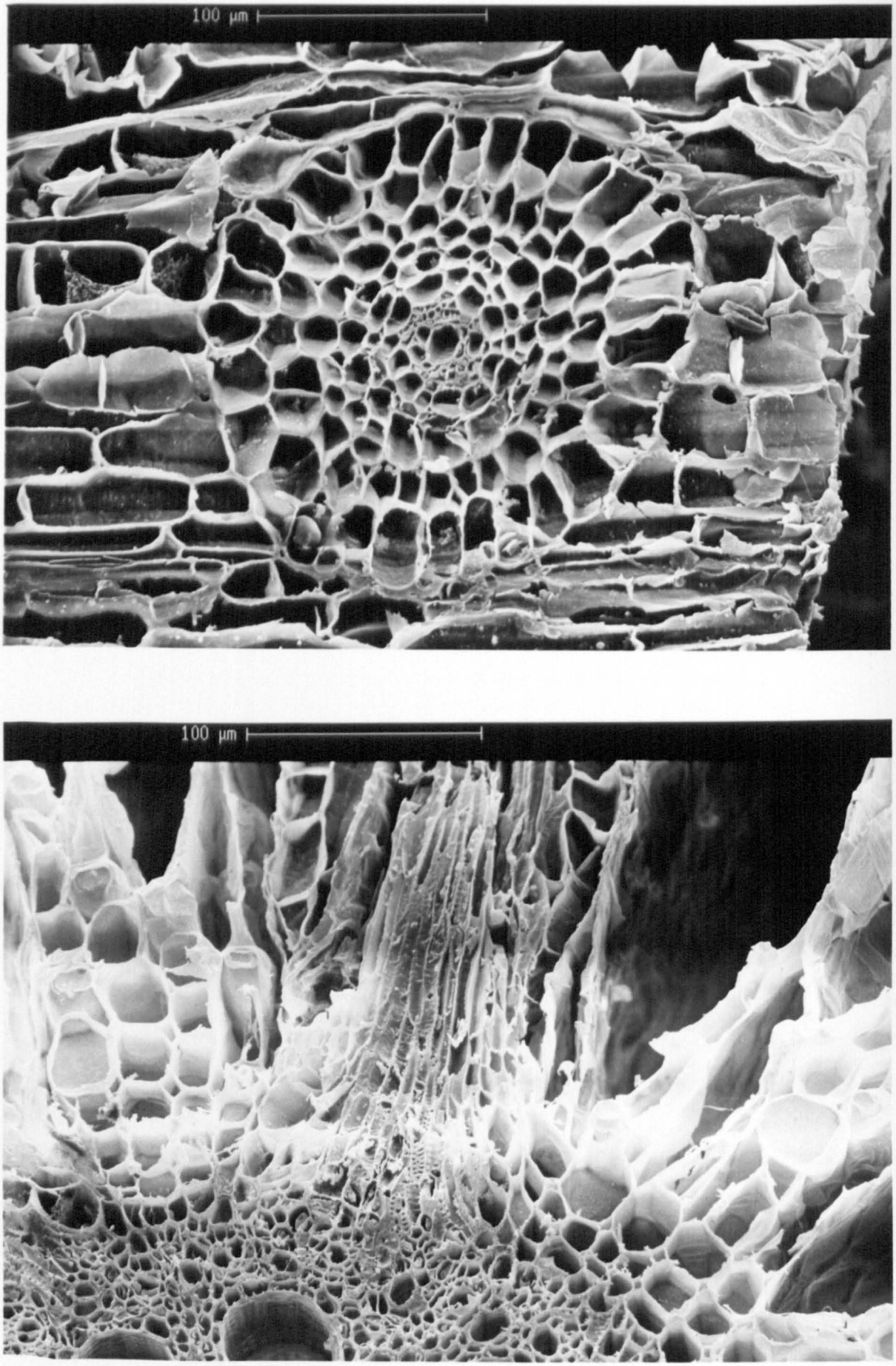

FIG.3.30

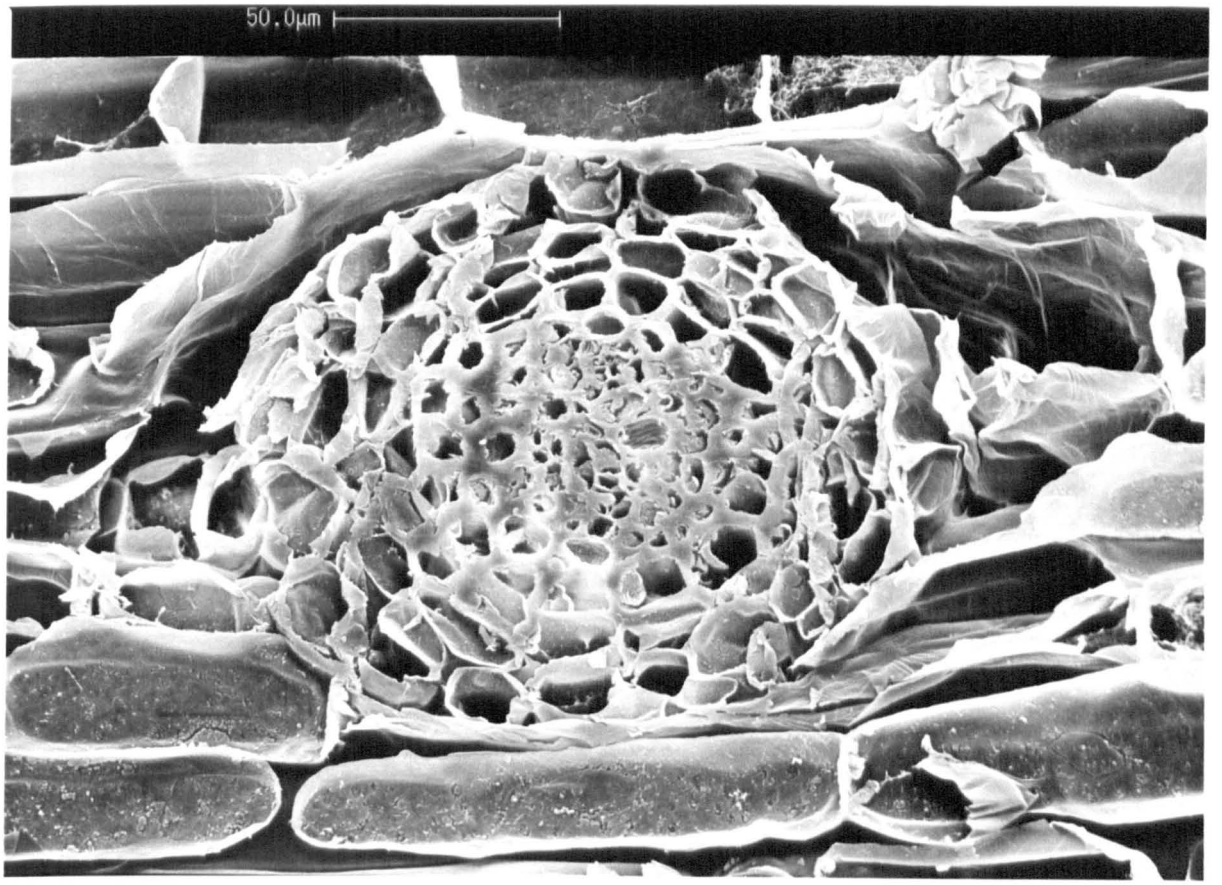

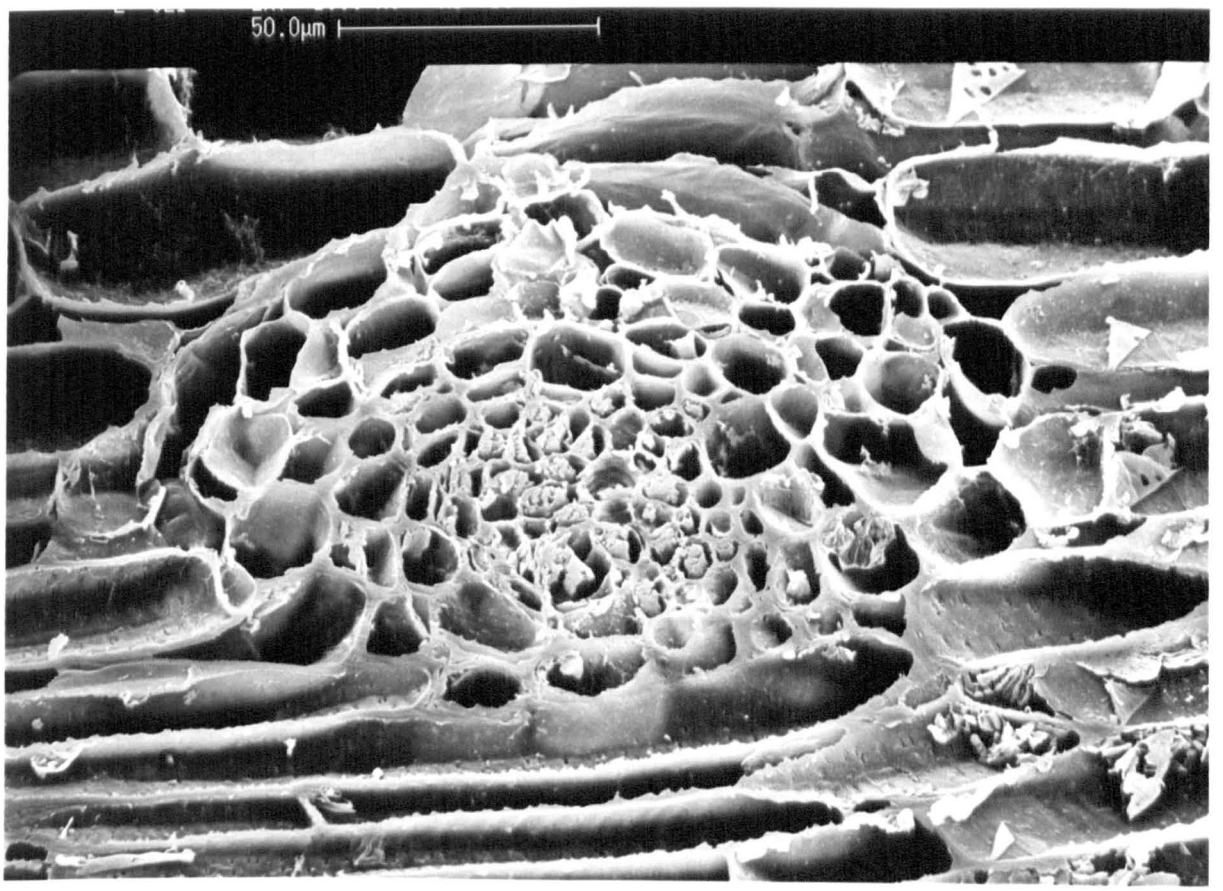

FIG. 3.31

Figure 3.32 (overleaf)

Fig. 3.32. Fresh, hand-cut, transverse sections from previously illuminated basal regions of adventitious root (length ca. 200 mm).

(a) Note chlorophyll in persistent cells between cortical aerenchyma and lack of chlorophyll in hypodermal layers and the stele. (X 140).

(b) photographed in green light showing chlorophyll fluoreacing red. (X 175).

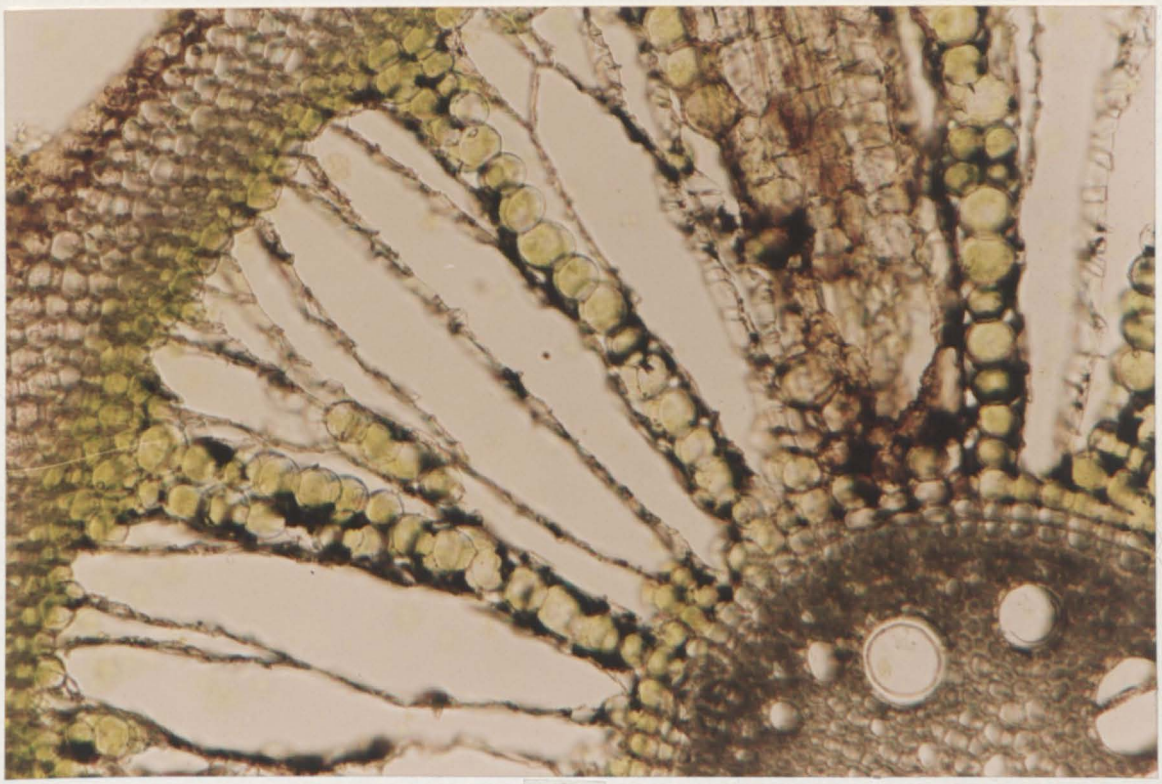

(a)

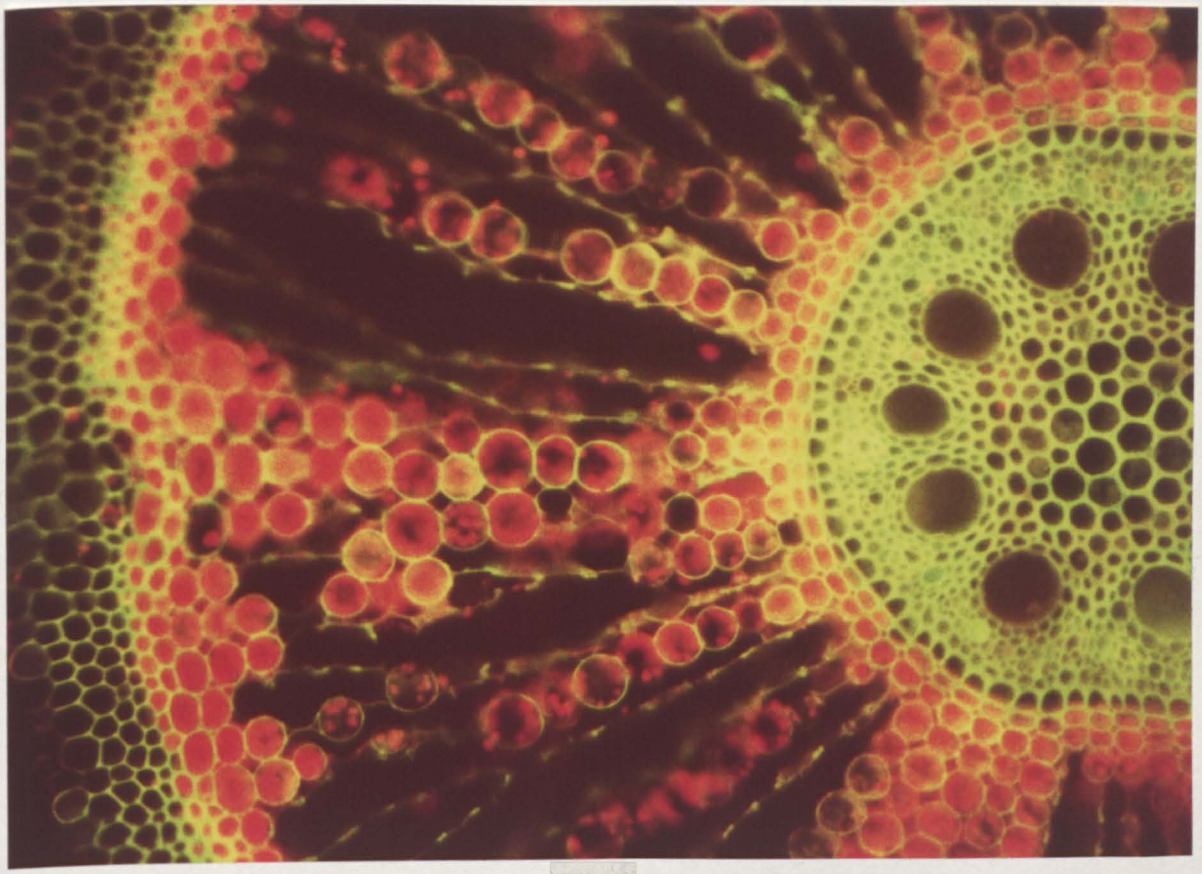

(b)

Figure 3.33 (overleaf)

Fig. 3.33.

Above. Part of tangential section of cortex of previously illuminated basal region of adventious root (length ca. 200 mm) showing lateral root in transverse section. Note chlorophyll development in cortex of lateral root and its absence from the stele, epidermis and hypodermis. (X230).

Below. Tangential section through previously illuminated basal lateral root. Note chlorophyll development in cortex and its absence from the epidermis and hypodermis. (X350).

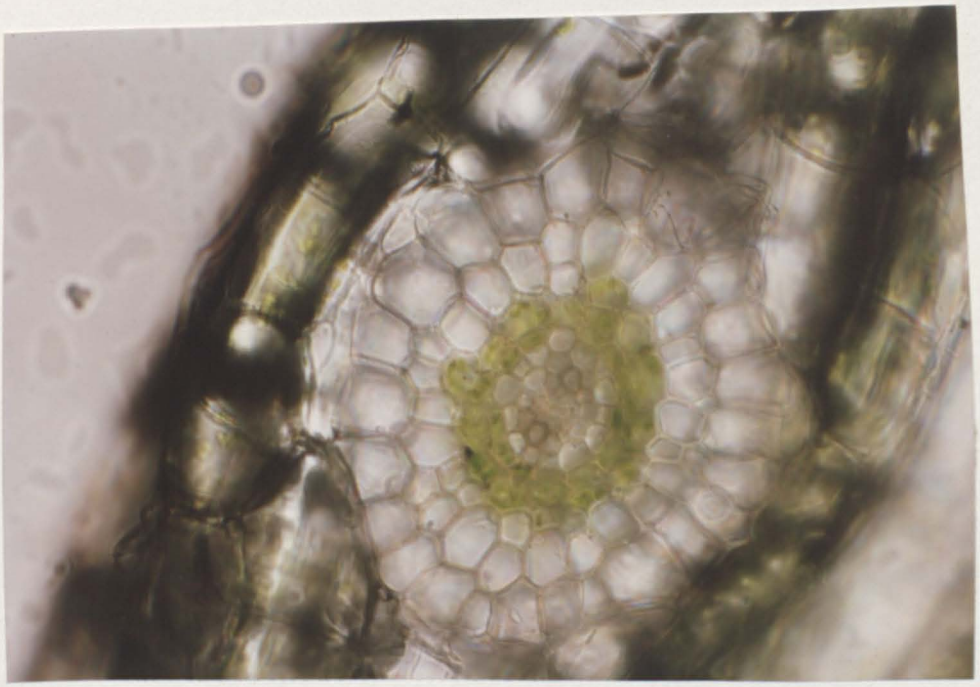

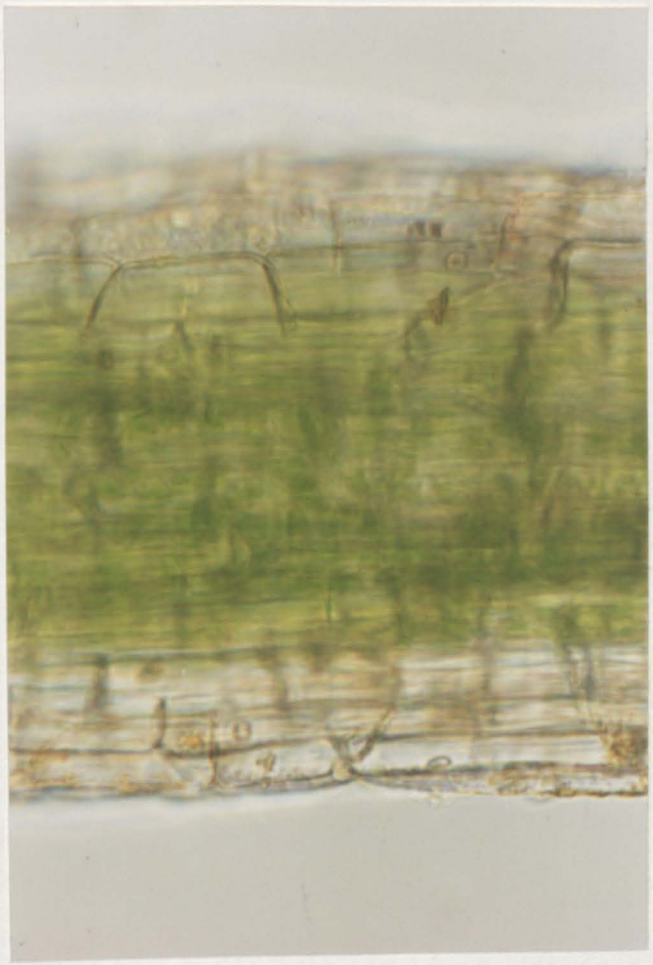

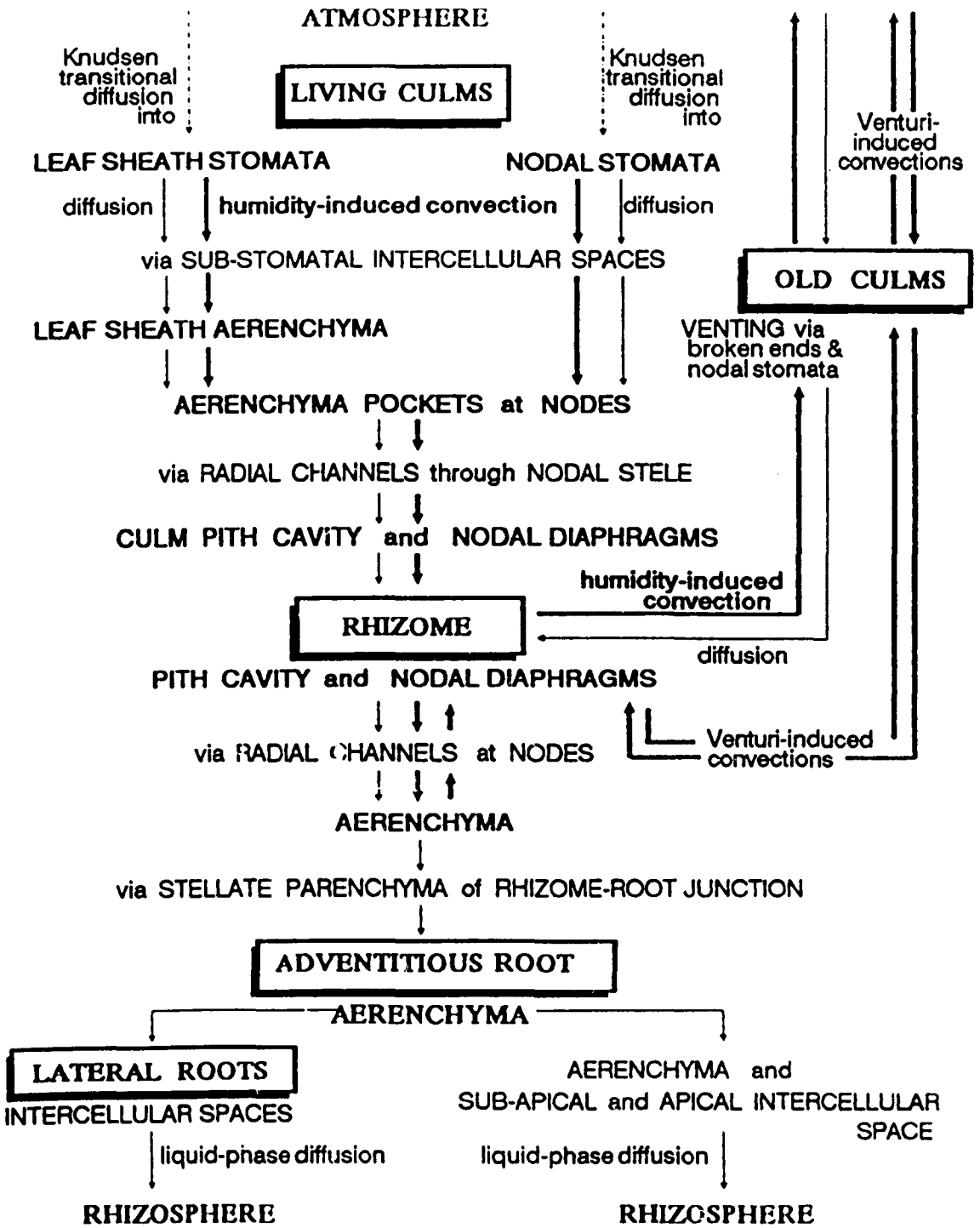

Fig. 3.34 Pathways of convection and diffusion of oxygen in *Phragmites*.

CHAPTER 4

QUALITATIVE AND QUANTITATIVE STUDIES OF OXYGEN RELEASE BY THE RHIZOME AND ROOTS OF *PHRAGMITES*

4.1 INTRODUCTION

Of major importance in the root-zone treatment of effluents by *Phragmites* beds is thought to be the extent to which the plant can maintain oxidised zones around its roots (Chapter 1). Initial attempts by Danish workers, to sample oxygen in water collected in porous pots from the rooting zone of P*hragmites* beds, failed to detect any free oxygen (Brix and Schierup *personal communication*). Hence, it was supposed that little or no oxygen diffused from these roots, and these findings in no small way appear to have led to feelings of disenchantment and a discrediting of the principles of the root-zone method by some workers. Furthermore, many beds in Denmark and in Britain were functioning sub-optimally, especially in respect of NH_4^+ removal. (It must be mentioned, however, that in many such beds, there was considerable surface run-off, so that the effluents could not reach the rooting zone of the bed.)

However, very large numbers of wetland plants are capable of sustaining oxidised rhizospheres at significant soil depths (Armstrong & Boatman, 1967; Justin & Armstrong, 1987; Laan *et al* 1989). The extensive system of large, interconnecting gas-spaces within *Phragmites*, (Sections 2.3, 3.3.2, 3.3.3, 3.3.4 & 3.4), together with the presence of highly porous rhizome-root junctions, (Section 3.3.4), suggested that this plant would probably be no exception. Concerning the Danish workers' "free oxygen" experiments, it was felt that under

such conditions one would not expect to detect any free oxygen, since it would be rapidly used up by the soil micro-organisms.

The initial experiments were qualitative, to see which parts of the plant would oxidise reduced methylene-blue dye, (MeB), in dilute aqueous agar. Attempts were also made to see which layers of the rhizome were permeable to oxygen. *Phragmites* was also planted in soil containing reduced MeB, and redox measurements were made of various regions within the soil to see the extent to which oxidised rhizospheres could be created and maintained. Also, longitudinal root profiles of radial oxygen loss, (ROL), and root surface [O_2] were obtained by polarographic methods using sleeving platinum electrodes around adventitious roots. Finally, a "circulation experiment" was designed to see if oxygen could be detected polarographically in previously deoxygenated, fresh, distilled water after it had passed over a root.

4.2. MATERIALS AND METHODS

4.2.1. *Plant material*

Horizontal rhizomes, 150-600 mm long, were placed in 20% Hoagland's solution in darkened Perspex tanks in a growth room until leafy shoots *(c.* 320-670 mm tall) were produced, and healthy adventitious roots with fine laterals were present at the shoot-bearing nodes. The growth room was maintained at approx. 20°C, day length was 18h and PAR approx. 100 μmol m^{-2} s^{-1}.

4.2.2. *Methylene-blue oxidation in agar by rhizomes and roots*

Dye solutions, prepared by dissolving either 0.012 or 0.024 g of methylene-blue per litre of agar-water medium (0.05 % w/v), were de-oxygenated by gassing with oxygen-free nitrogen, and reduced by

the addition of 0.26 g of sodium dithionite ($Na_2S_2O_4$). The dye is colourless when reduced and blue when oxidized. The blue colour is due to the presence of conjugated single and double bonds over the whole molecule, an arrangement which is absent in the reduced form (Barton & Hollis, 1979). For reduction by dithionite the reaction is:

$$MeB^+ + 2H_2O + S_2O_4^{2-} \rightleftarrows MeBH + Cl^- + 3H^+ + 2SO_3^{2-} \quad (4.01),$$

whilst the oxidation of the leucomethylene-blue by oxygen is:

$$MeBH + {}^1/_2O_2 + H^+ \rightleftarrows MeB^+ + H_2O \quad (4.02).$$

To test for oxidation by rhizomes and roots the solutions were used in Perspex vessels, kept in the dark and sealed from the air as far as possible by a rigid plastic barrier which held the plants in position (similar to the arrangement shown in Fig. 4.06b). Only the aerial shoots and cut basal ends of rhizomes were exposed to the air and a stream of nitrogen was passed between the plastic support and the liquid surface as an additional measure to prevent oxidation by the air. The presence or absence of visible oxidizing activity and the approximate radial dimensions of oxidized zones were recorded at various intervals. Quantifying the oxidation more exactly was not possible because of varying colours of oxidized halo, difficulty in estimating the exact halo boundaries and incomplete knowledge of oxidation-reduction dynamics within an oxidized zone and its boundary. Horizontal rhizomes were tested: (a) with dormant and with non-dormant tips but with no roots; (b) without tips or roots, and with windows (24 mm^2) or collars of tissue removed to test for oxygen permeability in the various tissue layers; (c) with and without aerial shoots and with new adventitious roots (2 - 170 mm), some with basal laterals; some rhizomes had old brown adventitious roots, the latter carrying several secondaries (40 - 120 mm) with tufts of fine basal laterals. (Methylene-blue oxidation was also used to test dead culms for

any sites of oxygen permeability. Each intact culm was inverted in a 4 litre measuring cylinder containing reduced MeB in aqueous agar as above with only the basal cut end emergent.)

4.2.3. Methylene-blue oxidation in soil by roots together with redox measurements.

Methylene-blue dye was added to a loam soil (1g MeB in 1200 cm^3 soil) waterlogged under 30 - 50 mm of water, and kept in an incubator at 25°C. After 3-4 weeks the soil showed no blue colouration except at the surface, showing that bacterial and chemical activity in the soil had reduced the dye to the colourless form. The soil was then transferred to a clear-sided 8-litre Perspex tank and planted with small clumps of *Phragmites* which had begun to develop shoots after transference to the laboratory. The tanks were transferred to a cool position (16-18°C) near a north-facing window, the sides of the tank were covered in black polythene, and the soil was flooded under 40 - 70 mm of water. Platinum-wire electrodes were then placed: (i) in the surface water, (ii) in the surface 7 mm of soil, (iii) near living roots, (iv) in the middle of a clump of old roots, and (v) in the soil remote from any roots. In conjunction with saturated Ag-AgCl reference half-cells, and using a high impedance electrometer, oxidation-reduction potentials (E_7, mV) at each electrode were recorded mostly at least twice a week for 12 weeks. Observations were also made on the size and colour of zones of oxidation in the soil.

4.2.4. *Radial oxygen loss from roots*

Short single-noded pieces of rhizome each bearing a shoot and roots were used. With the shoot in air and the roots in a 0.05% de-oxygenated nutrient medium, oxygen flux from the root was measured

polarographically using a cylindrical Pt-electrode (diameter 1.125 mm; length 5.0 mm) in conjunction with a Ag/AgCl anode as described by Armstrong 1979. To obtain a profile of oxygen release the electrode was moved up the root in stages starting with the 2 - 7 mm region immediately behind the apex. The equilibrium oxygen flux was recorded at each stage, the diameter of the root corresponding to each current reading was measured using a travelling vernier microscope, and from these values it was possible to calculate the rate of oxygen release (radial oxygen loss, ROL) and the concentrations of oxygen at the root surface.

The assessment of the oxygen status of roots using cylindrical platinum electrodes is given in detail elsewhere (Armstrong & Wright, 1975; Armstrong, 1979). When the cylindrical platinum electrode is drawn into place around the root; a shell of liquid of uniform thickness separates the root from the inner (reactive) electrode surface. Under an appropriate polarizing voltage the platinum acts as a sink for oxygen (the oxygen concentration at the electrode surface is effectively maintained at zero), and if the root is internally aerobic, a diffusion gradient is set up between the root and electrode. At equilibrium, the radial oxygen loss (ROL) from that part of the root lying within the electrode can be determined from the following equation:

$$Q/t = 4.974\ I_t\ /\ 60 \qquad \text{ng s}^{-1} \qquad (4.03)$$

where Q/t is the radial diffusion of oxygen from the root (Q) per unit time (t)(ng s^{-1}) and I_t is the current (μA) due to the electrolytic reduction of oxygen at equilibrium time (t). If required, the oxygen concentration, C_W, at the surface of the root can be estimated from the following equation:

$$Q/t = D_W\ A_R\ C_W\ /\ (a \log_e b/a) \qquad (4.04),$$

where D_W is the diffusion coefficient (cm^2 s^{-1}) of oxygen in the

bathing medium, A_R is the surface area of root (cm^2) within the electrode, *a*, the radius of the root (cm), *b*, the inner radius of the platinum cylinder (0.1125 cm), and C_W, the liquid-phase oxygen concentration ($g\ cm^{-3}$) at the root surface (Armstrong, 1979). The concentration C_W can subsequently be expressed as an oxygen partial pressure in kPa.

4.2.5. *Oxygen Release from Roots into a Circulating Anaerobic Water Stream*

The oxygen flux from single roots still attached to single-noded short lengths (30-100 mm) of shoot-bearing rhizomes, were measured in a circulating water system (flow rate 30 $cm^3\ min^{-1}$; velocity 6 mm s^{-1}; Fig. 4.08). The water, de-oxygenated at every cycle by passage through a N_2-primed gas-exchange system, flowed from the exchanger and over the roots to a Clark-type polarographic electrode situated in the stream just beyond the basal regions. Various adventitious roots up to 250 mm long, and with and without laterals, were monitored.

4.3. RESULTS AND DISCUSSION

4.3.1. *Methylene-blue oxidation in agar by rhizomes and roots*

The results are presented in Table 4.01 and Figs. 4.01 & 4.02. When oxygen-free nitrogen was applied to the exposed cut ends of the rhizome or rhizome-root system no long-term re-oxidation of the dye occurred. Consequently, assuming that dye re-oxidation indicates a passage of oxygen from the plant, the results suggest that the outer cuticle, epidermis and outer cortical layers prevent a leakage of oxygen from the rhizomes themselves. Also, there appears to be no significant lateral gas transport between the hollow pith and aerenchyma channels

in the internodal regions (Fig. 4.01 & Table 4.01). (The small oxidized halo developing around the stelar cylinder after two days may have indicated a change in permeability or a reduced respiratory demand of this tissue due to treatment in the dye medium.) Oxygen appears to diffuse readily from the growing tips of both horizontal and vertical rhizomes, but only to a very small degree from dormant rhizome tips. No oxygen efflux from the old brown regions of adventitious roots of the previous year could be detected, but there was clearly a ready diffusion of oxygen from the surfaces of young adventitious roots and from basal laterals (Fig. 4.02). Indeed, the extent of the oxidation around the laterals seems to indicate that these zones may effect the greatest release of oxygen from the rhizome-root system in *Phragmites.*

These results are consistent with anatomical findings which indicate oxygen impermeability of the rhizome wall due to cuticularisation and suberisation (Section 3.3.3), and of the adventitious root hypodermal layers due to suberisation and lignification (Section 3.3.4). The results also agree with the applied pressure experiments (Section 2.3), which showed small gas bubbles emerging from the growing tips of rhizomes. On the other hand, it is to be concluded that the lack of lignification and suberisation in the outer layers of young parts of adventitious roots and in the outer layers of the laterals is probably responsible for these parts being permeable to ROL. The very prominent and coalescing oxidised halos (Fig. 4.02b) around the fine laterals suggest that these roots, could be very important in the root-zone treatment of effluents. The rather rapid development of oxidised halos around these roots when the aerial parts are in air is consistent with the presence of pathways of high porosity linking the atmosphere with the aerial shoots, rhizomes and roots.

Oxidised halos only appeared around the nodal stomatal regions

Table 4.01 *Oxidation of reduced methylene-blue by rhizome and roots*

Region of plant showing oxidation	Approx. radial thickness of oxidized halo (mm)	Time
(i) Dormant horizontal rhizome: apical 1–3 cm	1–2	24 h
(ii) Growing horizontal rhizome: apical 1·5 cm	1	20 min
	5	2 h
	8	24 h
(iii) Windows cut in horizontal rhizome wall		
(*a*) Outer cuticle and epidermis only removed	0	24 h
(*b*) Epidermis + 2–3 layers of outer cortical tissue removed	0	24 h
(*c*) Most of tissue external to aerenchyma channels removed	1	2 h
	4	24 h
(*d*) Outer tangential wall of aerenchyma + tissues external to them removed	2	1 h
	8	24 h
(*e*) Submerged cut end of rhizome	2	1 h
	8	24 h
(vi) (*a*) Horizontal rhizome: collar of tissue removed including all aerenchyma tissue (cut ends of aerenchyma sealed with lanolin)	0	24 h
	1	48 h
(*b*) Submerged cut end of rhizome	7	24 h
(v) The root system		
(*a*) Thick brown adventitious roots of previous year	0	12 h
(*b*) Young adventitious roots	1–2	15 min
	4	1·5 h
(*c*) Secondaries:		
main root	2	15 min
	4	1·5 h
region of basal laterals	1–2	15 min
	10	1·5 h

In all cases the dye remained colourless round all other regions of the rhizomes. It was noted that as soon as an adventitious root emerged from the rhizome, it produced a zone of oxidation; prior to emergence, no oxidation was visible. The halos produced in the zones of basal laterals were deeper in colour than those around the adventitious roots. In the early stages of oxidation (15 min) there appeared to be a colourless halo around the main secondary root in the zone of basal laterals. This gradually disappeared as oxidation by the laterals increased.

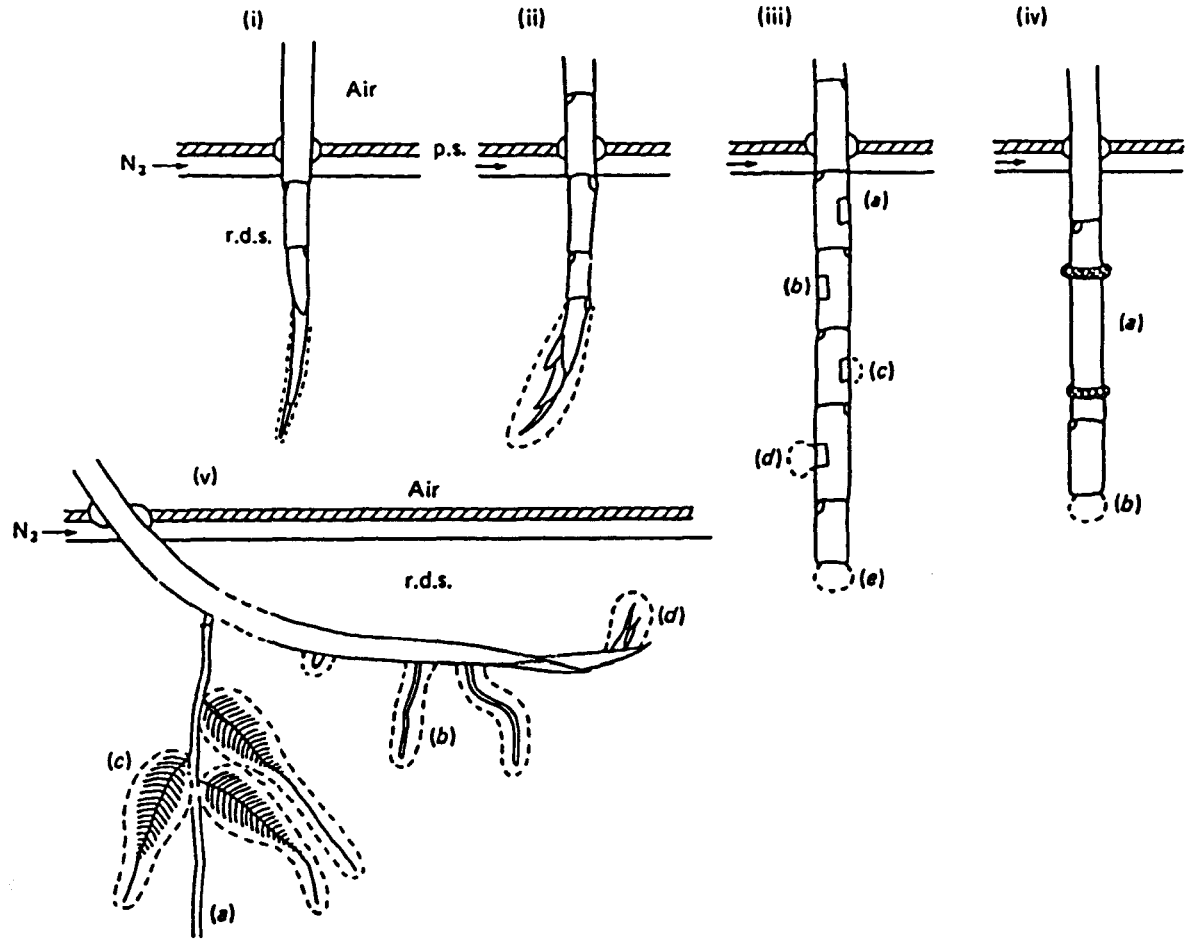

Fig. 4.01 The patterns of methylene-blue oxidation around horizontal rhizomes and roots. Zones of oxidation are indicated by broken lines. (i) Dormant rhizome apex (24 h), (ii) Growing rhizome apex (24 h), (iii) Oxidation at 'windows' cut from horizontal rhizome (24 h): (*a*) cuticle and epidermis removed; (*b*) epidermis and outer 2–3 layers of cortical cells removed; (*c*) epidermis and most of cortex external to aerenchyma removed; (*d*) all cortex external to aerenchyma removed; (*e*) end of rhizome removed, (iv) (*a*) Collar of cortical tissue including aerenchyma removed (24 h); (*b*) cut end of rhizome (24 h). (v) Oxidation around roots and growing rhizome apex (1·5 h): (*a*) old adventitious root; (*b*) young adventitious roots; (*c*) secondaries and tufts of basal laterals; (*d*) growing rhizome apex (very pale). p.s., plastic support; r.d.s., reduced dye solution.

Figure 4.02 (overleaf)

Fig. 4.02. Oxidation of reduced methylene-blue dye in dilute agar by young adventitious roots and their laterals. Note the lack of oxidised halos around old brown parts of adventitious roots in (a), and around the rhizomes in (a) & (b). In (a) the medium contained 0.012g MeB l^{-1} of medium and photograph was taken after 45 min of oxidation. In (b) the medium contained 0.024g MeB l^{-1} of medium and the photograph was taken after 2 h.

FIG. 4.02

(a)

(b)

of the partially submerged culms, suggesting that for intact senescent culms, these will be the only points at which oxygen would normally enter.

4.3.2. *Dye oxidation and redox measurements in soil*

The development of oxidation-reduction potentials at the various electrodes over a period of twelve weeks is shown in Fig. 4.05. The intitial potentials in the soil were approx. -100 mV. Subsequent changes in potentials were as follows.

One month after planting the mosaic in the soil of oxidised zones around the roots, and clay coloured reduced zones, together with blackened reduced parts (possibly because of the presence of FeII sulphide), was as shown in Fig. 4.03.

Surface water and top 7 mm of soil. Here conditions had become considerably oxidising after 4-weeks: +600-630 mV, and remained at these values throughout the experiment. The dye in the surface layer of soil became blue and oxidised to a depth of 5-7 mm within the first week and remained so until the end of the experiment. The water, although at a high redox potential, remained colourless, the dye having been absorbed by the soil.

Living roots. After two-weeks, where new roots were developing, conditions were obviously less reducing (+100 mV). Within the oxidised halos of the rhizospheres, they had risen to +530 mV after 3½ weeks, and remained so until the 6th week. In effect, this represented a raising of the redox potential by *ca.* 800 mV relative to the surrounding soil. Blue halos were present around the young adventitious roots, and were especially extensive around the zones of fine laterals where they reached maximum diameters of 20-30 mm after

Figure 4.03 (overleaf)

Fig. 4.03. Waterlogged soil covered by 40–70 mm of water and containing 1g of MeB in 1.2 litres of soil planted with *Phragmites*, and photographed after 4 weeks. Note the mosaic of oxidised and reduced zones within the soil, with blue oxidised halos around young adventitious roots and their laterals (redox = +530 mV), and the blue oxidised soil surface (redox = *ca.* +600 mV). Redox potentials in the regions remote from the roots where the dye remains in the reduced form *were ca.* -270 mV.

FIG. 4.03

Figure 4.04 (overleaf)

Fig. 4.04.

(a) Close up view from Fig. 4.03 of rhizosphere oxidation at 4 weeks after planting. The orange precipitate close to the adventitious root is probably composed of hydrated iron III oxides.

(b) The same root from (a) photographed 12 weeks after planting when the shoots had died and probably this root also. Note that the blue halo has disappeared (redox now *ca.* -80 mV).

(a)

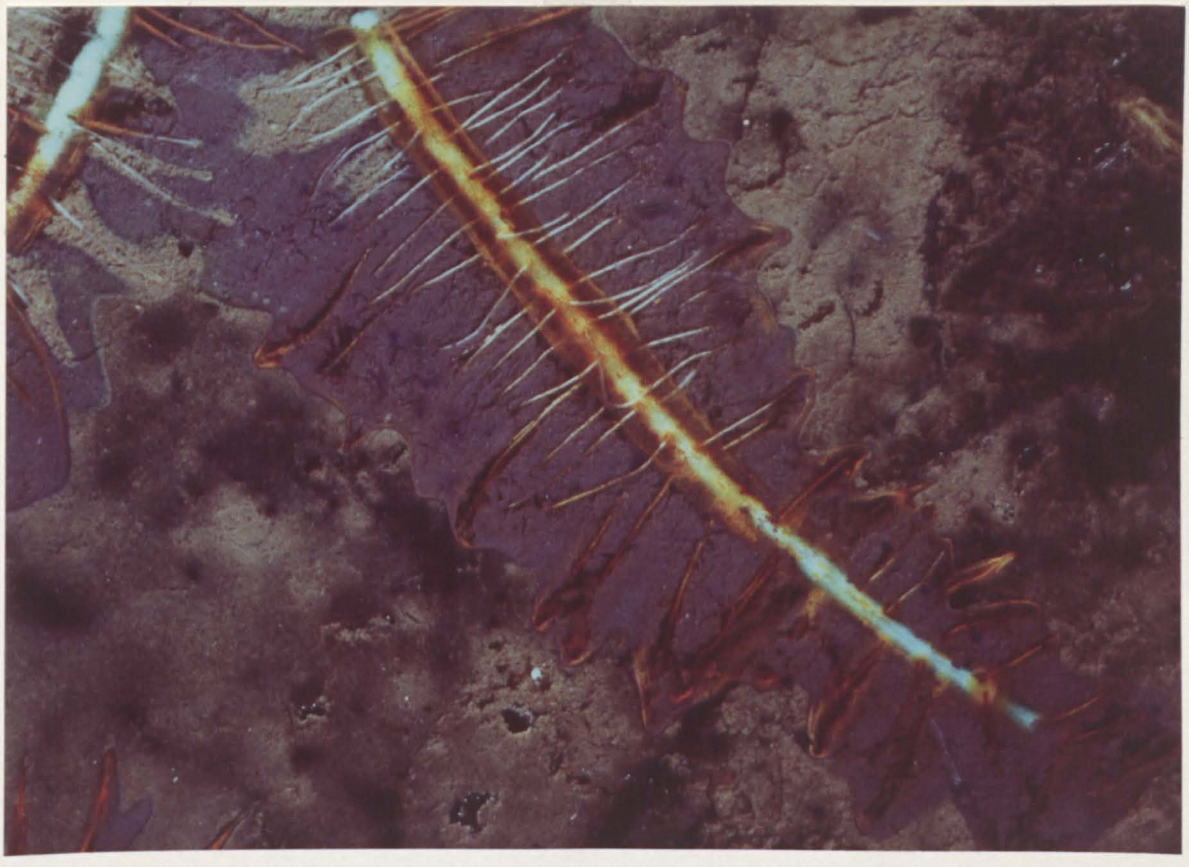

(b)

FIG. 4.04

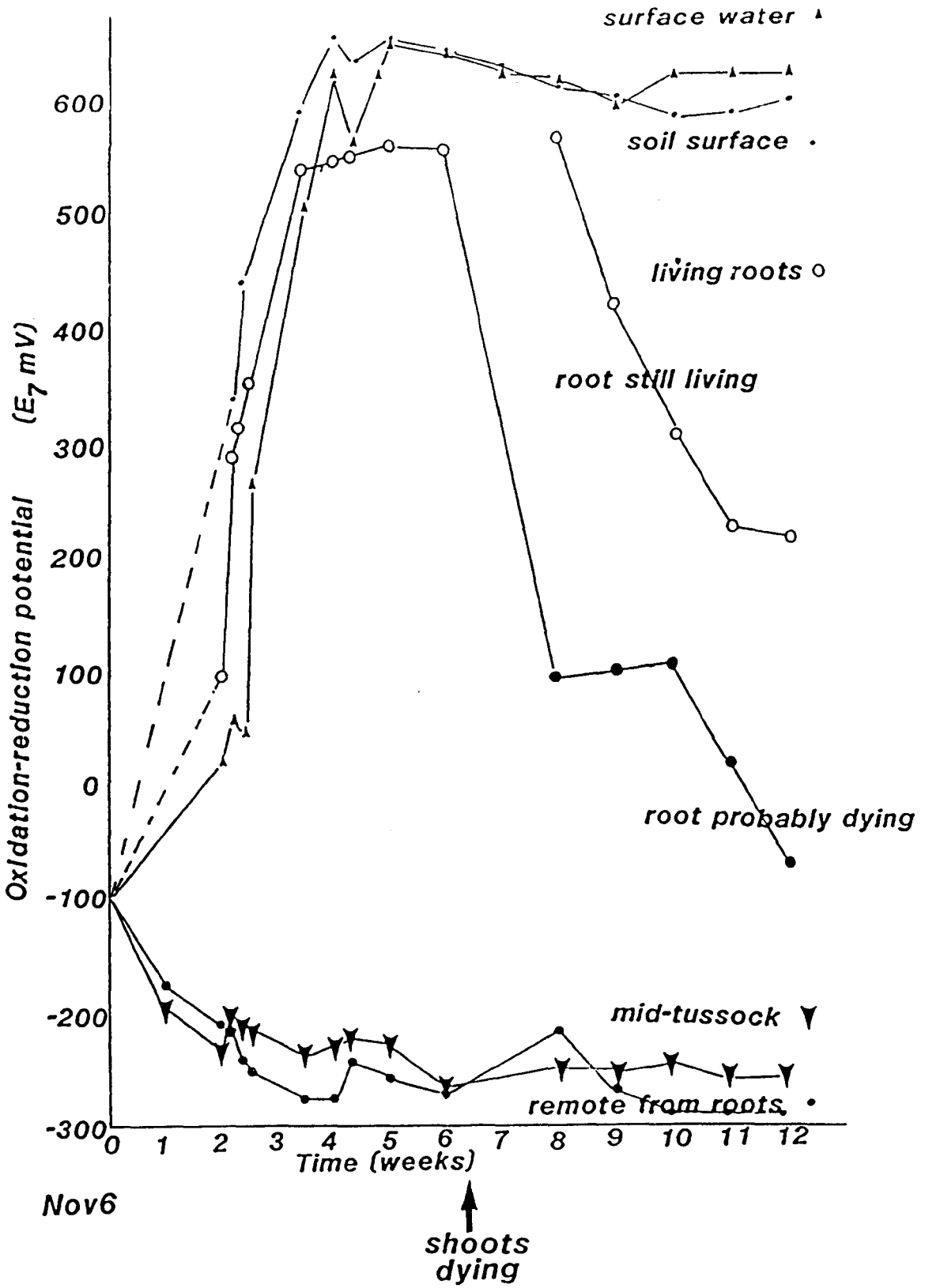

Fig. 4.05

Changes in Oxidation–Reduction Potential in Soil Planted with Phragmites

6-8 weeks (Fig. 4.04a).

At around 6 weeks the shoots began to senesce, the result of a combination of aphid damage and winter temperatures and lighting. Coincident with this die-back, potentials around some roots had fallen to +100 mV after 8-9 weeks, and after 12 weeks were *c.* -80 mV with the halos clearly fading; in some cases, the halos had completely disappeared (Fig. 4.04b), and potentials were -200mV. Here, the lateral roots were clearly dying and the surfaces of the parent roots had probably lost much of their permeability to oxygen. However, around many other roots the blue halos persisted, although they had decreased somewhat in diameter at 12 weeks and were paler; here, the laterals still appeared healthy and potentials were at +212 - 230 mV. Zones of yellow hydrated FeIII-oxides at the rhizosphere boundary of adventitious roots and laterals provided further evidence of the root oxidising activities; by twelve weeks, there was also iron oxide deposition on some root surfaces which again probably indicated a substantial reduction in root wall oxygen permeability (Armstrong 1967). As in other dye-oxidation experiments (Armstrong & Armstrong 1988), at no time did oxidation occur at the rhizome surface.

Old dead roots and soil remote from roots. After 2-weeks, conditions had become more intensely reducing (-200 to -300 mV), and the values stayed very low throughout the experiment. No dye oxidation occurred in these regions, the soil remained buff-coloured, and decaying roots showed up as black zones.

4.3.3. *Radial oxygen loss from adventitious roots*

A typical profile of root surface oxygen for a young adventitious root, transformed from measurements of the radial oxygen loss to a cylindrical Pt-electrode, is shown in Fig. 4.07. It can be seen that ROL

Figure 4.06 (overleaf)

Fig. 4.06.

(a) Clear-sided Perspex tank used for growing and experimenting on *Phragmites* plants, showing horizontal rhizomes and architecture of adventitious roots and laterals.

(b) Some of the apparatus for measuring ROL polarographically using cylindrical Pt-electrodes sleeving the sub-apical regions of adventitious roots. Pt-wire electrodes were placed among lateral roots and in the medium remote from the roots.

(a)

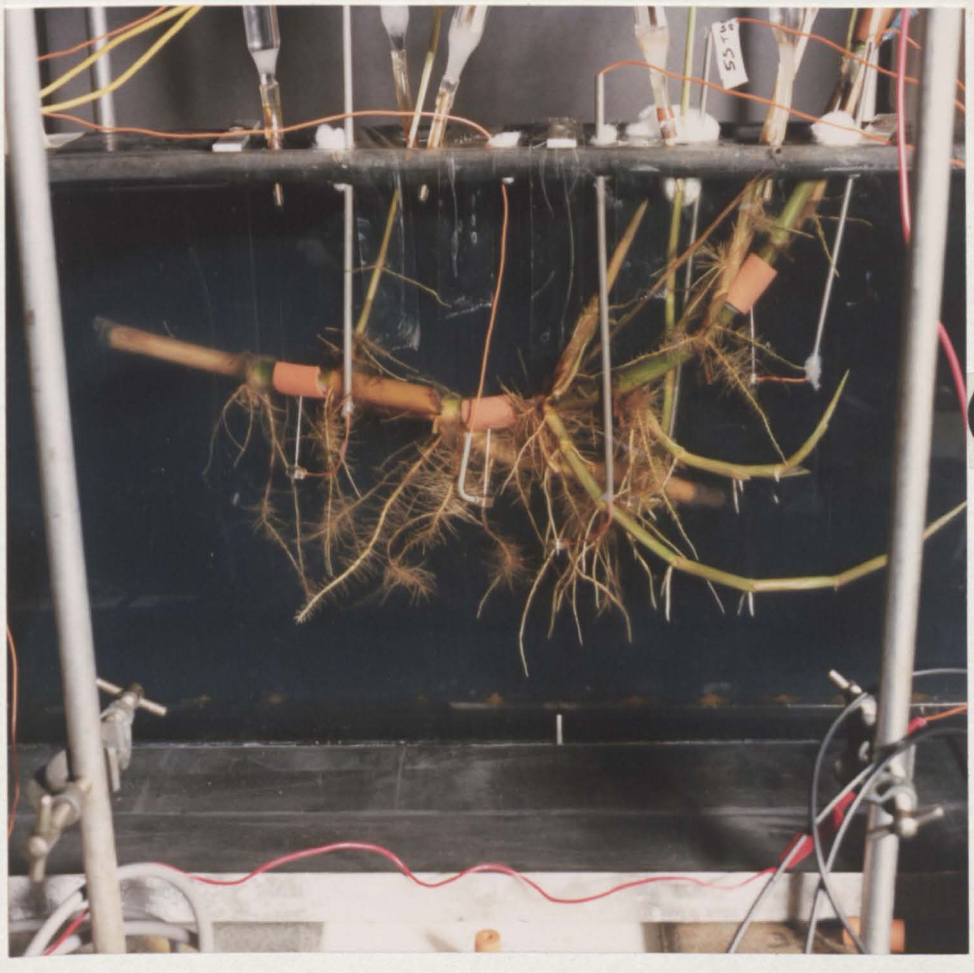

(b)

FIG. 4.06

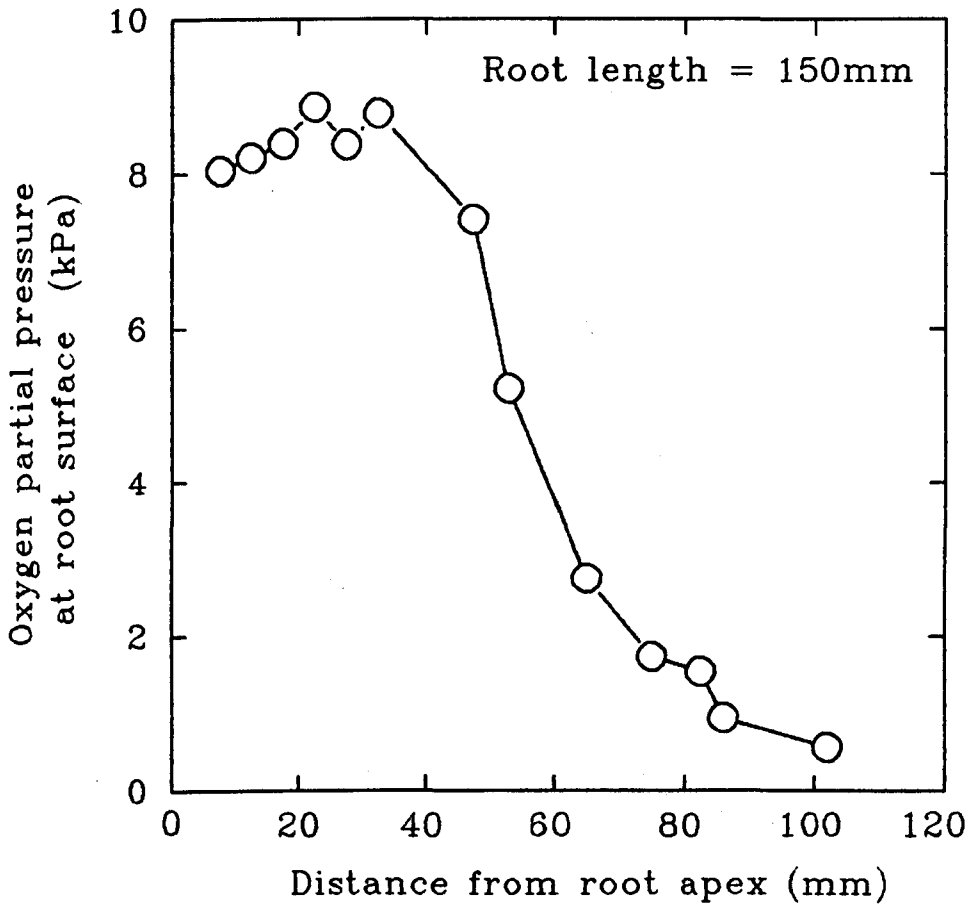

Fig. 4.07. Typical root surface oxygen profile for young adventitious root. Note that apical regions are more permeable to ROL than those greater than 50 mm from the apex..

begins to decrease markedly at 40 - 50 mm from the apex, and that there is very little ROL from the basal region. These observations are consistent with anatomical findings of increased lignification and subserisation of the hypodermal layers a few centimetres behind the apex (Section 3.3.4), and with the inability of old brown basal regions of adventitious roots to oxidise methylene-blue (Section 4.3). Also, in Sections 5.3.1.5 & 5.3.1.7, it is shown polarographically that oxygen diffuses readily from the basal laterals. The significance of this pattern of ROL from adventitious roots which has been found in other wetland plants e.g. rice and *Eriophorum angustifolium* (Armstrong, 1971; Gaynard & Armstrong, 1987) is discussed in Section 8.2.2.

4.3.4. *Oxygen release to streaming de-oxygenated waters*

It is not an easy matter to measure the full potential for oxygen release to anaerobic media from whole root systems, or even individual roots. If root systems are immersed in a stagnant or stirred oxygen-free medium, the rate of oxygen release will be at a maximum for a relatively short period only. Thereafter, diminishing concentration gradients between root and medium will reduce the net release. Also, if the water is stirred, the oxygen released from one part of the root system may readily be absorbed again by another. The circulation system described in the methods section was designed to mimick a strong and constant soil oxygen sink on individual adventitious roots and any attached laterals: the streaming velocity of *c.* 6 mm s^{-1} should have imposed a very thin diffusion boundary layer (≥150 μm; Madsen, 1984) between the root surface and the anoxic oxygen-depleting stream, and also there was restricted opportunity for the released oxygen to be re-absorbed elsewhere. Since the roots were attached to short lengths of rhizome, the cut ends of which were in contact with the

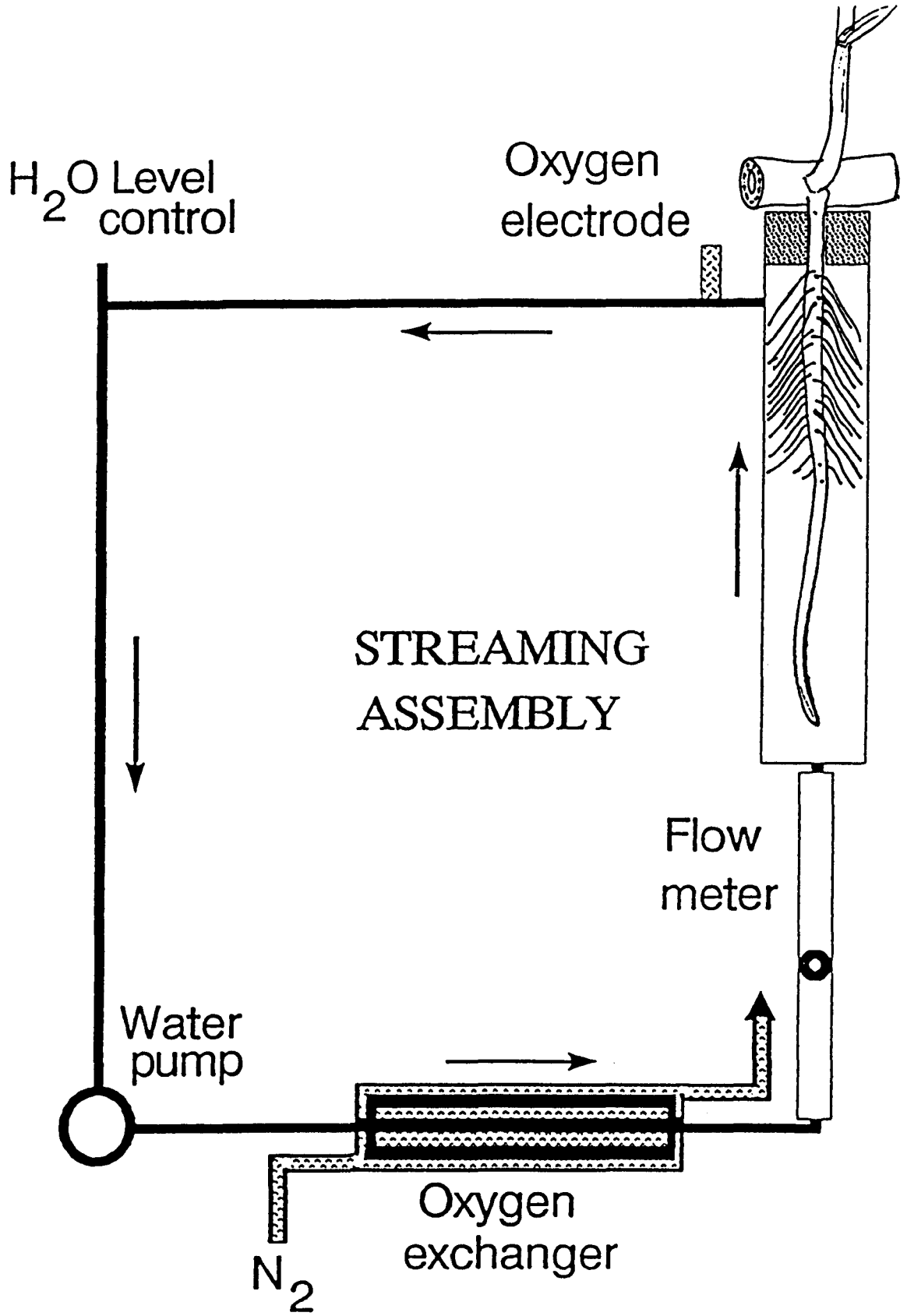

FIG. 4.08 Apparatus for measuring oxygen release from Phragmites roots into a stream of deoxygenated water

atmosphere, it can be assumed that the oxygen concentrations within the root-shoot junctions will have been at approximately 20.5%. A radial path length of 150 μm from root to sink could equate with a soil oxygen demand of 1500 ng cm^{-3} s^{-1} (130 g O_2 l^{-1} d^{-1}) around lateral roots, and *ca.* 750 ng cm^{-3} s^{-1} around adventitious roots. Since the laterals were orientated at 90° to the water stream, however, it is likely that boundary layers will have been much thicker than 150 μm in the shadows of the roots, and the oxygen demand perhaps much less than the above figure.

The individual roots, which ranged in length from *ca.* 100 - 250 mm, and bore varying numbers and lengths of laterals, released between 2.7 and 6.7 x 10^{-6} g O_2 min^{-1} to the water stream. Translated to the field situation on the assumption of 150 shoots m^{-2} and 10 adventitious roots per shoot, then, if over a twenty-four hour period, oxygen at the root-shoot junction were to average 17%, the potential for oxygen release from roots to sediment would amount to 5 - 12 g O_2 m^{-2} d^{-1}.

4.4 FINAL COMMENTS

The diffusion of oxygen from the young parts of adventitious roots and their laterals has been demonstrated by MeB dye oxidation and by polarographic methods. In the root-zone treatment of wastewaters it seems likely that such roots, especially the fine laterals are important. It was also obvious that these roots can locally raise considerably the redox state of a reduced, waterlogged soil so that a mosaic of oxidised and reduced regions is created in which bacterial oxidation reactions (*e.g.* $NH_4^+ \rightarrow NO_2^- \rightarrow NO_3^-$), and bacterial reducing reactions (*e.g.* $NO_3^- \rightarrow NO_2^- \rightarrow N_2O$ & N_2) could be respectively promoted. The results thus

accord with the findings of Hansen & Andersen (1981), and the more recent results of Geller *et al* (1990) and Hofmann (1990).

However, the extents to which root ROL and soil oxidations occur in winter must depend upon the survival of the roots, the degree to which they remain permeable to ROL, and upon the degree of rhizome aeration. The latter is discussed in Section 7.4. In winter these effects may be somewhat diminished compared to summer values and more research is needed to investigate the winter condition as this has an important bearing on overall reed-bed performance.

Furthermore, the extent to which the oxygen diffusing from the roots is available for the effluent treatment is still the subject of controversy. It seems certain that some of this oxygen will be used in the soil in processes which are not connected with the sewage treatment *e.g.* in the degradation of the dead parts of the plant itself. Even without the input of waste-waters a reed-bed must have its own intrinsic BOD. Also, the degree to which the roots, especially the laterals, will tolerate additional BOD and phytotoxins in the form of various concentrations of waste-waters urgently needs clarification. In the stagnant system, as described in this chapter, the roots produced persistent oxidised rhizospheres, but in a "moving liquid regime" the situation would be different as the roots would be exposed to greater concentrations of reductants and phytotoxins.

Both the dye-oxidation and redox measurements in the soil provided evidence of atmospheric oxidation of the surface layers of the rooting medium. This occurred in the soil even when the soil surface was submerged. In a reed-bed the relative amounts of oxygen contributed directly by the atmosphere and by the roots needs to be clarified. Already there is some enthusiasm for "vertical-flow" treatment beds which make greater use of the direct atmospheric contribution

(Cooper & Findlater 1990).

In Chapter 8 attempts are made to quantify by mathematical modelling the amounts of oxygen passing out of the root system and through the soil surface. The extent to which these quantities may satisfy the effluent's demands are discussed in the final chapter.

4.5. SUMMARY

Oxygen release from rhizome and roots was studied qualitatively by means of experiments involving methylene-blue dye oxidation. Only the tips of growing rhizomes, the young parts of adventitious roots, and lateral roots showed oxidising capacity.

Quantitatively, oxidising activity was studied in soil by taking redox potential measurements. The young parts of adventitious roots and the basal laterals were capable of considerably raising locally the redox potential of an anaerobic soil and maintaining it at a value >800 mV above that of the surrounding soil. This produced a mosaic of oxidising and reducing zones in the soil.

In an aqueous medium, polarographic measurements of radial oxygen loss profiles along young adventitious roots indicated that the oxygen permeability in apical and sub-apical regions was much greater than in the basal parts.

Oxygen release to streaming de-oxygenated water as it passed over young adventitious roots bearing laterals was also measured polarographically. The individual roots, which ranged in length from *ca.* 100 - 250 mm, and bore varying numbers and lengths of laterals, released between 2.7 and 6.7 x 10^{-6} g O_2 min^{-1} to the water stream. These figures were used to estimate the potential for oxygen release to anaerobic sediments.

CHAPTER 5

HUMIDITY-INDUCED CONVECTIVE GASEOUS THROUGHFLOW AND ITS EFFECT ON RHIZOME AND ROOT AERATION.

5.1. INTRODUCTION

Until quite recently it had been generally assumed that the only significant ventilating mechanism in wetland plants was the reciprocating gas-phase *diffusion* of oxygen and carbon dioxide through the interconnecting aerenchyma and the non-aerenchymatous intercellular cortical gas-spaces of shoot and root. Bulk-flows of gas were not unknown *e.g.* the inrush of air into mangrove root systems exposed on the ebb-tide (Scholander *et al.* 1955), but it was not appreciated that *convection* might *often* play a significant role in the aeration process.

The first recent reports of a *throughflow* convection in plants were those of Dacey (1980, 1981) and Dacey and Klug (1982a,b). Using the water-lily *Nuphar lutea*, they noted the following: (i) small, but significantly raised gas pressures, (up to 250 Pa), in the youngest emergent leaves during daylight hours, (and sometimes also at night, if lake waters were warm; Dacey and Klug 1982b), (ii) an inflow of gases from the atmosphere into these leaves (the influx leaves) against the pressure gradient, (iii) by means of an ethane tracer gas, a convection from these *influx* leaves to rhizome and back to the atmosphere through older, more mature (and more porous) *efflux* leaves, and (iv) that there was a diurnal rhythm to the flow: flows increased from near zero at dawn, peaked around mid-day and declined again to ca. zero at dusk. The convective flows at mid-day were particularly impressive

with petiolar velocities from the *influx* leaves of up to 50 cm min^{-1} (volume flux: 60 ml min^{-1}) and, except for the higher water-vapour (humidity) in the gas of the midrib of these *influx* leaves, there was no measurable difference between the composition of the lacunar gases and the atmosphere. Isotope studies confirmed that most of the oxygen in the flow originated in the external atmosphere and not from photosynthesis, and integrated predictions from the pressure: flow data indicated that 22 litres of air (4.6 litres of oxygen) could be moved down a single petiole during the hours of daylight.

There have also been reports of convective flows in *Nymphoides peltata* (Grosse and Mevi-Schutz 1987), and the Lotus - *Nelumbo nucifera* (Dacey 1987; Mevi-Schutz and Grosse 1988a,b), and during the present study very substantial flows from the leaves of *Nymphaea alba* have been observed (Armstrong *et al* 1990b). ***Throughflow*** in *Nelumbo is* particularly interesting, with *influx* and *efflux* apparently occurring within the same leaf, (Dacey, 1987; Mevi-Schutz and Grosse, 1988a). Air is thought to enter the leaf across the expanse of the lamina, and petiolar *influx* channels transport the gases to the rhizome. *Efflux* channels in the same petiole transport the venting gases back to the atmosphere via a highly porous disc-like region at the centre of the lamina directly above the petiole. The only data available on the rates of convection in *Nelumbo* are those of Mevi-Schutz and Grosse (1988a), who estimated volume fluxes as 10 cm^3 min^{-1}. Although this is somewhat lower than the maxima of 60 ml min^{-1} reported by Dacey for *Nuphar*, it is nevertheless a substantial flow and translates into a petiolar velocity of ca. 30 cm min^{-1}, a quite similar figure to the petiolar velocities of Dacey. During the present study, using soap-film flowmeters, flows of 50 cm min^{-1} (15 cm^3 min^{-1}) in *Nymphaea* were detected. However, if convection is deliberately blocked, younger leaves may develop higher

static pressures than older, more expanded leaves, but the potential for convection from the older leaves is greater and in proportion to their greater area. Also, whereas an infra-red light source enhances convection, considerable flows can still develop in darkness provided that the atmosphere is moving and is relatively dry. It can be deduced from equation (2.03), that provided the resistance to convection through the plants is low, the "dynamic" pressures developed in the *influx* leaves will be, and only need to be, small to drive appreciable flows.

The anatomical studies on the interconnecting and extensive gas-space system within the culm, rhizomes and roots of ***Phragmites australis*** (Cav.) Trin. ex Steud., reported in Chapter 3 and elsewhere (Armstrong and Armstrong, 1988), and pressurised gas-flow studies (Chapter 2 and Armstrong *et al.*, 1988) led to the suspicion that a ***convective throughflow*** of gases might occur here as in *Nuphar*.

The experiments reported below established that convective throughflows do indeed occur in *Phragmites* (see also Armstrong & Armstrong 1987, 1990a, 1991; Armstrong, Armstrong & Beckett 1990a, 1992). The chapter describes the procedures used for investigating convective throughflows in *Phragmites* in the laboratory, and under varying conditions of illumination, temperature and humidity in the field, and it is shown that *throughflow convection* substantially increases rhizome aeration and root radial oxygen loss.

In *Phragmites* convective flow can be driven in a variety of ways: by an isothermal (or thermally-enhanced) ***humidity-induced*** Knudsen diffusion (or transitional Knudsen diffusion) of atmospheric gases into the plant, by ***thermal transpiration*** (Reynolds, 1879; Mason and Evans, 1969), and by ***Venturi effects*** (Chapter 6). Photosynthetic oxygen production from the fixation of carbon sources from the

transpiration stream may be also be involved to a minor extent (Brix 1988). Convection has been found to be particularly rapid under conditions of low atmospheric humidity and warm, sunny conditions (Armstrong & Armstrong 1990a, 1991; Armstrong *et al*, 1990a). It is shown in this chapter that the major mechanism driving the flows under these conditions is the process which may be described as *humidity-induced convection* (HIC). Probably supplementing this to a certain extent is the process known as *thermal transpiration* (Reynolds 1879); both mechanisms are further investigated and discussed in Chapter 6.

A ***non-throughflow convection*** is also known to occur in *Phragmites* and other plants. It is driven by a pressure deficit caused by respiratory carbon dioxide dissolving in the soil water (Raskin & Kende, 1983, 1985; Brix 1988; Koncalova, Porkorny & Kvet 1988). However, it has been demonstrated recently that this fails to support root aeration adequately, and that diffusion contributes at least 80 % of the oxygen transported (Beckett *et al.*, 1988).

5.2. MATERIALS AND METHODS

5.2.1. *Plant material*

This was of three types:

(a) Horizontal rhizomes, 150-600 mm long, were placed in 20% Hoagland's solution in covered clear perspex tanks near the laboratory windows or in a growth room until leafy shoots (320-670 mm) and adventitious roots with laterals had been produced. The temperature was maintained at *ca.*20°C; daylength was 16 h and the maximum PAR was *ca.* 100 μmol m^{-2} s^{-1}.

(b) Horizontal rhizomes (length 100-400mm) with living roots and

bearing autumn culms (1-2 m) with dead leaf sheaths and laminae, but with the basal 5-6 internodes still green, were collected in the field and transferred to the laboratory for immediate use.

(c) Leafy culms (1-2 m) *in situ* in the field, or excised and used immediately in the field.

5.2.2 *Measurement of convective flow and static pressure*

5.2.2.1. *Leafy and autumn culms in the laboratory*

The apparatus for laboratory measurement of convective flow and static pressure, ΔP_s, is shown in Fig. 5.01.

With the rhizome system submerged and the culms emergent, convective flow rates were measured using a soap-film flow-meter (length, 400 mm; bore, 5 mm) attached by rubber tubing to the cut submerged end of a rhizome, or to an old emergent culm. Flow rates have generally been expressed as $m^3\ s^{-1}$, but sometimes, to make it easier to visualise rates of flow, the gas velocities through the flow meter are quoted also. Static pressure, ΔP_s, i.e. the maximum pressure above atmospheric developed in the plant with the vent closed, was measured by diverting the flow to a water manometer or pressure transducer (Furness Controls Ltd.) only, by means of a 3-way tap.

Care was taken to ensure that the rhizome was not flooded and that it had no callus development in the nodal septa which could have impeded the flow (Armstrong and Armstrong, 1988). Humidity and light flux were varied as required during experiments by means of a gas-train humidifier (A.D.C. Instruments, U.K.) and by adjusting the position of the light source: a 400W high-pressure Na-vapour lamp. To reduce the heat loading, a watercooled heat sink was placed between the plants and the lamp.

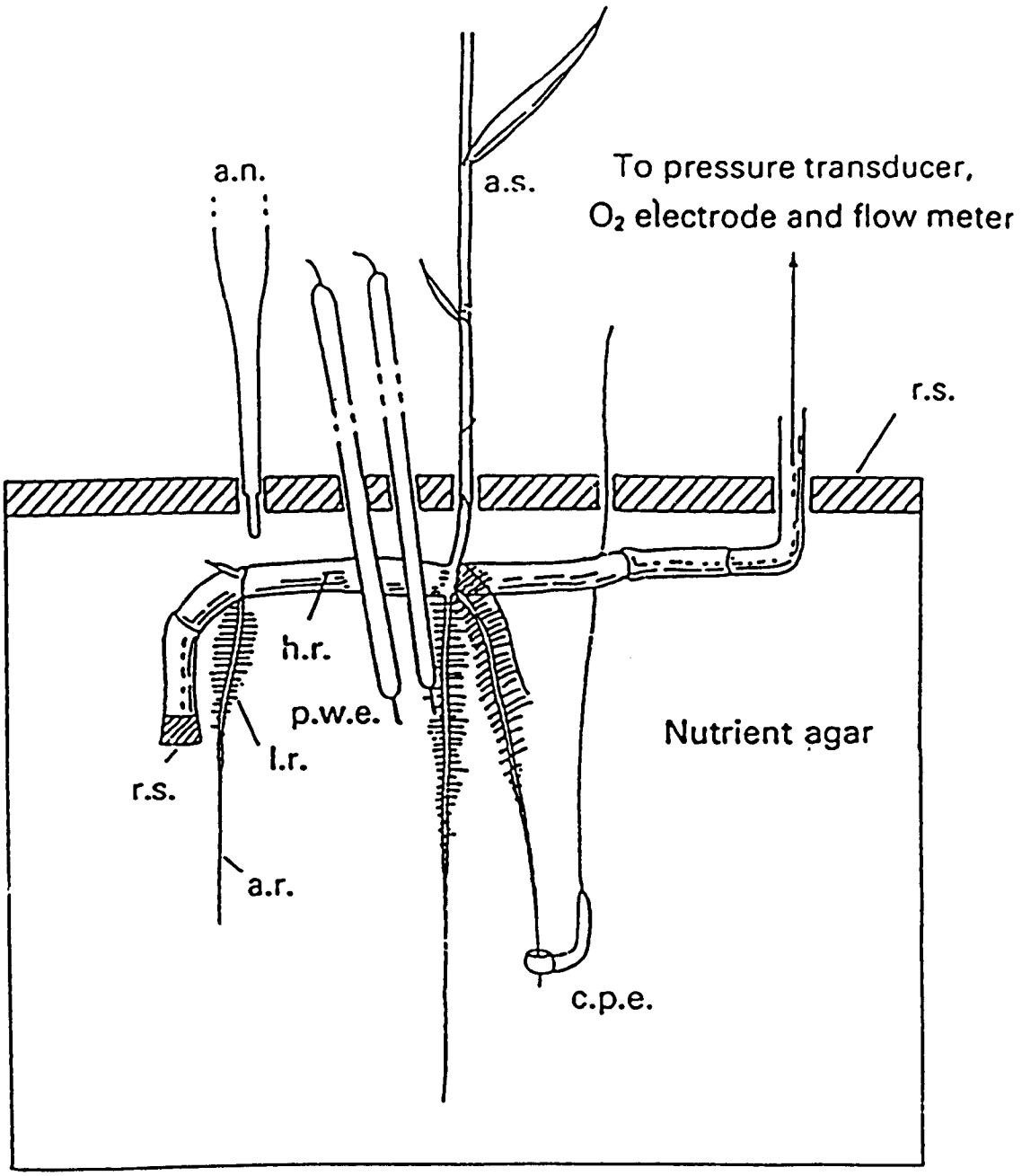

Fig. 5.01 Diagrammatic representation of assembly for measuring convection, static pressure differentials, root oxygen efflux and oxygen concentrations in venting gases. a.s., aerial shoot; r.s., rubber seal; a.r., adventitious root; l.r., lateral roots, h.r., horizontal rhizome; c.p.e., cylindrical platinum electrode; p.w.e., platinum wire electrode; a.n., anode: silver–silver chloride (only one shown).

5.2.2.2. *Leafy culms in the field*

Static pressure differentials and convective flow rates were measured on single leafy culms of undisturbed plants. Firstly, the culm's lowermost nodal region and part of the pith cavity above were flooded to prevent venting via the rhizome system, by injecting with water above the nodal diaphragm using a hypodermic syringe. Since nodal diaphragms are very hydrophobic, the water remained on the upper surface of the diaphragm, so blocking the gas flow path. The wound was sealed with silicone rubber. Another needle was then inserted and sealed into the pith cavity above the flooded region, and from this needle plastic tubing was connected via two 3-way gas taps to a flow-meter and a water manometer or the portable pressure transducer. In some instances the venting gases were re-routed back into the plant via the flow-meter and a second syringe inserted into the internode below.

An alternative, more convenient method was also used for measuring convective flow and ΔP_s. Here, the culm was cut off at the base and immediately attached to the flow-meter or the pressure transducer.

5.2.3. ***Measurement of dynamic pressure differentials (ΔP_d) in the field***

Dynamic pressure differentials (ΔP_d) are the pressures above atmospheric within the rhizome and culm system when throughflow is occurring. These pressures were usually measured in the living culms and hence represent the magnitude of the total pressure drop across the system. The measurements were made by connecting the pressure transducer directly to a living culm by means of a syringe needle which was sealed in with Si-rubber.

5.2.4. *Radial oxygen loss (ROL) from roots*

Radial oxygen loss from *Phragmites* adventitious and lateral roots was measured in the laboratory with whole plants using a polarographic method. Cylindrical platinum electrodes (length 5 mm; inside diameter, 2.25 mm) were placed around the sub-apical regions of adventitious roots, while solid platinum electrodes (length, 10 mm; diameter, 0.6 mm) were placed among the fine basal lateral roots, and also 30 mm away from these roots in the agar (Fig. 5.01). The platinum cathodes were used in conjunction with saturated Ag-AgCl anodes and the oxygen was assayed polarographically as described in Section 4.2.4. The cylindrical platinum electrodes enabled the root surface oxygen concentration to be computed as well as the rate of oxygen efflux from the root.

5.2.5. *Oxygen concentration in venting gases*

For both laboratory and field experiments, the gases venting from the field culms (or from rhizomes in the laboratory) were passed across a Clark-type electrode having a Si-rubber membrane and which was specially developed during this study for long-term monitoring of gas-phase oxygen concentration. A sensitive polarograph calibrated to an accuracy of 0.05 kPa O_2 was used for the measurements in conjunction with a chart recorder. In the field a portable Goerz Multiscript chart recorder was used. Calibration of the electrode was periodically checked by flushing with atmospheric air.

In the laboratory, the tube from rhizome to electrode was 360 mm long (bore: 3 mm). From the electrode to the flow meter the tubing was 600 mm long (bore: 3 mm) and this appeared to be sufficient to minimise back diffusion from the flow-meter during low rates of convection at night when the soap film could not be replaced continuously.

In the field the venting gases emerged via a syringe from the internode above a flooded node, passed across the end of the Clark electrode, then through the flow-meter, and back via a second syringe to the internode below.

5.2.6. *Measurement of temperature differentials, and relative humidity*

For both laboratory and field experiments, temperatures within culms were measured by digital thermometer (RS components) using thermocouples (diameter 1 mm) sealed into the pith cavities. The air temperature external to a culm (5 mm away) was measured using a similar thermocouple.

Atmospheric relative humidity was monitored using a portable humidity probe (Vaisala H.M.P.32UT).

5.2.7. *Variation and measurement of PAR*

The light source was a 400 W high-pressure sodiumvapour light screened by a water-cooled heat sink; neutral filters were used to vary the light flux. PAR was measured using a Lambda Instruments Quantum-meter.

5.2.8. *Measurements of leaf sheath area and culm numbers.*

Leaf sheath areas were calculated from measurements of exposed lengths and diameters using the formula ($2\pi rL$) for the surface area of cylinders.

Numbers of dead to living culms were measured within metre quadrats.

5.3. EXPERIMENTS, RESULTS AND DISCUSSION

The experiments were designed to locate the sites of initiation of the convective flow and to determine the mechanism, which was thought to involve light, humidity differentials, and possibly temperature differentials between the inside and outside of the plant.

5.3.1. *Laboratory experiments*

5.3.1.1. *Leafy culms : the effect of variations in atmospheric humidity and temperature on convective flow*

At low light flux and a PAR of 100 μmol m^{-2} s^{-1}, convective flow rates were measured at 18°C and at various relative humidities: 31-96% (Fig. 5.02a). Also at a PAR of 20 μmol m^{-2} s^{-1}, rates of convective flow were measured at an ambient temperature of either 24 or 17°C for various humidities: 41-96% (Fig. 5.03).

Increasing the atmospheric humidity greatly reduced convective flow rates, e.g. at 18°C, HI flow rate at an RH of 31.4% was 36X the rate when the RH was 96.5% (Fig.). Also at 24°C, the rate of HIC when RH was 41%, was 3.5X the rate when RH was 73.4% (Fig. 5.03). In both figures, extrapolation indicated that at 100% RH, the flow would have virtually stopped. The rate of flow also appeared to be slightly increased at higher temperatures, (Fig. 5.03). This could be explained in terms of higher diffusivities and diffusion gradients at the higher temperatures (section 5.4). Similar effects of RH and temperature were obtained when Nuclepore membranes were used to mimick HIC (Fig. 5.02b and Sections 6.3.3 & 6.3.6a).

Phragmites: Effects of Atmospheric Humidity on Humidity-Induced Convective Through-flow n.b. virtually no flow at 100%RH

Single shoot, ht.:0.7m , Temp.:18°C, Light flux:100μmol $m^{-2} s^{-1}$

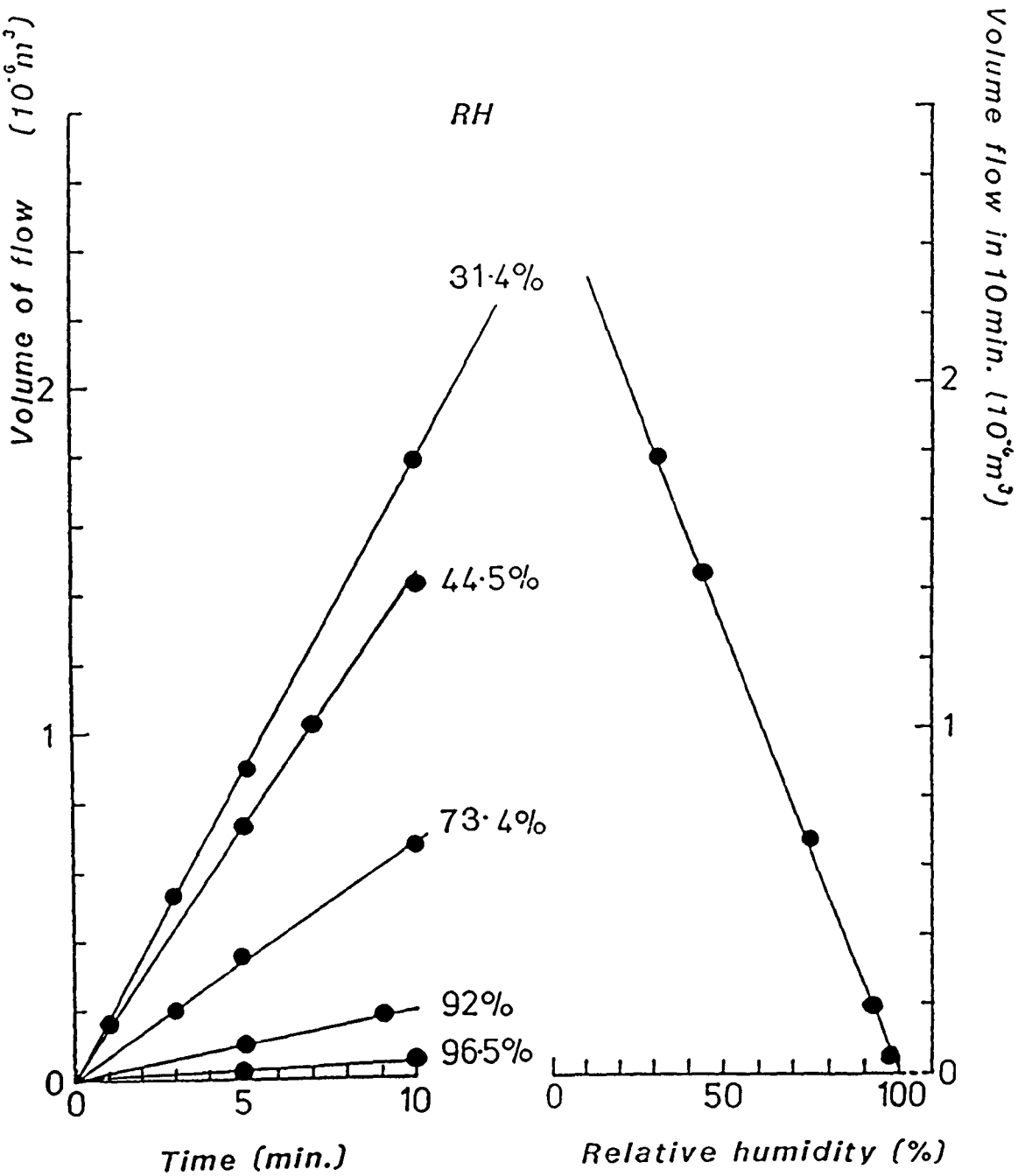

Figure 5.02 a

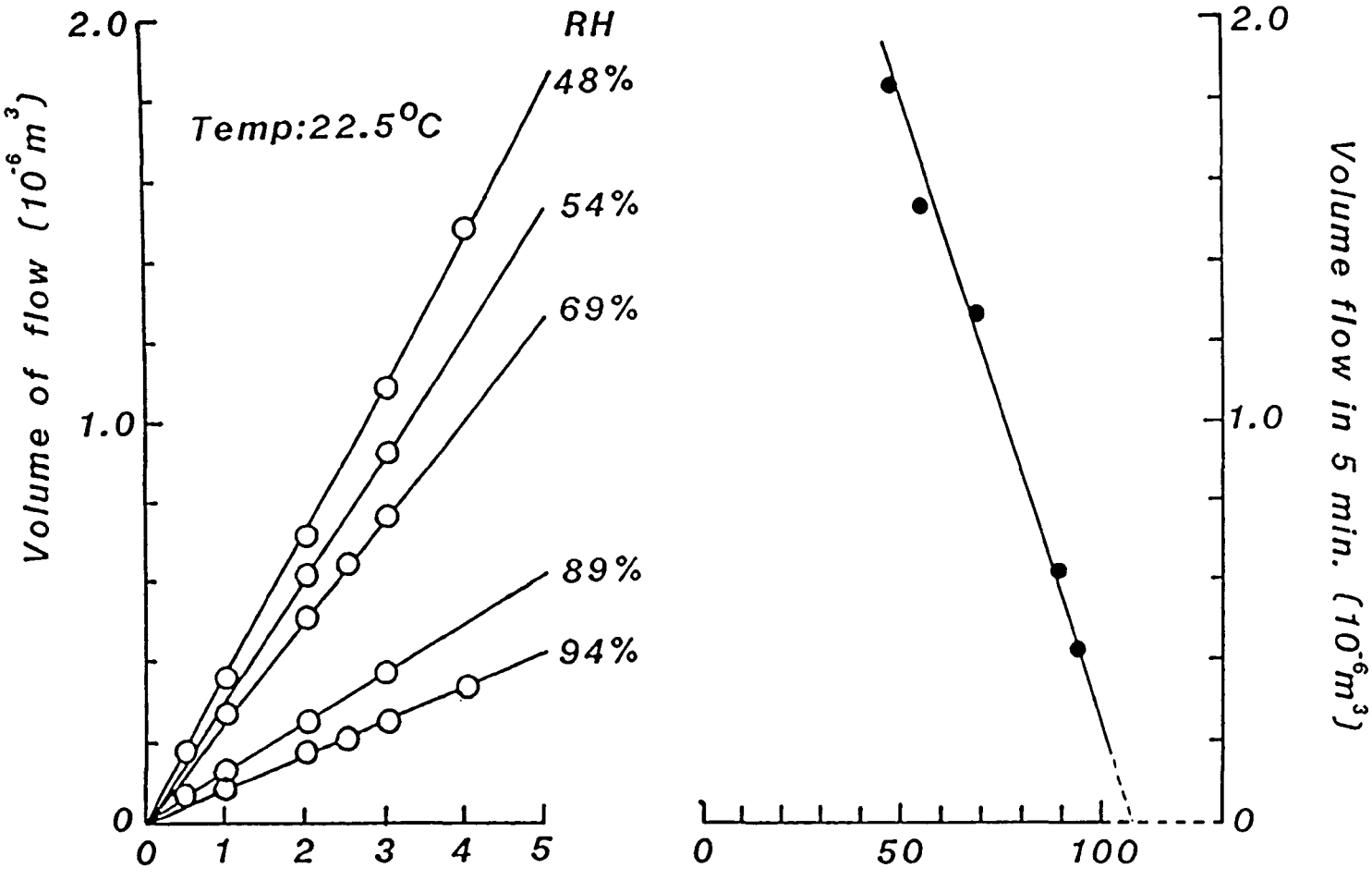

FIG. 5.02b

Effects of Atmospheric Humidity on Gaseous Convection through Nuclepore Membrane above Humidified Chamber (pore diam.:0.2μm,pore no.:c.0.5−1X10^9) n.b. virtually no flow at 100%RH

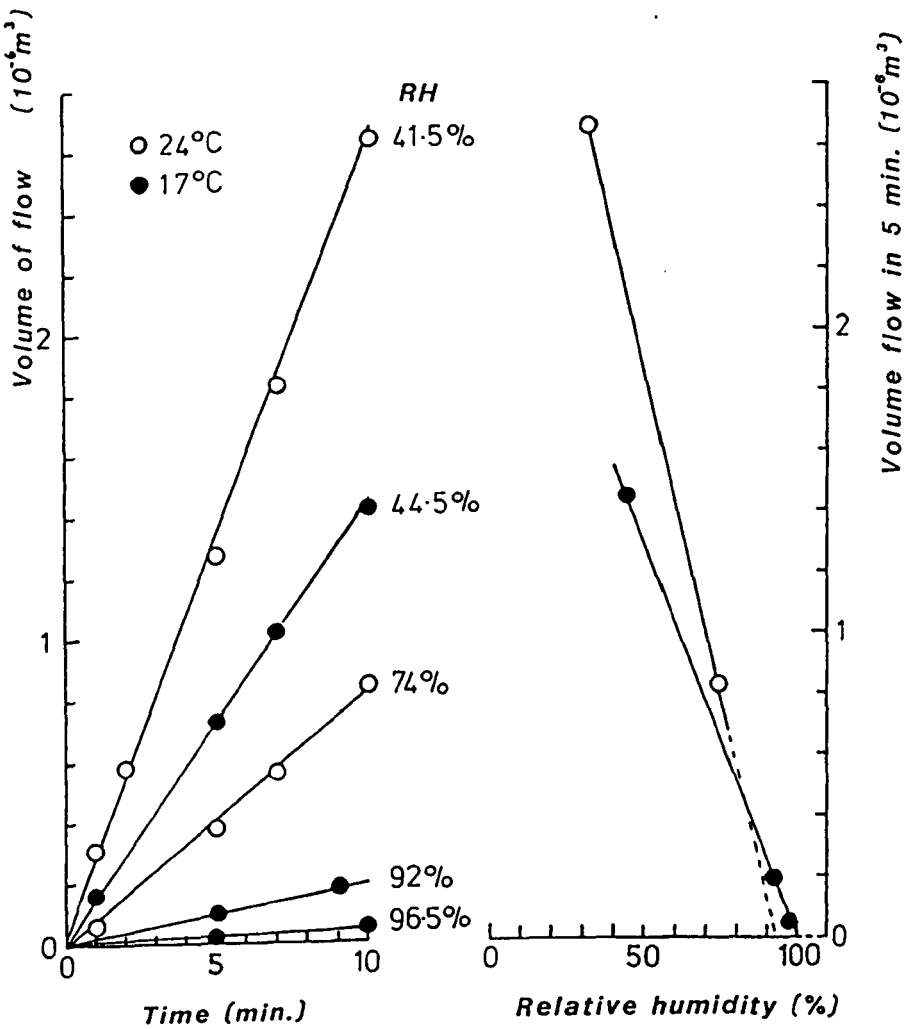

Convective gas-flow in *Phragmites*: young leafy shoot, vertical and horizontal rhizome. The relationship between flow and RH at two temperatures is shown, together with extrapolations which indicate very slow to zero flow at 100% RH.

Figure 5.03

5.3.1.2. *The effect on convective flow and static pressure differentials of cutting and resealing leaf laminae and sheaths*

The following experiments were performed at 20°C, light flux of 180 μmol m^{-2} s^{-1} and RH 45% for two leafy shoots (heights 0.9 and 0.95 m) on the same rhizome.

(i) Convective flow rates and ΔPs were measured (a) with aerial shoots intact and (b) when all but the terminal laminae were cut to within 5 mm of the lamina-sheath junction.

(ii) With the shoots "delaminated", the ΔPs were measured (a) with the leaf sheaths intact, (b) with the two lowermost healthy leaf sheaths cut on each shoot as near to the top of the sheath as possible, and (c) with the cut leaf sheaths of (b) sealed with silicone rubber.

Whether the cut ends were sealed or unsealed, the cutting of leaf laminae had no appreciable effect (not shown). However, cutting through just the one basal living leaf sheath per shoot markedly reduced ΔPs (and hence the flow rate)(Fig. 5.04). Pressure was regained when the sheaths were sealed again. This accords with the presence of aerenchyma in the sheaths, but not in the leaf laminae.

5.3.1.3. *Leafy culms partly covered in "clingfilm"; convective flow and static pressure*

For two shoots (heights 0.9 and 0.95 m) at 19.7-20°C, light flux 180 μmol m^{-2} s^{-1} and RH 47%, the ΔPs and convective flow rates were measured with the aerial shoot uncovered and when the following parts were covered in cling film: leaf laminae only, leaf sheaths only, and both leaf sheaths and laminae.

Convective flow rates and ΔPs were virtually unaffected by covering the laminae alone (Table 5.01). However, there was a marked reduction in both when the leaf sheaths were covered, even though the

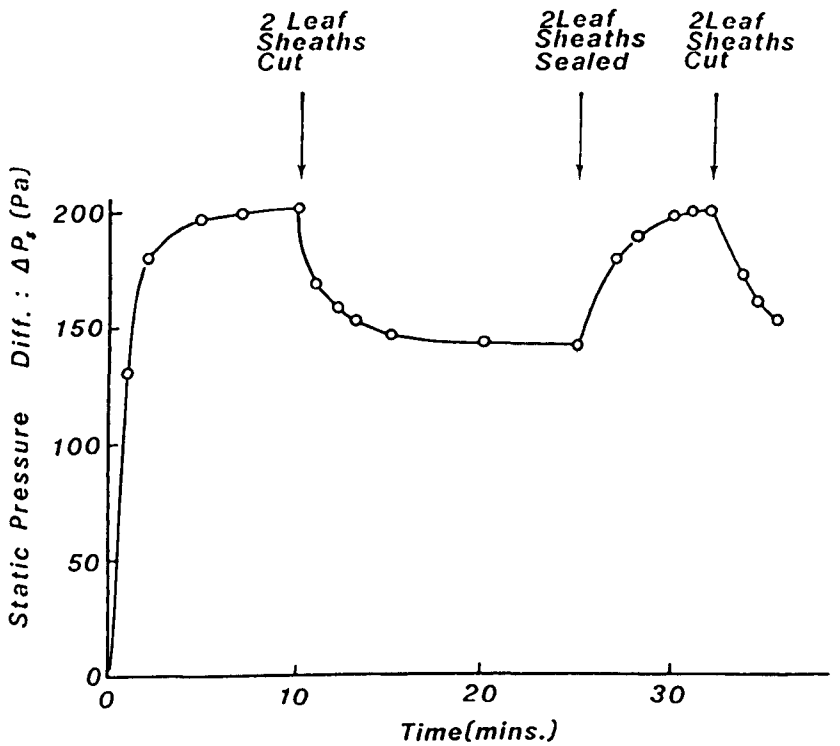

Fig. 5.04 Static pressure differential (ΔP_s). The effects of cutting and resealing the tops of living leaf sheaths of two shoots of heights 0.9 and 0.95 m and basal diameters 3–4 mm are shown. The laminae were removed and the tops of the two basal living sheaths on each shoot were cut. The figure shows the fall in ΔP_s upon cutting and the regaining of pressure when the cut ends were sealed. Light flux: 180 μmole m^{-2} s^{-1}; temperature: 20°C.

total leaf sheath area was only 0.17 times that of the total lamina area. It is not certain why exposed leaf laminae do not contribute to the pressurisation and flow; the topic was not further investigated. However, high gas-flow resistance in the lamina-sheath junction may be one reason, another may be a greater degree of stomatal opening in leaf laminae stomata.

The reason for cling-film reducing the convective flow rates was probably due to the production of high humidities around the leaf sheaths (cf. Figs. 5.02a & 5.03).

5.3.1.4. *Convective flows in progressively shortened leafless culms*

At a light flux of 20 μmol m^{-2} s^{-1}, RH 42% and air temperature 19.4°C, two autumn culms attached to the same rhizome were cut back to heights of 0.49 and 0.54 m, respectively, so as to leave five basal green internodes on each. The cut ends were then sealed with silicone rubber. With venting through the rhizome, the culms were further cut in stages and the rates of convective flow were measured at each successive cutting, and on resealing. Each shortening involved the removal of one node and half an internode on either side of the node on each culm. Convective flow rates for these autumn culms, whose leaf sheaths and laminae had died, were slow (Fig. 5.05) compared to leafy culms under similar conditions (Figs. 5.02a & 5.03) presumably because of the very much lower stomatal numbers. Removal of an internode alone had no effect on flow rate, but removal of each section of internodal tissue with a nodal region clearly reduced the flow rate. A cut open culm produced no convective flow and zero ΔPs. Flow rates decreased when the number of nodes present was decreased because of a reduction in the number of nodal stomatal zones which allow gases into the culm. (It was interesting that if these stomatal zones were

Table 5.01

Phragmites australis: Effects on convective flow and static pressure differential when parts of two aerial shoots are covered in cling film. Illumination: 180 μmole m^{-2} s^{-1}; temperature: 19.7–20°C; RH: 47.2–47.4%; shoot heights: 0.9 and 0.95 m; basal diameter: 0.003 m

	Static pressure differential (Pa)	Convective flow (10^{-6} m^3 s^{-1})
Whole plant exposed	204.4	0.0097
Leaf laminae only covered (area 376.5×10^{-6} m^2)	200	0.01
Leaf sheaths only covered (area 62.57×10^{-6} m^2)	96.4	0.0052
Leaf sheaths and laminae covered	92.6	0.0053

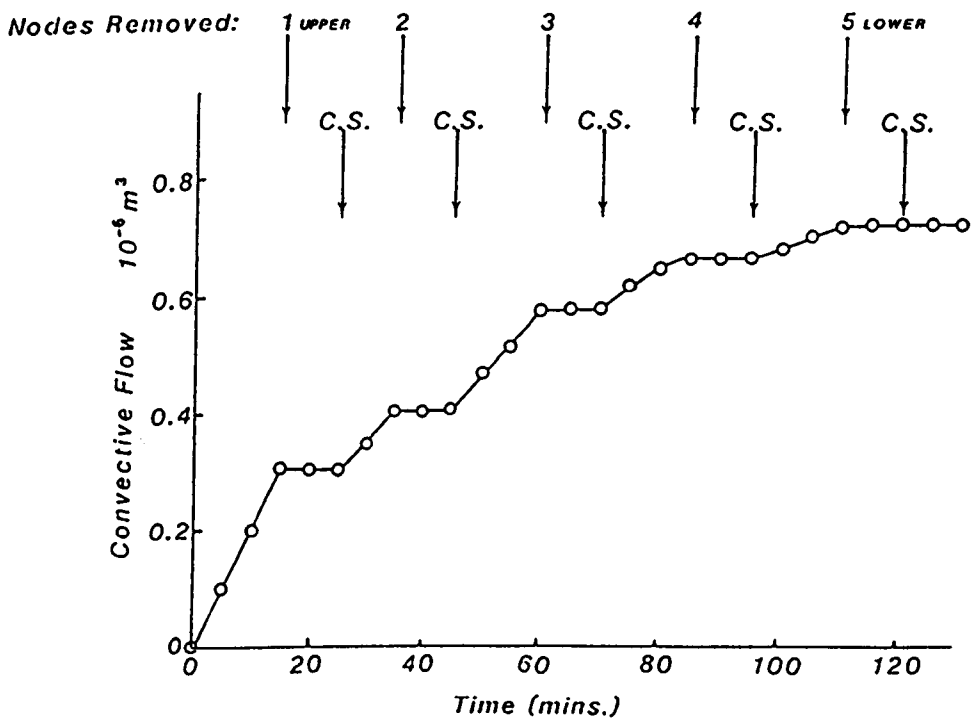

Fig. 5.05 Convective flow: effects of cutting and resealing leafless late autumn culms. Each cut removed a node and half of each of the adjoining internodes. The figure shows the progressive reduction in flow rate which can be attributed to the successive removal of nodal stomatal zones. Flow stopped whenever the cut end of the culm was unsealed, but resumed on sealing. C.S. = culm end sealed. Light flux: 20 μmole m^{-2} s^{-1}; RH: 42%; temperature: 19.5°C; culm heights: 0.49 and 0.54 m; basal diameters: 6 mm.

progressively covered by moist tissue, flow rates similarly decreased).

5.3.1.5. *Effects of light and darkness on convective flows and on rhizome and root aeration*

Convective flow rates, the concentration of oxygen in the gases venting from the rhizome, and ROL during periods of light and darkness were measured on intact plants set up as shown in Fig. 5.01.

The enhancement of convective flows in light had a considerable influence on rhizome and root aeration: in the example shown in Fig. 5.06, darkness caused a rapid fall in the convection rate from 38 nm^3 s^{-1} to 0.86 nm^3 s^{-1}. It also resulted in a 36% reduction in the oxygen composition of gases venting from the rhizome, and a 50% and a 70% decline in oxygen efflux from adventitious and lateral roots respectively. For the adventitious root, ROL in the light was 18.8 μg m^{-2} s^{-1}, representing a root surface oxygen concentration equivalent to 6.1 kPa. Similarly, when the lights were switched on again after a night period, convection rate and rhizome oxygen levels were soon restored to high values, as was ROL from the roots; in the case of the adventitious roots this involved a rise of 135%, while for the laterals the figure was *ca.* 85%. In contrast, the oxygen flux at a control electrode 30 mm away from the roots remained close to zero throughout.

The patterns of ROL and [O_2] venting from the rhizome during the night show some interesting features; similar features were found in other examples not presented. Firstly, after the initial steep decline in the oxygen regimes of rhizome and roots, there was a small but significant rise in oxygen efflux from adventitious root and laterals (Fig. 5.06). A little later the response is reflected also in the levels of oxygen venting from the rhizome. From around dawn ROL began to fall

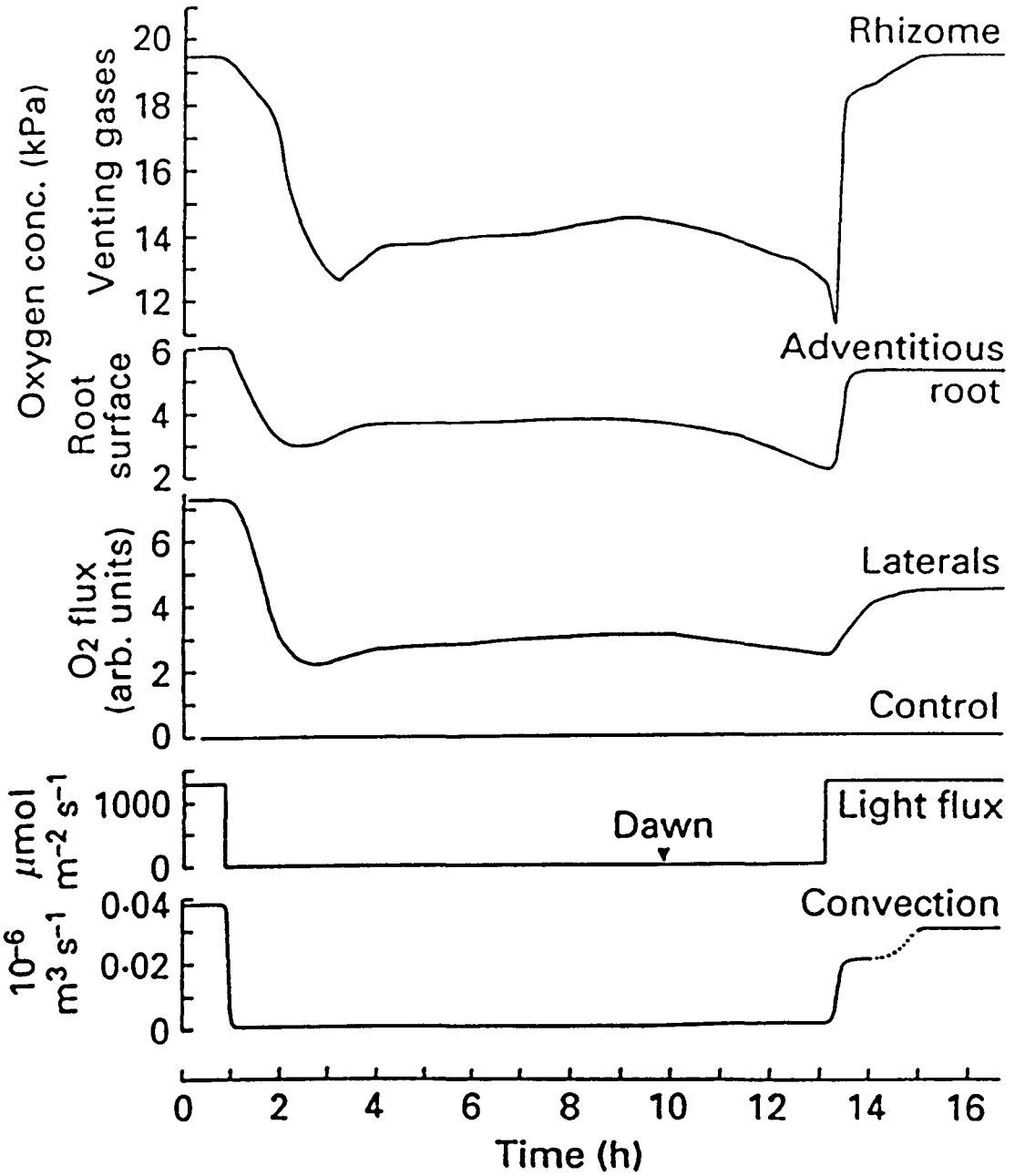

Fig. 5.06 Effects of light and dark periods on convective flows, on oxygen concentrations of gases venting from rhizome, and on root oxygen efflux. Rhizome length was 65 mm; 3 culms present (heights 0·6 m); depth of culm submergence, 170 mm; adventitious root, young and 65 mm long (diam. approx. 1·5 mm); lateral roots (approx. lengths 15 mm) formed dense coating on older adventitious roots; control electrode was 30 mm away from lateral roots. Dawn, is natural dawn.

again, as did the oxygen regime in the venting gases. During this period the light flux rose from zero to approx. 50 μmol m^{-2} s^{-1}. Convection also rose marginally. The first of these two sets of features is probably due to a decline in respiration somewhere within the rhizome and/or root system since the response was first evident in the root oxygen data rather than more remotely at the venting oxygen sensor. It is conceivable that this could be caused by the onset of hypoxia/anoxia in some of the tissues because of the lower convection rate, or it might be the result of a reduction in substrate supply because of the cessation of photosynthesis. At dawn, the gradual decline in oxygen levels suggests increased respiration and this may be due to the alleviation of hypoxia in some tissues because of the marginally raised convection rate, or because of substrate renewal on the restoration of some photosynthesis. Other points of interest are (i) the inverted peak in the rhizome oxygen trace which represents a flushing out of the stale, oxygen-depleted rhizome gases when the convection again accelerates under the influence of the higher light flux at 13.00 h, and (ii) the very quick response in ROL which accompanied the acceleration in convection; such a rapid response is quite consistent with a diffusion of oxygen from rhizome to root, (Armstrong & Beckett, unpublished modelling data).

In another experiment involving only one shoot, the plant had not been allowed to vent for the preceding 2 h of darkness and the light was turned on after 0.15 h (Fig. 5.07). Radial oxygen losses and oxygen concentrations at the Clark electrode remained low, as they had in the dark period. Only when convective throughflow was restarted by opening the exit from the rhizome at 0.8 h did the oxygen values rise. As before the control electrode remote from the roots showed consistently very low readings. This experiment suggests that neither

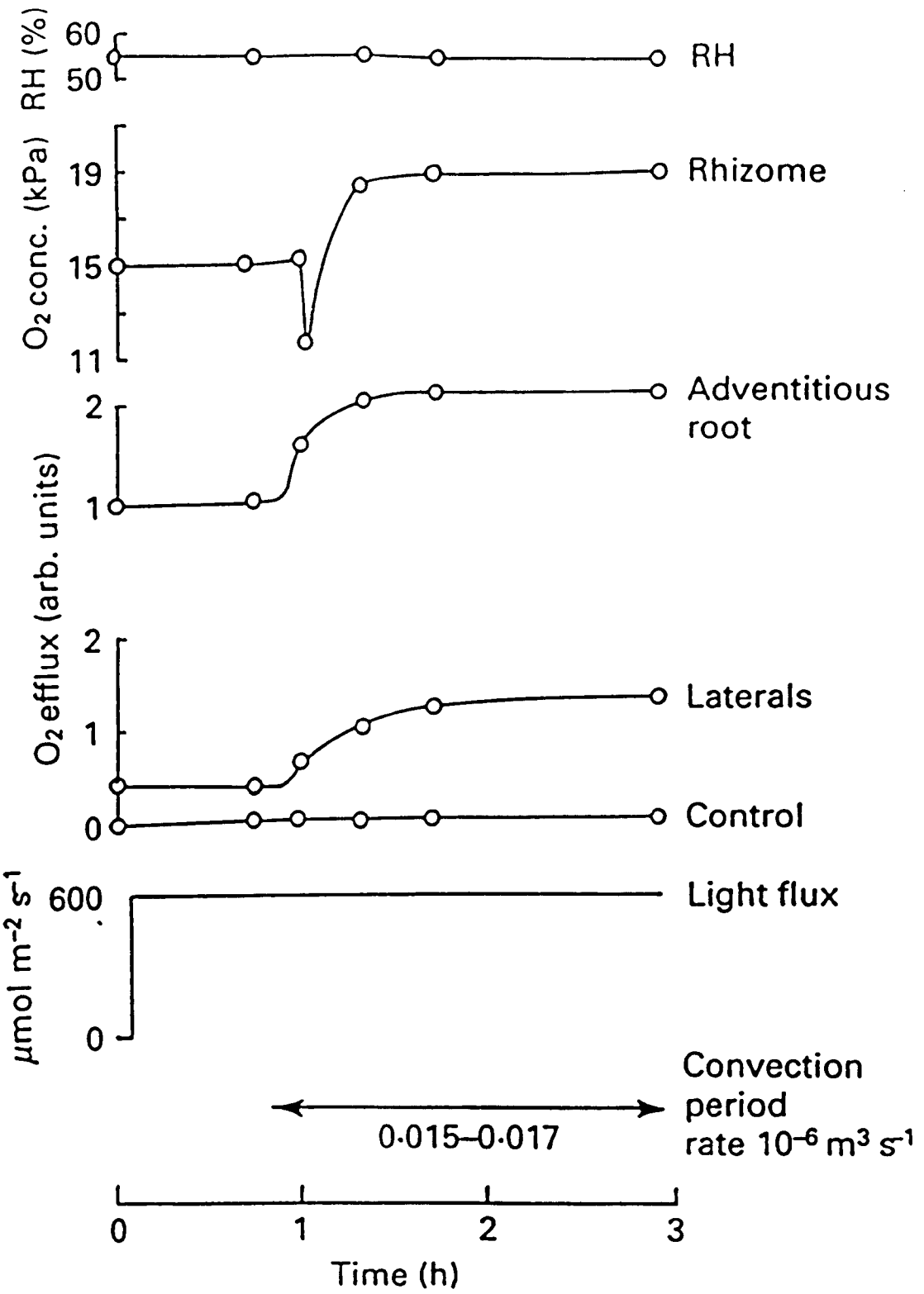

Fig 5.07 Effects of presence or absence of convection on rhizome oxygen concentrations, and on root oxygen efflux at high light intensity. Rhizome length 80 mm; one shoot, height 0·62 m; depth of submergence 100 mm; adventitious root length 165 mm.

light nor photosynthesis *per se*, in the absence of convection, has significant effects on the concentration of oxygen of the rhizome or on ROL. It shows also that, when rhizome and root aeration are dependent entirely upon diffusion, the oxygen deficits which develop in the rhizome are much greater than in the presence of rapid convection. As in the previous experiment, a resumption of rapid convection caused a flushing out of oxygen-depleted gas from the rhizome, evident as a sharp but brief reduction in oxygen concentration of the venting gases. It should be noted, however, that if more than one shoot is present in this type of experiment a small rise in oxygen efflux from the roots may occur when light is restored during an imposed non-convective period. This can be attributed to a small convection between the living shoots.

5.3.1.6. *Effects of variations PAR flux on humidity-induced convective flow, ΔP_s and ΔT*

Convective flow rates ΔP_s, and ΔT (i.e. the temperature differential between the culm pith cavity and ambient), were measured at various values of PAR: 0 - 780 μmol m^{-2} s^{-1}. Atmospheric humidities and external temperatures were reasonably constant : RH 33-35%; temperature, 21.2 ± 0.2°C.

Convective flow rates and ΔP_s can increase markedly in response to photosynthetically active radiation (Fig. 5.08). The greatest response occurred within the range below 200 μmol m^{-2} s^{-1}. A small amount of internal warming also accompanied the increases in light flux: $\Delta T \leq 2$°C. However, convective flow rates and ΔP_s values approached zero in darkness as in section 5.3.1.5.

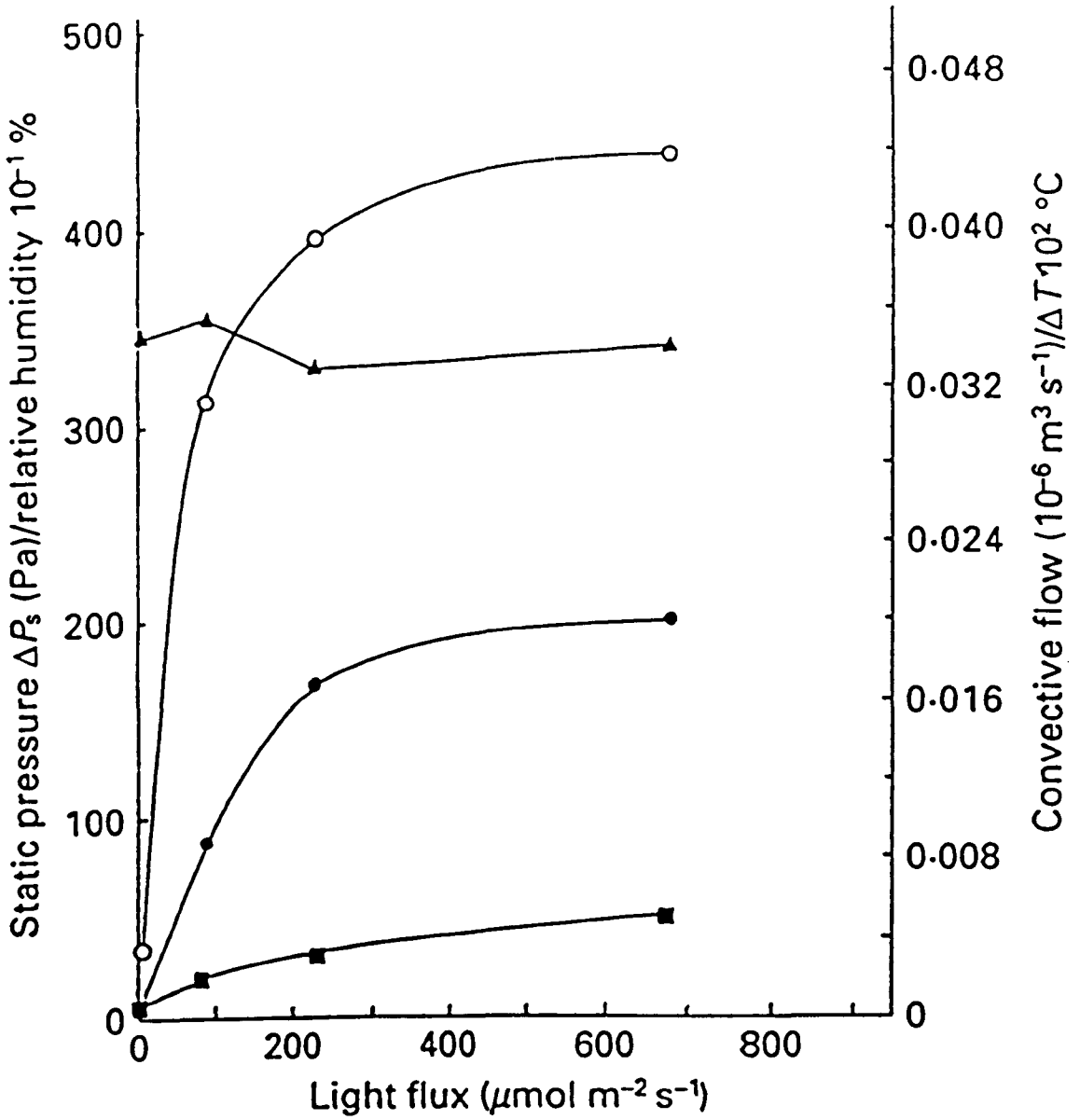

Fig 5.08 The effect of varying light flux (PAR) on static pressure differentials and convective flow, and on temperature differentials between the culm pith cavity and ambient. Atmospheric relative humidities also shown. Rhizome bearing 4 young shoots of heights 0·24–0·32 m. ○, ΔP_s; ▲, RH; ●, convective flow; ■, ΔT.

5.3.1.7. *Effects of variations in PAR on humidity-induced convection and on rhizome and rhizosphere aeration*

In this type of experiment light flux was varied (PAR: 0-1600 μmol m^{-2} s^{-1}) using neutral filters. At the various light flux, measurements were made of the convective flow rate, the oxygen concentrations of gases venting from the rhizome, the oxygen efflux from adventitious and lateral roots, and the oxygen regime in the agar 3-5 mm. away from the laterals.

The experiment was repeated twice on different, but similar plants. The effect of a greater range of PAR (0-4000 μmol m^{-2} s^{-1}) on convection rate was made on a separate occasion. Throughout these experiments the atmospheric humidity was 45 ± 3 %.

The results in Fig. 5.09 demonstrate clearly how increases in radiation (measured as PAR) lead to a more rapid throughflow convection: from 0.86 nm^3 s^{-1} (2.6 mm min^{-1}) at zero PAR to 32 nm^3 s^{-1} (98 mm min-1) at 1400 μmol m^{-2} s^{-1} PAR. This in turn caused substantial increases in ROL and rhizome oxygen concentrations, while the control electrode 3-5 mm away from the laterals recorded an oxygen concentration of virtually zero. From 0-200 μmol m^{-2} s^{-1} PAR, convective flow increased 13-fold, while radial oxygen losses from the laterals and apical region of the adventitious root increased by approx. 2.3x and 3.1x respectively, and rhizome [O_2] almost doubled. At 200 μmol m^{-2} s^{-1} convection amounted to 11.4 nm^3 s^{-1} (34 mm min^{-1} through the flow-meter), comparable to the Venturi effect at a wind speed 5.3 m s^{-1} (19 km h^{-1})(Sections 7.3.1 & 7.3.2), and although convection continued to increase at light fluxes greater than 200 μmol m^{-2} s^{-1} (Fig. 5.09), further effects on aeration were very small.

In the replicates of this experiment using different plants, the results showed a similar pattern. Also, rhizome [O_2] never exceeded

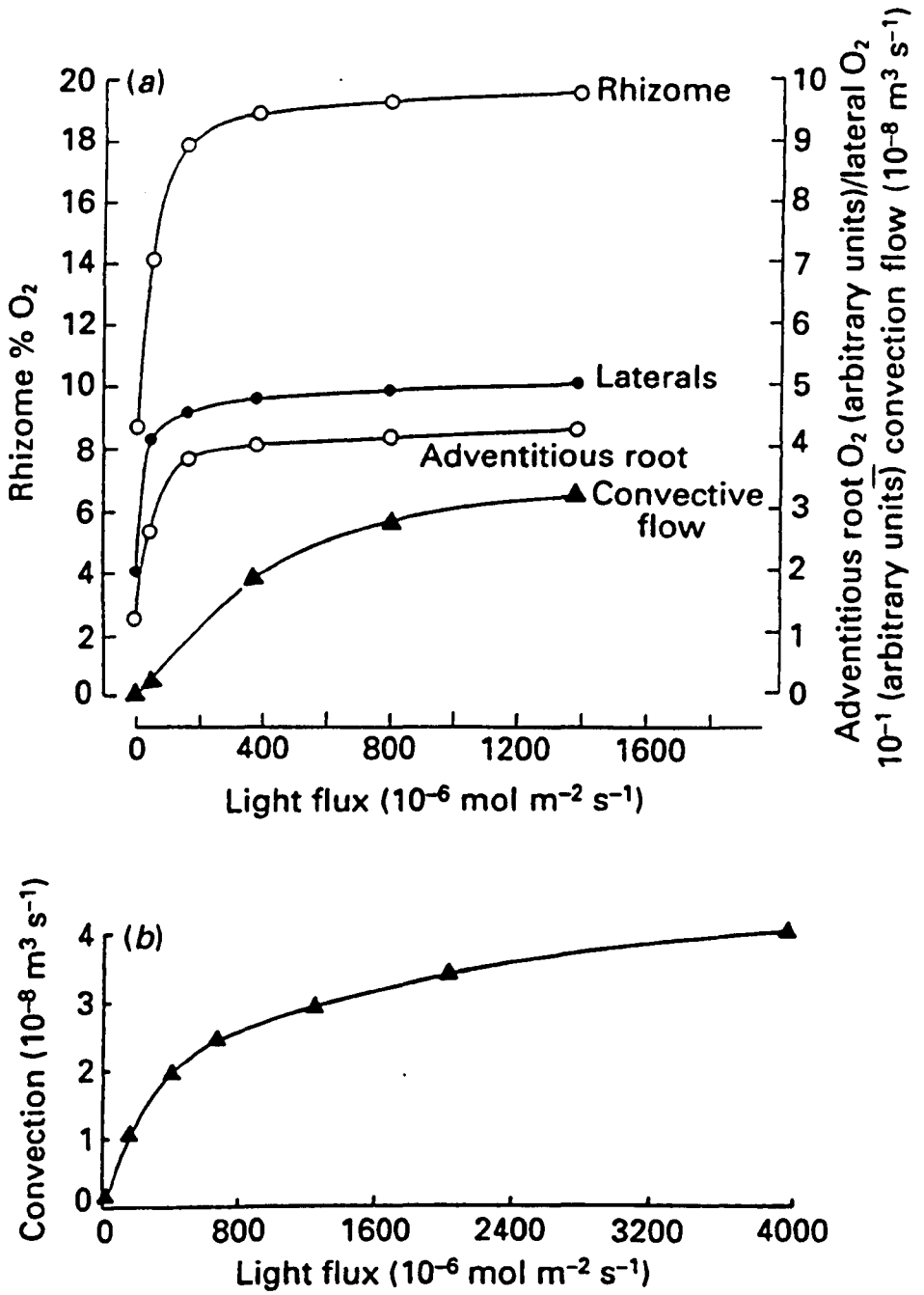

Humidity-induced convection. (*a*). The effects of varying light flux on humidity-induced convection, [O_2] venting from the rhizome, and root oxygen efflux. Rhizome length 0·36 m; rhizome submerged at 100 mm; 3 shoots (h = 0·6 m); 13 adventitious roots (lengths 0·02–0·29 m); root assayed for oxygen efflux was 113 mm long; r.h. 40–43 %; T = 22–23 °C. (*b*). The effects of varying light flux on humidity-induced convection. Rhizome length 0·3 m; rhizome submerged at 0·7 m; 5 shoots (h = 0·23–0·56 m); adventitious root number = 17, root lengths 0·02–0·19 m; r.h. = 41–45 % ; T = 21–22·5 °C.

Figure 5.09

atmospheric, and thus it seems unlikely that photosynthesis *per se* plays more than a minor role in the convection process (Armstrong & Armstrong, 1990a).

5.3.2. *Field Experiments*

5.3.2.1. *The effects of leaf surface area on convective flow and* ΔP_s

Convective flows were measured in the field on a cloudless September day using living freshly-excised culms of differing leaf sheath areas. Relative humidity was in the range 54-62%, and temperature 19-22°C.

The results (Fig. 5.10b, and Armstrong & Armstrong 1991), indicate that the potential for convection increases with leaf sheath area, and hence stomatal numbers. The large degree of scatter was probably due primarily to variations in external conditions during the time it took to make all the measurements, but differences in water potentials between the various shoots, and differences in the degree of stomatal opening could also have been contributory factors. The data seem to indicate a curvilinear relationship between convection and leaf surface area which could be a function of lower venting resistance in the wider culms which are also those with the higher leaf sheath areas.

It was also noted that the larger the culm the more rapidly are the ΔP_s values achieved. However, the level of ΔP_s achieved is relatively independent of leaf sheath area (Fig. 5.10a) probably because the pressure depends chiefly upon pore size and humidity differentials (see also Section 6.3.4 & 6.3.6).

These results can be correlated with experiments using different areas of Nuclepore membrane (Section 6.3.7).

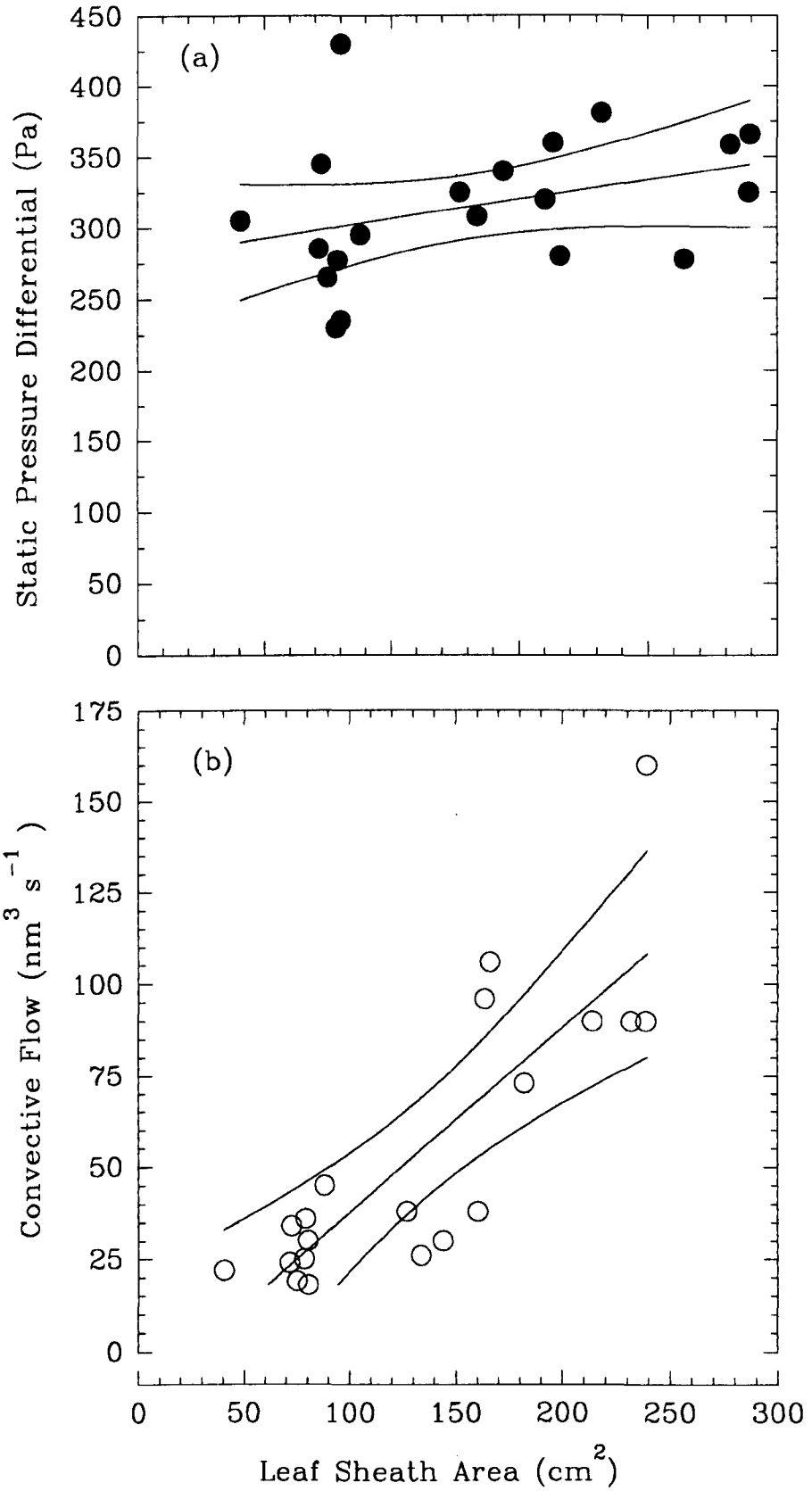

Fig. 5.10. Showing the relationship found between leaf sheath area and (a) static pressure differential and (b) convective flow, from excised culms in the field. 95% confidence limits shown.

5.3.2.2. *Variations in dynamic pressure differential with different proportions of dead and living culms.*

Dynamic pressure differentials in several reed beds were measured on the banks of the Humber Estuary on a September day with hazy sunshine with relative humidity in the range 54-62%, and temperature 19-21°C. The pressures were then plotted against the ratio of dead to living culms in the bed (Fig. 5.11). From the pattern of these results one may conclude that the lower dynamic pressures in long-established reed beds (ratio dead:living culms >0.1) were due to the presence of the relatively large numbers of dead persistent culms. These would provide a venting pathway of low resistance, able to carry high flow rates under a very low pressure gradient. Conversely, in newly established beds with relatively few dead persistent culms (old:new culm ratio <0.1) it may be deduced that the greater values of ΔP_d were the result of a higher venting path resistance. In other words because of high venting path resistance, a higher pressure difference has to develop to drive the flows.

Thus, it can be concluded that a reed bed does not reach its full potential for rhizome aeration until several years have elapsed and there are large numbers of old persistent culms to provide a low resistance venting pathway. From the graph it would seem necessary to have at least one dead to ten living culms but greater numbers of dead culms would be desirable.

Old culms can persist for at least 2-3 years, and unlike dying rhizomes and senescing leaves they do not develop callus which would block the connexion between the pith cavity of the rhizome and that of the culm. They do, however, tend to become snapped off, and even those which appear entire often develop cracks near the apex.

Venting can also occur through the nodal stomata of these old

Phragmites australis: Field Variations in Dynamic Pressure Differential with Different Proportions of Dead : Living Culms

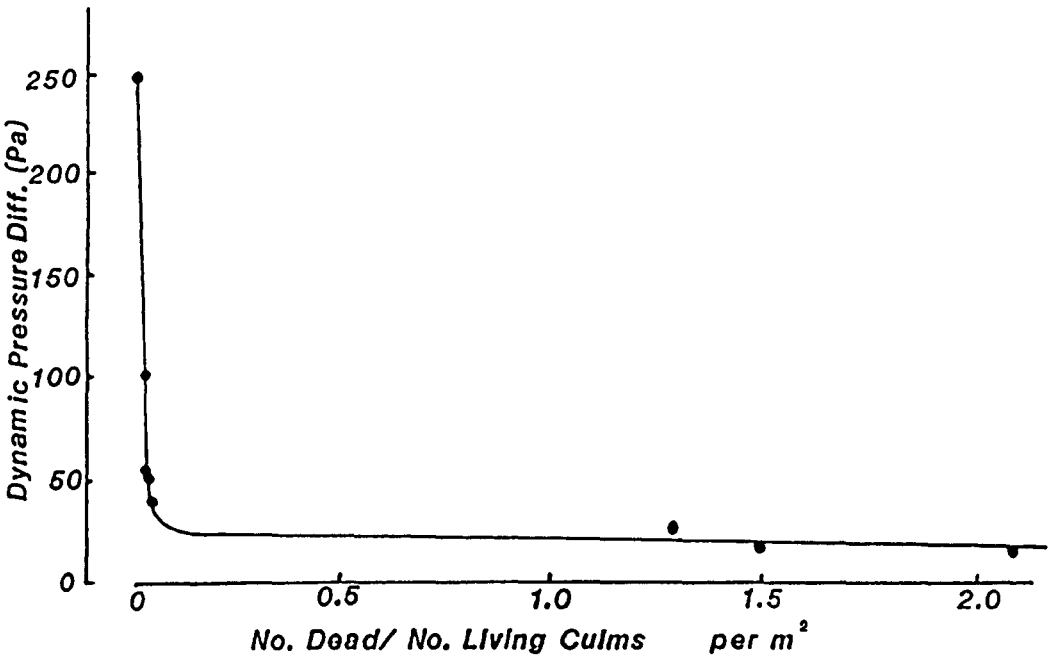

Figure 5.11

culms, and this may be important for ventilation in newly dead and senescing culms whose flowering apex is entire.

The presence of large numbers of old culms is also important during the winter since they provide the means of achieving a Venturi-induced convection (see Chapter 7), as well providing pathways for the diffusive aeration of the rhizome.

5.3.2.3. *Leafy culms : diurnal variations in convective flow, ΔP_s, ΔT and venting O_2 concentrations.*

Static pressure differentials, convective flow rates, oxygen regimes of gases venting from the rhizome, temperature differentials between the culm pith cavity and outside air, and the atmospheric relative humidity were measured during the daytime for intact plants in the field (culm height *ca.* 2 m) during August (Fig. 5.12). As with our laboratory experiments, ΔP_s decreased as convective flow rates decreased. As the humidity increased and the light flux decreased (15:0021:00 h), the convective flow rates decreased to almost zero at sunset 20:50 h) when the humidity was 92%. Conversely, at mid-day under sunny conditions and fairly low humidity (42%), the flow rates reached a maximum (266 $nm^3\ s^{-1}$), but the rate decreased (12:00–15:00 h) when the illumination decreased with diffuse cloud and the humidity increased moderately. At high light intensities, the temperature differential was greater (*ca.* 2°C), with warmer conditions prevailing in the culm. However, with decreasing illumination (15:00–20:23 h), this differential became very low (0.3°C). Around sunset and thereafter the differential became slightly negative (–0.5°C) with cooler conditions prevailing in the culm. Measurements of the oxygen concentration of gases venting from the culm showed that it was only slightly higher than that of the air, but it must be noted that these were only daytime measurements.

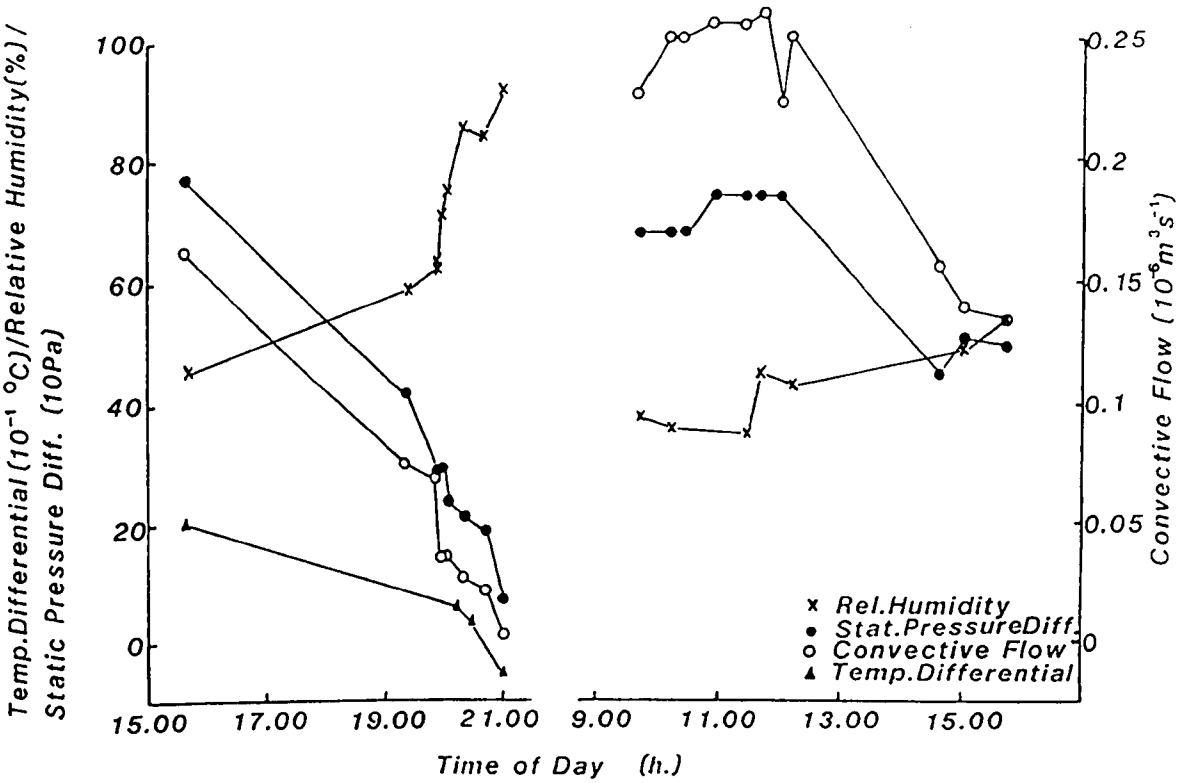

Field measurements showing diurnal variations in convective flow, the static pressure differential in relation to humidity and the temperature differential between shoot and atmosphere. Data are from single leafy culm of an intact plant in situ. Shoot height: 2.85 m; diameter: 10 mm; ×: atmospheric relative humidity; ●: static pressure differential; ○: convective flow; ▲: temperature differential.

Figure 5.12

5.4. *DISCUSSION*

From the results in sections 5.3.1.2, 5.3.1.3 and 5.3.2.1, it would appear that the convective flow reported here is caused by an inflow of gases from the air via stomatal pores on living leaf sheaths and culm nodes (the latter to a minor extent), and greater flow rates are found the larger the leaf sheath area. For a particular plant, static pressures increased concomitantly with convective flow rates. HIC is much lower in winter when the leaf sheaths die, and the latter are sealed from the culm by callus development (Section 3.3.5). In summer, however, while static pressure differentials could be high (up to 800 Pa) the dynamic pressures were usually very low: $\leq$ 5 Pa for venting through an open culm. These observations are in keeping with the small resistances to pressured gas flow within the plant (Section 2 and Armstrong *et al.*, 1988). Furthermore, in *Phragmites* beds in the field, where there are plenty of broken culms, the values of ΔPd under sunny summer conditions (Fig. 5.11) were much lower than the static pressures. This indicates that there is a throughflow of gases into the underground system. Also, ΔP_d values for *Phragmites* beds were lower the greater the numbers of dead to living culms. However, it should be noted that senescing intact culms offer a much higher resistance to venting and indeed when their basal regions are green, they can actually generate a small convective flow (Section 5.3.1.4). For an influx of gases against temperature and pressure gradients, such as those which develop in water lilies and in *Phragmites*, it appears that the pores must be such as to help to create an appropriate balance between inward diffusion and an outward Poiseuille flow. Pores small enough to allow Knudsen diffusion, i.e. $\leq$ 0.1 μm can best effect this, but the studies of pressure flow through stomata, and scanning electron micrographs of

culm and leaf-sheath stomata, indicated internal stomatal pore widths of *ca.* 0.13-0.25 μm. The depth of the pore may also be significant: *ca.* 15 μm for stomata. The significance of pore width, and the proximity of the evaporating surface to the lower opening of the pore were explored using Nuclepore membranes and are discussed in some detail in Chapter 6.

The effects of humidity on convective flow both in the plant (Section 5.3.1.1) and for Nuclepore membranes (see Section 6.3.6) suggest that the humidity differential between the inside and outside of the plant is very important: flow rates are slow if roots are few or damaged. Also, if the evaporating surface within Nuclepore chambers is low, static pressures are low (Section 6.3.6c). It seems reasonable to conclude that the humidity within the plant, by a tendency to displace a proportion of the oxygen and nitrogen, initiates an inward diffusion of atmospheric gases from the comparatively dry air outside the plant. It must be noted that when the humidity differential is zero, at RH 100%, there is virtually no convective flow for either the plant (Figs. 5.02a & 5.12) in the dark, or Nuclepore membrane (Fig. 5.02b), or where there is no heating effect. Because of the relatively small difference in the concentration of water vapour in air between 0 and 100% RH, i.e. 2-3%, the direct contribution of the internal evaporation of water to the total convective flow must be small. This is somewhat contrary to Dacey's suggestion of a "biological steam engine" (1981), which implies that the convective flow is "driven" solely by water vapour.

Relative humidity within the plant will be high because of constant evaporation from the cells adjoining the gas-spaces, and this water vapour will have the effect of reducing the concentrations of N_2 and O_2 relative to those in the drier air outside. Thus, the lower the external RH, the steeper will be the diffusion gradients and this will

result in a more rapid diffusion of air into the plant and a faster diffusion of water vapour outwards. However, if the water vapour within the plant is replaced by evaporation as rapidly as it is lost, the internal water vapour partial pressure will tend to be sustained, whilst the total gas-pressure within the plant will rise because of the inflow of the atmospheric gases. For the plant to pressurise significantly the resistance to the inward diffusion of gases must be effectively less than the resistance for a reverse Poiseuille flow from the leaf sheath to the atmosphere. If this resistance was very high and convective throughflow was prevented, then, in dry atmosphere, the total pressure in the plant (Pi) should approach numerically the atmospheric pressure (Pa) plus the saturated watervapour pressure (P_{wv}) at that temperature according to the equation:

$$Pi = P_a + P_{wv} \qquad (5.01)$$

At 296°K this would amount to 1041 kPa, and a ΔP_s of approx. 2808 Pa would have been created. Thermal transpiration (Reynolds, 1879), which accounts for a proportion of the convective flow in water-lilies (Dacey, 1981, 1987; Schroder *et al.*, 1986), also may have contributed to the flows observed in *Phragmites*, but a temperature differential is always necessary. Under ideal Knudsen conditions, the pressure differential is governed by the relationship:

$$Pi = P_a \sqrt{(Ti/Ta)} \qquad (5.02)$$

and a ΔP_s of only 170 Pa per °K can be expected. In the light, the highest ΔT recorded between the culm pith cavity of *Phragmites* and the atmosphere did not exceed 2°K, and hence, it follows that the potential for pressurization by thermal transpiration in these experiments should have been very much less than for one which was humidity-induced.

Clearly, resistances to a Poiseuille outflow from *Phragmites* leaf-

sheaths to the atmosphere are not sufficient to allow the creation of really high pressure differentials by humidity-induced diffusion or thermal transpiration. Indeed the exact nature of the resistance is still uncertain, but it seems to involve the stomata. It has been shown elsewhere (Schroder *et al.*, 1986) that pore sizes within the Knudsen regime (pore diameter <0.1 μm, (i.e. less than λ, the molecular mean free-path) will be most effective for minimising Poiseuille flow. However, as shown in Chapter 6, appreciable humidity-induced pressurisations can arise with pore sizes $>10^{-7}$ μm, provided that internal rates of evaporation and partition resistance to Poiseuille flow are still sufficiently high.

It is very difficult to determine the width of stomatal apertures in living *Phragmites* leafsheaths because of surface waxes and the sunken position of the narrowest part of the aperture. From scanning electron micrographs and pressurised-flow measurements, however, the effective widths of nodal stomatal apertures appeared to be of the order of 0.13 - 0.25 μm and the depth, 15 μm.

There may be several reasons why PAR should lead to an increase in the convective flow:

(a) Si-rubber impressions appeared to show that light causes some opening of the stomata, and the very low flow rates in darkness, even at low RH may have been due to closed stomata. It could seem paradoxical that the opening of stomata should enhance humidity-induced diffusion, however, since the more open the stomata, the less resistance will they offer to outward Poiseuille flow. In the "closed" condition, however, projecting waxes obscure the opening. It is conceivable that these could help to reduce the humidity gradient across the pores by introducing additional boundary layers. Also, it may be that the degree of stomatal opening is critical and achieves an

optimum balance for diffusive inflow and Poiseuille outflow. (It is interesting that in water-lilies it has been suggested that pores beneath the palisade layer could be the major partition resistance. Further investigation of this aspect of the convection phenomenon is required).

(b) Light can increase ΔT, and warmer conditions within the plant will increase the water-vapour partial pressure and lead to a steepening of the diffusion gradients for the entry of atmospheric N_2 and O_2. This can described as *thermally enhanced humidity-induced diffusion.* The potential for this enhancement is approx. 6% per degree in the range 293-303°K.

(c) Higher internal temperatures in the light would increase the tendency for the entry of cooler gases by thermal transpiration.

(d) There may be a small direct pressurization by photosynthetic oxygen produced during the fixation of transpiration-stream carbon sources found by Brix (1988).

The results have highlighted how convective flows can increase the oxygen regime of gases venting through the rhizome, and, by enhancing the supply of oxygen to the root-rhizome junctions, cause an increased diffusion of oxygen to the fine laterals and young parts of adventitious roots, followed by outward radial diffusion. Previous experiments have indicated that more oxygen may diffuse from the basal laterals than from the adventitious roots (Armstrong & Armstrong, 1988; Conlin & Crowder, 1989, and Chapter 4); also, that even in solution culture, anoxic conditions can prevail a short distance away from the lateral root zone (Section 5.3.1.5 & 5.3.1.7).

It is shown in Chapter 2 that the gas space of the roots is continuous with that of the rhizome at the rhizome-root junction . It would seem, however, that because of an apparent lack of a through-

flow pathway in the root, root aeration must occur principally by gas-phase diffusion (see also Armstrong, 1979; Koncalova *et al.*, 1988; Beckett *et al.*, 1988) and that enhancement of root oxygen by the through-flow convection is because it sustains higher oxygen concentrations at the root-shoot junctions.

It must be emphasized, that when throughflow convection does not occur, the underground parts will be chiefly aerated by diffusion (Beckett *et al.*, 1988). The results suggest that should there be no convection or only slow convection at night (e.g. in the absence of wind, see Chapter 7), the oxygen concentrations within the rhizome and roots are likely to decline markedly. In the examples shown, night-time oxygen concentrations of 11% (11 kPa) are indicated, whereas in the light, values in excess of 19 kPa were recorded. The results of the laboratory experiments (Section 5.3.1.5), together with the field experiments on intact culms (Section 5.3.2.3), suggest that especially in summer, the onset of rapid daytime convective flows may help to flush out stale O_2-depleted, CO_2 and ethene-enriched gases accumulated in the underground parts on still nights (i.e. when there is no Venturi convection).

Thus, there could be diurnal fluctuations in root aeration and in the dimensions of the oxygenated rhizospheres. The size of these fluctuations will of course depend upon several factors. Among these are the degree of submergence of the culms, culm frequency, and rhizome lengths. In the case of the roots, the distance of the tissues from the nearest venting point will be important. It can be envisaged that, in some parts of the root system, perhaps stelar zones and the apices of long roots, very low oxygen concentrations may prevail during the night. If convection were to lead to a renewal of oxygen in these parts during the day, the rise in oxygen status or in oxygen

efflux could be enormous in percentage terms. It should also be noted that under conditions of high humidity, or during rain, when HIC is very low, rhizome aeration will depend upon wind-generated Venturi-convection (Chapter 7) and upon diffusion.

Although light clearly plays a major role in the convection, there is no evidence in these experiments for any substantial photosynthetic enrichment of the oxygen supply from the shoot system. Earlier investigations of oxygen concentration gradients within the *Phragmites* culm and rhizome system also indicate this (Yamasaki 1984; Brix 1988), and oxygen concentrations in gases venting directly through syringes inserted into living culms in the field were only marginally greater than atmospheric (Fig. 5.12 & Armstrong & Armstrong, 1991). Therefore, it may be assumed that this is because the processes involved in driving the convection will always tend towards a dynamic equilibrium in which the oxygen concentration within the leaf sheaths and culm will be sustained at a level only marginally above atmospheric, primarily because of the N_2 inflow by diffusion stimulated by the tendency for internal oxygen concentrations to rise. The results of Brix and of Yasmasaki also indicate the existence of convective flows since their results cannot be explained in terms of diffusion alone.

Finally, extrapolating from the data presented here, where flows of up to 260 nm^3 s^{-1} were recorded from sturdy 2 m long culms in the field, indicate that convection can transfer up to 0.3 kg_A/m^2 of oxygen into the underground parts of a *Phragmites* stand in a 12 h light period at a shoot density of 100 m^{-2}. This rate of transfer is more than 30-100x greater than could be achieved by diffusion alone (calculations assume a respiratory demand of 7.5 mg m^{-3} s^{-1} and a rhizome porosity of 50%). Extrapolating from the highest HIC rates measured in the present experiments, where the shoots were young and relatively short, gives a

transfer rate of only 0.025 kg O_2 m^{-2}. However, even this would be about 3 - 11x the amount which could be transported by diffusion alone. It must be recognised that not all of this oxygen will be used in respiration or in release to the soil: a large proportion could be vented back to the atmosphere. Nevertheless, a major impact of the convection will be to increase the availability of oxygen for release from root to soil than would be the case if *Phragmites* aeration depended entirely upon diffusion.

SUMMARY

The first direct evidence of a *humidity-induced* convective throughflow of gases in a grass is reported for *Phragmites*. The flow appears to be initiated in living leaf sheaths and in the living nodal stomatal regions of the culm. The convected gases are transmitted via gas-spaces in the culm and underground rhizome, and are vented via old broken culms. The convection is particularly rapid at low atmospheric humidities and increases with increasing PAR. It is shown that the *Humidity-induced convection* causes direct enhancement of rhizome aeration, and by increasing the oxygen regime (a.a. conc.) at the root-rhizome junction, results in a greater diffusion of oxygen into the roots and into the rhizospheres of adventitious roots and their laterals. Substantial diurnal fluctuations in rhizome oxygen regimes and in root oxygen efflux may be attributed to humidity induced convection *per se*.

Static pressure diferentials up to 800 Pa and flow velocities of up to 800 mm min^{-1} per leafy shoot (flow rate, 960 x 10^{-6} m^3 h^{-1} per shoot) were recorded in the field. It is estimated that because of this type of convection up to 0.31 kg of oxygen d^{-1} m^{-2} may enter the rhizome system of vigorous stands of *Phragmites* during summer months. By comparison, diffusion alone could be expected to supply less than 0.01 kg m^{-2} d^{-1}.

It is shown that the mechanism of *humidity-induced convection* is probably based chiefly on humidity-induced diffusion into the plant under the influence of a steep concentration gradient caused by the humidity differential which is generated between the plant and the atmosphere.

CHAPTER 6

THE USE OF NUCLEPORE MEMBRANES TO INVESTIGATE THE CONVECTIONS CREATED BY HUMIDITY-INDUCED DIFFUSION & THERMAL TRANSPIRATION

6.1. INTRODUCTION

Papers by Dacey, Grosse and others (Section 5.1), suggested that convective gas-flows in water-lilies are driven by the process known as *thermal transpiration*; Dacey (1981) later concluded, however, that what has been called here "humidity-induced diffusion" might be the primary mechanism underlying the flows. Central to both of these mechanisms of pressure-generation and flow is the presence of a porous membrane : in the case of the water-lilies this is thought to be a cellular floor bearing the palisade layer; in the case of *Phragmites* it probably involves the stomatal surfaces of the leaf sheaths and, to a minor extent, the stem nodes (Chapter 5). A crucial property required of such membranes is that they should be permeated by pores of narrow diameter, preferably less than the mean free path length of the diffusing molecules.

Dacey (1987) used artificial microporous membranes (Nuclepore membranes) to extend his investigations on water-lilies. These thin (10 μm) polycarbonate Nuclepore membranes have discrete pores in one of a number of sizes in the range (MPD, 0.015 to 3 μm). By comparing changes in the N_2:Ar ratio of gases passing through leaves and also through membranes of known pore size, he estimated the effective pore size in *Nelumbo* to be in the Knudsen regime at *ca.* 0.03 μm.

Physical models have often provided valuable information on the aeration of both animals and plants, and for the present study the Nuclepore membrane seemed to offer many possibilities of studying the convective flow mechanism more easily than using the *Phragmites* plant. Consequently a physical model was designed with the object of further investigating what was perceived as *humidity-induced* pressurisation, and of elucidating the relative importance of *thermal transpiration.*

In this model, Nuclepore membranes of known pore size were attached to small glass chambers, and convective flows of gases and static pressure differentials (impeded flow condition) were studied in relation to a variety of conditions imposed on opposite sides of the membrane. Data were obtained in relation to (a) pore size and porosity of membranes, (b) temperature gradients, (c) humidity gradients (d) gas species, and (e) membrane area. In addition, microcapillaries in series were used to produce resistances to convective flow, and the effects of this venting resistance on dynamic pressure differentials and flows was measured.

Ancillary to the experimental work, a theoretical treatment of humidity-induced pressurisation and flows in the Nuclepore assembly was also undertaken. The equations used are introduced in section 6.2.3, while the results arising from their application are commented upon there and under appropriate headings in Section 6.3.

Abbreviations

HIC = humidity-induced convection.

λ = molecular mean free path length (μm).

MPD = membrane (of) pore diameter (μm).

ΔP_d = dynamic pressure differential. Pressure differential across the membrane under conditions of convective throughflow.

ΔP_s = static pressure differential. Pressure differential developed with convective flow blocked. Positive pressure differential indicates a higher pressure beneath the membrane and *vice versa*.

S = velocity of horizontal gas-flow across membrane (m s^{-1}).

ΔT = temperature differential vertically across membrane; positive value indicates a higher temperature beneath the membrane, and *vice versa*.

W = distance between water surface and membrane (mm).

6.2. MATERIALS & METHODS

6.2.1. *Physical Model*

A sectional view of the apparatus is shown in Fig. 6.01.

Nuclepore membranes (diameter 25 mm, thickness 10 μm, and advertized pore diameters of either 0.015, 0.03, 0.08, 0.1, 0.4, 1.0 or 3.0 μm) were attached with Si-rubber to one end of a water-jacketed cylindrical glass-chamber (diameter, 20 mm; length 90 mm), which could be filled with water to within a few millimetres of the membrane in order to create a humidity gradient. The diameter of membrane left exposed was 18-20 mm. The porosities of the membranes were claimed by the manufacturers to be 10 *per cent*. The other end of each glass chamber contained a rubber bung supporting three glass tubes (diameter, 3 mm), two of which protruded sufficiently to bring them close to the lower surface of the membrane. A Ni:Cr thermocouple attached to a digital thermometer (RS components) was fused into one of these, and the thermocouple tip was positioned as close as possible to, but not touching the lower surface of the membrane; the second opened 1-2 mm below the membrane surface and directed any convective flow out of the chamber via a three-way tap to either a soap-film flow meter (length 300 mm ; inside diameter 5 mm) or to a pressure transducer (Furness Controls Ltd). The third (short) tube was used to fill or drain the chamber of water.

For studying humidity-induced diffusion and thermal transpiration, the membrane end of the chamber projected through a neatly fitting hole into a Perspex "wind" tunnel. Through this, gas was blown at different rates horizontally over the membrane to modify the surface boundary layer above the membrane, and at different humidities to develop a range of humidity gradients vertically across

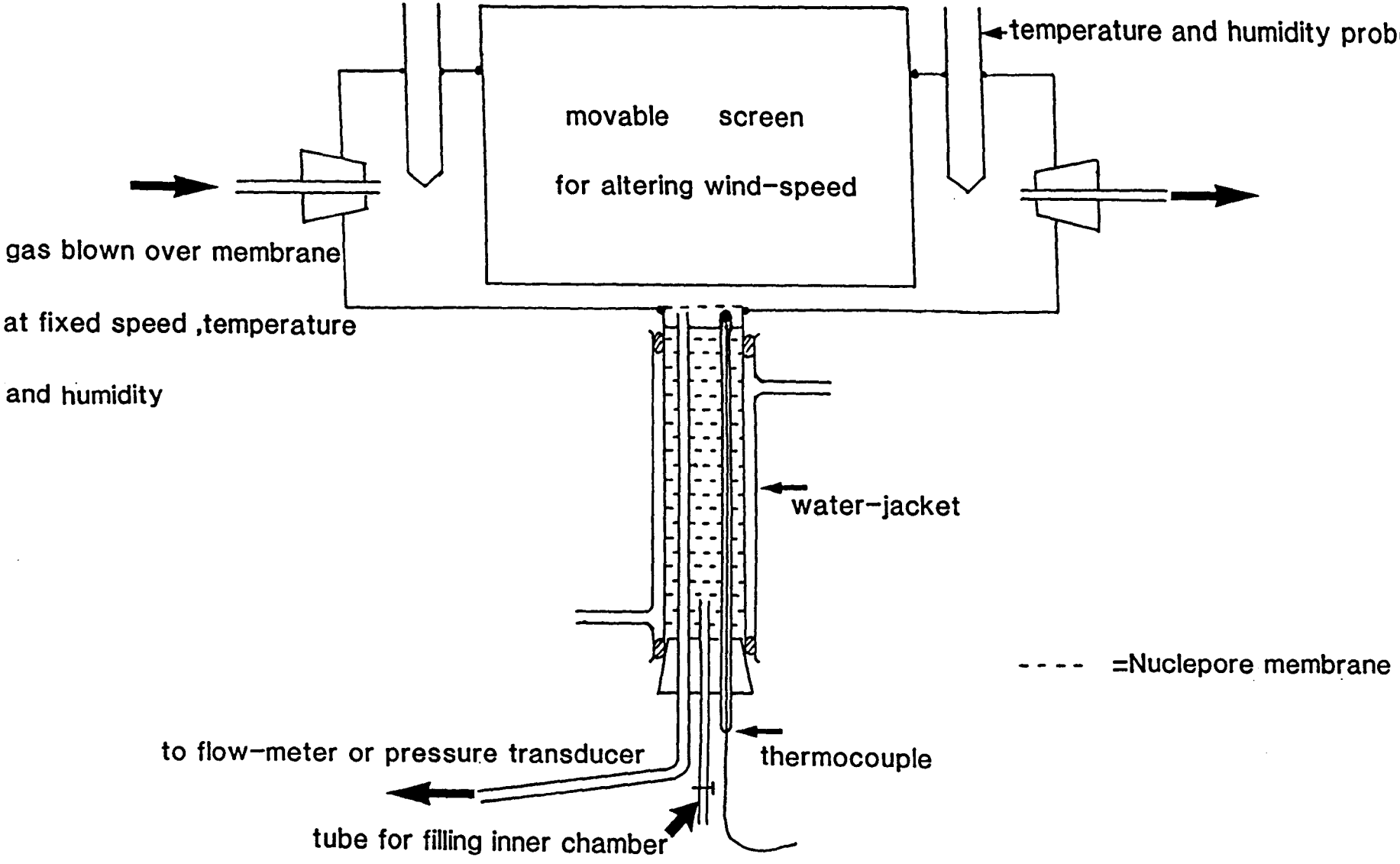

Fig.6.01

APPARATUS FOR INVESTIGATING HUMIDITY-INDUCED CONVECTION USING NUCLEPORE MEMBRANES

the membrane. The temperature and humidity of the gas before and after passing over the membrane were detected by humidity / temperature probes (Vaisala, Sweden) inserted into the "wind-tunnel". Temperature differentials vertically across the membrane were produced by circulating water at various temperatures through the water-jacket surrounding the chamber. For this a combination of a heated water-bath and refrigeration assembly (Grant Instruments Ltd., Cambridge) was used. The temperature of the gas immediately above the membrane was monitored using a Ni:Cr thermocouple and digital thermometer as above (not shown in Fig. 6.01).

For studying 'Poiseuille' flow through the membranes, the chambers were not inserted into the wind tunnel.

6.2.2. *Experiments*

6.2.2.1. *Measurements of pore diameters and porosities of membranes*

Having found some anomalous results for HI convection rates and ΔP_s values in some preliminary experiments, it was felt necessary to check the porosities and pore diameters of the various membranes to see if they corresponded to the manufacturer's specifications. Small portions of each membrane, (MPD= 0.03 - 3 μm), were sputtered with as fine a coating of gold as possible so as not to obscure the pores, and examined by scanning electron microscopy.

6.2.2.2. *Poiseuille flow through Nuclepore membranes*

With neither a humidity nor a temperature differential across the membrane, the rate of flow of dry air through each membrane was measured, (MPD = 0.022 - 3 μm), at various dynamic pressures: 100 - 400 Pa for MPD = 0.022 - 0.046 μm, and for the membranes with larger pores, at pressures between 2 and 40 Pa. By extrapolation the

Poiseuille flow rate through each membrane was found for a ΔPd of 100 Pa.

6.2.2.3. *Effects of a temperature differential across the membrane, with or without a humidity gradient.*

For membranes of MPD 0.015 μm or 0.046μm, convective flow rates and ΔP_s values were recorded for different ΔT values across the membrane: -4 to +7.5 °K.

(i) ***No humidity gradient.*** The chamber beneath the membrane contained silica-gel granules to 15 mm below the membrane to ensure a dry atmosphere below the membrane, and dry air was passed over the membrane at a velocity of 0.056 m s^{-1}.

(ii) ***With humidity gradient :*** Here, W = 4.5 mm ; S (dry air) = 0.056 m s^{-1}.

6.2.2.4. *Effects of pore diameter*

Humidity-induced convective flow rates and ΔPs values were measured for membranes as follows: MPD = 0.015-3 μm; S (dry air) = 0.056 m s^{-1}; W = 4 mm; ΔT=0. Also, various predictions of ΔPs and convection for the Nuclepore assembly were made based chiefly on values of W = 4 mm and a membrane porosity of 10%. For comparison with HIC in the plant, ΔPs and HIC values were predicted for MPD = 0.2 - 3 μm, external RH = 50%, W = 10 μm and, for convenience a membrane porosity 1%. It was difficult to determine leaf sheath porosity accurately; it seemed to lie between 0.4 and 1.0%.

6.2.2.5. *Effects of different gases*

At an early stage of the Nuclepore investigations it was decided to test the pressurising effects of gases other than air. To this end humidity-

induced convection rates and ΔP_s values were measured for "winds" of different dry gases across the membranes: MPD = 0.015 or 0.046 μm; S = 0.053 m s^{-1}; W = 4 mm; ΔT= 0. The gases used were H_2, He, CH_4, N_2, O_2 and Ar, whose diffusivities in water-vapour ranged from <0.2 to 1 cm^2 s^{-1} and whose relative molecular masses varied between 2 and 42.

6.2.2.6. ***Effects of varying the humidity gradient***

(a) varying the humidity of "wind" across membrane with and without a temperature differential : Humidity-induced convective flow rates and ΔP_s values were measured for MPD = 0.046 μm, S= 0.0393 m s^{-1} and W = 4mm, and the humidity of the air streaming across the membrane was varied between 0.7 and 65% (using an ADC humidity generator). The ΔT was zero or +1.4°K.

(b) Varying dry-air wind speed over the membrane : Humidity-induced convective flow rates and ΔP_s values were measured at a range of dry-air wind speeds across the membrane for a membrane of MPD 0.046 μm, and with the evaporating water surface at 4 mm below the membrane. The humidity loading in the air after it had passed over the membrane was also recorded using a humidity probe.

(c) Varying distance between membrane and underlying water surface. The depth to the evaporating water surface was varied over the range 2-35 mm for two membranes, MPD 0.046 and 0.075 μm, and the static pressures and flows recorded at a dry air wind speed over the membrane of 0.046 m s^{-1}.

6.2.2.7. ***Effects of membrane area***

HI convection rates and ΔP_s values were measured for the entire membrane area, and subsequently for progressively smaller areas, by gradually covering the membrane with Sellotape. MPD = 0.03μm; W= 4mm;

S (dry air) = 0.0393 m s^{-1}; ΔT = 0.

6.2.2.8. *Increasing resistance to venting using "Microcap" capillaries*

HI convection rates and ΔP_d values were measured for different resistances to venting by placing microcaps (each of 1 μl volume) in series between the exit tube and the flow meter. MPD = 0.046 μm; W= 4mm; S (dry air) = 0.0532 m s^{-1}; ΔT = 0.

NB Unless otherwise indicated, experimental points relating to any particular membrane are based on the mean of 3 readings; variation was so small that standard errors are within the symbol size.

6.2.3. HISTORICAL & THEORETICAL

The pressurisation and gas-flows which can be created by the establishment of temperature and/or humidity differentials across microporous partitions are phenomena which appear never to have been widely appreciated; even in physics texts, humidity-induced pressurisations are rarely mentioned, and temperature-induced gas-flows are usually dealt with briefly if at all. Also, considerable confusion now surrounds their terminology, and it seems appropriate to try to clarify this before proceeding to any theoretical treatment.

The temperature-induced flow which occurs (colder to warmer) when ***dry*** gases are separated by a microporous partition was strictly defined and described by Reynolds (1879) and termed ***thermal transpiration.*** Unfortunately in contemporaneous and subsequent studies the terms ***thermal-osmosis*** and ***thermo-diffusion*** were coined, sometimes being used to describe thermal transpiration, sometimes to describe what must have been pressurisation involving both thermal transpiration and humidity dependent factors. Denbeigh & Raumann

(1955) used ***thermo-osmosis*** to describe movements in which the diffusing species dissolved in the partition.

In view of the historical precedence set by Reynold's description it seems appropriate to retain the term ***thermal transpiration*** for the "dry" component of any plant pressurisation process, and to invoke some new term to specify any humidity-dependent component. In the case of the experiments with Nuclepore membranes described in this chapter the thermal transpiration component proved to be very small.

The term ***diffusion hygrometrique*** was used by Dufour (1874) in connexion with pressurisation induced by the presence of a wet gas on one side of a microporous partition. More recently, Dacey (1981) has referred to the mechanism as ***hygrometric pressurisation***, but this term can give the impression that the water vapour component in the gas directly causes the pressurisation and alone drives the convective gas-flows described in this and the previous chapter. However, it is evident from the following results that the incoming gases play an equally crucial part in the mechanism and form the bulk of the convective flow. In this thesis, the terms ***humidity-induced diffusion*** and ***humidity-induced convection*** have been adopted in preference to *hygrometric pressurisation* since they seem more descriptive of the processes involved.

In his first report on convective gas-flow in water-lilies Dacey (1980) suggested that the mechanism underlying the pressurisation and convection was *thermal transpiration*, but later suggested that *hygrometric pressurisation* (HIC in this thesis) might be a more important mechanism; Grosse and his colleagues have continued to maintain that *"thermal-osmosis"* is the dominant process.

A pre-requisite for both thermal transpiration and humidity-

induced diffusion is the presence of a porous partition in which the pore diameters are very small (Section 5.4). Ideally pore diameter, d, should be much less than λ, the mean free path length between intermolecular collisions (*ca.* 0.1 μm at normal pressure). Here, the rate of diffusion of one species is independent of all others because intermolecular collisions are rare compared with those between the molecule and the pore walls. This is Knudsen diffusion. When pore diameters are large compared to λ, diffusion depends upon concentration gradients and upon the frequency and types of intermolecular collisions and is termed *continuum diffusion.* At intermediate values of d, the *transition region*, diffusion is significantly influenced by both types of collision.

Although Dacey (1987) has claimed that the maintenance of a pressure differential in water-lilies implies that the average pore diameter must be $\ll$0.1 um, this is not supported by predictions in Schroder *et al* (1986) or by the experiments on HIC reported elsewhere in this chapter. In connexion with thermal transpiration in water-lilies, Schroder *et al* predicted the effect of pore diameter on pressurisation using an empirical formula which was derived by Takaishi & Sensui (1963) from experiments on the thermal transpiration of hydrogen and some other gases. The results (Fig. 6.02) show that significant pressurisation can be expected at pore diameters well in excess of λ, a situation in which Poiseuille Flow and *continuum diffusion* should be the governing processes. It seems reasonable to conclude from this, that for pressurisation to occur, it is only necessary that the effective resistance to Poiseuille flow should exceed that for *continuum diffusion.* The figure also shows that the relationship $Pi = P_a \sqrt{(Ti/Ta)}$ (equ. 5.02) will be approached at extremely small pore diameters only.

From the literature examined, it is not clear at exactly which

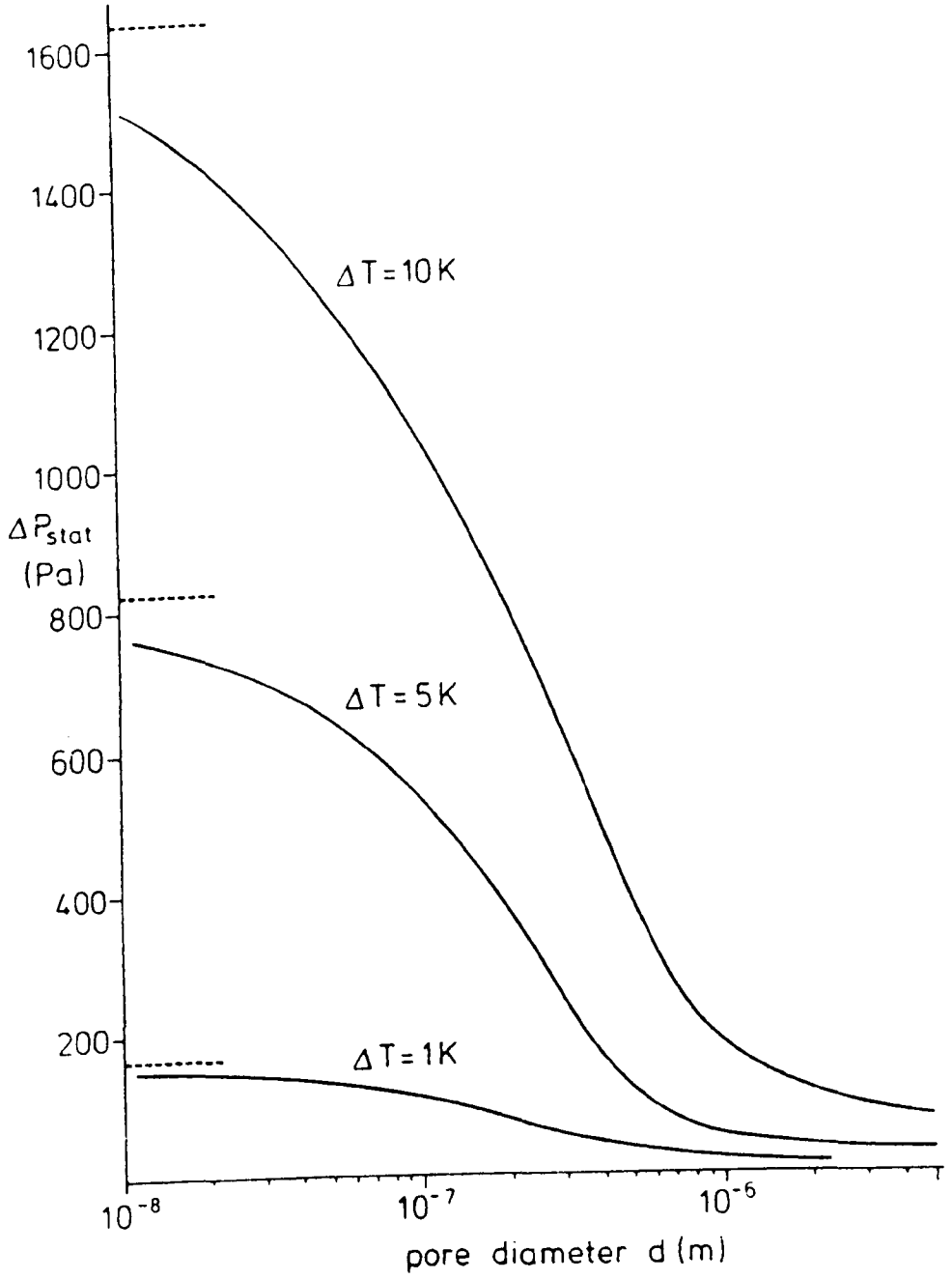

Fig. 6.02. Thermo-mechanical pressure difference $(\Delta P)_{stat}$ (zero net flow) as a function of the pore diameter, d, and at a pressure of 100 kPa and a temperature ΔT of 300°K (1 Pa = 1.02×10^{-4} m H_2O). The curves refer to nitrogen and are calculated on the basis of an empirical equation proposed by Takaishi & Sensui (1963). Parameter is the temperature difference between the bulk phases. The dashed lines indicate the Knudsen limits calculated on the basis of equation 6.13. [After Schroder, P., Grosse, W. & Woermann, D. (1986)]

pore diameter viscous flow will effectively cease. Takaishi & Sensui's experimental approach was dictated by the lack of any rigorous treatment for dealing with the transitional region, and in his book "Kinetic Theory of Gases", Present (1958) stated that no quantitative kinetic theory existed to deal with flow in the transition region where λ and d/2 are comparable. However, where λ is smaller that d/2, Present states that it is customary to apply the Poiseuille formula to any pressure flow. Hence, in the treatment developed below for predicting humidity-induced pressurisation in the Nuclepore assembly, it has been assumed that the Poiseuille formula (equ. 2.04) can be applied at all pore diameters $\geq$0.2 μm.

Attempts to induce the degree of thermal transpiration indicated by the Takaishi & Sensui equation were unsuccessful using the Nuclepore membrane assembly shown in Fig. 6.01 (see Section 6.3.3), and it has been concluded that it might not have been possible to maintain the intended temperature gradient across the membrane.

With humidification of the Nuclepore-topped chambers, substantial pressures were obtained but these did not approach the pressures predicted by equation 5.01, and, except with the smallest pore diameters, they also fell short of the pressures obtained with *Phragmites* where pore widths seemed always to exceed 0.1 μm in the light. The following mathematical treatment was derived to help to explain these observations and hopefully to provide among other things, an alternative means of assessing the effects on humidity-induced diffusion of such factors as pore diameter, pore length and porosities. Although the series of equations represents a relatively non-rigorous approach, the results obtained from them suggest that they represent a good appproximation to reality.

In the experimental assembly (Fig. 6.01), the diffusion path for

the escape of water-vapour evaporating from the free water surface can be treated as three segments. These are : (a) the header space between the water surface and the membrane, with diffusive resistance R_h, (b) the pore space through the membrane, with diffusive resistance R_{md}, and (c) any unstirred boundary layer above the membrane with resistance R_B. Following normal convention (Armstrong 1979), the diffusive resistance (s m^{-3}) of the header space can be determined from the equation:

$$R_h = L_h / (D_o A), \qquad (6.01),$$

where L_h is the distance (metres) between the water surface and the membrane, D_o is the mutual diffusivity (m^2 s^{-1}) of water-vapour and air, and A is the cross sectional area (m^2) of the chamber (equal to the area of the membrane). Similarly the diffusive resistance of the membrane can be obtained from the equation:

$$R_{md} = L_m / D_{md} \epsilon A, \qquad (6.02),$$

where L_m is the membrane thickness, ϵ the fractional porosity, and D_{md} will be the water-vapour diffusivity. The value assigned to D_{md} will vary according to the membrane pore diameters (MPD): if MPD is greater than 0.1 μm, D_{md} can be represented by D_o as in the header space, but for MPD $\leq$ 0.1 μm, it becomes a Knudsen Diffusion Coefficient (D_K), and is calculated from the following equation:

$$D_K = (d/3)\sqrt{[8RT/ (\pi M_i)]} \qquad \text{(Leuning, 1983)(6.03)},$$

where M_i is the molecular mass of the diffusing species i. For water vapour, the relationship between the Knudsen diffusion coefficient and pore diameter is shown in Fig. 6.23.

The boundary layer resistance is given by the equation:

$$R_B = L_B / D_o A, \qquad (6.04),$$

where L_B is the thickness of the unstirred layer, a function of the surface dimensions of the membrane and the wind speed in the

chamber above it. At wind speeds of 0.056 m s^{-1} the value used most frequently in the Nuclepore experiments, the boundary layer thickness appeared to be *ca.* 700 μm.

It follows that the diffusion rate (kg s^{-1}), J_C, for water-vapour loss from the free water surface within the Nuclepore chamber will be:

$$J_C = \Delta C / (R_h + R_{md} + R_B), \qquad (6.05)$$

where ΔC is the water-vapour concentration difference between the water surface and the upper limit of the unstirred boundary layer. If partial pressure difference is substituted for ΔC , and dry air is maintained above the boundary layer, then at 20°C and normal atmospheric pressure (P_a) the equation may be re-written:

$$J_v = (2.337 / P_a) / (R_h + R_{md} + R_B), \qquad (6.06)$$

where the water-vapour pressure at 20°C is 2.337kPa, P_a is 101.3 kPa, and 2.337/101.3 is therefore a concentration difference in fractional volume terms (m^3 m^{-3}). Since the presence of H_2O-vapour is at the expense of the other atmospheric gases, there will be a difference in partial pressure of these gases, ΔP_{on}, across the membrane, and this will be numerically equal to $J_v R_{md}$, i.e.:

$$\Delta P_{on} = J_v \times R_{md} \qquad (6.07).$$

This difference in partial pressure will generate a diffusion of atmospheric gases, J_a, into the chamber, the rate of which will be given as follows:

$$J_a = (J_v R_{md} / P_a) \times 1 / R'_{md} \qquad (6.08).$$

This approximately equates numerically with the maximum potential rate of convective gas flow. If the MPD $\leq$ 0.1 μm, D_{md} in R'_{md} (the membrane diffusive resistance to air) will be the average Knudsen diffusion coefficient for air for the appropriate pore size calculated from equation 6.03. It should be noted that Knudsen diffusion coefficients will always be less than D_o (Fig. 6.24) and also that, in

these cases, the outward diffusion of H_2O-vapour through the membrane will exceed any diffusive inflow of atmospheric gases.

If the escape tube from the chamber is now diverted solely to the pressure transducer (i.e. convection is blocked), there will be for a short time only, a net entry of atmospheric gases into the chamber, and because H_2O-vapour levels will be sustained by constant evaporative replacement, the total pressure in the chamber will rise. If MPD $\leq$ 0.1 μm, it is assumed that the pressure will rise until the partial pressure gradient for atmospheric gases disappears, i.e. "diffusion in" will then equal "diffusion out", and the total pressure in the chamber should equal $P_a + J_vR_{md}$; the static pressure differential will therefore be numerically equal to J_vR_{md} kPa. Where MPD $\leq$ 0.1 μm it is assumed that there will either be no Poiseuille backflow or this will be insignificantly small [see Fig. 6.04A(i)]. Where MPD > 0.1 μm, however, any tendency to pressurise will be counteracted by a Poiseuille backflow through the membrane, and the potential static pressure differential (numerically J_vR_{md}), will not be realised; rather, there will be some lower value attained at which a diffusive inflow will be balanced by Poiseuille backflow. This "real" pressure differential, ΔP_{rl} (elsewhere in this thesis ΔP_s), can be determined using the following equation where the potential static pressure differential, J_vR_{md} is represented as ΔP_{ps}:

$$(\Delta P_{ps} - \Delta P_{rl})/P_a \times 1/R_{md} = \Delta P_{rl}/R_{mP} \qquad (6.09)$$

For membranes with MPD $\geq$ 0.2 μm, the Poiseuille Flow resistance, R_{mP}, may be found from the expression $8\eta L_m/(\epsilon A r_1^2)$ (see equations 2.03 & 2.05).

The expression $(\Delta P_{ps} - \Delta P_{rl})/P_a \times 1/R_{md}$, will be the diffusive inflow ($m^3\ s^{-1}$) under the partial pressure gradient of atmospheric gases numerically equal to $\Delta P_{ps} - \Delta P_{rl}$, while P_{rl}/R_{mP} will be the

Poiseuille backflow (m^3 s^{-1}) at the resultant "real" pressure differential ΔP_{rl}.

To predict the convective flow rates from the experimental assembly, it is necessary to incorporate the resistance to venting through the outlet tube and soap film flow-meter. If pores are within the Knudsen regime, an equation having a similar form to equation 6.09 may be used, but in which R_{mP} is replaced by the resistance of the venting path, R_{vP}, and in which ΔP_{rl} becomes the dynamic pressure, ΔPd:

$$(\Delta P_{ps} - \Delta Pd)/P_a \times 1/R'_{md} = \Delta Pd/R_{vP} \qquad (6.10)$$

The convective flow, HIC, is then given by:

$$HIC = \Delta Pd/R_{vP} \qquad (6.11).$$

If the pore diameters are outside the Knudsen regime there will be two Poiseuille flow resistances acting in parallel, that of the membrane, R_{mP}, and that of the venting path, R_{vP}. It is necessary, therefore, to determine first the resultant resistance to Poiseuille flow, R_{TP}, from the relationship:

$$1/R_{TP} = 1/R_{vP} + 1/R_{mP} \qquad (6.12),$$

and then to use R_{TP} in place of R_{vP} in equations 6.10 & 6.11.

The results obtained from this theoretical approach are presented at appropriate points in the Section 6.3 below. However, it is particularly interesting to note that, as with output from the Takaishi & Sensui equation, significant pressurisation and convective flows are possible at pore diameters greatly in excess of λ (e.g. Fig. 6.17). Only when the pore diameters become greater than *ca.* 10 μm do the resistances to Poiseuille outflow become so small relative to that for diffusion, that no significant pressurisation or convective flows are obtained.

6.3. RESULTS AND DISCUSSION

6.3.1. Pore diameters and porosities of membranes

The pore diameter and porosity of the large-pored membrane (MPD = 3 μm), were approx. as advertised, but those with smaller pores often differed considerably from the manufacturer's specifications: see Table 6.01. This was first detected when different batches of membranes said to be of MPD 0.03 μm, produced very different static pressure differentials under identical conditions. Scanning electron microscopy (e.g. Fig. 6.03) confirmed the differences and was used to determine the true pore diameters. Thus, in most of the following experiments it is the corrected values of MPD that are cited. However, the electron micrographs also revealed that the random neutron bombardment used to create the pores had resulted in a scatter of much larger holes, the result of partial overlapping, (Fig. 6.03a). To some extent these larger holes are bound to have caused some lowering of static pressure differentials and some raising of the convective flows in the experiments. However, no attempt to quantify the incidence of such holes or their effects has been attempted.

During the course of the experimental work it became evident that in most cases membrane porosity also differed from the manufacturer's published specification. To ascertain the correct porosities, however, proved less straightforward than determining pore diameters. Scanning electron micrographs covered such a small field of view, and revealed such a clumped distribution of pores in some cases, that many more preparations would have been required to clarify the situation. Other attempts to resolve the question of membrane porosity are reported in the following section.

TABLE 6.01. Nuclepore membranes : details of specified and estimated pore sizes and porosities.

MPD (μm)		Porosity (%)			
(a) advertised	(b) measured SEM	(a) advertised	(b) SEM	(c) Poiseuille method	(d) From HIC ΔP_s
0.015	≤ 0.015	10.0	0.80	-	1.3
0.03(1)	0.022	10.0	0.54	1.1	2.7
0.03(2)	0.037	10.0	0.61	2.2	3.8
0.03(3)	0.046	10.0	1.08	10.4	8.3
0.08	0.095	10.0	2.50	17.4	15.7
0.10	0.075	10.0	1.51	14.75	12.6
0.20	0.018	10.0	9.26	20.6	22.5
0.40	0.595	10.0	20.30	18.9	≤ 30.0
1.00	0.90	10.0	10.33	18.9	≥ 30.0
3.00	3.00	10.0	-	9.9	-

Note: The figures in brackets under MPD column (a) indicate different batches of membranes. The figures in porosity columns (c) could be under-estimates by up to 20% because of the variable thickness of protruding silicone rubber fixative securing the membrane.

Figure 6.03 (overleaf)

Fig. 6.03. Scanning electron micrographs of a selection of Nuclepore samples: (a) MPD 0.9 µm - manufacturer's spec. 1.0 µm: note overlapping pores top left; (b) MPD 0.596 µm - manufacturer's spec. 0.4 µm; (c) MPD 0.046 µm - manufacturer's 0.03 µm; note clumping of uneven distribution of pores.

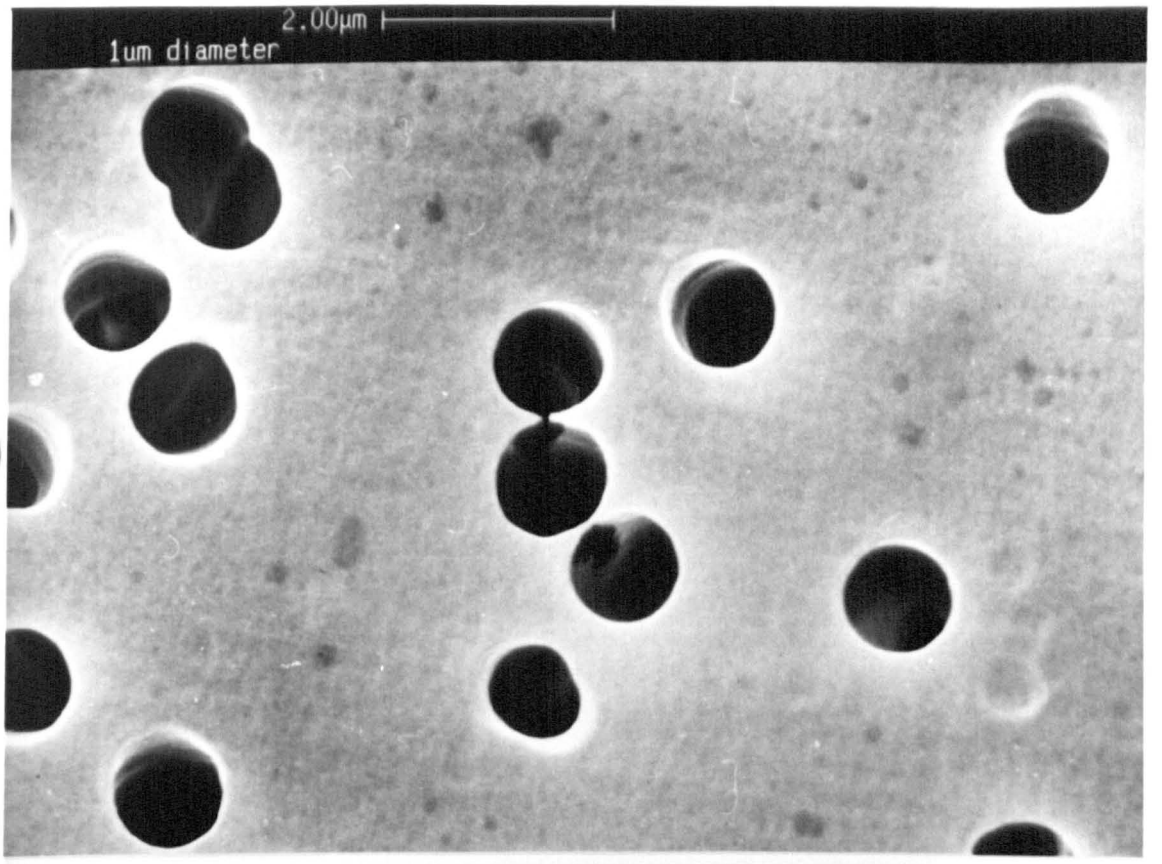

(a)

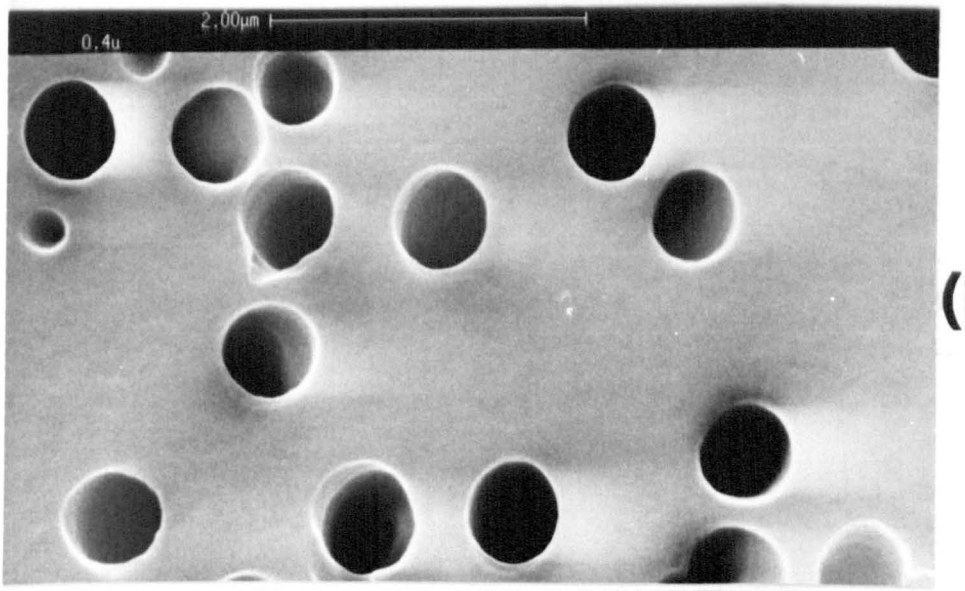

(b)

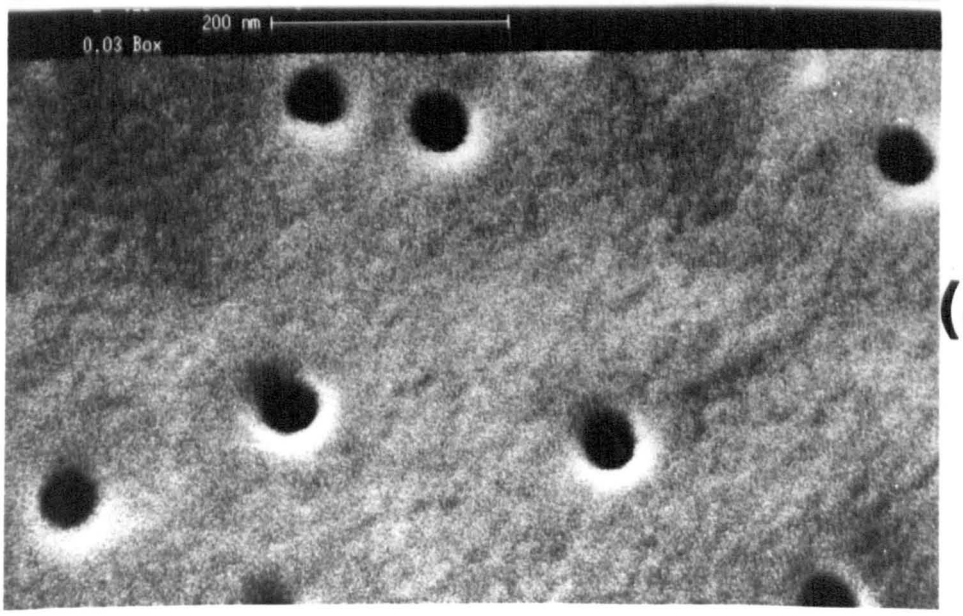

(c)

6.3.2. *Poiseuille and diffusive flows through membranes pressurised by dry air.*

Creating and measuring outflows from a dry Nuclepore chamber was conceived as a possible way of clarifying the porosity of membranes; it has also served to illustrate the dominance of diffusion at small pore diameters.

If a pressure differential is maintained by forcing dry air into a dry Nuclepore assembly through what is normally the outlet pipe, there will be a net outflow of gas from the assembly via the Nuclepore membrane. At pore diameters $\leq$ 0.1 μm this flow should be almost entirely diffusive (Section 6.2.3), and caused by the density gradient induced across the membrane by the compression of gas within the assembly. With a pressure differential of 100 Pa this will amount to approx. 100/101,300 m^3 m^{-3}. The flow should be calculable from the expression (100/101,300) x $1/R'_{md}$, and will decline with declining pore diameter through the reduction in the value of the Knudsen diffusion coefficient. At pore diameters >0.1 μm the outflow will have both a diffusive and a convective component. The diffusive component will again be given by the expression (100/101,300) x $1/R'_{dm}$ but should be independent of pore diameter, and provided that membrane porosities do not differ, should be the same for all membranes. However, the Poiseuille flow component should vary in proportion to the fourth power of the pore radius (equ. 2.03). However, if it were possible to apply the Poiseuille formula irrespective of pore size (i.e. even at pore diameters <0.2μm), then for membranes of diameter 20 mm, porosity 10% and with an applied pressure of 100 Pa, the Poiseuille component of any flow should decline with decreasing pore size as shown in Fig. 6.04(i). If the diffusive component is now plotted for all values of pore

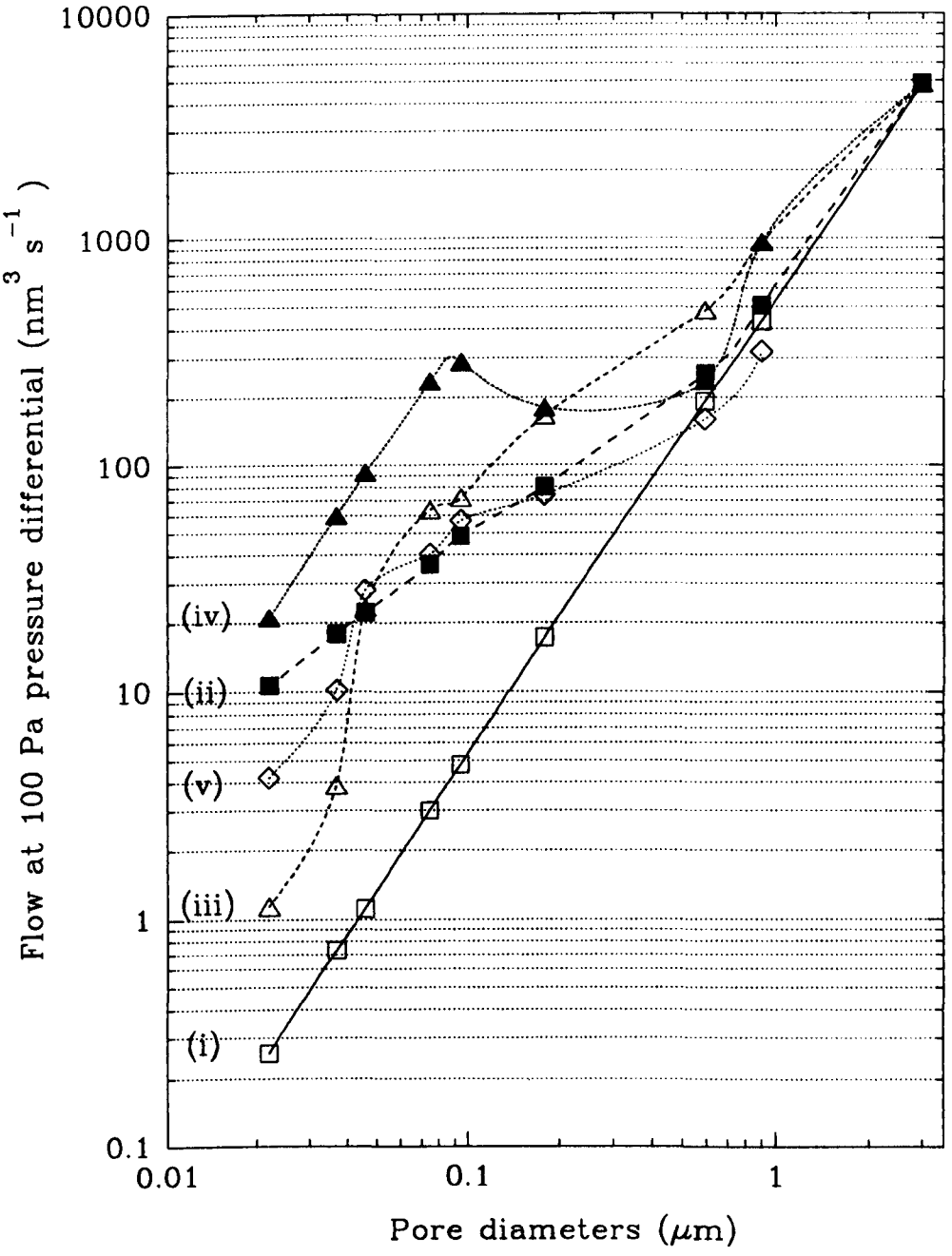

Fig. 6.04. Predicted and experimental gas flow through Nuclepore membranes under an applied pressure of 100 Pa dry air. (i) prediction for Poiseuille flow only (ii) prediction for Poiseuille flow and diffusive flow arising from the density gradient created by the 100 Pa pressure differential, (iii) experimental data uncorrected for porosity, (iv) as (iii) but corrected for porosity on basis of SEM findings, (v) as (iii) but corrected from results of HIC experiments and the type of data shown in Fig. 6.17.

diameter ≤ 0.1 μm, and the sum of diffusion and Poiseuille flow is plotted where pore diameter is >0.1 μm, the relationship between flow and pore size deviates from the previous plot and is shown in Fig. 6.04(ii). These results indicate that Poiseuille flow becomes subordinate to diffusion at pore diameters of approx. 0.3 μm and below. Also, it may be seen that even if there was a Poiseuille flow at pore diameters <0.1 μm, such flows would be very small compared to diffusion.

When the experimental data were plotted without adjusting for any porosity differences between membrane batches, the curve [Fig. 6.04(iii)] was obtained. Although, as expected, this plot lies above the Poiseuille flow plot [Fig. 6.04(i)], the correlation with curve (ii) is not good probably because of porosity differences between the membranes. Adjustments based on the porosities found from the scanning electron microscopy changed but did not really improve the picture [Fig. 6.04(iv)], but a correction based on porosities deduced from the humidity-induced flows and theoretical plots for humidity-induced flows gave curve (v) which shows a tolerably good agreement with the expected result, curve (ii). These porosity values together with those necessary to convert curve (iii) to curve (ii) are shown in Table 6.01, together with the values derived from the scanning electron microscopy. It is concluded that the closest to the true porosities are probably those derived from the Poiseuille flow method.

Although Poiseuille flow is shown to dominate at pore diameter >0.3 μm, it becomes evident from an application of the appropriate equations in Section 6.2.3, and from the results of subsequent experiments (sections 6.3.6c), that when HID operates, diffusive inflows can be large enough compared to Poiseuille backflow to create significant pressurisation and convective throughflows with the

Nuclepore assembly up to pore diameters of at least 3 μm.

6.3.3. *Effects of varying* ΔT

With no humidity gradient and an MPD of 0.046 μm, virtually no pressurisation could be detected over the range of ΔT shown : -3 to +8°K. Even when MPD was 0.015 μm, ΔP_s values were low: +50Pa and -20Pa when ΔT was +8 and -2.8°K respectively (Fig. 6.05b). As expected, however, zero pressurisation is indicated when ΔT= 0. However, the flow rates for this membrane (MPD = 0.015 μm) were very slow and difficult to measure accurately; this was attributed to its unexpectedly low porosity (Table 6.01).

On the other hand, when a humidity gradient was maintained (Fig. 6.05a), ΔP_s values for MPD 0.015 μm were high : 1240 Pa, and 1560 Pa for ΔT's of -2° & + 3.5°K respectively, but again, due to the low porosity of this membrane, flow rates were much lower than expected. Similarly ΔP_s values for MPD 0.046 μm were substantial when a humidity gradient was maintained : 85 Pa and 147 Pa for ΔT's of -3.5° & +5.5°K respectively (Fig.6.06a). Convective flows for this membrane were easily measured : 13 & 22 $nm^3\ s^{-1}$ for the above ΔT's (Fig. 6.06b).

In theory, for pore diameters of 1 μm and below (Schroder & Grosse, 1986), the increase in pressure due to *thermal transpiration* should be as shown in Fig. 6.02, and for pores as small as MPD 0.015μm, the static pressure differential, ΔP_s, should approach that given by the equation:

$$\Delta P_s = P_a \sqrt{(T_i/T_a)} - P_a, \qquad (6.13)$$

where $P_a \sqrt{(T_i/T_a)}$ is the total internal pressure, P_a = atmospheric pressure (101 KPa), T_a = external temperature (°K) and T_i = internal temperature (°K). For each degree rise in temperature one can thus

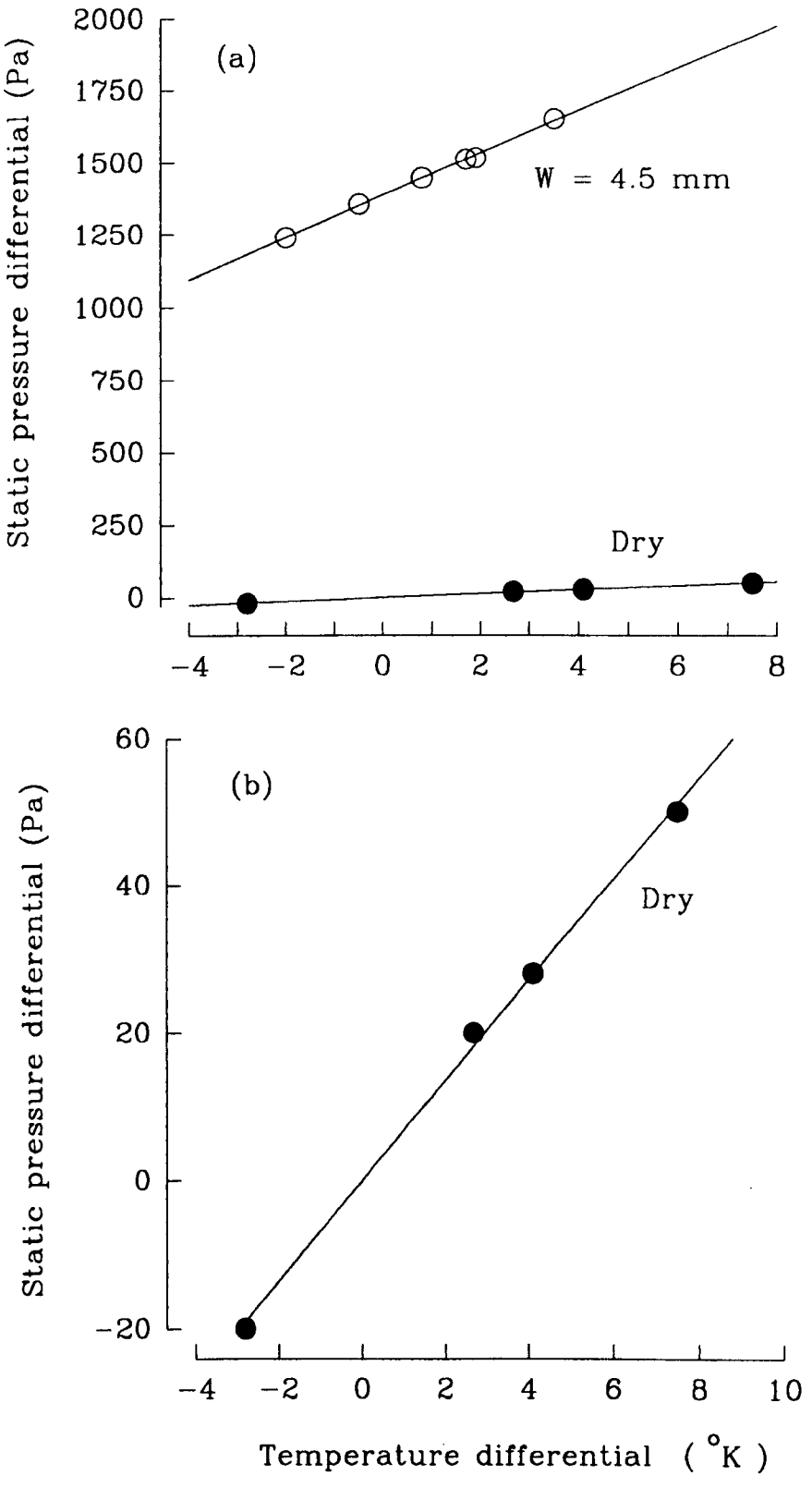

Fig. 6.05. The relationship between static pressure and temperature differentials (a) with, & without, and (b) without, a humidity gradient. MPD=0.015 μm; S = 0.056 m s^{-1}.

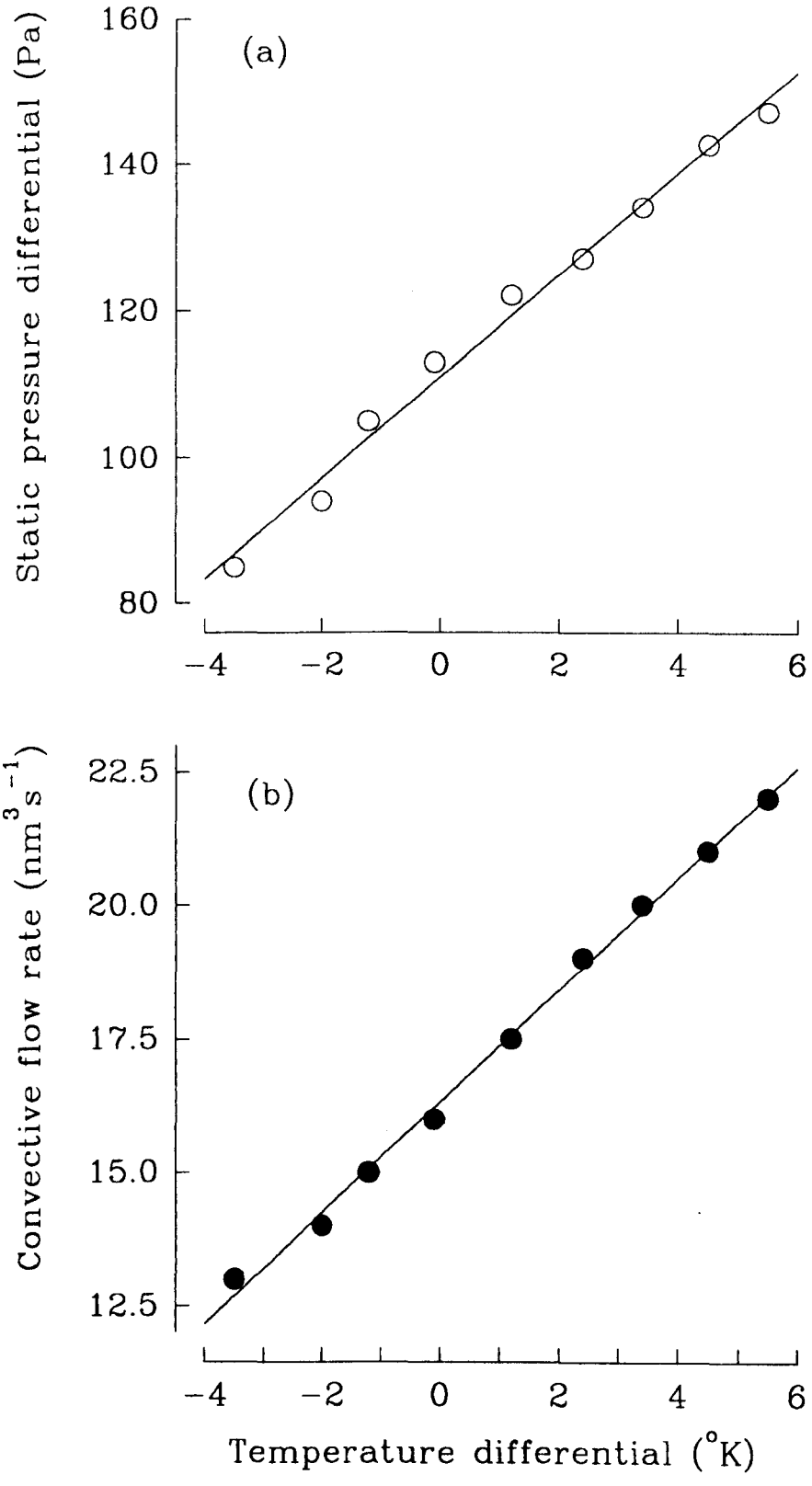

Fig. 6.06. The effects of temperature differentials on (a) static differential and (b) convective flow. MPD = 0.046 μm; S (dry air) = 0.056 m s^{-1}, W = 4 mm.

ideally expect a maximum increase in pressure due to thermal transpiration of 170 Pa. In Fig. 6.05b, however, the rise per degree was only 6.6 Pa. These results suggest that for Nuclepore membranes in the absence of a humidity gradient, considerable temperature differentials would have to prevail to produce pressurization and flows by thermal transpiration comparable with those induced by humidity-induced diffusion. It is possible that the thinness of the membranes (10 μm) prevents the development of steep temperature gradients across them. However, it must be noted that obvious pressurizations occur with a humidity gradient even when ΔT is negative (Fig. 6.05a). One may conclude that for these membranes, over the range of ΔT's studied (which is greater than the range found between the inside and the outside of the *Phragmites* shoot), a humidity gradient is more important for inducing convection than is a temperature gradient *per se*. Hence, it seems justifiable to refer to this flow as *humidity-induced* convection (see also Section 5.4) : the greater ΔP_s and flow values found when ΔT was positive, can be attributed to (a) a steepened humidity gradient due to a higher concentration of water-vapour below the membrane, and (b) a small thermal transpiration effect.

Increases in the partial pressure of water-vapour with rising temperature are expressed in Fig. 6.07: for every degree rise over the range 19-24°C (the same range as in the above experiments), the maximum increase in water-vapour partial pressure is *ca.* 137-170 Pa. Where MPD was 0.046 μm (Fig. 6.06a), a rise of <7 Pa *per* °K rise in temperature is indicated. Where MPD was 0.015 μm there was a rise of 75 Pa per °K. These represent about 4.6% and 48.5% of the theoretical maxima respectively. The difference between the two can be accounted for by the higher diffusive resistance of the smaller pored membrane, a function of (a) a very low porosity and (b) the smaller pores size

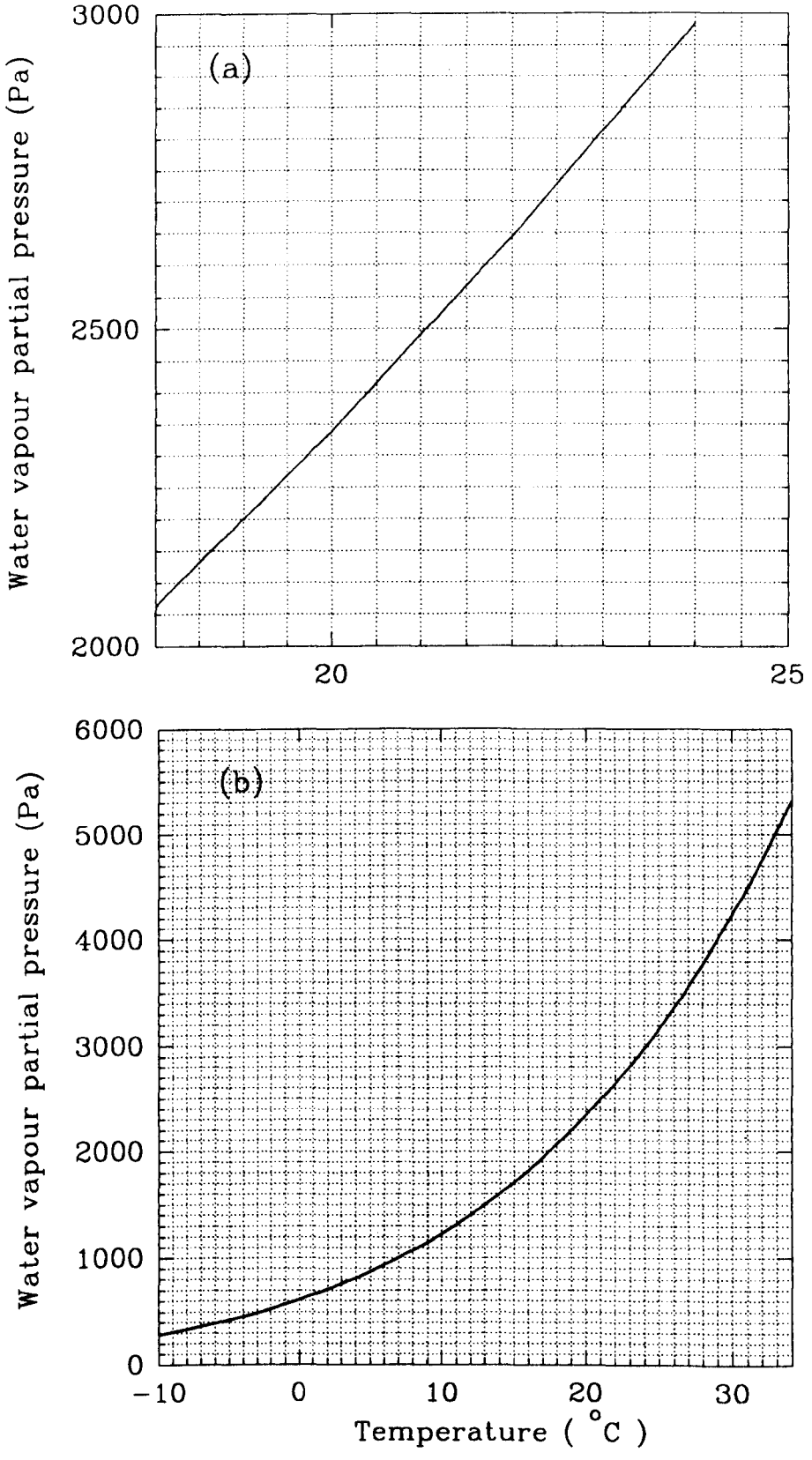

Fig. 6.07. The effect of temperature on the partial pressure of water vapour.

which is further into the Knudsen regime. This is supported by predicted values derived using equations 6.06 & 6.07. Assuming a porosity of 10% for MPD 0.046 μm, and 0.8% (from SEM's) for MPD 0.015 μm, and a boundary layer thickness of 700 μm, respective values of 5 Pa $^{\circ}K^{-1}$ and 96 Pa $^{\circ}K^{-1}$ were obtained for a rise in the internal temperature from 20 to 21°C.

6.3.4. *The effect of pore diameter*

The experimental values of ΔP_s (developed with the evaporating water surface at 4 mm below the membrane) versus MPD are shown in Fig. 6.08a, and it will be seen that the inverse relationship is similar to that predicted by Schroder *et al* (1986) for thermal transpiration (Fig. 6.02). If the data are also compared with predictions based on Section 6.2.3, there is again encouraging agreement (cf. Figs. 6.08a & 6.08b), although the experimental data do not follow such a smooth curve, and the pressures at MPD values of 0.015, 0.022 & 0.037 μm are very much greater than predicted. However, this can be explained in terms of the much lower than expected porosities of these three membranes. At an MPD of 0.046 μm there is close agreement between the experimental and predicted data. At higher values of MPD, the lower experimental values are probably a function of the higher than expected porosities of the membranes used.

Of particular interest was the unexpected relationship found between convective flow and MPD (Fig. 6.08c). It had been assumed that the relationship would follow a similar pattern to that of ΔP_s *vs* MPD, but instead convection rose to a peak around 0.1 μm MPD, and then declined with decreasing pore size. At first it was thought that the explanation again lay in the lower porosity of the smaller pored membranes. However, results derived from the equations presented in

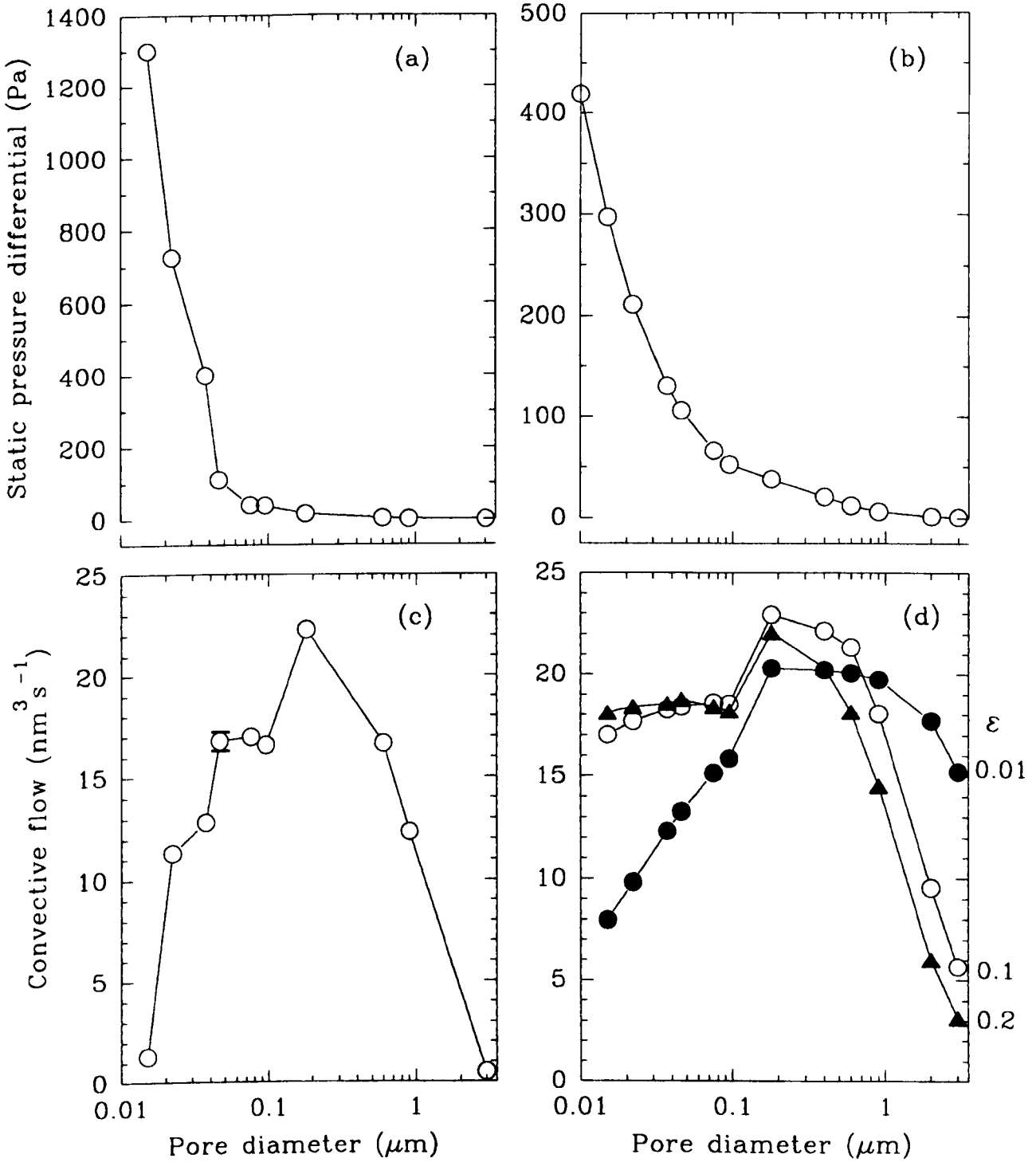

Fig. 6.08. The relationships between static pressure and pore diameter: (a) experimental, (b) predicted, and between convective flow and pore diameter (c) experimental, (d) predicted. The predicted data are for a water distance, W of 4mm as are the experimental, and an assumed boundary layer thickness of 700 μm. ε = fractional porosity. For MPD 0.046 μm the experimental data represent the mean of results from five membranes. For static pressure the standard error lies within the symbol size; for convective flow the SE is indicated by bars.

Section 6.2.3 show that the pattern is broadly that which is predicted (cf. Figs. 6.08c & 6.08d). although probably modified to varying degrees by the porosity differences. For example, the flow for the 0.015 μm MPD membrane was very much lower that expected, and this accorded with a very much higher than expected ΔP_s. From the SEM's it was estimated that the pore size in this membrane was $\leq$ 0.015 μm, and porosity was *ca.* 0.8%, and before the experimental data had been compared with the predicted values of pressure and flow, it had been thought possible that the gold sputtered onto the membranes might have narrowed the appearance of the pores and perhaps totally covered others. The very low flows, and the very high pressures, with this membrane suggest that this was not so, and thus broadly support the SEM findings.

The differences between the experimental and predicted ΔP_s data are more evident if the log:log plots (Figs. 6.09a & 6.09b) are compared. The "bulge" in the theoretical plot is a function of the constant diffusivity employed at pore diameters >0.1 μm, and decreasing Poiseuille flow resistances of the membranes which vary inversely as the 4th power of the pore radius.

The theoretical approach also makes it possible to predict the relationship between ΔP_s, and MPD over a much extended range of pore sizes (Fig. 6.09c). Here again it was assumed that all membrane porosities were 10% and that W was 4 mm as in the experiment, but no boundary layer was programmed. The predicted pressures increase with decreasing pore size along an *apparently* smooth curve beginning at *ca.* 3 - 10 μm MPD, but for the reasons given above there is of course a change in the curve when MPD exceeds 0.1 μm and the diffusivity becomes independent of pore size. Since the porosities were all assumed to be 10% no aberrant points are seen, and the data is seen

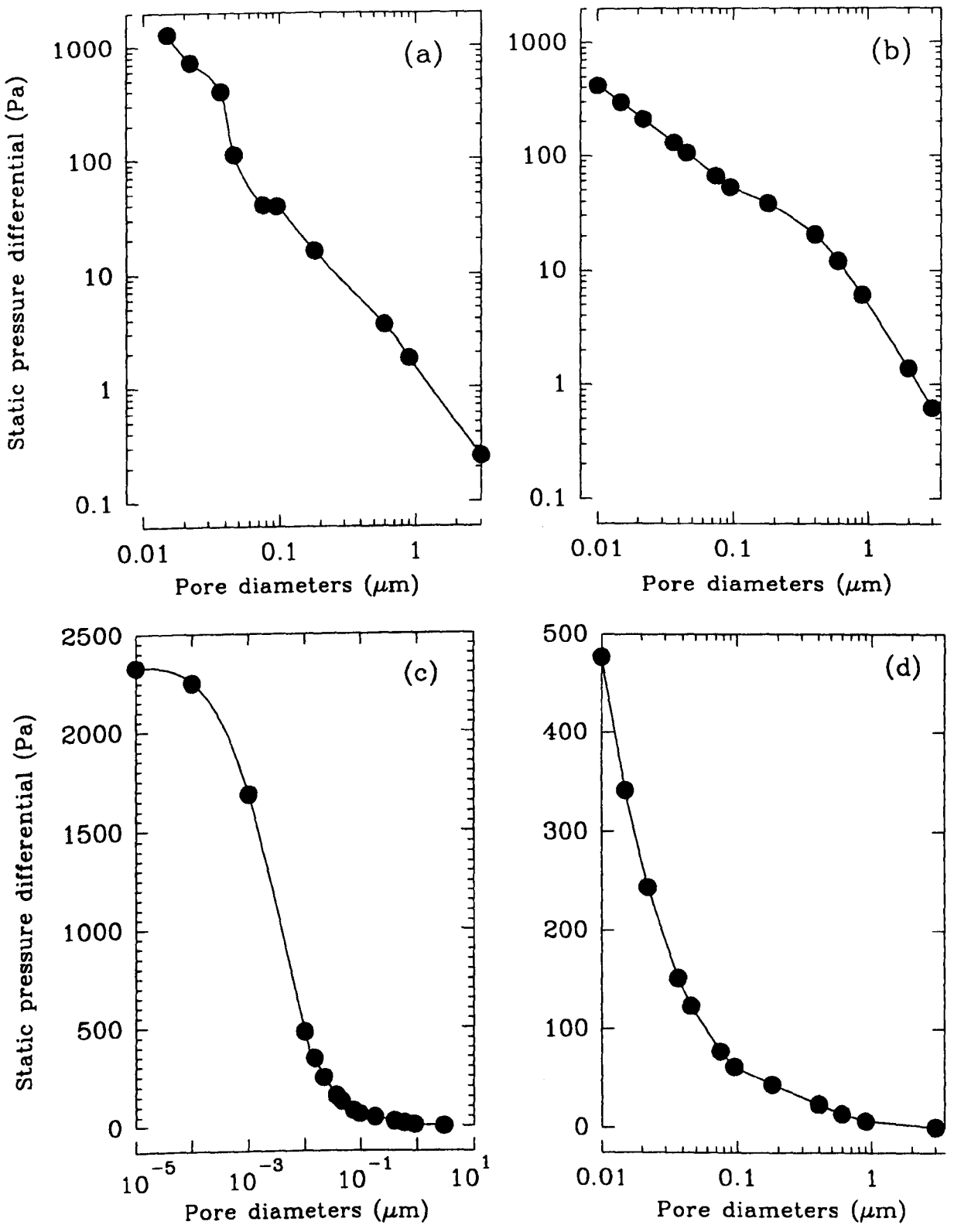

Fig. 6.09. The development of static pressure as a function of membrane pore size: (a) experimental data; (b) data predicted for equiporous (10%) membranes with 700 μm boundary layer; (c) as for (b) but no boundary layer; (d) relevant portion of (c) enlarged.; $S = 0.056$ m s^{-1}; $W = 4$ mm.

eventually to be asymptoting at a pressure numerically equal to the partial pressure of water vapour. In these particular cases, though, where W was at 4 mm, it can be seen that the pore sizes necessary to cause the plots to asymptote (Fig. 6.09c) are beyond the bounds of possibility, being less than the diameter of the diffusing molecules. Later, however, it is shown that if the evaporating water surface is placed much closer to the membrane (Fig. 6.16), the plots asymptote at pore diameters well within the membrane MPD range.

6.3.5. *Different gases*

The ΔP_s values and HIC were highest for the lighter, faster-moving gases, (of low RMM) : H_2, He, and lowest for the heavier gases: O_2, Ar, (e.g. Fig. 6.10 : MPD = 0.046 μm). In general terms this accords with Graham's Law of Diffusion: $D \propto 1/\sqrt{RMM}$, but the static pressures developed in the case of H_2 and He were somewhat lower than expected. Where MPD was 0.015 μm (Fig. 6.11), the ΔP_s values were much closer to predicted values but the data fitted more closely to a straight line if plotted against published values for the mutual diffusivities of the gases and water vapour. Possibly this is because there is some degree of reaction between the gas species and the solvent water-vapour molecules.

6.3.6. *Effects of varying the humidity gradient*

(a) Varying the humidity of the wind across the membrane

For MPD = 0.046 μm, ΔP_s and HIC were highest, the lower the RH of the air above the membrane, i.e. with the steepest humidity gradient across the membrane. This applied when ΔT was zero (Fig. 6.11a), or +1.4°K (Fig. 6.12b).

Increasing the humidity of the external atmosphere when ΔT was

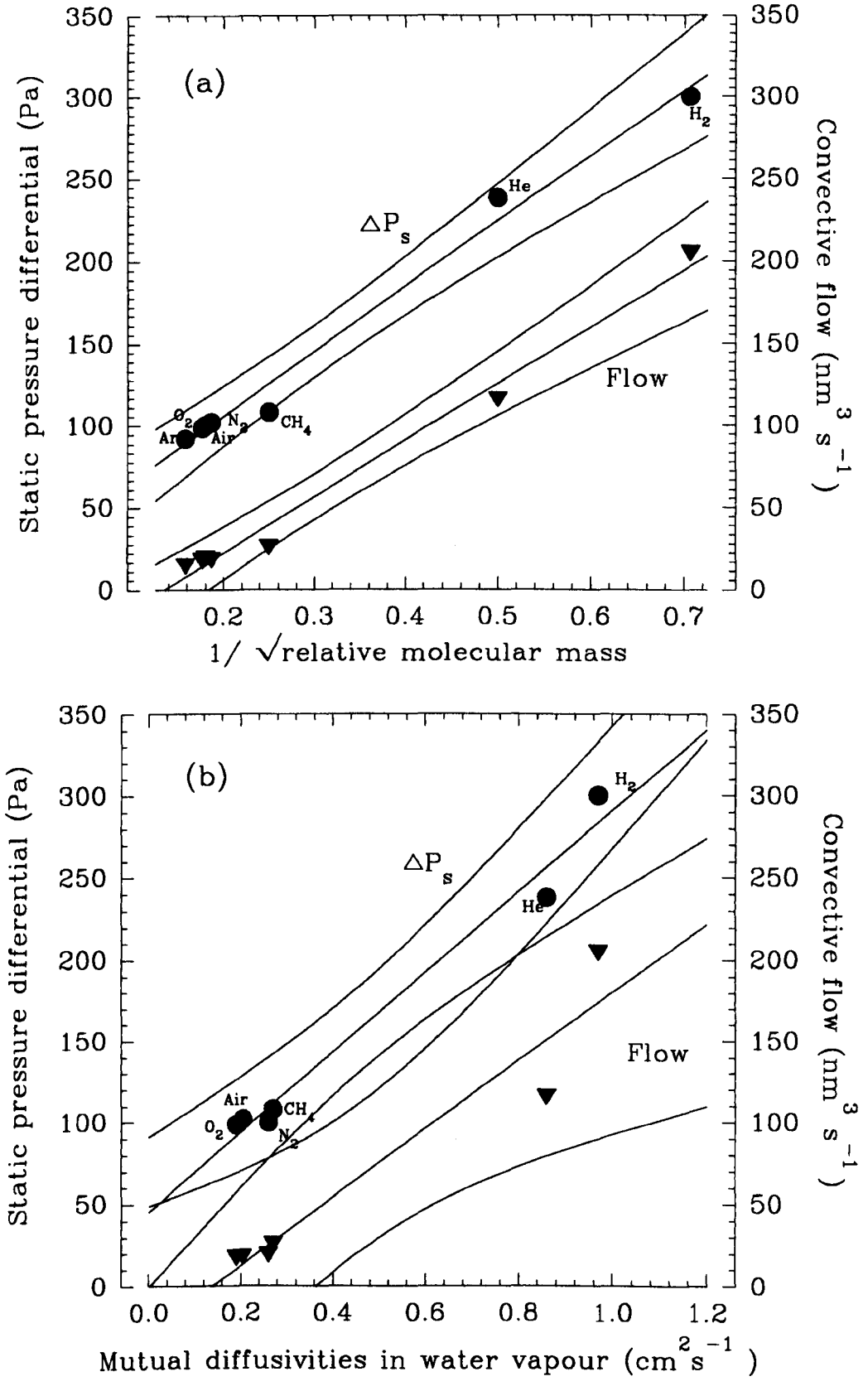

Fig. 6.10. Humidity induced convection and ΔP_s for different gases: H_2, He, CH_4, N_2, Air, O_2 and Ar.: (a) versus $1/\sqrt{}$ RMM, and (b) versus mutual diffusivities of gases and water vapour.. MPD = 0.046 μm; W = 4 mm; s (dry air) = 0.053 m s^{-1}.. Regressions with 99% confidence intervals.

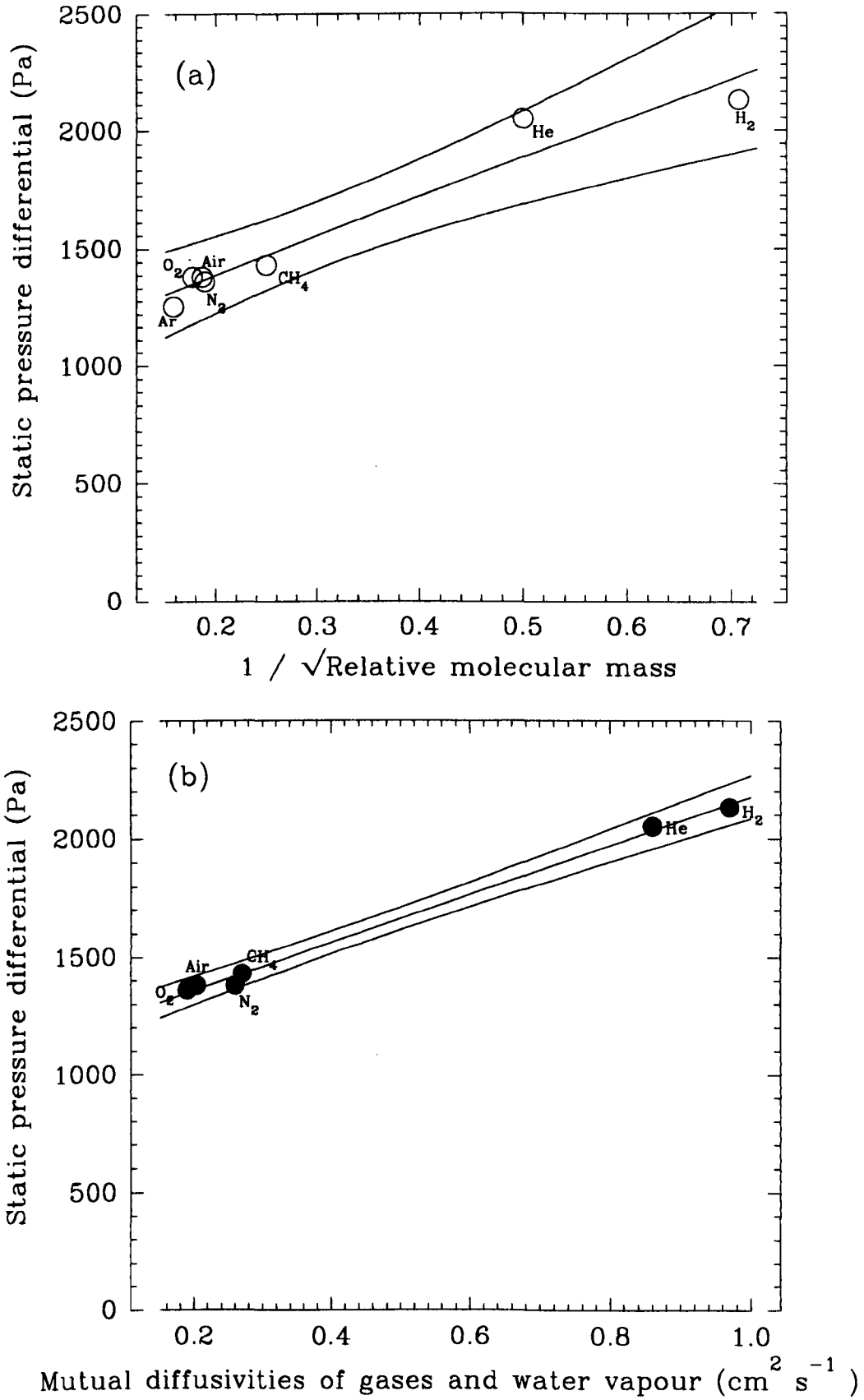

Fig. 6.11. Humidity induced P_s for different gases: H_2, He, CH_4, N_2, Air, O_2 & Ar : (a) versus $1/\sqrt{RMM}$, and (b) versus mutual diffusivities of gases and water vapour.
MPD = 0.015 μm; S (dry air) = 0.053 m s^{-1}; W = 4 mm.
Regression with 99% confidence limits.

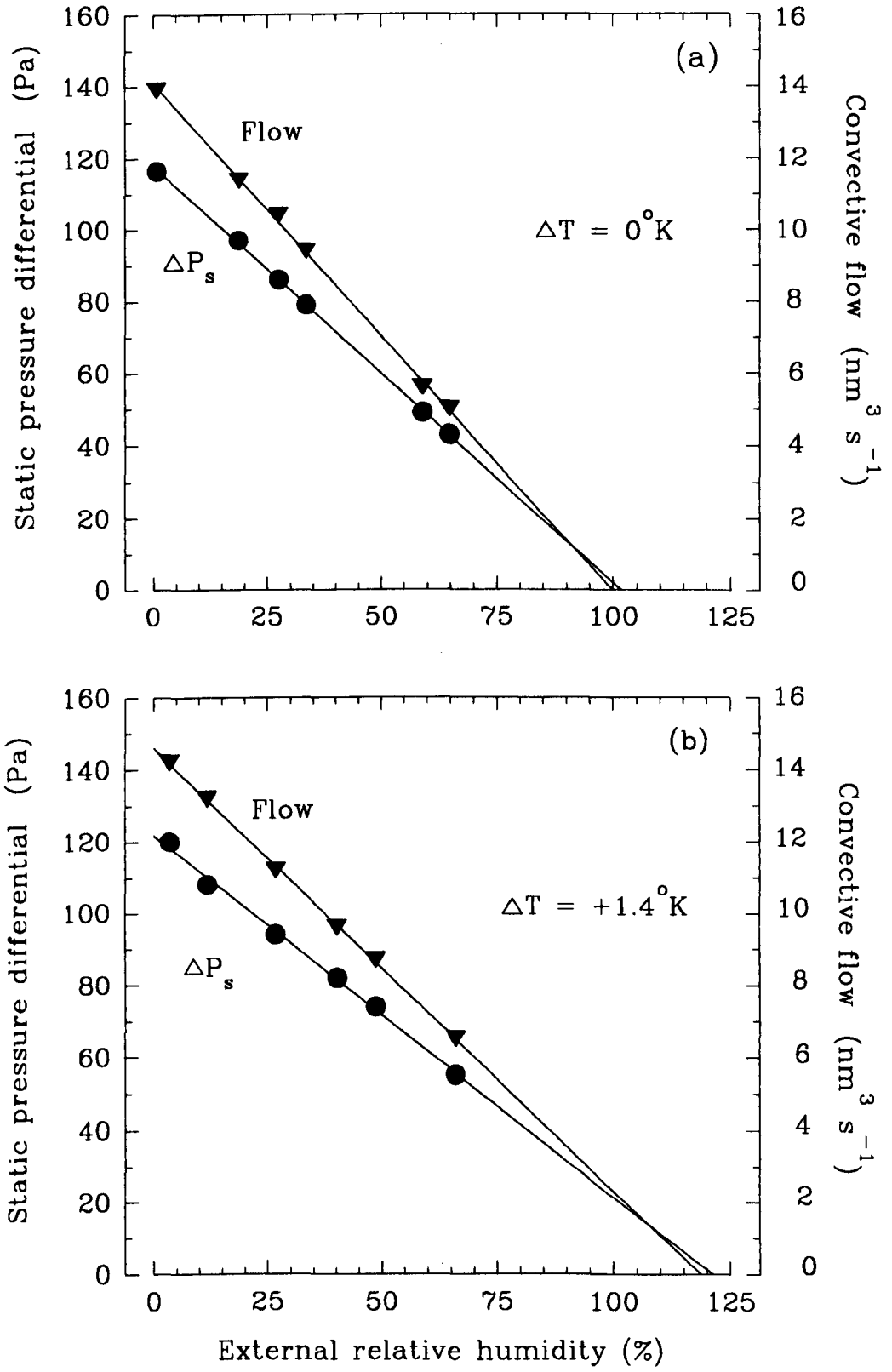

Fig. 6.12. Showing the effect of humidity differential on static pressures and humidity–induced convection for two values of ΔT. MPD = 0.046 μm, S (dry air) = 0.0393 m s^{-1}, W = 4 mm.

zero, resulted in lower HIC and ΔP_s values, until at 100% RH there was virtually no pressurisation or flow, because there was no humidity gradient, and hence no concentration gradient for the inflow of atmospheric gases. However, when ΔT = 1.4°K there was still a small degree of pressurization and flow at 100% RH. These effects can be attributed primarily to a higher concentration of water-vapour internally because of the higher temperature; secondarily there might have been a small thermal transpiration effect. These findings accord with the observed effects of external humidity on the HIC and pressurisation in *Phragmites* (Sections 5.3.1.1 & 5.3.1.3).

(b) Varying dry-air wind speed over the membrane

Both ΔP_s and HI-convection rates increased with increasing wind speed (Fig. 6.13). The greatest effect was between 0 and 20 mm s^{-1} and this coincided with the greatest reduction in RH in the air venting from the wind tunnel. It is concluded that the stream of dry air had the effect of creating steeper humidity gradients across the membrane by reducing the boundary layer above the membrane: the faster the wind speed, the thinner the boundary layer. The parabolic relationship reflects the increasing difficulty of reducing boundary layer thickness the thinner it becomes. A boundary layer of *ca.* 700 μm was required to predict the ΔP_s values observed at wind speed 0.056 m s^{-1} but this is considerably less than the thickness that is predictable from the well known relationship $0.4\sqrt{(L/u)}$ (units in cm & cm s^{-1}; Nobel 1974) for leaves. It is by no means certain, however, that this relationship would apply in the context of the geometry of the "wind-tunnel" system used here.

When the volume flow of water-vapour through the membrane was calculated from the humidity of the gas which had passed over the

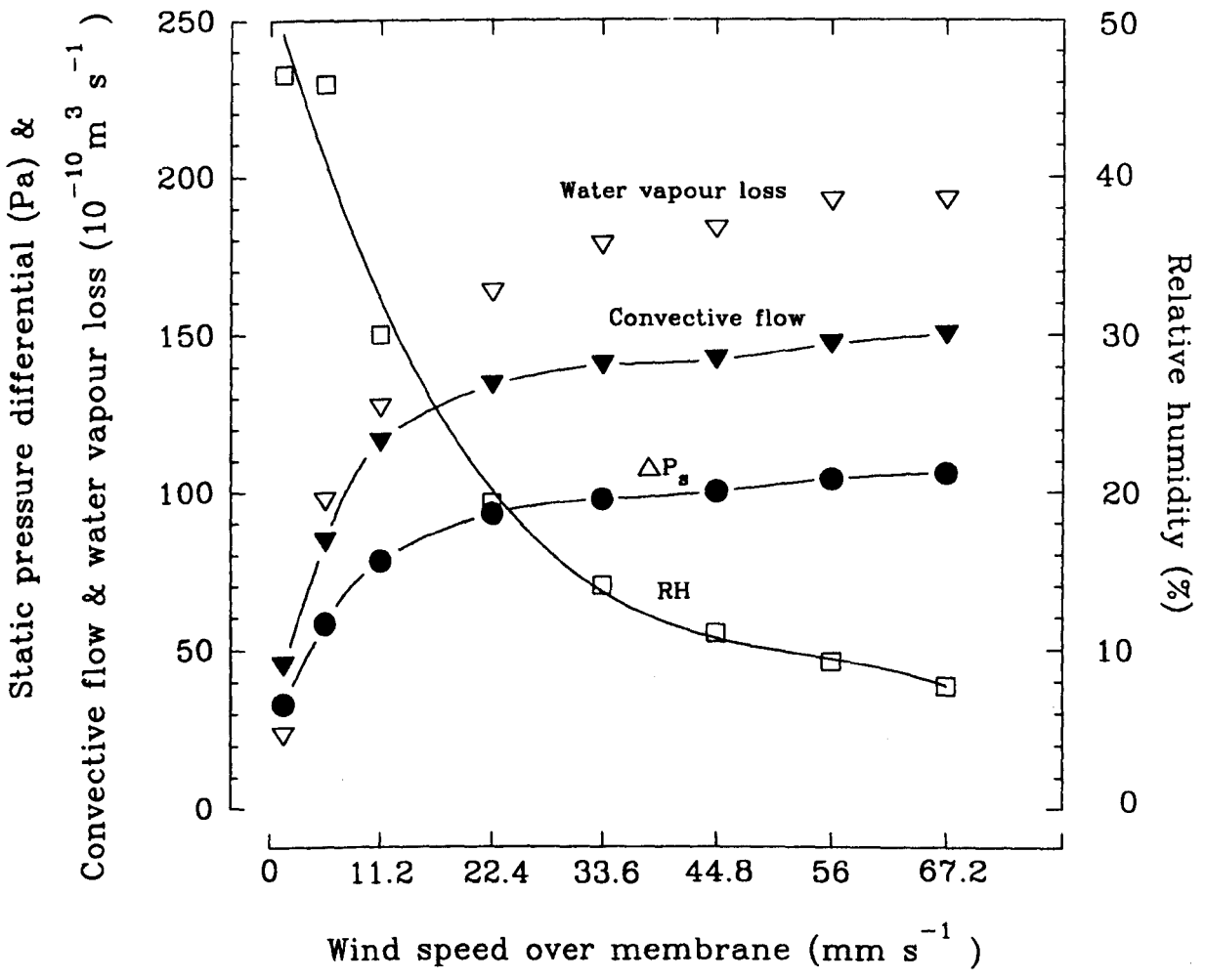

Fig. 6.13. The effect of windpeed onΔP_s, HI–convection, humidity of air stream after passing over the membrane, and water vapour. loss through the membrane MPD = 0.046 μm; W = 4 mm..

membrane and the wind speed, it can be seen that the water vapour losses were greater than the corresponding values of HIC. At the highest wind speeds the ratio between the rate of water-vapour loss through the membrane and HIC was 1.26:1, and it is interesting to note that this is approximately the ratio between the Knudsen diffusion coefficient for water-vapour and the mean of the coefficients for oxygen and nitrogen through a membrane of pore diameter 0.046 μm. The result is thus consistent with expectations concerning the HIC mechanism. Also encouraging are the flow predictions which were 21.67 $nm^3\ s^{-1}$ and 17.14 $nm^3\ s^{-1}$ for the water vapour and air respectively, which are very close to those observed.

(c) Varying distance between membrane and underlying water surface.

As has already been mentioned, the distance between the membrane and the evaporating water surface in the Nuclepore assembly can be expected to have a very great influence on the magnitude of ΔP_s and convective flows. This is because of the magnitude of the diffusive resistances of this header space relative to those of the membrane and boundary.

The two experimental examples shown (Fig. 6.14) are for two different membranes, MPD 0.046 μm and MPD 0.075 μm, and hence effects due to pore size and porosity, as well as W, can be seen. In both examples, ΔP_s and HIC increase as the distance W decreases, but at each depth the pressure attained at MPD 0.046 μm is greater. The flows were fairly similar, however, and although this was unexpected at the time, the theoretical predictions are for a slightly greater flow at an MPD of 0.075 μm. The slightly lower flow here may have been due to a smaller surface of exposed membrane.

Unfortunately because the membranes could be easily wetted

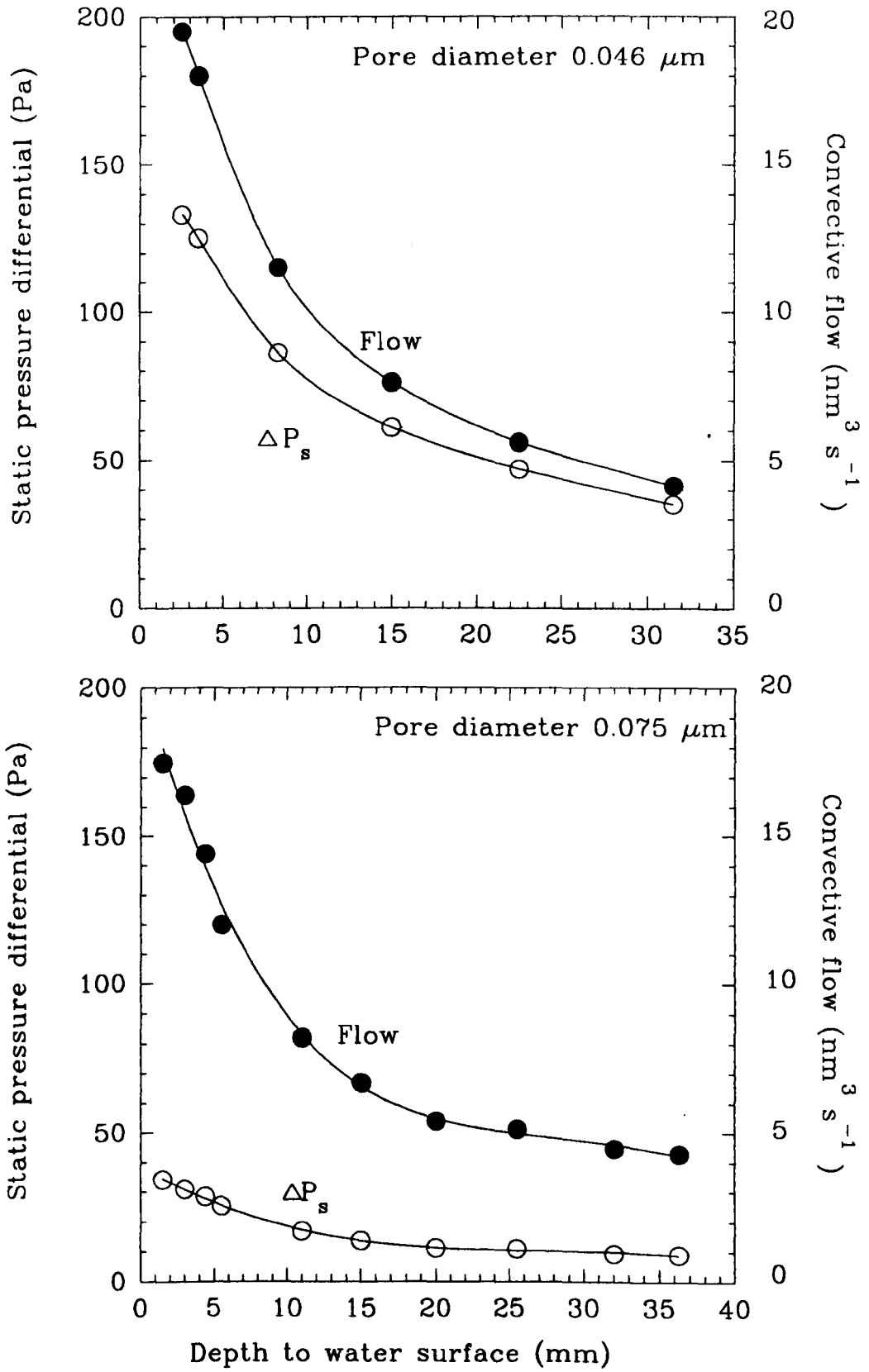

Fig. 6.14. The effect of distance between membrane and water surface on static pressures and HIC for two membranes differing in their MPD.. S (dry air) = 0.04 m s^{-1}.

accidentally by the meniscus if the water in the chamber was raised too far (<2-3 mm), it was not possible to extend the experimental data further to try and more effectively mimick *Phragmites* where the evaporating surfaces must come to within a few μm of the base of the pores. Indeed in *Phragmites* the pore itself, in its lower reaches, might be a significant part of the evaporating surface. Nevertheless, by the use of the equations in Section 6.2.3, it has been possible to explore the likely effects of moving the evaporative surface much closer to the membrane.

The results obtained demonstrate a quite remarkable potential for convective flows even where pore diameters are beyond the Knudsen range (MPD >0.1 μm). In Fig. 6.15 the effects of raising the water surface from 100 mm to within 1 μm of the membrane surface are shown for an MPD of 0.046 μm and a membrane porosity of 10%; no boundary layer was included for this prediction. It is particularly interesting that the plot approaches a static pressure numerically equal to the water vapour pressure at W = 10 μm. On the same figure it can be seen that with an atmosphere of hydrogen this same value is approached at W = 100 μm. If the evaporating surface is very close to the membrane (e.g. W = 10 μm) not only does the asymptotic static pressure numerically approach that of the vapour pressure of water, but very substantial pressures are predictable for pore diameters outside the Knudsen regime (Fig. 6.16).

Another factor which can cause higher static pressure differentials to be achieved relative to pore diameter, is lower membrane porosity, and such an effect is illustrated in Fig. 6.17, where it is interesting to note that porosities of 1% are those more normally associated with leaf surfaces. Even more interesting in relation to *Phragmites* are the data shown in Fig. 6.18 where the effect of pore

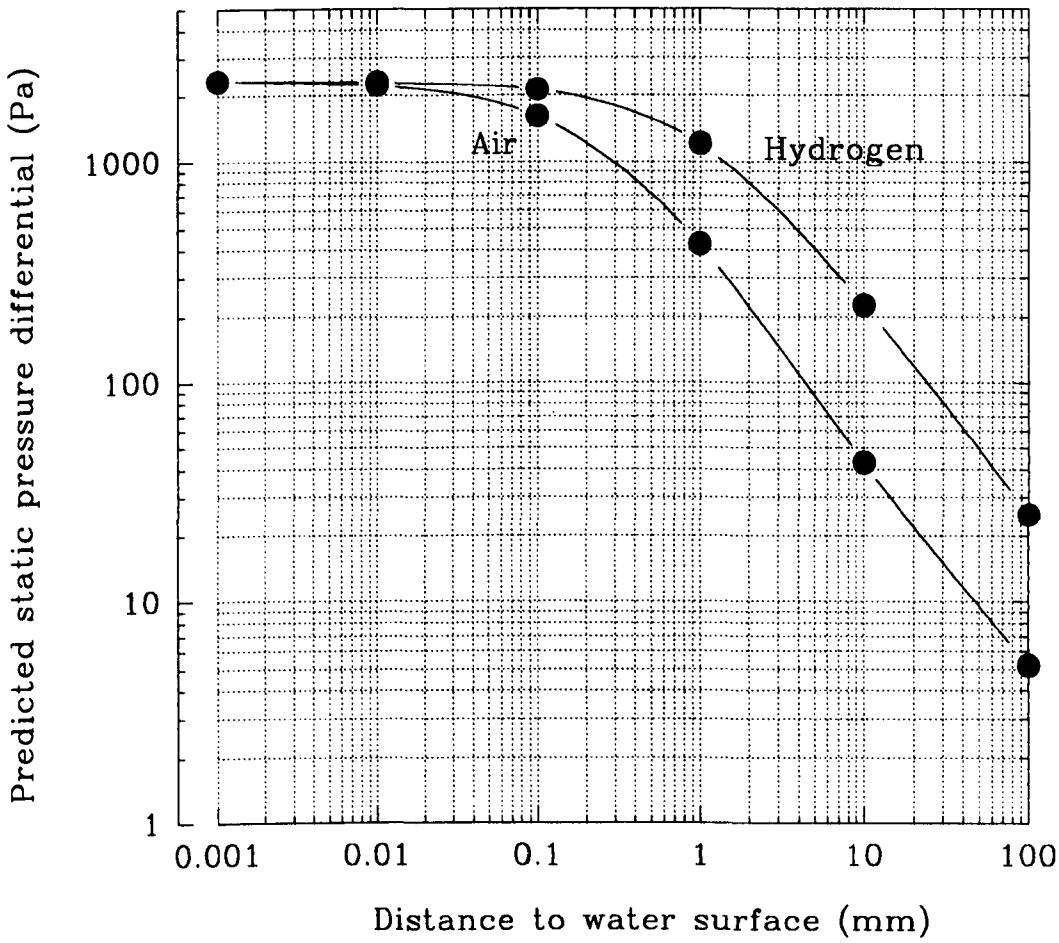

Fig. 6.15. Predicted relationship between static pressure differential and distance of membrane above the water surface for air:water vapour and hydrogen:water vapour. MPD = 0.046 μm, no boundary. layer above the membrane, T=20°C and membrane porosity 10%.

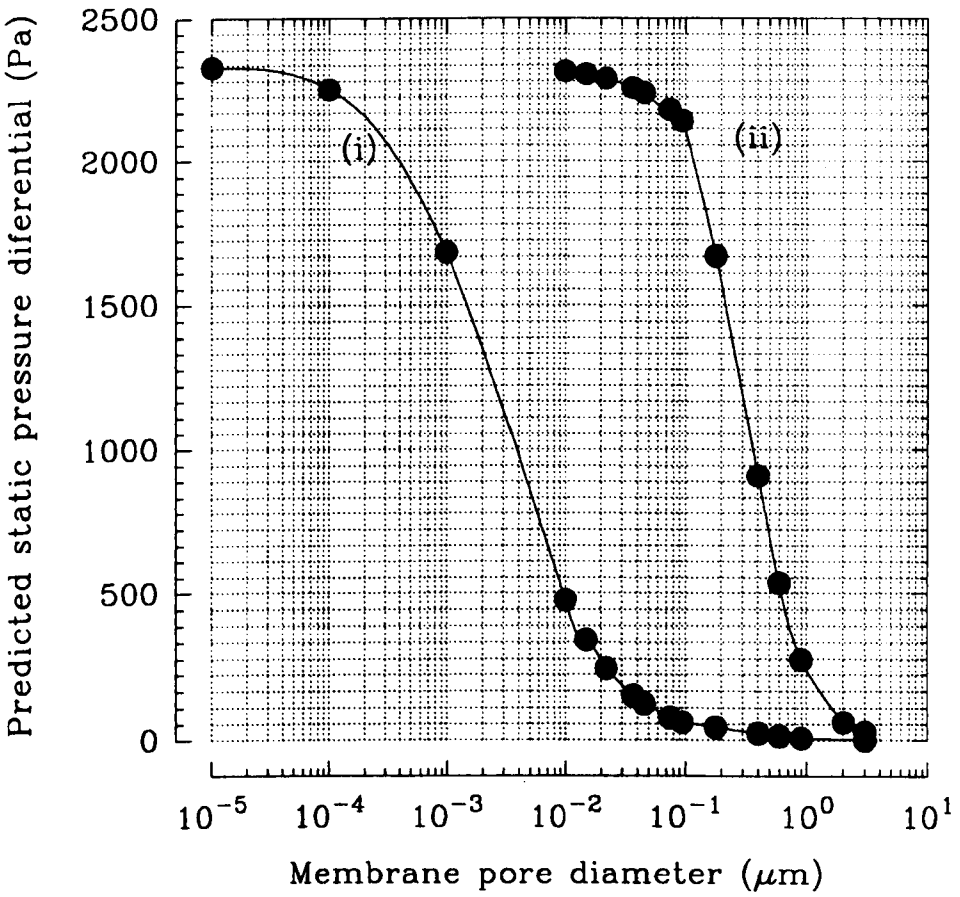

Fig. 6.16. Predicted relationship between static pressure differential and membrane pore diameter: (i) evaporating water surface 4 mm below membrane, and (ii) evaporating surface 10 μm below the membrane. Predictions based on a membrane porosity of 10%, and Knudsen diffusion where pore diameter <0.12 μm.

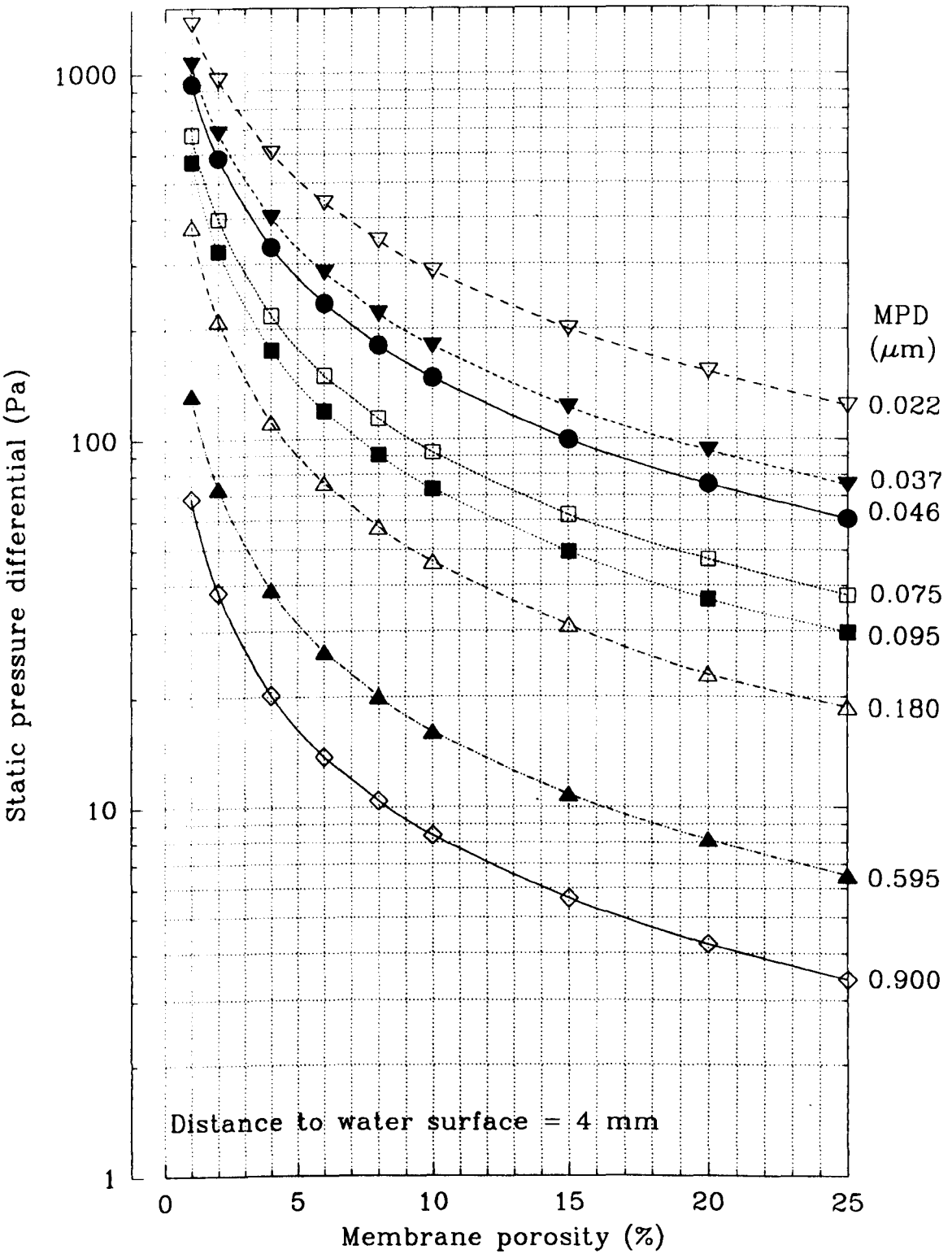

Fig. 6.17. Predicted relationships between static pressure and porosity for membranes having the pore diameters used in the present study. Boundary layer not progammed.

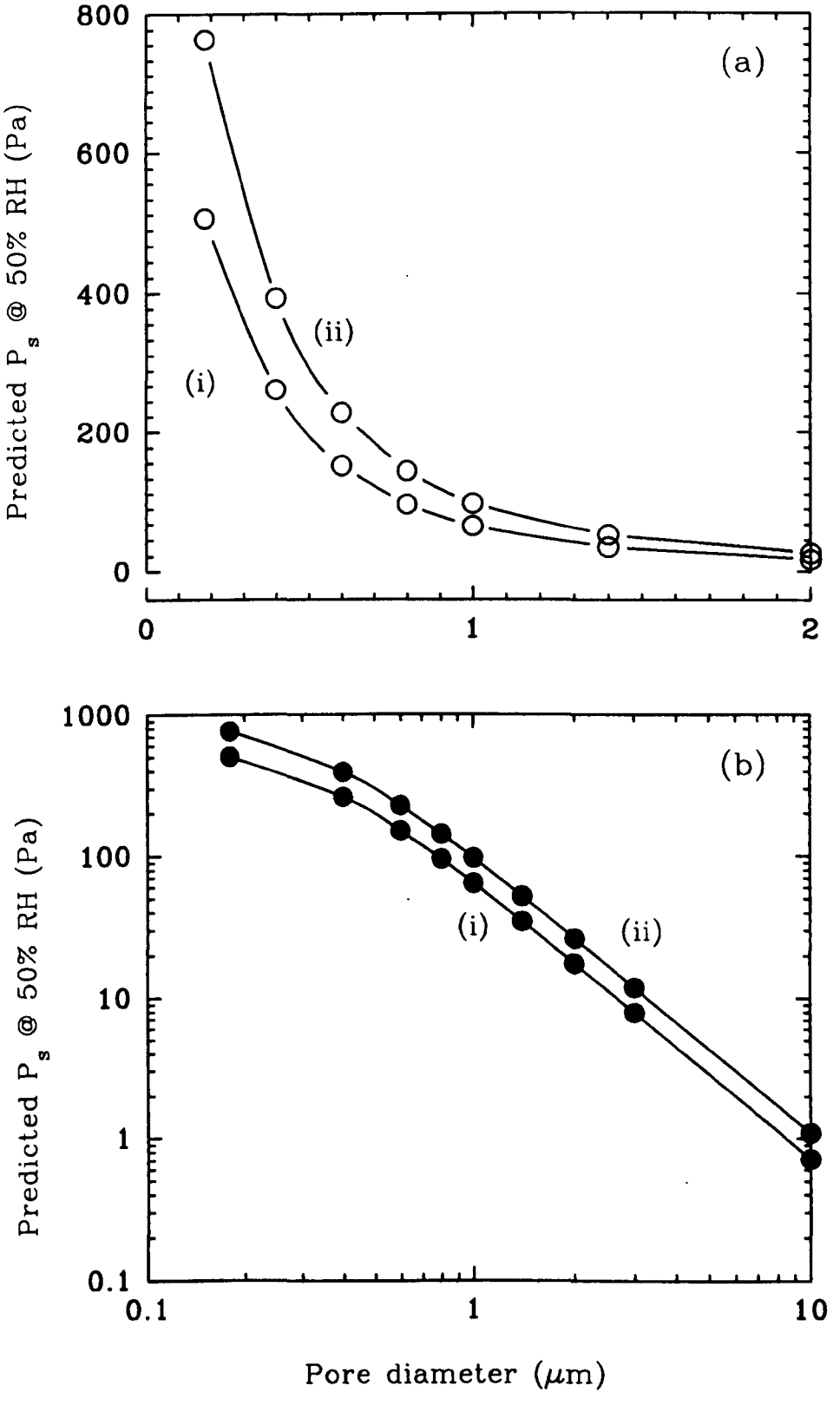

Fig. 6.18. Predicted static pressure in relation to pore diameters for membranes of 1% porosity, with outside humidity 50%, water surface 10 μm below the membrane, and boundary layer thickness either 700 μm (i), or 200 μm (ii).

diameter on static pressure development is predicted for W = 10 μm, and a membrane porosity of 1% ; also, the relative humidity imposed above the membrane was 50%, a common atmospheric level in *Phragmites* stands in Britain. This figure shows that very significant pressures can be expected to develop even at an MPD of 3 μm, and that at pore sizes having some equivalence to those in *Phragmites* e.g. >0.2 - <1 μm, static pressures within the range found for *Phragmites* are predictable. The very significant effects exerted by boundary layer thickness is also revealed in the figure.

6.3.7. *Exposed membrane area*

As expected, HI-convection increased as area of exposed membrane increased (Fig. 6.19). However, there was comparatively little change in ΔP_s values which actually decreased slightly, the greater the area of membrane exposed. This latter effect could have been due to the ratio of membrane area to header space area and / or to "humidity-shadowing" i.e water vapour emanating from the leading edge of the membrane reducing humidity losses from the trailing edge downwind. The latter would have the effect of reducing humidity gradients across the shadowed portion, and consequently reducing the static pressure developed. There is also a suggestion of this effect in the convective flow data at the highest area of membrane exposed.

With *Phragmites* a similar relationship is found between leaf sheath surface area and ΔP_s, and HIC, as shown in Fig. 5.10.

6.3.8. *Effects of increasing the resistance of the venting path*

As the resistance to venting was increased by stepwise addition of 1 μl Microcap capillaries to the venting path, the flow rate decreased exponentially, while ΔP_d rose and approached its limit as the resistance

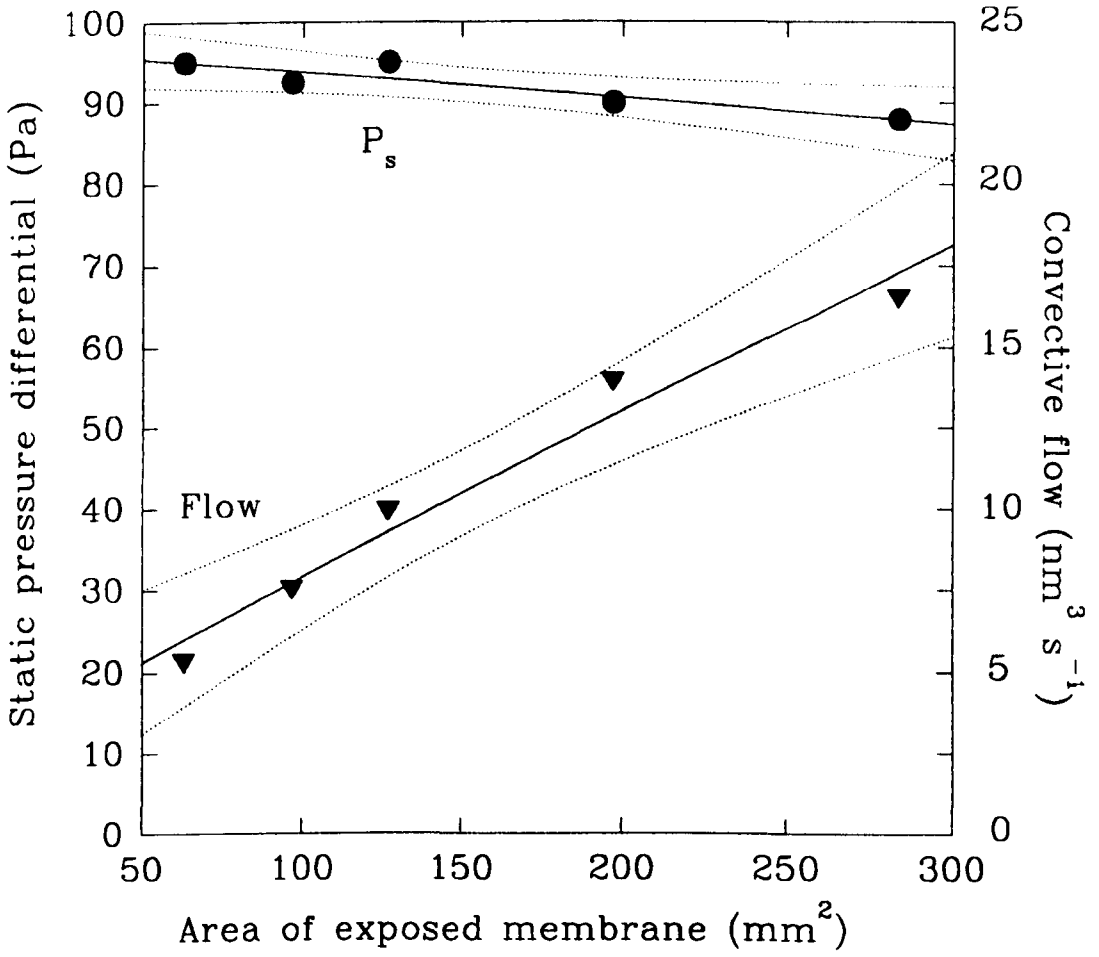

Fig. 6.19. The effect of exposed membrane area on the rate of convective flow and the development of static pressure where S (dry air) = 0.0393 m s^{-1}; MPD = 0.046, & W = 4 mm. Regressions with 95% confidence intervals.

increased (Fig. 6.20a). Flow through a capillary at a given pressure is given by the Poiseuille equation :

$$\Delta P = F\ (8\eta L\ /\ \pi r^4), \qquad (6.14)$$

where ΔP is the pressure difference between the ends of the capillary; F, the volume flow rate ($m^3\ s^{-1}$); η, the viscosity of air, (1.84×10^{-6} $kg\ s^{-1}\ m^{-1} \equiv N\ s\ m^{-2}$); L, the length of capillary (m), and r, the radius of capillary (m). Since resistance to flow, $R = 8\eta L/\pi r^4$ ($Pa\ s\ m^{-3}$), then $R \propto 1/F$ as shown in Fig. 6.20b, and as the number of Microcaps approaches 8, and the flow is greatly impeded, the ΔP_d value approaches what was the ΔP_s for this membrane (112Pa). It should be noted that ΔP_d is the pressure at which the convected gas is passing through the flow meter, and this pressure increases the greater the resistance to flow because the tendency for gases to enter the system, $\equiv \Delta P_s$, is constant, and created mainly by the humidity differential. It is possible to envisage that increasing the resistance to venting does somewhat affect the humidity differential, but it was not possible to quantify this effect.

It is encouraging to note that, using equation 6.11, the predicted value for flow through 8 Microcaps at the pressure differential shown in Fig. 6.20a (105 Pa) is 0.79 $nm^3\ s^{-1}$; the experimental value was 0.86 $nm^3\ s^{-1}$. Similarly, for one capillary, the ΔP_d was approx. 78 Pa, the predicted flow 4.7 $nm^3\ s^{-1}$, and the experimental flow 5.1 $nm^3\ s^{-1}$. It also encouraging to find that if the humidity-induced diffusion through the membrane is calculated from the diffusion equation (6.08), using the calculated Knudsen diffusion coefficient (equ. 6.03) for air through pores of 0.046 μm (the true diameter of this batch of 0.03 μm membranes), and a concentration difference based on the ΔP_s (i.e. 112 Pa *or* $112/101300\ m^3\ m^{-3}$), the value obtained is approx. 19.8 $nm^3\ s^{-1}$; the experimental figure obtained with no Microcaps in the system (i.e.

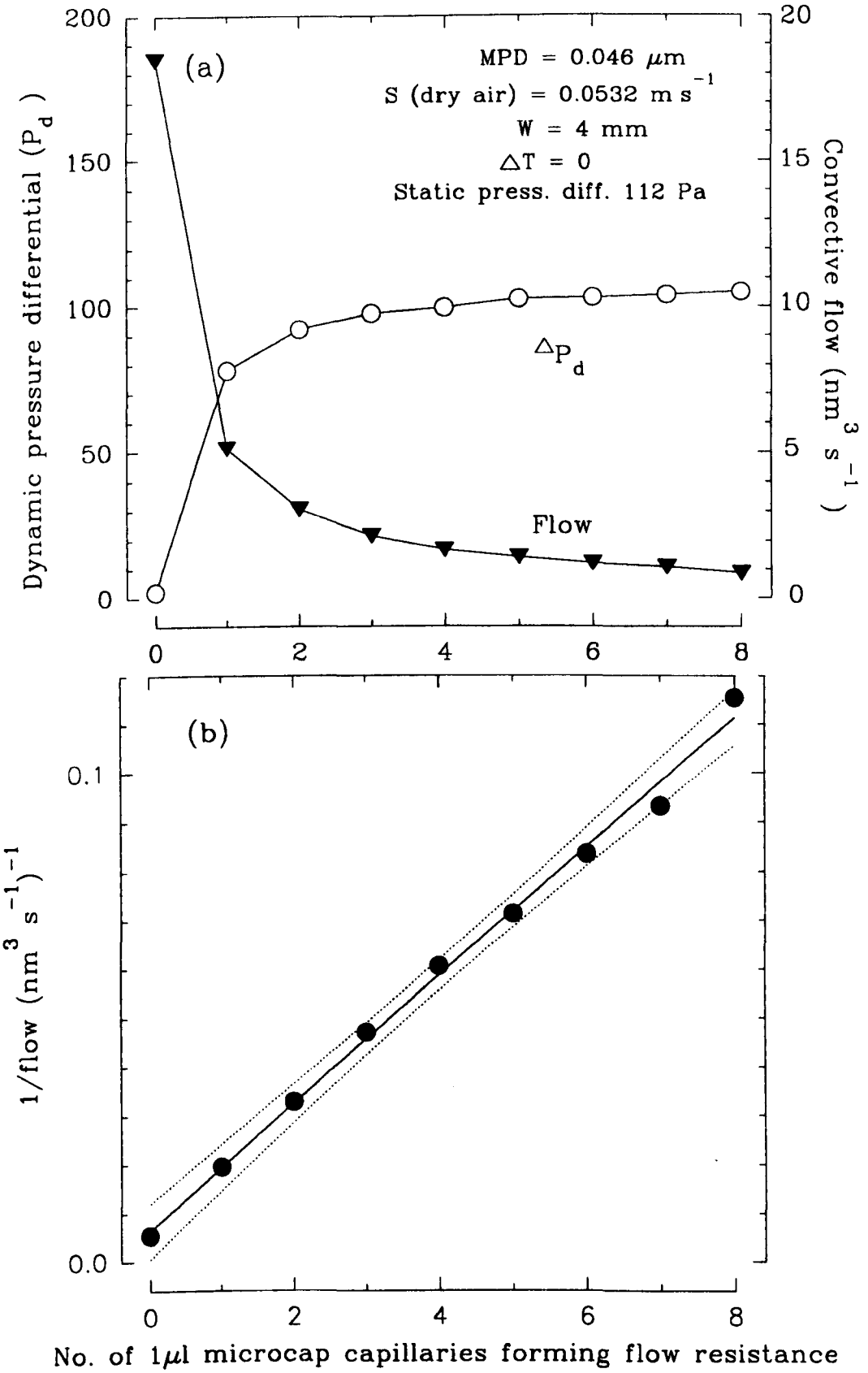

Fig. 6.20.. (a) The effect of increasing resistance to throughflow (HIC) on the development of dynamic pressure and flow rates. (b) Shows the relationship between 1/flow and increasing resistance to flow. Regression with 99% confidence limits.

'zero' resistance) was 18.5 $nm^3\ s^{-1}$. The 'zero' resistance condition in the experiment did not take account of the resistance of other pipe work or the resistance of the soap bubble to travel.

The increase in ΔP_d with increasing numbers of microcaps was also investigated by substituting the microcap resistance for R_{MP} in equation 6.09; again, excellent agreement with the experimental results was obtained.

This section points to the importance of low throughflow resistances for HIC in *Phragmites*. The maximum potential for convective flow will only be realised at the lowest throughflow resistance of all i.e. zero. The higher this resistance the higher will ΔP_d become, and for leaf sheath pores outside the Knudsen range the theory indicates that more of the diffusive inflow of air will immediately leak back once more through the stomata by Poiseuille flow, rather than contributing to the convective flow through the plant. (For pores in the Knudsen range, more of the inflow gas would diffuse back through the stomata rather than contributing to throughflow convection). Again, therefore, this emphasises the likely importance of high ratio of outflow to inflow culms in a reed bed as originally indicated in the data shown in Fig. 5.10b. Other examples of the effects of venting resistance are given in the next section and in Section 6.3.10.

6.3.9. *Membrane Porosity*

The problems of Nuclepore membrane porosity in this work have already been alluded to, and to date, a thoroughly satisfactory method of determining their porosities has not been found. However, it has been possible to explore the likely influence of membrane porosity on HIC using the equations given in Section 6.2.3.

Most importantly the results have revealed that the influence of

membrane porosity can be quite substantial at large values of W such as the 4 mm value used in much of the experimental work (see. Figs. 6.17 & 6.21 : note that the convective flows in Fig. 6.21 are potential flows only and require a zero venting path resistance). As W is reduced, porosity exerts a much smaller influence on ΔP_s although the presence of a boundary layer increases its influence once more (Fig. 6.22). Also, whereas an increase in membrane porosity lowers the achievable ΔP_s it actually increases the potential for convective flow. Whether actual flows will be increased, however, appears to depend very much upon the venting resistance to convection. For instance, in connexion with the examples shown in Fig. 6.22, it can be calculated that where membrane porosity is 1% and the outflow resistance is that of the soap film flow meter only (70 MPa s m^{-3}), the convective flows would be 51.3 nm^3 s^{-1} if there was no boundary layer, and 39.1 nm^3 s^{-1} in the presence of a 700 μm boundary layer ; at a porosity of 20% the respective flows would be 919 nm^3 s^{-1} and 137 nm^3 s^{-1}. If, however, the venting path was through a 1 μl outflow tube (R_{PT} = 1.676 x 10^{10} Pa s m^{-3}), convective flows for a 1% porous membrane would be 37.4 nm^3 s^{-1} if there was no boundary layer and 28.6 nm^3 s^{-1} in the presence of the boundary layer, while with membrane porosity at 20% the respective flows would be 112.8 nm^3 s^{-1} and 16.8 nm^3 s^{-1}. There is thus a big influence of porosity on flows in the presence or absence of a boundary layer provided that venting resistance is relatively low. If the venting resistance is high then flows generated with a low porosity membrane can become greater than with a high porosity membrane. This is because of the potential of the lower porosity membrane to generate higher dynamic pressures.

In *Phragmites* the effective distance W is likely to be very small and leaf sheath porosity low, and there will be a boundary layer

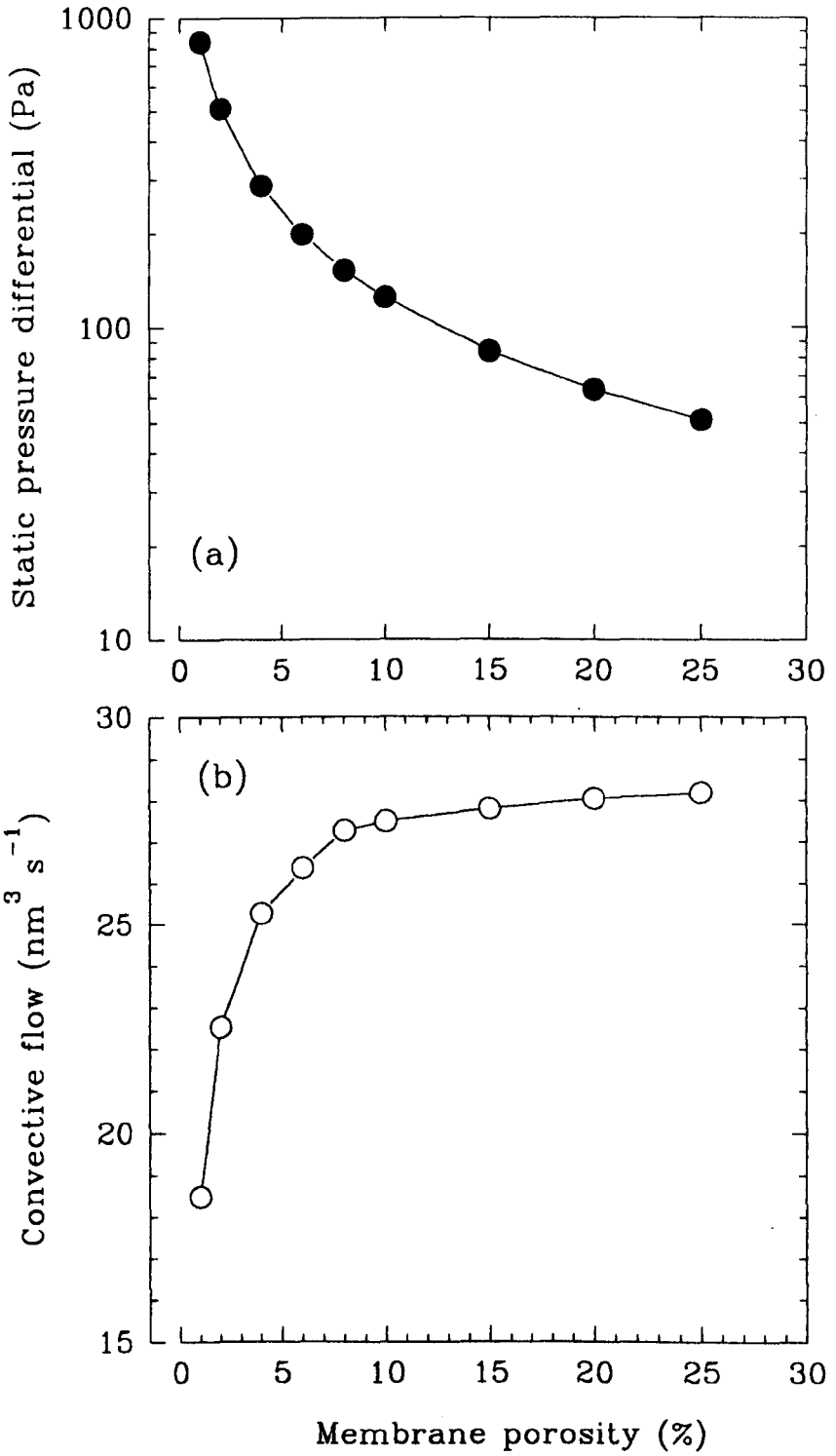

Fig. 6.21. Predicted effects of porosity on static pressures and potential convective flow for membrane of MPD = 0.046 μm; W = 4 mm; no boundary layer and T = 20°C.

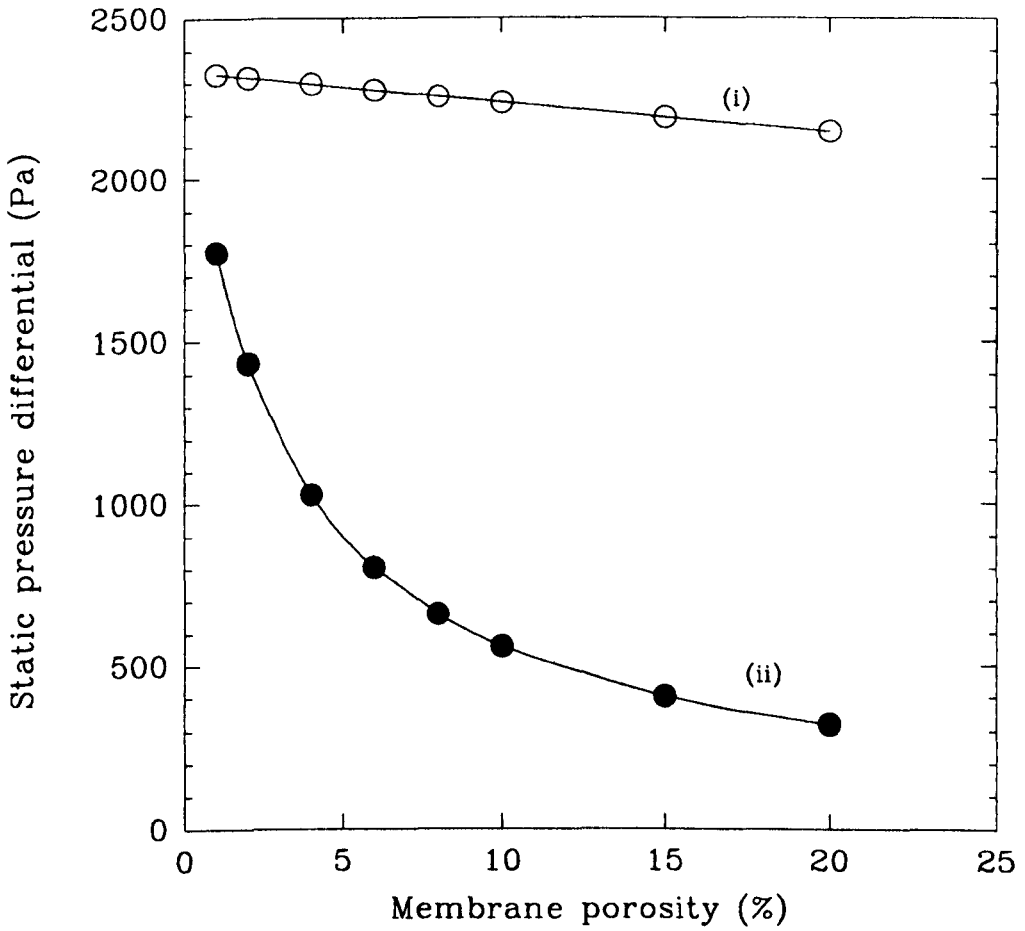

Fig. 6.22. Predicted effect of membrane porosity on the static pressure: (i) no boundary layer and (ii) a boundary layer of 700 μm. MPD = 0.046 μm. W = 10 μm

resistance. Consequently low leaf sheath porosity may be an advantage for overcoming resistance in the throughflow path. However, in the examples just cited it must be recognised that the venting resistance imposed by one 1 μl capillary is probably very much greater than that of quite long lengths of rhizome (see Chapter 2).

6.3.10. *Pore length*

Since increasing pore length increases the value of R_{md}, then just as ΔP_s increases with decreasing pore diameters and decreasing membrane porosity, so it will with increasing pore length (see Fig. 6.23). Thus it is predicted that for an MPD of 0.046 μm, with W at 4 mm and a 700 μm boundary layer, ΔP_s should rise from 54 Pa at a pore length of 5 μm to 448 Pa at a pore length of 50 μm (Fig. 6.23 b).

The results also show that at a low venting path resistance of 70 MPa s m^{-3} (equivalent to the resistance of the soap-film flow meter with its pipe work and one soap film), the dynamic pressure differentials and flows are not greatly affected by pore length where W = 4 mm : there are small decreases only with increasing pore length (Fig. 6.23a); when W is reduced to 10 μm, the ΔP_d and flows are halved for this same increase in pore lengths (Fig. 6.23c). However, when the venting path resistance is increased, although flow rates fall, the relationship between flow and pore length is gradually altered, and eventually reversed in slope. Thus at W = 4 mm and a venting path resistance of 7000 MPa s m^{-3}, the flows and dynamic pressures at the 50 μm pore length are more than double those for 5 μm long pores (Fig. 6.23b). If W is 10 μm, similar effects are noted, although at the venting resistance of 7000 MPa s m^{-3} the flows for the 10 & 50 μm long pores are similar and only 1.4x higher than for the 5 μm pores (Fig. 6.23d). Thus, as was the case with membrane porosity, the

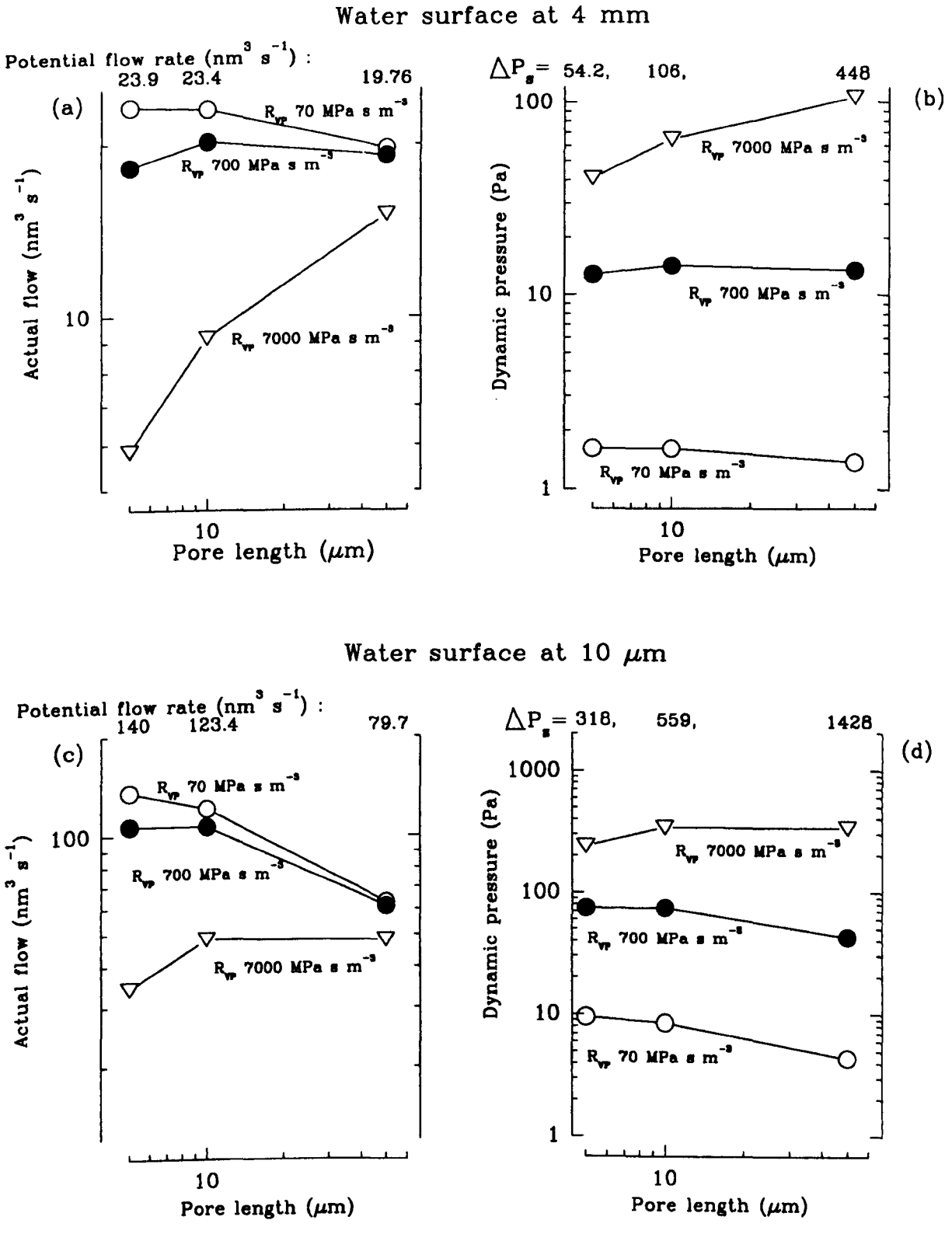

Fig. 6.23. Prediction showing the effect of pore length and venting resistance on dynamic pressures and convective flows for Nuclepore membrane of MPD 0.046 μm and boundary layer of 700 μm.

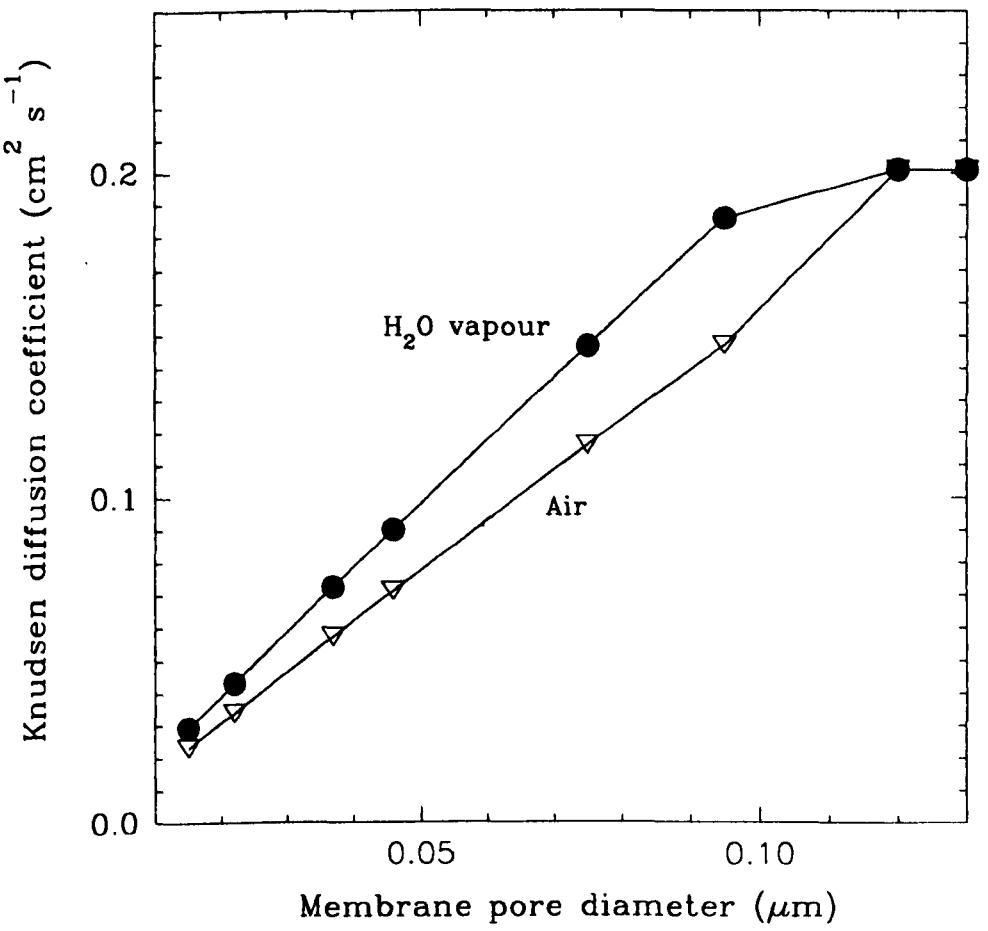

Fig. 6.24. Calculated Knudsen diffusion coefficients for water vapour and air at 20°C.

potential to achieve high pressures increases in importance as venting resistance becomes greater.

6.4. FINAL COMMENTS

Experimenting with Nuclepore membranes was perceived originally as a relatively simple way of studying the convective flow processes which appeared to be operating in *Phragmites* and the water lilies. The *Phragmites* plant, because of its bulk and awkward shape, is not an easy experimental subject. Unfortunately, however, because the Nuclepore membranes failed in so many instances to match the manufacturer's specifications, the study proved less simple and took much longer than had been anticipated. Nevertheless, the results obtained have been helpful in furthering our understanding of the humidity-induced convective flow mechanism, and the use of the Nuclepore membranes also stimulated the development of the theoretical treatment described in Section 6.2.3. The broad agreement obtained between the experimental work and the mathematical predictions is encouraging since the use of mathematical modelling has introduced a flexibility into the study which could never be achieved with either the physical Nuclepore model or the *Phragmites* plant.

In this respect perhaps the most important findings to emerge from the modelling are : (a) that very significant pressurisation and convective flows can be achieved from membrane pore diameters well outside the Knudsen regime provided that the evaporative surface can be established close to the base of the pore, (b) that convection can peak at pore diameter *ca.* 0.1-0.2 μm, and (c) that the role of membrane resistance becomes more critical the greater the venting path resistance.

This has helped to clarify the position regarding *Phragmites*. All the evidence seemed to point to the leaf sheath surface with its stomata as being the effective microporous membrane, but the stomatal pore width appeared to lie only on the fringes of, or outside, the Knudsen regime. Further to this, static pressures up to 800 Pa could be found in the field, and pressures *ca.* 250-400 Pa were the norm even in dull daytime conditions at relative humidities of 30-50%. The theoretical findings (Fig. 6.18) show that pressures of 300 Pa should be possible at a pore diameter of 0.4 μm, a boundary layer thickness of 200 μm and an external relative humidity of 50%. Also, greater pressures would be obtained if the evaporative surface was closer to the membrane, if the external humidity was lower or if the boundary layer was thinner.

Experimentally, humidity-induced pressurisation and flows were measurable for Nuclepore membranes of MPD 0.015 - 3 μm, apparently under similar conditions of humidity differential to those recorded for *Phragmites* living leaf sheaths (Chapter 5). In both cases convective flows are enhanced by low atmospheric humidity, by a positive temperature gradient, and by greater areas of porous membrane exposed.

However, there is the important difference that light was necessary for appreciable HIC convection in the plant, but not in the case of the membranes. This is to be expected, since it seems that light is necessary in the plant for the opening of stomata. Also a dry wind blowing over a Nuclepore membrane markedly increased HI convection rates and ΔP_s, but these effects were not so marked in the plant when a fan was used to create a wind. This was perhaps because the stomata of the leaf sheaths are located in grooves and the pores themselves are surrounded by wax, (Fig. 3.02), features which might prevent the

wind from disturbing the boundary layer of water vapour around the pores. Also, it is difficult to blow a wind under controlled conditions across leaf sheaths in the same way as across a smooth flat membrane. Nevertheless, one can envisage that a wind blowing dry air into a reed bed would enhance HIC by removing the comparatively humid air which could accumulate around the shoots under still conditions.

When the wind speed of dry air over the 0.046 μm-pored membrane was increased it was found that the rate of water vapour loss through the membrane was greater than the rate of entry of air, and this accorded with modelling predictions. However, the modelling shows that where the micropores are outside the Knudsen regime, the two flows should balance. It follows that convective air flows from *Phragmites* should give an approximate measure of transpirational water loss from the sheaths.

Nuclepores membranes did not prove to be very successful for studying thermal transpiration. Compared to the convection induced by a humidity gradient, the effects due to temperature differentials were small, even when ΔT was +8°K. This may have been due to the difficulty in maintaining a steep temperature gradient across the shallow pores of the Nuclepore membrane, possibly because the membrane itself heats up. On the other hand, one could envisage that a humidity gradient could be maintained more easily than a temperature gradient could in the Nuclepore assembly or the plant, since it largely depends upon molecular movement. With the plants, the measurements of ΔT rarely exceeded +2°K, and hence it seems unlikely that thermal transpiration plays more than a minor role in convection in *Phragmites*.

Further to this the Nuclepore experiments have confirmed that, whereas any thermal transpiration effect is reversed if the temperature under the membrane falls below ambient, the humidity-induced

pressurisations and flows remain substantial under small negative temperature differentials.

6.5. SUMMARY

Experiments are described in which Nuclepore microporous membranes were used to study thermal transpiration and the development of humidity-induced pressurisation and convective flows in relation to pore diameter, humidity and temperature differentials, external wind speed, membrane surface area and venting path resistance.

Mathematical modelling was employed to help to interpret the experimental results and to extend the study by exploring the effects of factors which were difficult or impossible to vary experimentally.

The experiments confirmed that considerable pressures and convective flows can be created when a humidity differential is imposed across a microporous membrane, and that for equi-porous membranes, the pressure differential will increase with decreasing membrane pore diamter. On the other hand, the potential for convective flow peaks at pore diameters around 0.1 - 0.2 μm. Thus it would appear that significant pressures and flows can be generated by pores outside the Knudsen regime, and the mathematical modelling showed that to achieve static pressures similar to those found in *Phragmites* does not require that the pore diameter be in the Knudsen regime.

Both the experimental and modelling data emphasised the importance of having the internal evaporative surface close to the base of the micropores, and confirmed that convective flow inceases linearly with humidity differential and with membrane surface area. Static pressures and convective flows increased with increasing wind speed over the membrane, while dynamic pressures increased and convective flows decreased, as resistance to convective flow was increased.

The mathematical modelling demonstrated the likely effects of membrane porosity and pore length on pressurisation, and an interaction between porosity and boundary layer effects. The results suggested that as the convective venting flow-path resistance increases, membranes of higher gas-flow resistance (caused by low porosity or narrower or longer pores) can become more effective than membranes of lower resistance for driving convective flows.

The Nuclepore membranes were not very successful for the study of thermal transpiration. Only the smallest pored membrane (0.015 μm) gave measurable pressures over the temperature differential range found in *Phragmites*, and it was again concluded that humidity-induced diffusion is likely to be the dominant pressurising mechanism in the plant.

CHAPTER 7

VENTURI-INDUCED CONVECTION AND ITS EFFECT ON RHIZOME AERATION AND ROOT RADIAL OXYGEN LOSS

7.1 INTRODUCTION

The beneficial effects of *humidity-induced convection* on rhizome and rhizosphere aeration in a reed bed are anticipated in Section 5.4, but this type of convection can only operate effectively in the growing season, in the light and when there is a humidity differential between the inside and outside of the plant. These aspects led to fears that the capacity of reed beds to treat waste-waters might be hampered during the winter and under conditions of darkness and/ or very high atmospheric humidity. In these circumstances rhizome aeration would depend largely upon the diffusion of oxygen from the aerial parts and this might be insufficient to meet the oxygen demands of the effluents (see also Section 8.2.1). However, the present study has shown that another major type of *throughflow convection* occurs in *Phragmites* namely ***Venturi-induced convection***, which depends upon the wind. It can operate both during the growing season, in winter, and is unaffected by conditions of darkness and high humidity. A gas-space continuum between dead snapped-off culms and the rhizome system is essential. Wind blowing across tall dead culms creates a suction pressure throughout the system resulting in a throughflow of gases, air being sucked out through the tall culms and in via culms snapped off closer to ground level where wind speeds are slower.

It is interesting that Vogel (1978) drew attention to a Venturi-

ventilation of the underground tunnels of the prairie-dog. It has also been suggested that small-scale Venturi-ventilation might operate within leaves (Dacey, 1981a). The present study appears to be the first instance in which a Venturi convection has been identified and quantified in a plant.

The investigations which led to the discovery of the Venturi-effect in *Phragmites* are described in this chapter and effects of wind speed on rhizome and rhizosphere aeration are quantified.

7.2 MATERIALS AND METHODS

7.2.1. *Plant material*

Horizontal rhizomes of *Phragmites*, collected from the banks of the Humber estuary were placed, with one end emergent, in stagnant 20% Hoagland's solution at 15°C to resume root and shoot production. The plants chosen for the experiments each consisted of a piece of horizontal rhizome bearing living shoots 0.3-0.6 m tall, and adventitious roots 0.01-0.3 m long.

Old dead culms of various diameters and open at the top, were also collected.

7.2.2. *The effects of wind speed on Venturi-induced convection.*

Single, excised dead culms were used ; the upper pith cross sectional areas ranged from 0.096-0.283 cm^2, and each culm had six nodes. The upper, open end of the culm was sealed into a T-piece junction, so that air at various wind speeds could be blown across it at right angles to the plane of the aperture. This created a variety of suction pressures and convective flow rates. Wind-speed was calculated by means of an air-flow meter, and from the internal dimensions of the T-

piece junction. The basal end of the culm was connected directly to a pressure transducer (Furness Controls Ltd., Bexhill) to measure the static pressure differentials developed (ΔP_s, i.e. non-throughflow condition) , or alternatively was connected to a soap-film flow-meter (length 500 mm, I.D. 5 mm) to measure convective flow rates through the culm. The measurements were made at imposed wind speeds of *approx.* 2 to 16 m s^{-1}.

It should be noted that the ID of the flow meters used in this study lay within the range of pore space diameters which characterise *Phragmites* rhizomes and culm bases. Consequently, throughout the results sections, to make it easier to visualise rates of flow, the gas-flow velocities through the flow-meter (mm min^{-1}) are quoted in addition to the volume flow rates (m^3 s^{-1}).

7.2.3. *Effects of Venturi-induced convection on rhizome and rhizosphere aeration.*

Each plant consisted of a piece of horizontal rhizome, 3-5 nodes and 0.3-0.4 m long, bearing living shoots and roots. One end of the rhizome was connected to a short, dead, emergent culm, (with 2 nodes and upper pith cavity diameter = 5 mm), to allow an inflow of air. The other end was indirectly connected to another emergent dead culm (6 noded ; upper pith cavity diameter = 3.5 mm), and T-piece to induce Venturi-convection as in the previous experiment. Between the rhizome and this latter dead culm was a Clark-type electrode for monitoring the $[O_2]$ of air as it emerged from the rhizome, and a soap-film flow-meter to measure the convection rate (Section 5.2.2). The rhizome and roots were immersed in 8 litres of a stagnant 20% Hoagland's solution made up in 0.05% w/v agar : water, in a transparent Perspex container (600 x 50 x 280 mm). The medium was de-oxygenated by gassing with

oxygen-free nitrogen for 24 h before measurements commenced, and for this series of experiments the shoots were kept in darkness to minimise humidity-induced convection. Oxygen efflux from both adventitious and lateral roots and the oxygen regime in the agar, 3-5 mm. from the laterals were measured polarographically according to methods previously described (Armstrong, 1979; Armstrong and Armstrong, 1990a; and Section 5.2.4).

7.2.4. *Venturi-induced convection in the field.*

Evidence of Venturi effects in the field was sought in the winter when the leaf sheaths had died and when very little humidity-induced convection could occur.

Excised culms, one to two metres tall with basal pith cavity diameters of 4 - 6 mm, and which had lost their flowering heads, were used to determine static pressures in relation to wind speed. Values of ΔP_s were obtained using a portable digital pressure transducer (Furness Controls Ltd) attached via a plastic three-way tap to the basal end of vertically held culms. Wind speeds across the top of the culms were measured using a simple hand-held Anemo (Casella, London) rotating wind speed indicator without any averaging facility.

Convective flows from rhizome to culm were demonstrated by connecting a soap-film flow-meter in series between the stump and the base of an excised 2 m culm (pith cavity diameter, 5 mm).

Convective flows into the rhizome system were demonstrated by attaching a soap-film flow-meter to the protruding stump of an isolated snapped off culm which was surrounded only by tall persistent culms. The isolated stump was chosen to maximise the chances of measuring inward convective flow. If there had been other short stumps in the vicinity they could, because of underground linkages, have acted in

parallel, and depending upon the geometry of the underground system could have substantially reduced the flow into the chosen stump.

7.3. RESULTS AND DISCUSSION

7.3.1. *The effects of wind speed on Venturi-induced convection.*

The Venturi-effect of wind blowing across an open tube is quantified by Bernoulli's equation (Milne-Thomson, 1960): $\Delta P = - 0.5\ \rho\ V^2$, where ΔP is the pressure differential developed (Pa), ρ is the density of air (approx. 1.20–1.25 kg m^{-3}), and V, the wind velocity (m s^{-1}). Thus, ΔP should be directly proportional to V^2 and independent of the culm's internal resistance, and hence of its cross-sectional area. This is confirmed by the results shown in Fig. 7.01b where, at each wind speed, similar ΔP_s values were obtained for the four culms of differing cross-sectional areas. On the other hand, the convective flow rate is a function of wind speed (Fig. 7.01a,b), namely inversely proportional to the wind-speed^2 (Fig. 7.03b), and is more or less proportional to the cross sectional area of the culm (Fig. 7.02). In the latter figure the possible curvature in the relationship between convection and cross-sectional area could be due the greater influence of the internal drag factor the narrower the culm. Like the static pressure differential, the convective flow rate also is directly proportional to the square of the wind speed (Fig. 7.03b).

From the above it can be deduced that the aerating effect of Venturi-induced convection in a reed bed will be greater the greater the incidence of tall, wide, persistent dead culms which are connected to the internal gas-space system of the rhizomes. It was found that dead culms can persist in this way for at least 2–3 years.

When the basal ends of the culms were deliberately blocked to

Figure 7.01 (overleaf)

Fig. 7.01. Venturi-induced convection and static pressures differentials developed at different wind speeds in dead 'decapitated' excised culms. Each culm had 6 nodes and culm lengths varied from 0.67 - 1.07 m.

Phragmites: Venturi- Induced Convective Flows and Static Pressures in Dead Culms at Different Wind Speeds

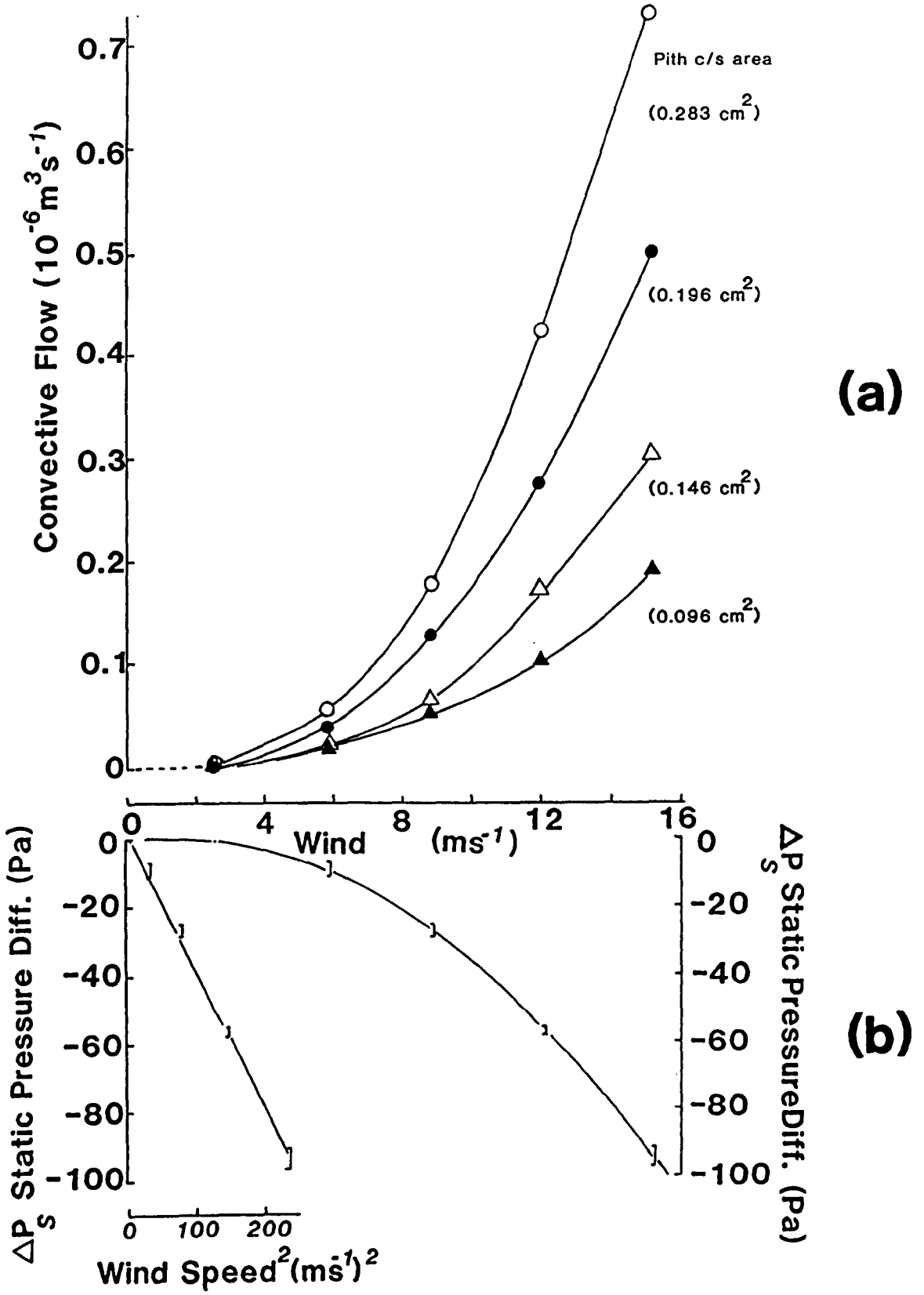

Figure 7.01

Phragmites : variation in Venturi-induced convection with pith x-sectional area and wind speed.

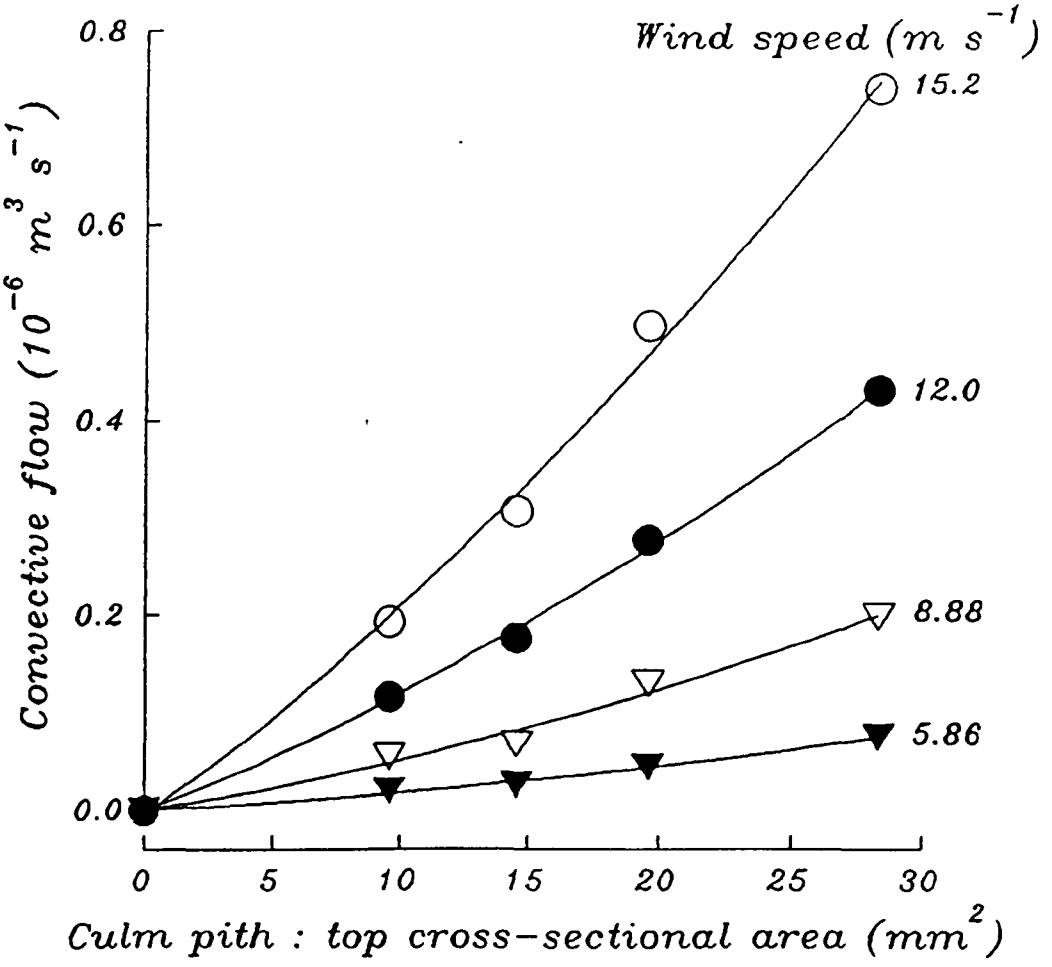

Fig. 7.02

Figure 7.03 (overleaf)

Fig. 7.03. Venturi-induced convection.

(a) Effects of wind speed on the convective flow, on [O_2] venting from rhizome, and on root oxygen efflux. The experiment was performed in the dark to minimise humidity-induced convection. Adventitious root 1, length = 70 mm; adventitious root 2, length = 98 mm. Inflow culm : two noded; length 240 mm; pith cavity diameter 5 mm. Outflow culm (exposed to controlled wind): six noded; length 790 mm; upper pith cavity diameter 3.5 mm. Temperature 21-22.5°C; RH=42-48%.

(b) Relationship between convective flow and (wind speed)^2, calculated from data in 3(a).

PHRAGMITES: VENTURI-INDUCED CONVECTION: EFFECTS OF WIND SPEED ON RHIZOME (O_2) AND ROOT OXYGEN EFFLUX

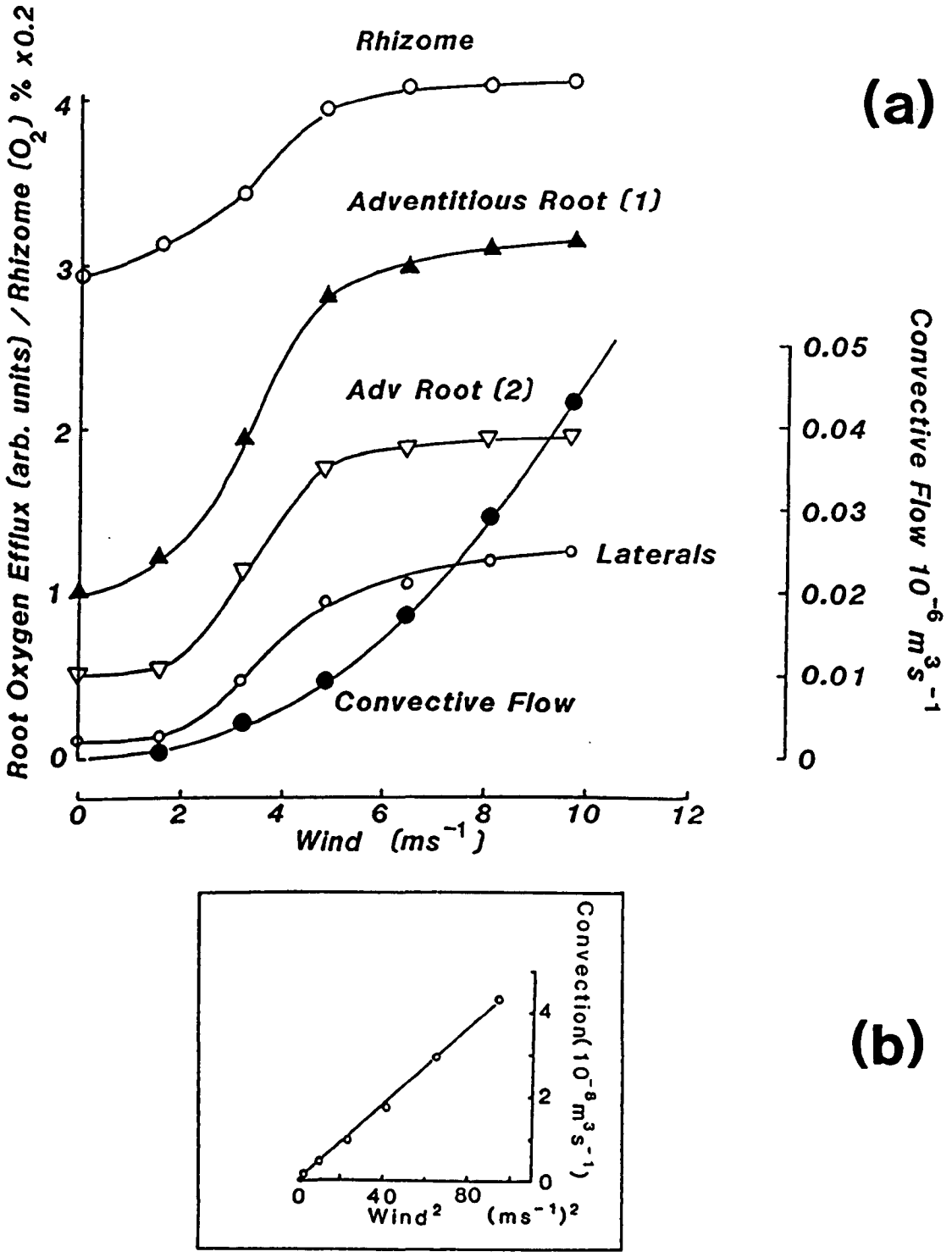

Fig. 7.03

prevent throughflow, the suction potential of the Venturi effect was measurable as a static negative pressure (Fig. 7.01b). These pressures amounted to approx. 60% of the values calculable from Bernoulli's equation. Glass tubes substituted for the culms developed pressures which were 85% of the predicted values. The lower suctions developed by the culms may have been due to the serrated nature of the pith cavity rims exposed to the wind stream. The possibility that leakages through the nodal stomata were the cause of the lower values was ruled out: blocking these stomata with silicone rubber raised the static pressures by no more than 1 Pa, but some culms were leaky due to longitudinal fractures, abscised buds and insect damage.

7.3.2. *Effects of Venturi-induced convection on rhizome and rhizosphere aeration.*

Convective flows induced by the Venturi effect markedly increased rhizome oxygen concentrations and oxygen efflux from both adventitious and lateral roots. In the case of the roots, it can be concluded that convective flow enhances the oxygen supply to the rhizome-root junctions, thereby causing increased oxygen diffusion through the roots and into the rhizosphere. In the example shown (Fig. 7.03a), rhizome [O_2] increased 1.4-fold (to 93% of atmospheric), lateral root O_2 efflux 8-fold, and O_2 efflux from adventitious roots 2.9- and 3.5-fold as the wind speed was raised from 0 to 5.3 m s^{-1}; and the convective flow reached 11.4 nm^3 s^{-1} (34 mm min^{-1} through the flow-meter, similar to rates achieved by HIC with a light flux of 200 μmol m^{-2} s^{-1} in Fig. 5.08 & 5.09). At wind speeds greater than 5.3 m s^{-1}, convection rates continued to rise proportionally, but further increases in rhizome [O_2] and root oxygen efflux were very limited. This aspect is further examined in the Chapter 8 on mathematical modelling.

The control electrode 3-5 mm. away from the laterals showed virtually zero oxygen flux throughout the experiments.

It is interesting to compare Figs. 5.09 and 7.03 which show that near maximum values for rhizome aeration and ROL are attained at comparatively low convective flow rates (approx. 0.1 m^3 s^{-1}) for both humidity-induced and Venturi-induced convection. For the latter, this was attained under laboratory conditions at wind speed 4.8 m s^{-1} blowing across a fairly narrow culm (upper pith cavity area 9.6 mm^2. Culms with wider exposed pith cavities would produce similar aeration effects at lower wind speeds (Fig. 7.02).

7.3.3. Venturi-induced convection in the field.

For the excised culms, static pressures varied from *ca.*-2 to -3 Pa at wind speeds of *ca.* 3 m s^{-1} to *ca.*-40 Pa at wind speeds of 12 m s^{-1}. The latter is a strong wind but average daily wind speeds of 3 m s^{-1} are common. At 12 m s^{-1} the static pressure is only 45% of the value calculable from Bernoulli's equation, and less than those obtained from excised culms in the laboratory. The discrepancy between the laboratory and field measurements may have been due to a number of factors: the gusting nature of the wind in the field made it difficult to measure wind speed and to co-ordinate wind speed and pressure differential measurements; also, it may be that the orientation of the open ends of the culms as a result of the bending of the reeds by the wind in the field may be such as to shield them from the full potential of the wind. The effects of gusting of the wind on rhizome aeration are considered in Section 7.4.

Despite the apparently lower realisable static pressures under field conditions, convective flows from rhizome to culm via the soap-film flow-meter varied from approx. 40 mm min^{-1} at wind speeds of 5-6

m s^{-1} to 100 mm min^{-1} at wind speeds around 10 m s^{-1}. Also, there was a pronounced Venturi-induced inflow of air into the rhizome system via the isolated stump described in the methods section, and a flow of 120 mm min^{-1} was recorded at wind speeds of around 10 m s^{-1}.

These preliminary studies confirm that Venturi-induced convection does indeed occur in *Phragmites* in the field, but much remains to be done to quantify the effects more exactly.

7.4. FINAL DISCUSSION

Although it is clear that Venturi-driven convection operates in the field and can cause considerable enhancement of aeration if generated in the laboratory, more information, and perhaps further modelling, are needed to gauge properly its role in *Phragmites* beds under field conditions. A knowledge of fluctuations in wind speed is particularly important, and wind speed averages expressed in m s^{-1} calculated from daily wind speed totals (km d^{-1}) are likely to be quite inadequate for assessing the field potential of the Venturi-effect. For example, because the pressure differential (and thus Venturi-convection) varies as the square of the wind velocity (Fig. 7.03b), the potential for rhizome aeration at an average wind speed of 3 m s^{-1} could be doubled if the average was achieved by a gusting of the wind at 6 m s^{-1} for 1 min followed by 1 min of stationary conditions. If the wind gusted at 12 m s^{-1} for 1 min, and was still for 3 min (again an average of 3 m s^{-1}) the aerating potential per minute is quadrupled. With higher velocity gusting the effects are further magnified. The wind regimes likely to provide optimum aeration remain to be determined, and will probably depend upon many factors including the influence of diffusion and the oxygen reservoir capacity of the rhizome during still periods, as well

as the respiratory demands of rhizome, root and rhizosphere, and the dynamics of activities in the rhizosphere. Also of importance must be the numbers of dead and broken culms per unit length of rhizome system, their heights above ground level, and the cross-sectional areas of exposed pith cavity. Since flow is directly proportional to culm cross-sectional area, and hence inversely proportional to Poiseuille flow resistance, the wider the culm, the greater will be the flow for any given wind speed (Fig. 7.02), and hence the more robust the culms and the higher their numbers per unit of rhizome, the greater should be the flows. Flows will not increase in direct proportion to an increase in culm numbers or accumulated cross sectional area, however, because as numbers or cross-sectional areas of culms increase, so the flow rate will become more dependent upon the internal resistance of the rhizome system itself. Hence, as culm cross-sectional area relative to rhizome cross-sectional area increases so will flow rates tend towards an asymptote. Winter (November-March) wind speeds on the Holderness Plain of East Yorkshire average on a daily basis approach approx. 3 m s^{-1}. (Average daily wind speeds for December 1974 are shown in Fig. 7.04). In the result shown in Fig. 7.03, a constant wind speed of 3 m s^{-1} produced a convection of 3 nm^3 s^{-1} (velocity 10 mm min^{-1}) which raised rhizome oxygen concentration to only 79% of its potential maximum, while fluxes from behind the apices of the adventitious roots rose only to 56 & 52% of their maxima. Gusting winds at 6 m s^{-1} on a 1 min on, 1 min off basis would have doubled the oxygen input to the system per unit time, and, therefore, would probably have increased rhizome oxygen to 90% of maximum, and root oxygen efflux to 81 & 79% respectively. Almost the same effect might have been achieved at a constant 3 m s^{-1} if two culms had been attached in parallel to the venting (Venturi-) end of the system, or one culm of twice the cross-

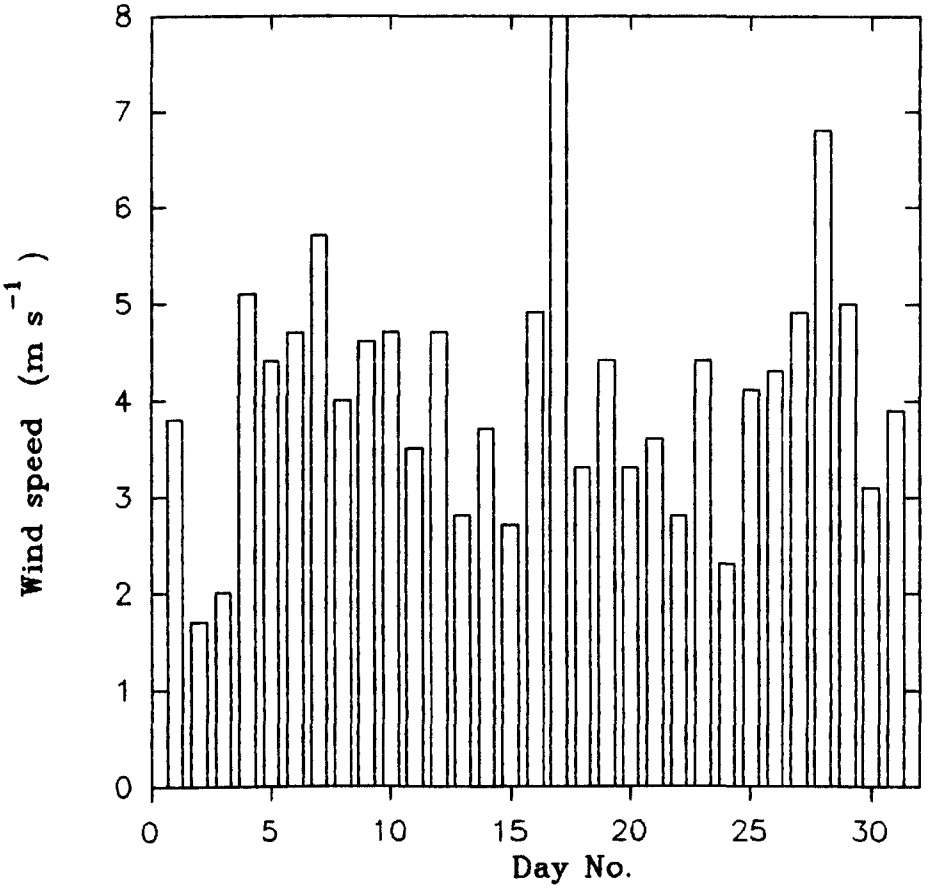

Fig. 7.04. Average daily wind speeds recorded at a meteorological station in Holderness, East Yorkshire, during December 1974.

sectional area (19.2 mm^2). Gusting at 12 m s^{-1} on a 1 min on, 3 min off cycle, would quadruple the convective effect, raising oxygen levels in rhizome and roots to between 92 and 96% of maximum.

Whereas both *humidity*- and *Venturi*-induced convections can operate in the growing season during the daytime, *Venturi*-induced convection should be the chief means of throughflow whenever *humidity*-induced convection cannot occur, or takes place very slowly such as at night when the relative humidity approaches 100%, and in the winter when the leaf-sheaths die. It would seem advantageous, therefore, for reed root-zone treatment beds to be planted in open conditions where they can benefit from the Venturi effects of the wind, and that old culms should not be cut so that maximum Venturi effects can occur. Old culms are also essential as venting points for humidity-induced convection, whereas *all* culms will be important for allowing the diffusion of oxygen into, and CO_2 out of, the underground system whenever convective flows are not operating. The wind in a reed bed could also help to reduce humidity and so aid humidity-induced convection. In this context, and that of Venturi-convection, it is interesting that Weisner (1988) found that *Phragmites* grows more vigorously in exposed rather than in sheltered sites.

SUMMARY

A ***Venturi-induced convection*** of gases through the ***Phragmites*** culm and rhizome system is described, and this is thought to be the first time that this type of convection in a plant has been reported. It is driven by a pressure differential created by wind blowing across tall dead culms which sucks air into the underground system via culms snapped off close to ground level. The results demonstrate how wind, by increasing ***Venturi-induced convection***, raises the oxygen concentrations in the rhizome system, thereby causing much greater fluxes of oxygen into root and rhizosphere than are achieved if rhizome aeration is by diffusion alone. The implications of wind gusting are also discussed. In laboratory experiments convective flow rates of as low as 7 - 14 $nm^3\ s^{-1}$ (approx. 20-40 mm min^{-1} in the rhizome) were sufficient to raise rhizome oxygen concentrations to 90% of atmospheric. The significance of this is discussed in connexion with pollution control by constructed wetlands.

CHAPTER 8

MATHEMATICAL MODELLING OF ROOT AND RHIZOME AERATION AND ROOT RADIAL OXYGEN LOSS

8.1. INTRODUCTION

The final goal of this project was to derive estimates of the quantities of oxygen which could be expected to enter the rooting medium *per* day, *per* m^2 of reed-bed.

Attempts to detect free oxygen in the soil water had previously failed (Brix & Schierup, 1986, *personal communication*), most likely as a result of the rapid utilization by the soil microorganisms of any oxygen released, and it was considered futile to attempt direct measurements of oxygen release in the field. It is possible make estimates of oxygen release based on the differences in the inflow and outflow BOD of sewage treatment beds (Gray *et al*, 1990), but such an approach was beyond the scope of this study.

Alternative approaches adopted here were (a) direct measurement of oxygen release from roots in the laboratory using circulation experiments (Sections 4.2.5 & 4.3.4) involving passing deoxygenated water over *Phragmites'* roots, the roots being in a more or less sterile medium and being subjected to as uniform an oxygen sink as possible; the results of such experiments could then be extrapolated to predict the degree of oxygen release which might be expected in the field (see Chapter 4), and (b) by mathematical modelling. To this end the multicylindrical mathematical model of Armstrong & Beckett (1987) was employed. The model enables a given level of soil oxygen demand and soil oxygen diffusivity to be programmed, together with the known

oxygen consumption and oxygen transport characteristics of the roots.

A second mathematical model (Beckett in Armstrong *et al*, 1990b) was developed in order to learn more of rhizome aeration including the likely effects of root and rhizosphere oxygen demands on the oxygen concentrations which might be maintained at the root-rhizome junctions, and the lengths of aerated rhizome which could be supported by diffusion and convection either together or separately. Results obtained using this model were also used to set the basal oxygen concentrations for the investigations using the multicylindrical root model.

In this chapter there are no separate results and discussions sections - discussion is incorporated immediately after comments on the models.

8.2. THE MATHEMATICAL MODELS

8.2.1. *Rhizome Aeration*

8.2.1.1. *Oxygen concentration in the rhizome.*

Having established that, in addition to diffusion, HIC (Chapter 5) and Venturi-convection (Chapter 7) can aerate *Phragmites* rhizomes, it seemed desirable to evaluate mathematically the relative importance of the processes of convection and diffusion, and to correlate this with the experimental findings. The aeration of the underground rhizome in *Phragmites* is of crucial importance in supplying the porous root-rhizome junctions with oxygen which will then diffuse into the adventitious root aerenchyma, and thence to the rhizosphere via the basal laterals and the oxygen-permeable apical regions of the adventitious roots themselves (Chapters 2 & 4). Thus, the greater the rhizome $[O_2]$ the greater should be the radial oxygen loss into the rhizosphere.

In the steady state, simultaneous ***throughflow convection*** and diffusion of oxygen through a rhizome of length L will be governed by the differential equation:

$$U\ dC/dx = D\ d^2C/dx^2 - Q \qquad (8.01),$$

where C(x) is the concentration at any distance along the convection or diffusion path, U is the convective velocity, D is the effective diffusion coefficient (i.e. $D_o\epsilon$, where ϵ is the fractional porosity and it is assumed that there is no tortuosity in the diffusion path; D_o is the oxygen diffusivity in air), and Q is the respiratory demand. It is assumed for convenience that Q and D are effectively uniform along the length of the rhizome.

By assuming that the concentration is maintained as C_o (e.g. atmospheric) at x=0 (the inflow point), and that there is no back-diffusion into the section at x=L (the outflow point), i.e. dC/dx = 0 at x=L, the concentration at any distance x from the inflow point is given by:

$$C(x) = C_o - Qx/U - (QD/U^2)\{e^{-UL/D} - e^{-U(L-x)/D}\} \qquad (8.02),$$

and the concentration at x=L is given by:

$$C(L) = C_o - QL/U + (QD/U^2)\{1 - e^{-UL/D}\} \qquad (8.03).$$

To facilitate comparison between the mathematical modelling and the laboratory experiments, the values assigned to constants C_o and D were those which pertain at room temperature (20°C).

It should be noted that equation 8.03 is only applicable if C(L) > 0. It is possible to prescribe a combination of parameters which yields a negative value for C(L), but in such cases the rhizome would not be fully aerobic and the basis on which the formula has been constructed is no longer valid.

Several types of prediction concerning the aeration of *Phragmites* can be made by the appropriate use of equation 8.03. As

written here the equation strictly shows the [O_2] at the end of a fixed length of rhizome through which gases are convecting at rate U. Hence, the relationship between convection rate and the degree of rhizome aeration in terms of achievable oxygen concentrations can be computed. Also, by appropriately varying the value of Q, it is possible to predict in a simplified way, the likely effects of root and rhizosphere oxygen demands; in particular to show to what extent an increased sink strength in the form of root and rhizosphere oxygen demand may influence the relationship between convective flow rate and the rhizome oxygen concentration C(L).

The extent to which convection can be expected to raise oxygen concentrations in a rhizome of fixed length is shown in Fig. 8.01, where oxygen concentrations in the gas venting from the rhizome, (i.e. concentration C(L) - equation 8.03), are plotted against the rate of convection. The length of active rhizome was fixed at 500 mm, the respiratory oxygen demand of the rhizome itself was set at 7.5 ng cm^{-3} s^{-1} in accordance with experimental measurements of rhizome oxygen demand made in the laboratory (Appendix III, and Yamasaki, 1987 - young rhizomes), porosity was taken as 60% (ϵ = 0.6)(Armstrong, Armstrong & Beckett, 1988), and rhizome diameter was assumed to be 6.45 mm. Curve A represents the condition in which the only oxygen demand is that of rhizome respiration ; curve B includes, in addition, the respiratory demand of 10 adventitious roots each bearing 600 laterals; for curve C a respiratory demand of 50 ng cm^{-3} s^{-1} and an oxygen diffusivity of 1×10^{-5} cm^2 s^{-1} was imposed in the rhizosphere of these roots. Curve D represents the case in which the oxygen demand of the rhizosphere is 500 ng cm^{-3} s^{-1}. The oxygen demands of roots and rhizosphere were determined by substituting appropriate values for porosity, oxygen demand, and root geometry into the

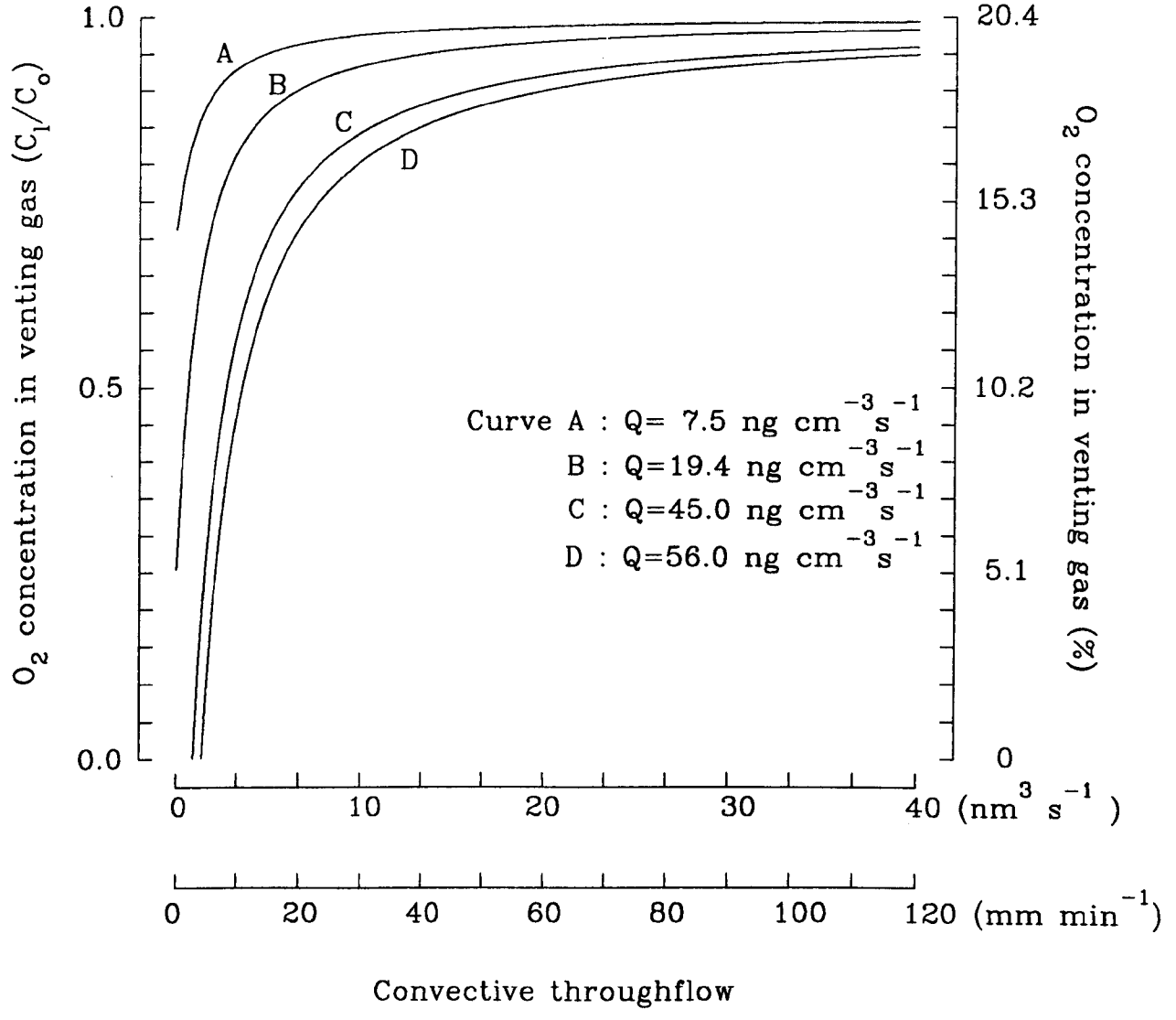

Fig. 8.01. Rhizome aeration modelling predictions. For different levels of oxygen demand shows how increasing rates of convection can be expected to influence the [O_2] in the gases vented from the rhizome :

Curve A, rhizome oxygen demand of 7.5 ng cm^{-3}s^{-1},

Curve B, as A, but with extra respiratory demand equivalent to that of 10 adventitious roots plus attendant laterals (600 per root),

Curve C, as B, but with additional demand due to oxygen consumption in the rhizosphere (soil oxygen demand 50 ng cm^{-3} s^{-1}),

Curve D, as C, but with rhizosphere demand raised to 500 ng cm^{-3} s^{-1}.

multicylindrical model of Armstrong & Beckett, 1987 (Appendix II).

The modelling predictions in Fig. 8.01 are in close agreement with the experimental observations recorded in Figs. 5.06, 5.09 & 7.03 for HIC and Venturi-induced convection respectively : in all cases rhizome aeration was greatly improved by relatively low rates of convection. In Fig. 8.01 (Curve A), where the oxygen demand is from rhizome respiration only, a convective flow of as little as 5 mm min^{-1} was sufficient to raise the rhizome venting oxygen concentration C(L) to 90% of its potential maximum . With the added respiratory demand of 10 roots, the same degree of aeration is achieved with a convective flow of approx. 20 mm min^{-1} (Curve B). To satisfy in addition the lower of the two rhizosphere oxygen demands, requires a rather larger increase in flow velocity to 47 mm min^{-1} (Curve C). To accomodate the further 10-fold increase in rhizosphere oxygen demands appears to require a relatively small further increase in flow to 60 mm min^{-1}. Although the rhizome could cope exactly as shown with an internal oxygen demand of 56 ng cm^{-3} s^{-1}, other modelling data have revealed that if the hypothetical root system was unchanged in its geometry and potential activity, the 10-fold increase in rhizosphere demand would probably cause some degree of root anoxia, particularly in the apices of the lateral roots (Armstrong, Armstrong & Beckett, 1990). In other words, no matter how rapid the convection might be through the rhizome, it might not be sufficient to support in full the potential oxygen demands of root and rhizosphere. However, it would be possible to support the same total demand if this were to be spread over more and shorter roots.

Concerning the above it is encouraging to note that in the experiments on HIC, (Section 5.3.1), a convection of approx. 13.3 nm^3 s^{-1} (40 mm min^{-1}) was sufficient to raise the venting oxygen

concentration to 90% of its presumed maximum , while for the Venturi-induced convection (Section 7.3.2), the 90% figure was achieved at a convective velocity of 6.7 nm^3 s^{-1} (20 mm min^{-1}). In the field, humidity-induced convective flows of 50–300 mm min^{-1} / culm were found on a cloudless day (temperature 19°C, RH 58%), and were a function of culm size, but, in particular, leaf sheath area (Section 5.3.2.1). The fastest flow rates recorded to date have been 800 mm min^{-1}. These were from 2 m tall robust culms in dry (RH 35%) sunny conditions.

The results in Fig. 8.01 also reveal some of the limitations of diffusion for effecting aeration in *Phragmites*. For example, diffusion *per se* would not support fully the aeration of rhizome and roots in the presence of even the lower of the two soil oxygen sink strengths (curve C at convective flow = 0). This further emphasizes the potential value of convection. Curves C & D also reveal the need for a threshold rate of convection to support fully rhizome aeration when the roots are subjected to moderate or high soil oxygen demand. However, it should be noted that, whereas rhizome oxygen demands *per se* are fully met above these threshold convection rates (approx. 2.5–5 mm min^{-1}, curves C–D), adequate root aeration may still require faster rates than this, while oxygen losses to the rhizosphere will always continue to increase as a function of rhizome oxygen concentration.

8.2.1.2. *Aerated length of rhizome*

A modification of equation 8.03 above gives the length L of aerated rhizome at a convection velocity of U, and the relative importance of diffusion and convection in terms of supportable aerobic rhizome length can be estimated by solving for L for a range of Q, D

& U. The equation is:

$$\exp(-UL/D) + UL/D = 1 + [C_oU^2/(QD)] \qquad (8.04)$$

where D is the effective diffusion coefficient, C_o is the $[O_2]$ at the inflow point L=0, and L is the length of aerated channel (i.e. the oxygen concentration becomes zero at L=L).

The equation also yields the length of rhizome which can be aerated either by diffusion alone, or by convection alone, and these limits are deduced by setting in the first case U=0 and in the second case D=0.

The results, Table 8.01a reveal that setting Q at 10 mg m^{-3} s^{-1} for *Phragmites* that at convective flows $\leq$ 1 mm min^{-1}, the length of rhizome which could be aerated by diffusion alone ($\leq$ 1050 mm) should be much greater than that aerated by convection alone ($\leq$ 450 mm). At 10 mm min^{-1}, diffusion alone would still aerate 1050 mm of rhizome, but by convection alone the aerated length would be 4483 mm. At convective flow rates >10 mm min^{-1} the effects of convection alone, increasingly should outweigh those of diffusion. Examples of the effects on aerated path length that higher rhizome oxygen demands would have are shown in Table 8.01b,c & d.

It should be noted also that a non-throughflow convection is known to occur in rhizomes and roots (Koncalova, Pokorny & Kvet, 1988; Brix, 1988). However, it has been demonstrated that this fails to support root aeration adequately, and that diffusion must account for at least 80% of the oxygen transported (Beckett *et al*, 1988). Also, with the non-throughflow convection functioning at its maximum efficiency, the degree of aeration achieved by diffusion alone is very close to that of diffusion plus the convection (Beckett *et al* 1988).

Table 8.01. Modelling predictions showing the length of rhizome which can be aerated by diffusion and or convection in *throughflow* convection.

Note : pg mm^{-1} s^{-1} = mg m^{-3} s^{-1} = ng cm^{-3} s^{-1}.

(a) The aerobic lengths for Q = 10 pg $mm^{-3}s^{-1}$

U (mm min^{-1})	Length by diffusion alone (mm)	Length by convection alone (mm)	Length by convection and diffusion (mm)
0.1	1050.2	44.8	1065.3
1.0	1050.2	448.3	1223.4
10.0	1050.2	4483.3	4606.3
100.0	1050.2	44833.3	44845.6
1000.0	1050.2	448333.3	448334.6

(b) The aerobic lengths for Q = 50 pg $mm^{-3}s^{-1}$

U (mm min^{-1})	Length by diffusion alone (mm)	Length by convection alone (mm)	Length by convection and diffusion (mm)
0.1	469.7	9.0	472.7
1.0	469.7	89.7	501.5
10.0	469.7	896.7	1019.6
100.0	469.7	8966.7	8979.0
1000.0	469.7	89666.7	89667.9

(c) The aerobic lengths for Q = 100 pg $mm^{-3}s^{-1}$

U (mm min^{-1})	Length by diffusion alone (mm)	Length by convection alone (mm)	Length by convection and diffusion (mm)
0.1	332.1	4.5	333.6
1.0	332.1	44.8	347.7
10.0	332.1	448.3	570.1
100.0	332.1	4483.3	4495.6
1000.0	332.1	44833.3	44834.6

(d) The aerobic lengths for Q = 200 pg $mm^{-3}s^{-1}$

U (mm min^{-1})	Length by diffusion alone (mm)	Length by convection alone (mm)	Length by convection and diffusion (mm)
0.1	234.8	2.2	235.6
1.0	234.8	22.4	242.5
10.0	234.8	224.2	339.4
100.0	234.8	2241.7	2254.0
1000.0	234.8	22416.7	22417.9

8.2.2. *The Modelling of Oxygen Release from Roots*

The rate of oxygen release from roots to sediments can depend upon so many variables that accurate predictions become very difficult. The most obvious of these variables are sediment oxygen diffusivities and demand, numbers, types and lengths of root, the magnitude and distribution of their gas-space provision and respiratory demand, the degree and distribution of root wall oxygen permeability, the numbers and physiological state of the aerial shoots, the porosity and oxygen demand within these shoots and the rhizomes, their lengths and the degree of submergence of the aerial shoots. A number of these variables may vary diurnally, some will certainly vary seasonally. Furthermore, roots are anatomically and physiologically multi-cylindrical, and porosity and respiratory demand vary both axially and radially. Oxygen transport in roots is, however, largely diffusive (Beckett *et al,* 1988), and diffusion is also thought to dominate in the oxygenation of the rhizosphere (Armstrong 1979). Consequently, root and soil aeration in wet soils has been modelled as a multishelled axial and radial diffusion system (Armstrong & Beckett, 1987). Data is input on an axial and cylindrical basis and accounts for variability in root respiratory demand, porosity and root wall permeability on the one hand, and soil oxygen demand and diffusivity on the other. Provided that the oxygen concentration at the root base is properly established, the model will determine among other things, the maximum possible length of aerated root and the amounts of oxygen released to the rhizosphere.

It would seem that because of convective throughflow, the daytime oxygen concentrations at the rhizome-adventitious root junctions in *Phragmites* will be close to atmospheric (for moist air 20.5%). At night (in still air), when rhizome aeration is more dependent

upon diffusion, concentrations will fall as a function of distance from the oxygen entry points on the aerial shoots. In the experiments reported in Chapters 5 & 7, the lowest oxygen concentrations recorded in the gases venting from rhizomes after a night period were approximately 11%. Thus, for a 16 h day it has been assumed that the average oxygen concentration at the rhizome-root junctions will be *c.*17% over the 24 h period.

In *Phragmites* there are also two very different root types (Section 3.3.4): the highly porous adventitious roots ($\epsilon \leq 0.5$), and their attendant laterals (porosities *c.*1.4%). The latter, which are short ($\leq$ 20 mm) and very narrow (radius 0.05 mm), are usually most frequent in the basal regions of the adventitious root where they can occur at frequencies of $\leq$ 120 cm^{-1}. Here, adventitious root porosity is at its highest, and respiratory demand (Appendix III and Yamasaki, 1987) and root wall oxygen permeability (Fig. 4.07 and Brix & Schierup, 1990) are at their lowest. Consequently, effective axial diffusive resistance in this region will be low, and oxygen consumption by the laterals should not markedly lower the oxygen concentrations within the basal lengths of adventitious root. Thus, for the purposes of modelling the aeration of individual laterals, the average oxygen concentration at the lateral-root : adventitious root junction was taken as 17%.

Adventitious and lateral roots were treated independently for modelling purposes: input porosity and respiratory data (Appendix II) were based on information obtained from anatomical and physiological studies of this (Appendix III) and other species (Yamasaki, 1987; Armstrong *et al*, 1990c), soil oxygen diffusivities varied from 0.33 (clay) to 0.84 (sand) x 10^{-5} cm^2 s^{-1} (Currie 1965), soil oxygen demand was varied between 50 and 500 ng cm^{-3} s^{-1}, and it was assumed that this

and root respiration would be independent of oxygen concentration until the point of anoxia; for convenience it had to be assumed also that there would be no significant overlap between the oxidised rhizospheres of adjacent laterals. A temperature of 20°C was assumed for comparison with data from the circulation experiments. At lower temperatures the potential for radial oxygen losses could be greater, for although lower temperatures reduce oxygen diffusivities, this can be more than compensated for by the reduction in plant respiratory demand, and increases in air density and oxygen solubility. However, for shorter roots (<15 cm) predictions (not presented) suggested that oxygen losses might be higher at 20°C than at 10°C, but that where adventitious root lengths exceeded 15 cm oxygen losses would became relatively greater at the lower temperature the longer the root.

The results predict a high potential for soil oxygenation by lateral roots, for although it is revealed that their respiratory demands and low porosities limit the lengths to which they can grow (viz. $\leq$ 20 mm)(Table 8.02), their high surface to volume ratios and their high surface permeability to oxygen makes them very efficient soil oxygenaters. In contrast the adventitious roots themselves have low surface to volume ratios, and towards their bases they become very impermeable to radial oxygen loss (Sections 4.3.1 and 4.3.4). Thus, for a lateral root 16 mm long in a sandy soil (soil demand 50 ng cm^{-3} s^{-1}), the modelling predicted an oxygen release of 0.58 x 10^{-10} g s^{-1}, and a ratio of root oxygen uptake to that released to the soil of 0.15 : 1 (Table 8.02). For an adventitious root 250 mm long, it will be seen that loss to the same soil amounted to 0.087 x 10^{-8} g s^{-1}, and the equivalent ratio of root : soil, of 13 : 1. By extrapolation, oxygen release *per day* would amount to approx. 5 g m^{-2} at a shoot density of 150 and adventitious roots at 10 per shoot. More oxygen would be

Table 8.02

Oxygen consumption by and release to soil from adventitious roots and laterals (g s^{-1})

Predictions based on a soil oxygen demand of 50 ng cm^{-3} s^{-1} and root details as in Appendix II.

Adventitious root length = 25 cm		**Lateral root** length = 1.6 cm	
Inner stele	0.924×10^{-9}	Inner stele	0.84×10^{-12}
Outer stele	0.636×10^{-8}	Outer stele	0.46×10^{-11}
Cortex	0.233×10^{-8}	Cortex	0.198×10^{-11}
Wall layers	0.390×10^{-8}	Wall layers	0.265×10^{-11}
Soil	0.103×10^{-8}	Soil	0.68×10^{-10}
Total	0.145×10^{-7}	Total	0.78×10^{-10}
Ratio Root : Soil	= 13.2 : 1	Ratio Root : Soil	= 0.15 : 1

$$\frac{\text{Oxygen release / lateral root}}{\text{Oxygen release / advent. root}} = \frac{1}{15}$$

Oxygen release from 600 laterals

= 40 x that from 1 adventitious root

released if there were greater numbers of shoots and roots; 20 roots per shoot would not be unusual. A greater oxygen demand in the sediments would also tend to induce extra oxygen release, but this could also lead to the spread of anoxia in the root system and reduce the effective lengths of root available to release oxygen. Other examples of predictions for a range of soil oxygen diffusivities, respiratory demand and root density (expressed as numbers of shoots) are shown in Table 8.03).

Where the water table extends only to the soil surface, the amounts of oxygen likely to diffuse into the sediment from the atmosphere may be estimated from the following equation:

$$C_o = M\ L^2\ /\ (2\ D_e) \qquad (8.05: \text{Currie } 1961),$$

where C_o is the oxygen concentration in air-saturated water (g cm^{-3}), M is the soil oxygen demand (ng cm^{-3} s^{-1}), L the aerated depth (cm), and D_e the *effective* oxygen diffusivity (cm^2 s^{-1}) in the sediment. For soil oxygen demand in the range 50 - 500 ng cm^{-3} s^{-1} and oxygen diffusivities of 0.33 - 0.84 x 10^{-5} cm^2 s^{-1}, predictions of 1.5 - 7.5 g m^{-2} d^{-1} are obtained (Table 8.04).

8.3. FINAL COMMENTS

The experimental results described in Section 4.3.2. demonstrated that a mosaic of oxidised and reduced regions does occur in soils planted with *Phragmites*. It has been shown also, that the potential for sediment oxygenation by *Phragmites*, during the growing season, is considerably enhanced by (a) daytime HI-convective throughflows of gases (Sections 5.3.1.5 & 5.3.1.7), and (b) in any season and day or night, by Venturi-induced convections if there is a wind (Section 7.3.2). Such convections should also enable the rhizomes to extend

Table 8.03. Potential for oxygen release into *Phragmites* beds based on mathematical modelling, assuming 600 laterals/root (shoot nos. are per m^2)

A.
Low porosity sands: oxygen diffusivity 0.4 x D_o

Soil O_2 demand (ng cm^{-3} s^{-1})	Predicted O_2 release (g m^{-2} d^{-1}) 100 shoots 10 roots/shoot	100 shoots 20 rts/shoot	200 shoots 20 rts/shoot
50	4.9	9.9	19.7
100	5.4	10.9	21.7
200	6.0	12.1	24.1
500	7.0	14.1	28.1
1000	8.0	15.9	31.8
1500	8.6	17.1	34.2

B.
High-porosity clay: oxygen diffusivity 0.156 x D_o

Soil O_2 demand (ng cm^{-3} s^{-1})	Predicted O_2 release (g m^{-2} d^{-1}) 100 shoots 10 roots/shoot	100 shoots 20 rts/shoot	200 shoots 20 rts/shoot
50	3.4	6.8	13.6
100	3.8	7.7	15.4
200	4.4	8.7	17.4
500	5.2	10.3	20.7
1000	5.9	11.9	23.7
1500	6.5	12.9	25.9

C.
Low-porosity clay: oxygen diffusivity 0.025 x D_o

Soil O_2 demand (ng cm^{-3} s^{-1})	Predicted O_2 release (g m^{-2} d^{-1}) 100 shoots 10 roots/shoot	200 shoots 10 rts/shoot	200 shoots 20rts/shoot
50	1.5	3.0	6.0
100	1.8	3.6	7.1
200	2.2	4.3	8.7
500	2.8	5.6	11.2
1000	3.4	6.8	13.6
1500	3.8	7.6	15.1

Table 8.04. Predicted oxygenation of beds by diffusion across the soil-atmosphere interface. Assumes that water table is at or below the soil surface.

Soil O_2 demand ($ng\ cm^{-3}\ s^{-1}$)	Predicted O_2 entry into bed ($g\ m^{-2}\ d^{-1}$) low porosity sand	high porosity clay	low porosity clay
50	2.4	1.5	0.6
100	3.4	2.1	0.8
200	4.8	3.0	1.2
500	7.5	4.7	1.9
1000	10.7	6.6	2.7
1500	13.1	8.2	3.3

Table 8.05. Potential for oxygen release into *Phragmites* beds based on measurements of oxygen *release to streaming oxygen free water.*

Soil O_2 demand ($ng\ cm^{-3}\ s^{-1}$)	Predicted O_2 release ($g\ m^{-2}\ d^{-1}$) 100 shoots 10 roots/shoot	100 shoots 20 rts/shoot	200 shoots 20 rts/shoot
≥ 500	3.3-8.0	6.6-16.0	13.2-32.0

deeper into the sediments than would be possible if plant aeration was dependent only upon diffusion. Because of convection, the total amount of oxygen which passes into the rhizome system in a 24-hour period must at times be very considerable indeed. A flow of 0.2 kg O_2 m^{-2} d^{-1} is probably not unusual, and at times much higher flows than this were recorded. However, it is certain that much of this oxygen must be vented back to the atmosphere and perhaps only 1/10 or less may find its way into the rhizosphere.

The mathematical modelling and the oxygen-free water streaming experiments provide a basis for predicting the potential for oxygen release in the field. It should be emphasised that the predictions of between 5 and 12 g m^{-2} d^{-1} are based on what is probably a conservative estimate of the number of roots in the beds (10 adventitious roots *per* shoot). Double this number is not uncommon in solution culture, and thus it is not beyond the bounds of possibility that oxygen release could approach 20 g m^{-2} d^{-1} (see also Chapter 9). However, it is much more difficult to predict whether such amounts will be sufficient to effect the requirements of NH_4^+ to NO_3^- conversion in effluents; it must very much depend upon competing oxygen demands generated directly or indirectly by other microorganism activities.

Although the potential for oxygen release from roots is some function of oxygen demand in the sediment, it is important to appreciate that any increase in oxygen demand might be offset by a reduction in the surface area of root from which oxygen can be released. This arises because the respiratory demand of the roots themselves and that of the sediment are in competition for that transported into the root system. If soil oxygen demand increases, the tendency will be for more oxygen to be released from the basal regions of adventitious roots via the lateral roots, and the apical regions of

both the adventitious and lateral roots may then be starved of oxygen. It could even lead to some root death.

Finally, although it is obvious that during the growing season, living *Phragmites* roots can locally raise the redox state of a soil considerably, the extent to which this occurs in winter must depend upon the survival of the roots and the degree to which they remain permeable to radial oxygen release. In winter, it is likely that root oxygen efflux is somewhat lower, but while humidity-induced convection may be only slight because of shoot senescence, convection may still reach significant proportions because of Venturi-effects across broken culms. More research is needed to investigate the winter condition which must have an important bearing on overall reed-bed performances.

Attempts to quantify the oxygen release in the field are based, therefore, on extrapolations from:

(i) ***direct measurement*** of oxygen release from single rhizome-attached adventitious roots plus laterals to streaming oxygen-free water, and

(ii) ***mathematical modelling*** based on known properties of *Phragmites* roots and waterlogged sediments.

It is encouraging that both methods have yielded similar values and the results are detailed in Tables 8.03 & 8.05. To summarise, it may be concluded that oxygen release by *Phragmites* in the field could range from <2 to >30 g m^{-2} d^{-1}, but that values of between 5 and 12 g m^{-2} d^{-1}, probably represent a conservative average for the growing season. Interestingly, the results reveal that high porosity substrates such as sands and gravels which help maintain suitable effluent flows should also optimize the oxygen flux from the roots. Also appended is a third table of predictions concerning oxygen diffusion from the soil surface where again the significance of high porosity sediments is

evident.

The laboratory and field experiments have revealed that, in the growing season, because of a *humidity-induced* convective gas-flow through the plant, oxygen levels in the *Phragmites* underground rhizome system can be close to atmospheric during the day: nearly double the night-time values in still air. For these reasons, the average daily oxygen concentration in the rhizomes was modelled as 17%. However, the existence of a Venturi-induced convection should ensure that in summer, winter, day and night, in the field there is likely to be some convective flow through *Phragmites* rhizomes, and that the use of a rhizome oxygen concentration of 17% could underestimate the potential for oxygen release. The laboratory experiments have shown that oxygen release from roots can be more than doubled by convections through the rhizome, and that quite slow rates of convection can be sufficient to produce almost maximal oxygen release.

Further studies are needed to measure the extent of rhizosphere oxidation in the reed beds, to clarify the potential for oxygen release in winter, and to quantify the Venturi-effects.

SUMMARY

Mathematical models have been used to estimate (a) the relative importance of convection and diffusion in aerating the rhizomes of *Phragmites*, (b) the extent to which root and soil oxygen demand might modify the aeration in the rhizome, and the role that convection might play in satisfying these demands, (c) the relative importance of adventitious roots and laterals as sources of oxygen release to the sediments, (d) the amounts of oxygen which might be released into the soil as a function of soil oxygen diffusivity, soil oxygen demand and root and shoot density.

The results support the experimental findings in showing that relatively small rates of convection can have a considerable influence on rhizome aeration. flow rates of as little as 6.7 $nm^3\ s^{-1}$ were shown to be sufficient to raise oxygen concentrations to 90% of atmospheric in a 500 mm long rhizome supporting the additional respiratory demand of ten 250 mm adventitious roots and attendant laterals. Further oxygen demand introduced by programming for high rates of soil oxygen demand (500 $ng\ cm^{-3}\ s^{-1}$) was similarly satisfied by a convection rate of *ca.* 2.3 $nm^3\ s^{-1}$ (60 $mm\ min^{-1}$ velocity), a figure well within the rates of convection found in the field.

It was shown that the oxygen release from the lateral roots *in toto* is likely to exceed greatly that released by the adventitious roots; the ratio of root oxygen demand to oxygen release by lateral roots was found to be 0.15 : 1 compared with 13 : 1 for adventitious roots.

Finally it was predicted that the release of oxygen from *Phragmites* could amount to a figure in excess of 30 $g\ m^{-2}\ d^{-1}$ in low porosity sands (high oxygen diffusivity) with high oxygen demand, and high shoot and root numbers.

CHAPTER 9

FINAL COMMENTS

Since the main topics of the thesis are discussed within the chapters themselves, the purpose of this section is to summarise the main conclusions, and to relate them to recently published papers on *Phragmites* aeration, and to the plant's role in waste-water treatment.

The general conclusions to be drawn from the project are:

1. *Phragmites* has a particularly well-developed internal gas-space system with unusually porous root-rhizome junctions.
2. *Phragmites* roots, especially the numerous laterals release oxygen to the soil, markedly raising the redox potential of the rhizosphere.
3. Convective gas-flows are a feature of *Phragmites* aeration : atmospheric oxygen is convected quickly (compared to diffusion) through the underground rhizomes by Venturi- and/or Humidity-induced convections.
4. For efficient convection there must be adequate venting via dead culms.
5. Many tall, dead, persistent culms will ensure effective Venturi convection in the wind, and gusting at higher wind speeds could be more effective than continuous wind at lower velocities.
6. The rate of HIC is proportional to leaf sheath area, hence, the highest rates of flow can be expected with many tall living robust culms ; the Nuclepore membrane work revealed that pores within the Knudsen regime are not necessary to effect this type of flow.
7. Convection probably increases the depth to which *Phragmites* rhizomes can penetrate.

8. Comparatively slow rates of convection result in large increases in root oxygen efflux, compared to values for diffusion alone.
9. Conservative values for oxygen release from roots to soil, based on laboratory measurements of ROL and modelling data range from 5 to 12 g m^{-2} d^{-1}, but could be greater than 30 g m^{-2} d^{-1}, or less, depending upon root numbers and their physiological state, and soil oxygen demand and diffusivities.
10. Points 4-6 suggest that ROL will not reach a maximum until a reed bed has been established for a number of years, and that cutting of reeds should be avoided.
11. When planting reed beds from rhizome cuttings they should not be completely submerged, and it would seem to be desirable for a dead culm to form part of the cutting to aid ventilation. It should be noted that Brändle (1985) found that the rhizomes and roots of *Phragmites* had no exceptional capacity for withstanding prolonged anoxia.

Since this project was started several papers have been published in relation to the aeration of *Phragmites*. Weisner (1988) showed that, whereas the concentration of oxygen in the basal stems of *Phragmites* and the mean shoot length above water decreased in deeper water, the oxygen concentration in the basal stems was correlated to shoot length above water at a given water depth. He suggests that oxygen, transported from shoots to the below ground parts, is restricted by (a) small shoot length above water and (b) long distance for oxygen transport. Also, the concentration of oxygen in basal stems was always lower at sheltered rather than exposed sites. These findings accord with the present study which shows that humidity-induced convection is related to leaf sheath area and culm height; also, that greater rates of HIC, and especially Venturi-induced convection,

would give rise to better rhizome aeration at exposed sites.

Brix (1990) calculated that 35% of the total gaseous oxygen flux into a reed bed during winter was through the dead culms, the remainder being by diffusion through the surface of the bed. He also concluded that the majority of the oxygen entering through the culms was used up in the respiratory activities of the plant itself and that very little oxygen escaped into the rhizosphere. However, his experimental techniques prevented any Venturi-convections, and it is likely that his data very much underestimated the oxygen flux both into the rhizomes and the rhizosphere.

Yamasaki (1987) has also stressed the importance of dead culms in the aeration of *Phragmites*. He concluded that most of the oxygen flux for the roots was derived from standing dead shoots. However, it has been shown here that living shoots can also be very important for aerating the underground organs by HIC, and that dead culms are essential for venting in HIC and can themselves aerate the rhizomes and roots by Venturi-induced convection. Geller *et al* (1990) also realised the importance of dead culms and conclude that, "the harvesting of reeds is senseless and destructive as far as wastewater treatment plants are concerned". Ashworth (1991), found that with more sunlight, lower relative humidity and with exposure to wind, sewage treatment by *Phragmites* beds was more efficient, all these being features which can increase convective flows (Chapters 5, 6 & 7) and hence rhizome, root and rhizosphere aeration.

The same pattern of root radial oxygen loss reported here (Chapter 4), has also been shown for *Phragmites* by Conlin and Crowder (1989) using indicator dyes. They detected a lowering of pH in the oxidised rhizosphere and the deposition of an Fe^{3+} oxide plaque.

Recently, Hofmann,(1990), working on bacteria in the rhizosphere, has found that 16 species of nitrifying bacteria increased in the rooting zone of *Phragmites*, compared to the soil of an unplanted bed, *e.g. Nitrosomonas* increased by 17x, while *Nitrobacter* increased by 1.7x. Furthermore, the numbers of denitrifiers increased by 8.2x. Hofmann has also shown that dense bacterial clouds occur especially around the fine laterals and the young parts of adventitious roots, and he deduces that such roots are the most important oxygen sources for the rhizosphere. These latter findings are in accordance with the pattern of root oxygen efflux described in Chapter 4. Hofmann also concludes that the oxygen transport from root to rhizosphere seems to be about 4.5 g m^{-2} d^{-1}, as well as the 4 g m^{-2} d^{-1} estimated by Brix (1990) to be entering the bed directly from the atmosphere. He points to the importance of oxygen leaking from the roots in establishing a nitrifying bacterial population, but one must bear in mind that other root exudates may also be of significance (It is interesting that Hofmann also found that planted beds were more efficient in removing heterotrophic and enterotrophic bacteria from sewage sludge than unplanted control beds.)

At the moment opinions still vary concerning the oxygenating capacity of *Phragmites* roots in waste-water treatment beds. However there are some recent publications which report increases in redox values in the rooting zone, and estimations of quantities of oxygen supplied to the bed by the roots which agree with those presented in this thesis. Hofmann (1990) found redox potentials of +95 to +170 mV in the rooting zone of sludge de-watering beds compared to -60 to +60 in the unplanted control. Geller *et al* (1990) also found redox values of +100 mV near *Phragmites* root tips compared to -300 mV elsewhere in the waterlogged soil. In Chapter 4 redox values close to the roots were

up to 800 mV higher than elsewhere, but it should be noted that in this case the soil had not been amended with sewage or by the addition of any organic matter, and its reducing capacity would consequently have been lower than in the examples quoted above. Gray *et al*, (1990), have produced encouraging results in treating agricultural waste waters with horizontal-flow beds. In a healthy bed, which was functioning efficiently, they estimated that the *Phragmites* roots transmitted 24.2 g O_2 g m^{-2} d^{-1} to the soil; Reed *et al*, (1990), have similarly estimated 20 g O_2 g m^{-2} d^{-1}, while in this study (Chapter 8), *c.* 5 - 12 g O_2 g m^{-2} d^{-1} has been suggested as a conservative estimate, but the modelling data suggested that amounts up to 35 g O_2 g m^{-2} d^{-1} or more might be realised under good conditions of growth and weather conditions. All these values are within the range originally predicted by Kickuth: 5 - 50 g O_2 g m^{-2} d^{-1}. The much lower figures of 65-129 mg m^{-2} h^{-1} suggested recently by Gries *et al* (1990) are probably explained in terms of the experimental design of their solution sulture system which imposed a relatively weak oxygen demand (sink activity), did not allow convective gas-flow in the plant, and was such that oxygen released by one part of the root system could have been re-absorbed and consumed by more remote parts.

There still appears to be uncertainty about how much oxygen is required to meet the demands of the purification processes in a reed bed, or how much of the oxygen entering a reed bed is available for the purification processes themselves. It may be that a greater input of oxygen than formerly supposed is actually required in macrophyte-based schemes, partly because the plants themselves die and decay and contribute to the mass of degradable substances. At a recent conference on waste water treatment by constructed wetlands, (Cooper

& Findlater, 1990), there appeared to be increasing support for "vertical-flow beds", which tend to be better aerated by causing a greater intake of air into the bed, compared to the conventional "horizontal-flow" systems. It may be that a combination of vertical- and horizontal-flow beds are to be recommended in order to ensure adequate oxygenation of the bed, (Gray *et al* 1990); this could be especially relevant in the UK during the winter, when there is very little HIC and the roots may be less permeable to ROL. The direct supply of atmospheric oxygen into a bed can also be improved by adopting intermittent flow techniques. Bahlo and Wach (1990), found good results from a vertical and intermittent filtration system in sandy reed beds.

BIBLIOGRAPHY

ARBER, A. (1920). *Water Plants.* Cambridge University Press.

ARIKADO, H. & ADUCHI, Y. (1955). Anatomical and ecological responses of barley and some forage crops to the flooding treatment. *Bulletin of the Faculty of Agriculture, Mie Univer*sity, Japan. 11, 1-29.

ARIKADO, H. (1959). Supplementary studies on the development of the ventilating system in various plants growing on lowland and on upland. *Bulletin of the Faculty of Agriculture, Mie University, Japan.* 20, 1-24.

ARMSTRONG, J. & ARMSTRONG, W. (1987-88). *Rhizosphere oxygenation by Phragmites australis.* Contract reports 6 & 7 - Water Research Centre, Stevenage, U.K.

ARMSTRONG, J. & ARMSTRONG, W. (1988). *Phragmites australis*: a preliminary study of soil-oxidising sites and internal gas transport pathways. *New Phytologist* 108, 373-382.

ARMSTRONG, J. & ARMSTRONG, W. (1990a). Light enhanced convective throughflow increases oxygenation in rhizomes and rhizosphere of *Phragmites australis* (Cav.) Trin. ex Steud. *New Phytologist* 114, 121-128.

ARMSTRONG, J. & ARMSTRONG, W. (1990b). Pathways and mechanisms of oxygen transport in *Phragmites australis.* In: *The Use of Constructed Wetlands in Water Pollution Control.* (Ed. by P.F. Cooper and B.C. Findlater). Pergamon, Oxford, pp. 529-533.

ARMSTRONG, J. & ARMSTRONG, W. (1991). A convective throughflow of gases in *Phragmites australis. Aquatic Botany* 39, 75-88.

ARMSTRONG, J., ARMSTRONG, W. & BECKETT, P.M. (1988). *Phragmites australis:* a critical appraisal of the ventilatingpressure concept and an analysis of resistance to pressurised gas-flow and gaseous diffusion in horizontal rhizomes. *New Phytologist* 110, 383-389.

ARMSTRONG, J., ARMSTRONG, W. AND BECKETT, P.M. (1992). *Phragmites australis:* venturi- and humidity-induced convections enhance rhizome aeration and rhizosphere oxidation. *New Phytologist* (in press).

ARMSTRONG, W. (1964). Oxygen diffusion from the roots of some British bog plants. *Nature 204,* 801-802.

ARMSTRONG, W. (1967). Oxidising activity of roots in waterlogged soils. *Physiologia Plantarum* 20, 920-926.

ARMSTRONG, W. (1970). Rhizosphere oxidation in rice and other species. A mathematical model based on the oxygen flux component. *Physiologia Plantarum* 23, 623-630.

ARMSTRONG, W. (1971). Radial oxygen losses from intact rice roots as affected by distance from the apex, respiration and waterlogging. *Physiologia Plantarum* 25, 192-197.

ARMSTRONG, W. (1979). Aeration in higher plants. In: *Advances in Botanical Research, vol. 7* (Ed. by H.W. Woolhouse), pp. 226-332. Academic Press, London.

ARMSTRONG, W., ARMSTRONG, J. & BECKETT, P.M. (1990a). Measurement and modelling of oxygen release from roots of *Phragmites australis.* In: *The Use of Constructed Wetlands in Water Pollution Control,* (Ed. by P.F. Cooper & B.C. Findlater). Pergamon Press, 41-52.

ARMSTRONG, W., ARMSTRONG, J., BECKETT, P.M. & JUSTIN, S.H.F.W. (1990b). Convective gas-flows in wetland plant aeration. In: *Plant Life under Oxygen Stress* (*Ed.* by Jackson M.B. Davies, D.D. & Lambers, H.), SPB Academic Publishing bv, The Hague, The Netherlands. pp. 283-302.

ARMSTRONG, W. & BECKETT, P.M. (1987). Internal aeration and the development of stelar anoxia in submerged roots: a multishelled mathematical model combining axial diffusion of oxygen in the cortex with radial oxygen losses to the stele, the wall layers and the rhizosphere. *New Phytologist* 105, 221-245.

ARMSTRONG, W., BECKETT, P.M. JUSTIN, S.H.F.W. & LYTHE, S. (1990c). Modelling, and other aspects of root aeration by diffusion. In: *Plant Life under Oxygen Stress* (*Ed.* by Jackson M.B. Davies, D.D. & Lambers, H.), SPB Academic Publishing bv, The Hague, The Netherlands. pp. 267-282.

ARMSTRONG, W. & BOATMAN, D.J. (1967). Some field observations relating the growth of bog-plants to conditions of soil aeration. *Journal of Ecology* 55, 101-110.

ARMSTRONG, W. & WRIGHT.E. J. (1975). Radial oxygen loss from roots : The theoretical basis for the manipulation of flux data obtained by the cylindrical platinum electrode technique. *Physiologia Plantarum* 35, 21-26.

ASHWORTH, R. F. (1991). *The factors determining nitrogen removal from sewage using a gravel bed hydroponic treatment system.* Ph.D. Thesis (CNAA), Portsmouth Polytechnic, Civil Engineering Dept.

ATHIE, D. & CERRI, C.C. (Eds)(1987). The use of macrophytes in water pollution control: *Water Science and Technology*, vol. 19, No. 10, 73 pages (Review Journals, Pergamon Journals Ltd., Oxford).

BAHLO, K.E. & WACH, F.G. (1990). Purification of domestic sewage with and without faeces, by vertical intermittent filtration in reed and rush beds. In: *The Use of Constructed Wetlands in Water Pollution Control,* (Ed. by P.F. Cooper & B.C. Findlater). Pergamon Press, 215-221.

BARTLETT, R.J. (1961). Iron oxidation proximate to plant roots. *Soil Science* 92, 372-379.

BARTON, D.R.M. & OLLIS, W.D. (1979). *Comprehensive Organic Chemistry,* vol. 4, pp. 1105-1106. Pergamon Press, Oxford.

BECKETT, P.M., ARMSTRONG, W., JUSTIN, S.H.F.W. & ARMSTRONG, J. (1988). On the relative importance of convectlve and diffusive gas flows in plant aeration. *New Phytologist* 110, 463-468.

BOON, A.G. (1985). Report of a visit by members and staff of wRC to Germany (GFR) to investigate the root-zone method for treatment of waste-waters. Water Research Centre, UK. Report 376-S/1.

BRÄNDLE, R. (1985). Kohlehydratgehalte und Vitalität isolierter Rhizom von *Phragmites australis, Schoenoplectus lacustris, und Typha latifolia* nach mehrwöchigem O_2-Mangelstress. *Flora* 177, 317-321.

BRIX, H. (1987). Treatment of wastewater in the rhizosphere of wetland plants: The root-zone method. *Water Science & Technology* 19, 107-118.

BRIX, H. (1988). Light dependent variation in the composition of the internal atmosphere of *Phragmites austratis* (Cav.) Trin. ex. Steud. *Aquatic Botany* 30, 319-329.

BRIX, H. (1989). Gas-exchange through dead culms of reed *Phragmites australis* (Cav.) Trin. ex. Steudel. *Aquatic Botany* 35, 81-98.

BRIX, H. (1990). Gas-exchange through the soil atmosphere interface and through dead culms of *Phragmites australis* in a constructed reed bed receiving domestic sewage. *Water Research* 24, 259-266.

BRIX, H. & SCHIERUP, H-H. (1990). Soil oxygenation in constructed reed beds : the role of macrophyte and soi-atmosphere interface oxygen transport. In: *The Use of Constructed Wetlands in Water Pollution Control.* (Ed. by P.F. Cooper & B.C. Findlater), pp. 53-66. Pergamon Press.

BUCKSTEEG, K. (1990) Treatment of domestic sewage in emergent helophyte beds - German experiences and ATV-Guidlines H262. In: *The Use of Constructed Wetlands in Water Pollution Control.* (Ed. by P.F. Cooper & B.C. Findlater), pp. 505-516. Pergamon Press.

CHEN, C.C., DIXON, J.B. & TURNER, F.T. (1980). Iron coatings on rice roots: minerology and quantity influencing factors. *Soil Science Society of America Proceedings* 44, 635-639.

CONLIN, T.S.S. & CROWDER, A.A. (1989). Location of radial oxygen loss and zones of potential iron uptake in a grass and two non-grass emergent species. *Canadian Journal of Botany* 67, 717-722.

CONWAY, V. (1937). Studies in the autecology of *Cladium mariscus:* the aeration of the underground parts. *New Phytologist* 36, 64-96.

COOPER, P.F. & FINDLATER, B.C. (1990)(Eds). *The Use of Constructed Wetlands in Water Pollution Control.* 605 pages. Pergamon Press.

CURRIE, J.A. (1961). The importance of aeration in providing the right conditions for plant growth. *Journal of the Science of Food & Agriculture* 13, 380-385.

CURRIE, J.A. (1965). Diffusion within soil microstructure : a structural parameter for soils. *Journal of Soil Science* 16, 279-289.

DACEY, J.W.H. (1979). *Gas circulation through the yellow water lily.* Dissertation. Michegan State University, East Lansing, Michegan, USA.

DACEY, J.W.A. (1980). Internal winds in water lilies: an adaptation for life in anaerobic sediments. *Science* 210, 1017-1019.

DACEY, J.W.H. (1981). Pressurised ventilation in the yellow water-lily. Ecology 62, 1137-1147.

DACEY, J.W.H. (1981). How aquatic plants ventilate. *Oceanus* 24, 43-51.

DACEY, J.W.A. (1987). Knudsen-transitional flow and gas pressurisation in leaves of *Nelumbo. Plant Physiology* 85, 199-203.

DACEY, J.W.A. & KLUG, M.J. (1979). Methane efflux from lake sediments through water lilies. *Science* 203, 1253-1255.

DACEY, J.W.H. & KLUG, M.J. (1982a). Tracer transport in *Nuphar*: $^{18}O_2$ and $^{14}CO_2$ transport. *Physiologia Plantarum* 56, 361-366.

DACEY, J.W.H. AND KLUG, M.J. (1982b). Ventilation by floating leaves in *Nuphar. American Journal of Botany* 69, 999-1003.

DeLAUNE, R. D., SMITH, C. J. & PATRICK, W. H. Jr. (1983). Relationship of marsh elevation, redox potentials, and sulphide to *Spartina alterniflora* productivity. *Soil Science Society of America Proceedings* 47, 930-935.

DENBEIGH, K.G. & RAUMANN, G. (1951). The thermo-osmosis of gases through a membrane. I. Theoretical. *Proceedings of the Royal Society* 210A, 377-387.

DUFOUR, L. (1874). Sur la diffusion hygrometrique. *Bull. Nat. Sci. Soc. Vaudoise XIII*, 74, 608-641.

DUNBABIN, J.S., POKORNY, J. & BOWMER, K.H., 1988. Rhizosphere oxygenation by *Typha domingensis* Pers., in miniature artificial wetland filters used for metal removal from wastewaters. *Aquatic Botany* 29, 303-317.

ENGLER, R.M. & PATRICK JR., W.H. (1975). Stability of sulphides, manganese, iron, zinc, copper and mercury in flooded soil. *Soil Science* 119, 217-221.

ETHERINGTON, J.R. (1982). *Environment and Plant Ecology.* John Wiley, Chichester.

FETTER, C.W., SLOEY, W.E. & SPANGLER, F.L. (1978). Use of a natural marsh for waste-water polishing. *Journal of the Water Pollution Control* Federation 50, 290-307.

FINLAYSON, C.M. & CHICK, A.J. (1983). Testing the potential of aquatic plants to treat abattoir effluent. *Water Research* 17, 415-422.

GAMBRELL, R.P., KHALID, R.A., VERLOO, M.G. & PATRICK Jr., W.H. (1977). *Transformations of heavy metals and plant nutrients in dredged sediments as affected by oxidation-reduction potentials and pH.* Contract report D-77-4. U.S. Army Engineer Waterways Experimental Station, Vicksburg M.I., NTIS ADA-041468.

GAMBRELL, R.P. & PATRICK Jr., W.H. (1978). Chemical and microbiological properties of anaerobic soils and sediments. In: *Plant Life in Anaerobic Enuironments* (Ed. by D.D. Hook & R.M.M. Crawford), pp. 375-424. *Ann Arbor Science Inc., Ann Arbor.*

GAYNARD, T.J. & ARMSTRONG, W. (1987). Some aspects of internal plant aeration in amphibious habitats. In: *Plant life in Aquatic and Amphibious habitats* (Ed. by R.M.M. Crawford), British Ecological Society Special Symposium 5, pp. 303-320. Blackwell, Oxford.

GELLER, G., KLEYN, K. & LENZ, A. (1990). Planted soil filters for wastewater treatment : the complex system "planted soil filter", its components and their development. In: *The Use of Constructed Wetlands in Water Pollution Control.* (Ed. by P.F. Cooper & B.C. Findlater), pp. 161-170. Pergamon Press.

GERSBERG, R.M., ELKINS, B.V., LYON, S.R. & GOLDMAN, C.R.G. (1986). Role of aquatic plants in wastewater treatment by artificial wetlands. *Water Research* 20, 363-368.

GERSBERG, R.M., LYON, S.R., ELKINS, B.V. & GOLDMAN, C.R. (1985). The removal of heavy metals by artificial wetlands. *Proceedings of the Water Reuse Symposium, San Diego, California. Aug. 26-31, 1984.*

GOEBEL, K. (1905). *Organography of Plants.* Clarendon Press, Oxford.

GRAY, K.R., BIDDLESTONE, A.J., JOB, G. & GALANOS, E. (1990). The use of reed beds for the treatment of agricultural effluents. In: *The Use of Constructed Wetlands in Water Pollution Control.* (Ed. by P.F. Cooper & B.C. Findlater), pp. 333-346. Pergamon Press.

GREEN, M.S. & ETHERINGTON, J.R. (1977). Oxidation of ferrous iron by rice (*Oryza sativa* L.): a mechanism for waterlogging tolerance ? *Journal of Experimental Botany* 28, 678-690.

GRIES, C., KAPPEN, L. & lOSCH, R. (1990). Mechanism of flood tolerance in reed, *Phragmites australis* (Cav.) Trin. ex Steudel. *New Phytologist* 114, 589-593.

GROSSE, W. & MEVI-SCHUTZ, J. (1987). A beneficial gas-transport systern in *Nymphoides peltata. American Journal of Botany* 74, 947-952.

GROSSE, W. & SCHRODER, P. (1984). Oxygen supply of roots by gas transport in alder trees. *Zeitschrift für Naturforschung* 39C, 1186-1188.

GROSSE, W. & SCHRODER, P. (1985). Aeration of the roots and chloroplast-free tissues of trees. *Berichte der Deutschen Botanische Gesellschaft* 98, 311-318.

GROSSE, W., BUCHEL, B.H. & TIEBEL, H. (1991). Pressurized ventilation in wetlnd plants. *Aquatic Botany* 39, 89-98.

HANSEN, J.I. & ANDERSEN, F.O. (1981). Effects of *Phragmites australis* roots on redox potentials, nitrification and bacterial numbers in the sediment. In: *9th Nordic Symposium on Sediments* (Ed. by A. Broberg & *T.* Tiren), pp. 72-88.

HASLAM, S.M. (1969). The development and emergence of buds in *Phragmites communis* Trin. *Annals of Botany* 33, 289-301.

HOFMANN, K. (1990). Use of *Phragmites* in sewage sludge treatment. In: *The Use of Constructed Wetlands in Water Pollution Control.* (Ed. by P.F. Cooper & B.C. Findlater), pp. 269-278. Pergamon Press.

JONES, H.E. & ETHERINGTON, J.R. (1970). Comparative studies of plant growth and distribution in relation to waterlogging. I. The survival of *Erica cinerea,* L., and *E.tetralix* L., and its apparent relationship to iron and manganese uptake in waterlogged soil. *Journal of Ecology* 58, 487-96.

JONES, R. (1972). Comparative studies of plant growth and distribution in relation to waterlogging. VI. The effect of manganese on the growth of dune and dune slack plants . *Journal of Ecology* 60, 141-146.

JONG, J. De. (1976). The purification of wastewater with the aid of rush or reed ponds. In: *Biological Control of Water Pollution,* (Ed. by J. Tourbier & R. Pierson), pp. 123-132. Pennsylvania University Press, Philadelphia.

JONG, J. De, KOK, T. & KORIDON, A.H. (1977). The purification of sewage with the aid of ponds containing bulrushes or reeds in the Netherlands. *Rapport 1977-7. Bow. Leylstad, Netherlands. Rijksdienst voor de l'Jsselmeerpolders.*

JUSTIN, S.H.F.W. & ARMSTRONG, W. (1983). Oxygen transport in the salt marsh genus *Puccinellia* with particular reference to the diffusive resistance of the root-shoot junction and the use of paraffin oil as a diffusive barrier in plant studies. *Journal of Experimental Botany* 34, 980-986.

JUSTIN, S.H.F.W. & ARMSTRONG, W. (1987). The anatomical characteristics of roots and plant response to soil flooding. *New Phytologist* 106, 465-495.

KICKUTH, R. (1981). Abwasserreinigung in mosaikmatrizen aus aerober und anaerober teilbezirken. In: *Grundlagen der Abwassereinigung, Scriftenreihe Wasser, (*Ed. by F. Moser). - *Abwasser* 19, 639-665.

KICKUTH, R. (1984). Das Wurzelraumverfahren in der Praxis. *Landschrift Stadt.* 16, 145-153.

KONCALOVA, H., POKORNY, J. & KVET, J. (1988). Root ventilation in *Carex gracilis* Curt.: diffusion or mass flow? *Aquatic Botany* 30, 149-155.

KRASOVSKII, L.I. & CHASHCHUKHIN, V.A. (1974). Oxygen regime of the rootstocks of the common reed. *Soviet Plant Physiology* 21, 255-259.

LAAN, P., SMOLDERS, A., BLOM, C. W. P. M. & ARMSTRONG, W. (1989). The relative roles of internal aeration, radial oxygen losses, iron exclusion and nutrient balances in flood tolerance of *Rumex* species. *Acta Botanica Neerlandica* 38, 131-145.

LAING, H.E. (1940). The composition of the internal atmosphere of *Nuphar advenum* and other water plants. *American Journal of Botany* 27, 861-898.

LAWSON, G.J. (1985). *Cultivating reeds (Phragmites australis) for root zone treatment of sewage.* Contract report to Water Research Centre, UK, ITE (UK) project 965, pp. 1-64.

LEUNING, R. (1983). Transport of gases into leaves. *Plant, Cell and Environment* 6, 181-194.

MADSEN, T.V. (1984). Resistance to carbon dioxide fixation in the submerged aquatic macrophyte *Callitriche stagnalis*. *Journal of Experimental Botany* 35, 338-347.

MASON, E.A. and EVANS, R.B. (1969). Graham's laws: simple demonstrations of gases in motion. *Journal of Chemical Education* 46, 358-364.

MAY, E., BUTLER, J.E., FORD, M.G., ASHWORTH, R., WILLIAMS J. & BAGHAT, M.M.M. (1990). Chemical and microbiological processes in gravel-bed hydroponic (GBH) systems for sewage treatment. In: *The Use of Constructed Wetlands in Water Pollution Control.* (Ed. by P.F. Cooper & B.C. Findlater), pp. 33-40. Pergamon Press.

MEVI-SCHUTZ, J. & GROSSE, W. (1988a). A two-way gas transport system in *Nelumbo nucifera*. *Plant, Cell and Environment* 11, 27-34.

MEVI-SCHUTZ, J. & GROSSE, W. (1988b). The importance of water vapour for the circulating air-flow through *Nelumbo nucifera*. *Journal of Experimental Botany* 39, 1231-1236.

MILNE-THOMSON, L. M. (1960). *Theoretical Hydronamics.* Macmillan, London.

MOLISCH, H. (1888). Uber Wurzelausschiedungen und deren Einwerkung auf organische Substanzen. *Sitzungsber. Akad. Wiss. Wein. Math. Nat. Kl.* 96, 84.

NOBEL, P. S. (1974). *Biophysical Plant Physiology.* Freeman, San Fransisco.

PATRICK Jr., W.H. & GAMBRELL, R.P. (1976). The effect of pH and redox potential on heavy metal chemistry in sediment water systems affecting toxic metal bioavailability. In: *Dredging: Environmental Effects and Technology.* Proceedings of WODCON VII, San Francisco, July 10-12, 1976. The Conference, San Pedro, California, pp. 579-604.

PEZESHKI, S. R., PAN, S. Z., DeLAUNE, R. D. & PATRICK, W. H. Jr. (1988). Sulphide-induced toxicity: Inhibition of carbon assimilation in *Spartina alterniflora*. *Photosynthetica* 22, 437-442.

PONNAMPERUMA, F.N. (1984). Effects of flooding on soils. In: *Flooding and Plant Growth* (Ed. by T. T. Kozlowski), pp. 10-46. Academic Press, London.

PRESENT, R.D. (1958). *Kinetic Theory of Gases.* McGraw-Hill Book Company Inc., New York.

RACIBORSKI, M.M. (1905). Utleniajace: redukajace wlasnosei kómorki zywej. I, II, III. *Bull. Int. de L'Acad. Sciences (Cracovie)* 338-349, 668-693, 693-707.

RASKIN, I. & KENDE, H. (1983). How does deep-water rice solve its aeration problem ?. *Plant Physiology* 72, 447-454.

RASKIN, I. & KENDE, H. (1985). Mechanism of aeration in rice. *Science* 228, 327-329.

REDDY, K. R. & SMITH, W. H. (Eds)(1987). *Aquatic plants for water treatment and resource recovery.* Magnolia Publishing Inc., Orlando, Florida. 1032 pp.

REDDY, K. R., D'ANGELO, E. M. & DEBUSK, T. A. (1990). Oxygen transport through aquatic macrophytes : The role in wastewater treatment. *Environmental Quality* 19, 261-267).

REED, S.C., MIDDLEBROOKS, E.J. & CRITES, R.W. (1988). *Natural Systems for Waste Management and Treatment.* Chapter 6. McGraw-Hill, New York.

REYNOLDS, O. (1879). On certain dimensional properties of matter in the gaseous state. *Phil. Trans.* 170, 727-845.

ROBERTS, D.G., McCOMB, A.J. & KUO, J. (1984). The structure and continuity of the lacunar system of the seagrass, *Halophila ovalis* (R. Br.) Hook. f. *Aquatic Botany* 18, 377-388.

RUDESCU, L., NICULSCU, C. & CHIRU, I.P. (1965). *Monographia stufului dim delta Dunarii.* Editura Academiei Republicii Socialiste Romania, pp. 101-224.

SCHIERUP, H-H., BRIX, H. & LORENZEN, B. (1990) Wastewater treatment in constructed reed beds in Denmark - state of the art. In: *The Use of Constructed Wetlands in Water Pollution Control.* (Ed. by P.F. Cooper & B.C. Findlater), pp. 495-504. Pergamon Press.

SCHOLANDER, P.F.L., VAN DAM, L. & SCHOLANDER, S.L. (1955). Gas exchange in the roots of mangroves. *American Journal of Botany* 42, 92-98.

SCHREINER, O. & SULLIVAN, M.S. (1910). Studies in soil oxidation. *U.S. Dept. of Agriculture, Bureau of Soils Bulletin* 73, 1-57.

SCHRODER, P., GROSSE, W. & WOERMANN, D . (1986). Localisation of thermo-osmotically active partitions in young leaves of *Nuphar lutea*. *Journal of Experimental Botany* 37, 1450-1461.

SCULTHORPE, C.D. (1967). *The Biology of Aquatic Vascular Plants*. Arnold, London.

SEIDEL, K. (1967). New ways of biological treatment of waste waters which are difficult to purify. *Zucker* 20, 466-470.

SEIDEL, K. (1976). Macrophytes and water purification. In: *Biological Control of Water Pollution* (Ed. by J. Tourbier and R. W. Pierson), pp. 109-122. Pennsylvania University Press, Philadelphia.

SEIDEL, K. & HAPPEL, H. (1981). Sewage treatments using plants according to the Krefeld system. *Sicherheit in Chemie und Umwelt* 1, 127-129.

SLOEY, W.E., SPANGLER, F.L. & FETTER, C.W. (1978). Management of wetlands for nutrient assimilation. In: *Freshwater Ecological Wetlands Processes and Management Potential.* (Ed. by R.E. Good, D.F. Whigham & R.L. Simpson), pp. 321-340, Pennsylvania University Press, Philadelphia.

STENGEL, E., CARDUCK, W. & JEBSEMEN, C. (1987). Evidence for denitrification in artificial wetlands. In: *Aquatic Plants for Water Treatment and Resource Recovery*, (Ed. by K.R. Reddy & W.H. Smith), pp. 543-550. Magnolia Publishing.

TAKAISHI, T. & SENSUI, Y. (1963). Thermal transpiration effect of hydrogen, rare gases and methane. *Transactions of the Faraday Society* 59, 2503-2514.

TAYLOR, G.J., CROWDER, A.A. & RODDEN, R. (1984). Formation and morphology of iron plaque on roots of *Typha latifolia* L. grown in solution culture. *American Journal of Botany* 71, 666-675.

THURSBY, G.H. (1984). Root-exuded oxygen in the aquatic angiosperm *Ruppia maritima*. *Mar. Ecol. Progr. Ser.*, 16, 303-305.

TOTH, L.(1972). Reeds control eutrophication of Balaton Lake. *Water Research* 6, 1533-1539.

VAN RAALTE, M.H. (1941). On the oxygen supply of rice roots. *Annals of the Botanic Gardens, Buitenzorg* 51, 43-57.

VAN RAALTE, M.H. (1944). On the oxidation of the environment by the roots of rice (*Oryza sativa*, L.). *Hort. Bot. Bogoriensis, Java. Syokubutu-Iho* 1, 15-34.

VOGEL, S. (1978). Organisms that capture currents. *Scientific American* 239, 128-139.

WATHUGALA, A.G., SUZUKI, T. & KURIHARA, Y. (1987). Removal of nitrogen, phosphorus and COD from waste water using sand filtration system with *Phragmites australis*. *Water Research* 21, 1217-1224.

WEISNER, S.E.B., 1988. Factors affecting the internal oxygen supply of *Phragmites australis* (Cav.) Trin. ex Steudel., *in situ*. *Aquatic Botany* 31, 329-325.

WINTER, M. & KICKUTH, R. (1989a). Elimination of sulphur compounds from wastewater by root zone process - I: Performance of a large-scale purification plant at a textile finishing industry. *Water Research* 23, 535-546.

WINTER, M. & KICKUTH, R. (1989b). Elimination of sulphur compounds from wastewater by root zone process - II. Mode of formation of sulphur deposits. *Water Research* 23, 547-560

YAMASAKI, S. (1984). Role of plant aeration in zonation of *Zizania latifolia* and *Phragmites australis*. *Aquatic Botany* 18, 287-297.

YAMASAKI, S. (1987). Oxygen demand and supply in *Zizania latifolia* and *Phragmites australis*. *Aquatic Botany* 29, 205-215.

APPENDIX I

Pressurisation by thermal transpiration can be determined from the following empirical equation derived by Takaishi & Sensui (1963).

$$\frac{(P_2 / P_1) - 1}{\sqrt{T_2 / T_1 - 1}} = \frac{1}{A X^2 + B X + C \sqrt{X + 1}}$$

where T_2 is room temperature and T_1, the temperature of the chamber, is greater than T_2 .

Also : $X = 2 P_2 d / (T_1 + T_2)$,

and A, B, & C are constants specific to the gases concerned; being independent of temperature, these are :-

$$A = 1.4 \times 10^{4} \exp(0.507D),$$

$$B = 5.6 \times \exp(0.607D),$$

$$C = (110 / D) - 14.$$

where D is the collisional diameter in Angstroms, and d is the pore diameter in mm. For oxygen D is 3.98 Å, for nitrogen 3.7 Å.

APPENDIX II

Adventitious roots:

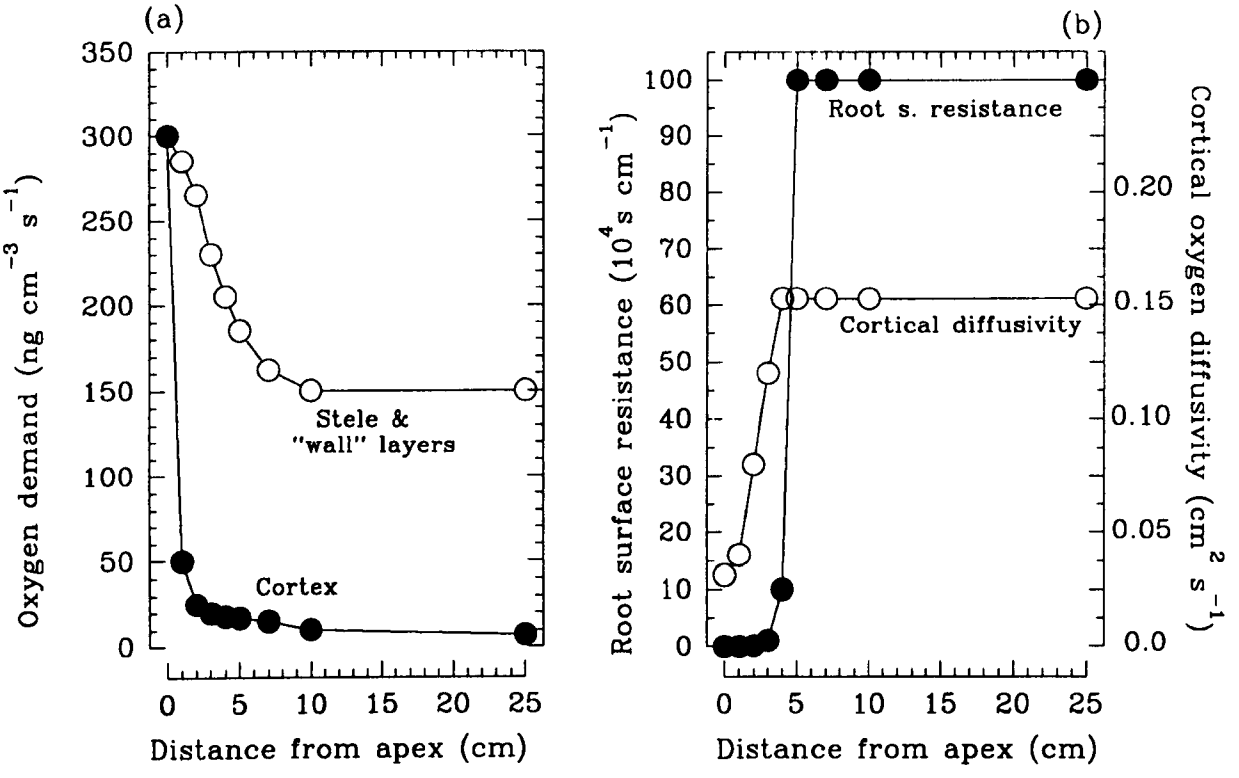

Lateral roots:

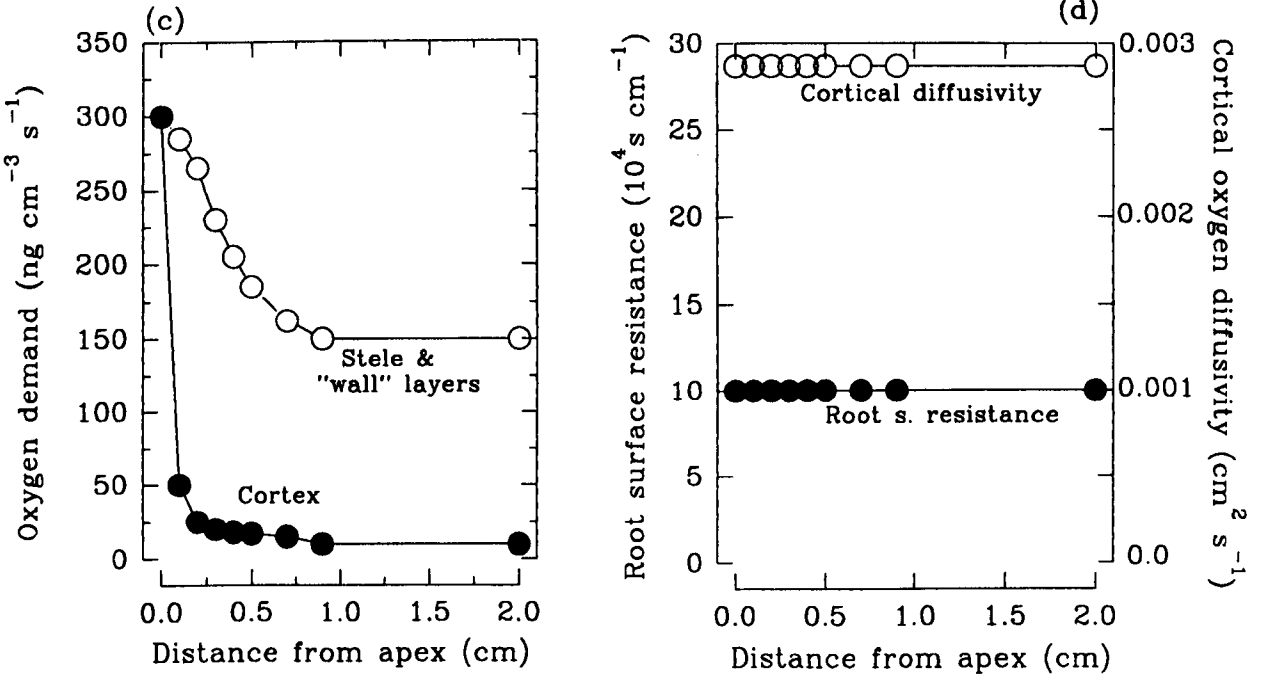

Summary of programming data for modelling oxygen consumption and release by *Phragmites* roots in connexion with Tables 8.02 & 8.03. Stelar diffusivities were taken as 0.7×10^{-6} cm^2 s^{-1}.

APPENDIX III

Respiratory oxygen consumption for *Phragmites'* rhizomes and roots at 20°C.

RHIZOME:

	O_2 uptake ng cm^{-3} tissue s^{-1} excluding gas space.
Node	40
Internode	8 - 10
Nodes + internodes	10 - 12

ADVENTITIOUS ROOTS

(i) including stele & cortex

	O_2 uptake ng cm^{-3} tissue s^{-1} including gas space.
Apex (0-5 mm)	425 - 255
20 - 50 mm	170 - 85
Basal (80 - 400 mm)	32 - 15

(ii) Stele without emerging laterals: young roots, at length 5-6 cm

150 - 220